JPL Publication 92-15, Vol. I

An Improved Approach for Flight Readiness Certification— Methodology for Failure Risk Assessment and Application Examples

Volume I

N. R. Moore
D. H. Ebbeler
L. E. Newlin
S. Sutharshana
M. Creager

June 1, 1992

NASA
National Aeronautics and Space Administration

Jet Propulsion Laboratory
California Institute of Technology
Pasadena, California

The research described in this publication was carried out by the Jet Propulsion Laboratory, California Institute of Technology, under a contract with the National Aeronautics and Space Administration.

List of Figures

Preface

This report presents the methodology for evaluating flight readiness developed by the Jet Propulsion Laboratory (JPL) under NASA RTOP 553-02-01 sponsored by the Office of Space Flight (OSF), NASA Headquarters. This methodology was developed as a part of the Certification Process Assessment task initiated by OSF due to concern about criteria for certifying flight readiness of the Space Shuttle propulsion system.

An early phase of this work included an extensive review of certification and failure risk assessment approaches used by the aerospace industry and government agencies. Based on the findings of this review,[1] further work was focused on defining, developing, and demonstrating an improved technical approach for failure risk assessment that can incorporate information from both test experience and engineering analysis to obtain a quantitative failure risk estimate. This approach, called Probabilistic Failure Assessment (PFA), is of particular value when information relevant to failure prediction, including test experience and knowledge of parameters used in engineering analyses of failure phenomena, is expensive or difficult to acquire. Under such constraints, a quantitative evaluation of failure risk based on the information available from both engineering analysis and operating experience is needed to make effective risk management decisions and utilize financial resources efficiently.

The PFA methodology is applicable to failure modes that can be characterized by analytical or empirical modeling of failure phenomena and is especially useful when models or information used in analysis are uncertain or approximate. PFA can be applied at any time in the design, development, or operational phases of a program to quantitatively estimate failure risk based on the information available at the time of the risk assessment and can be used to evaluate and rank alternative measures to control risk, thereby enabling the more effective allocation of limited financial resources.

The work documented in this report was carried out by a multidisciplinary team of JPL technical personnel, which was managed by N. R. Moore. This team was composed of individuals with expertise in statistics, systems modeling, and engineering analysis. D. H. Ebbeler formulated and structured the statistical methodology and directed its implementation. L. E. Newlin formulated and implemented probabilistic engineering models and implemented the statistical methodology. S. Sutharshana

---

[1] See [3] of *Section 1.0* references.

formulated probabilistic engineering analysis methods and models. M. Creager[2] made major contributions to defining and formulating the probabilistic modeling approach and engineering analysis procedures used in this work. Present or former JPL personnel who made substantial contributions in early phases of this work include D. L. Schwartz, W. E. Edmiston, and L. J. Grondalski. D. Goode and J. Ramsay typeset the manuscript, including graphics, using computerized desktop publishing methods, and E. Reinig edited the manuscript.

In developing the PFA methodology, the JPL team interacted with aerospace system manufacturers, the Marshall Space Flight Center, and the Lewis Research Center. Individuals of these organizations generously shared information and spent significant amounts of time with the JPL team. In particular, Rocketdyne, Canoga Park, California, and Pratt & Whitney, West Palm Beach, Florida, collaborated in performing the application examples given herein. In addition, technical comments on certification approaches and failure modeling were provided by the above-listed organizations and by General Electric, Cincinnati, Ohio; the Federal Aviation Administration; and the Wright-Patterson Air Force Base.

The PFA methodology, examples of its application to spaceflight components, and computer software used to implement PFA are documented in the three volumes of this report. Volume I documents the PFA methodology and the application examples, including the rationale for PFA and the analysis procedures used in the examples. Volume II contains user's guides and flowcharts for the computer software used to implement PFA in the application examples. Volume III presents the structure and listings of the computer programs.

---

[2] Currently of Structural Integrity Engineering, Chatsworth, CA.

Acknowledgments

The authors wish to acknowledge the guidance and encouragement provided by D. L. Winterhalter of the Office of Space Flight, NASA Headquarters, whose support made this work possible. The authors appreciate the encouragement of R. Bardos, J. Mulcahy, and other individuals of OSF. The review and comments on this work provided by R. Weinstock of Vitro, Washington, D. C. contributed substantially to its successful completion.

The application examples of this report were performed in collaboration with Rocketdyne, Canoga Park, California, and Pratt & Whitney, West Palm Beach, Florida. Several individuals at each organization contributed generously to this work, including E. P. Fox and C. G. Annis of Pratt & Whitney, and K. J. O'Hara and D. O'Connor of Rocketdyne. The authors worked particularly closely with E. P. Fox of Pratt & Whitney and K. J. O'Hara of Rocketdyne; their considerable contributions are gratefully acknowledged.

Present or former personnel of the NASA Marshall Space Flight Center, whose cooperation was instrumental in successfully performing this work, include J. Lombardo, J. S. Richards, G. W. Smith, L. D. Salter, H. P. Stinson, and J. Townsend.

The authors appreciate the technical comments provided by L. Beitch and A. Coles of the General Electric Co., Cincinnati, Ohio, on flight readiness certification approaches and fatigue life modeling. The effort of G. R. Halford of the NASA Lewis Research Center in providing information on materials fatigue life modeling is appreciated.

Throughout the course of this work constructive guidance was provided by the Liquid Rocket Engine Certification Subcommittee of Aerospace Division Committee G-11, Society of Automotive Engineers. The membership of this subcommittee included: W. E. Campbell, Aerojet; K. J. O'Hara, Rocketdyne; E. P. Fox, Pratt & Whitney; J. S. Richards and H. P. Stinson, NASA-MSFC; R. L. Doebler, Aerospace Corp.; and N. R. Moore, JPL.

Finally, the authors wish to acknowledge the review of the technical approach of this work provided by the late R. P. Feynman of the California Institute of Technology.

The authors express their gratitude to all those individuals who contributed to this work and regret that a complete listing is not feasible.

Abstract

An improved methodology for quantitatively evaluating failure risk of spaceflight systems to assess flight readiness and identify risk control measures is presented. This methodology, called Probabilistic Failure Assessment (PFA), combines operating experience from tests and flights with engineering analysis to estimate failure risk. The PFA methodology is of particular value when information on which to base an assessment of failure risk, including test experience and knowledge of parameters used in engineering analyses of failure phenomena, is expensive or difficult to acquire.

The PFA methodology is a prescribed statistical structure in which engineering analysis models that characterize failure phenomena are used conjointly with uncertainties about analysis parameters and/or modeling accuracy to estimate failure probability distributions for specific failure modes. These distributions can then be modified, by means of statistical procedures of the PFA methodology, to reflect any test or flight experience. Conventional engineering analysis models currently employed for design or failure prediction are used in this methodology.

The PFA methodology can be applied at any time in the design, development, or operational phases of a program to quantitatively estimate failure risk based on the information available at the time failure risk is assessed. Sensitivity analyses conducted as a part of PFA can be used to evaluate and rank such alternative measures to control risk as design changes, testing, or inspections, thereby enabling limited program resources to be allocated more effectively.

PFA is generally applicable to failure modes that can be characterized by analytical or empirical models of failure phenomena and is especially useful when models or information used in analysis are uncertain or approximate. Such failure modes include, but are not limited to, fatigue, flaw propagation, rupture, degradation and wear, and malfunction of mechanical or electrical systems.

It is often not feasible to acquire enough test experience to establish high reliability at high confidence for spaceflight systems. Moreover, the results of conventionally performed engineering analyses of failure modes can be subject to serious misinterpretation when uncertain or approximate information is used to establish analysis parameters and calibrate the accuracy of analysis models. Under these conditions, a quantitative evaluation of failure risk based on the information available from both test or flight experience and engineering analysis is needed to make effective risk management decisions.

This report describes the PFA methodology and presents examples of its application. Conventional approaches to failure risk evaluation for spaceflight systems are discussed, and the rationale for the approach taken in the PFA methodology is presented. The statistical methods, engineering models, and computer software used in fatigue failure mode applications are thoroughly documented.

Table of Contents

VOLUME I – Methodology and Applications

List of Tables

1.0 Introduction

Section 1.1
Flight Readiness Assessment

1.1.1 The Flight Readiness Assessment Problem

The occurrence of critical failures during the service life of such spaceflight systems as the Space Shuttle and planetary spacecraft must be established as extremely unlikely before missions are flown. The expectation of reliable operation over the service life of spaceflight systems typically has been established by a judgmental evaluation of limited test experience and deterministic engineering analysis, as discussed for the Space Shuttle in **[1]**, **[2]**, and **[3]**. It is rarely feasible to acquire enough test experience to establish high reliability at high confidence for spaceflight hardware, and deterministic analyses to predict failures can become arbitrary and subject to serious misinterpretation when information used to establish analysis parameters and to calibrate the accuracy of analysis models is not based on sufficiently extensive experience. The assessment and management of failure risk of spaceflight systems can be improved by using a risk assessment approach that can quantitatively incorporate information from both operating experience *and* engineering analysis. A discussion of the need for improved approaches for characterizing and managing failure risk, including comments on the approach presented in this report, is given in **[2]**.

Operating experience and engineering analysis are the two fundamental information sources on which any assessment of failure risk is based. For certain failure modes of spaceflight systems, directly applicable experience is sparse or does not exist; testing sufficient to establish high reliability is infeasible; consistently conservative engineering analyses result in unacceptable designs or service limits; and analysis parameters and/or models are too uncertain for less conservative deterministic analyses to be credible. Under these conditions, a quantitative assessment of failure risk that incorporates all of the available information is required in order to make effective risk management decisions.

The approach advocated in this report for assessing and managing failure risk uses engineering analyses and operating experience in a statistical structure in which uncertainties about the prediction or characterization of failure are quantitatively treated. The probabilistic analysis to characterize failure risk is carried out with the information available at the time of the analysis. This analysis can be performed with any amount of information at any time in the design, development, qualification/certification, or operational phases of a spaceflight project. The results of such a probabilistic analysis provides a quantitative measure of failure risk that is warranted

by what is known about a failure mode. In addition, the types of information having the largest impact in controlling failure risk can be identified and ranked.

This approach can be applied to any failure mode that can be described by analytical models of the failure phenomena, even when such models are uncertain or approximate. Such failure modes include, but are not limited to, fatigue, flaw propagation, burst or rupture, degradation and wear phenomena, and malfunction of mechanical or electrical systems. Examples of the application of this approach to high cycle fatigue and low cycle fatigue failure modes are presented in the following sections of this report. The application examples documented in this report are listed in *Section 1.4*. Additional applications will be presented in subsequent reports.

Fatigue, crack growth, and degradation are examples of damage accumulation failure modes wherein failure is a consequence of the cumulation of aging effects produced by repeated exposure to operating conditions or by environmental parameters which vary cyclically. In contrast, event consequent failure modes are those in which failure is independent of the extent of previous exposure to operating conditions; instead, failure is a consequence of an event such as applied stress exceeding ultimate strength.

Failure prediction for event consequent failure modes is usually much less uncertain than for damage accumulation failure modes. Moreover, it is often feasible to conduct testing programs to establish low failure probability with high confidence for event consequent failure modes, while such test programs are seldom feasible for damage accumulation failure modes **[4]**. As a result, the probabilistic analysis approach and methods presented in this report are most useful for damage accumulation failure modes when failure prediction by analysis is significantly uncertain and testing to demonstrate high service life reliability with high confidence is not feasible. Service life reliability is the probability of surviving the required service life without a failure.

Probabilistic analyses can yield particularly beneficial results for a subset of the critical failure modes identified by means of Failure Modes and Effects Analysis (FMEA) or other systematic procedures to identify and screen failure modes. Many of the failure modes identified by an FMEA can be shown to be extremely unlikely by means other than detailed probabilistic analyses. A probabilistic assessment of failure risk is appropriate for certain critical failure modes of components whose failure margins are of concern. That concern usually arises because analytical models for failure phenomena and/or information upon which to base failure prediction are uncertain. Under such circumstances, the probabilistic approach presented here can be used to more effectively organize and interpret the information available to characterize the likelihood of failure during service and evaluate such alternatives for

controlling failure risk as design changes, inspections, or tests to characterize environments, thereby enabling the more efficient use of limited financial resources.

In the following sections of this introduction, the limitations of conventional approaches to flight readiness or failure risk assessment are discussed, the probabilistic approach to failure risk assessment taken here is presented, and a description of the organization and contents of the remainder of this report is given.

1.1.2 Conventional Approaches to Flight Readiness Assessment

The flight readiness assessment process by which the expectation of reliable mission operation is established is referred to as certification or qualification. More definitively, certification of a system intended for use in a specific application is the process by which confidence is established that the system will perform as expected over a specified range of environmental and operating conditions. Certification of spaceflight systems has been typically based on a limited amount of testing of flight configuration systems considered in conjunction with deterministic engineering analysis. The deterministic engineering analysis may incorporate information from measurements of governing physical parameters taken during development testing. Approaches that have been used in certifying aerospace propulsion systems, including those of the Federal Aviation Administration and the U. S. Air Force, are discussed in **[3]**.

1.1.2.1 Testing to Establish Flight Readiness

The value of test experience in establishing low failure probability with high confidence for flight configuration systems is limited because testing is typically halted before failures are thought to be likely to occur. Failures during testing are avoided because the occurrence of critical structural failures of spaceflight systems can result in the loss of costly hardware and damage to expensive test facilities. The availability of failure experience for flight hardware is further diminished because failure modes discovered during development and testing are corrected by design changes which are intended to render their occurrence highly unlikely during subsequent mission operation. Consequently, test experience for spaceflight systems typically does not include failure data for flight configuration hardware, but instead consists of tests which are suspended before failures occur, i.e., "zero-failure" tests. Testing to establish flight readiness is discussed further in *Appendix 1.A*.

The exclusive use of zero-failure tests to establish with high confidence that failure risk is very low typically implies that an extremely extensive set of test data is required. For example, suppose that each mission simulation test can be treated as an identical independent trial with constant probability of failure p, so that the number of failures is Binomially distributed. The upper confidence limit for p at confidence level C is defined by

$$(1 - p_u)^n = 1 - C$$

where n is the total number of zero-failure mission simulation tests and p_u is the upper confidence limit for p. Reliability R at a service life M is the probability of survival to M. For the Binomial failure distribution with M expressed as a number of missions, reliability is

$$R = (1 - p_u)^M$$

Thus we have

$$n / M = \ln (1 - C) / \ln R$$

In order to have even 50% confidence that the probability of failure is no larger than 1/1000, 693M mission simulation tests without failure would have to be conducted.

Analogously, if failures are characterized by a Weibull distribution

$$R = \exp\left[-(M / \eta)^\beta\right]$$

If there are N zero-failure tests of duration $T_1, T_2, \ldots, T_N$, the lower confidence limit for η at confidence level C is defined by

$$\exp\left[-\sum_{i=1}^{N} (T_i / \eta)^\beta\right] = \exp\left[-N (T / \eta)^\beta\right] = 1 - C$$

where η and β are the Weibull location and shape parameters, respectively, and $T \equiv \left[\frac{1}{N}\sum_{i=1}^{N} T_i{}^\beta\right]^{1/\beta}$. Thus we have

$$T / M = \left[\ln (1 - C) / N \ln R\right]^{1/\beta} \qquad (1\text{-}1)$$

If the N zero-failure tests consist of testing N units for the same number of missions, then the duration of each of those unit tests is T missions, the service life is M missions, and the total test experience is NT missions.

Suppose two units are tested for the same number of missions. In *Figure 1-1*, the plot of *Equation 1-1* under that constraint shows reliability at 95% confidence as a function of the ratio of unit test duration to service life T / M for $\beta = 1$ and $\beta = 2$. For complex systems subject to multiple active failure modes, approximating the distribu-

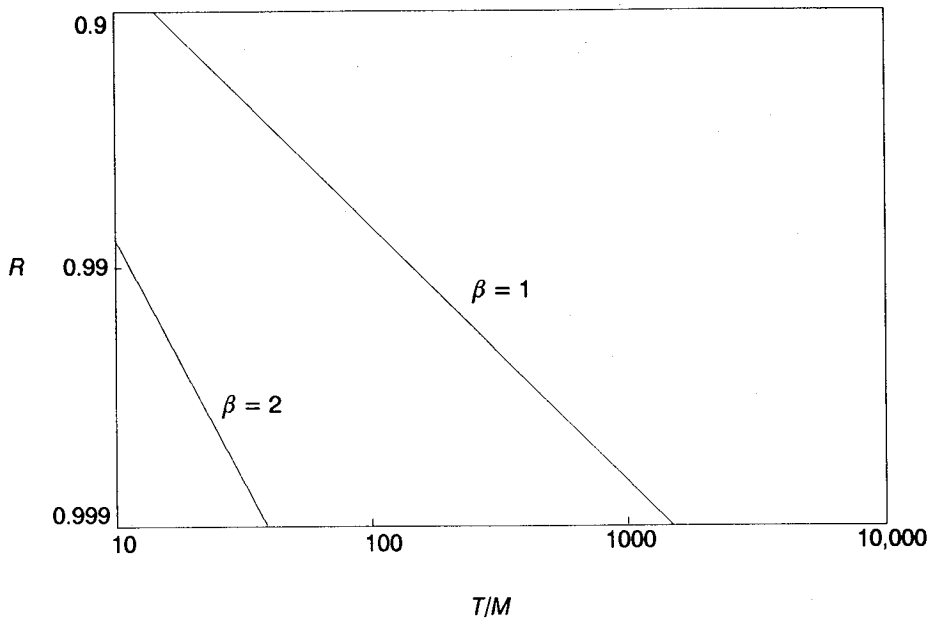

Figure 1-1 Reliability Demonstrated by Zero-Failure Operating Experience for $N = 2$ at 95% Confidence

tion of system failures by a Weibull distribution with $\beta = 1$ is more plausible than with $\beta = 2$. The system failure distribution problem is discussed in **[5]** (*Section 4.8*) and **[6]** (*Chapter 1.12*). *Figure 1-1* shows that, to establish a reliability of .999, at 95% confidence, $T / M = 1498$ for $\beta = 1$ and $T / M = 39$ for $\beta = 2$. Thus for $\beta = 1$ the unit test duration must be $1498M$ missions and for $\beta = 2$ the unit test duration must be $39M$ missions. For example, if the desired service life for a reusable system is 7 missions, then with $\beta = 1$ the unit test duration required to establish a reliability of .999 at 95% confidence is $T = 7 \times 1498 = 10{,}486$ missions.

The service life reliability that is demonstrated by accumulated operating experience on several reusable spaceflight components is presented in *Appendix 1.A*. In the absence of relevant failure data, it is not possible to estimate the shape parameter β of the Weibull distribution. Consequently, the value of that unknown β must be considered exogenous to the statistical analysis in order to calculate the service life reliability that is demonstrated by a component's zero-failure operating history. The figures given in *Appendix 1.A* show the effect of β on the service life limit below which service life reliability can be stated to be no less than a specified value. For example, given accumulated operating experience of 337,175 seconds for the component of *Figure 1-6* in *Appendix 1.A*, the service life limit for .999 service life reliability at 95%

confidence shown is about seven missions for $\beta = 3$ and about three missions for $\beta = 2$. Values of β between 1 and 3.5 are common for Weibull distributions for fatigue failures. Zero-failure testing is also discussed in **[6]** (*Chapter 5*).

When the data set consists of nonfailure operating experience, it is possible to avoid an exogenous specification of β by using the approach developed in **[7]**. Using this approach a service life limit can be derived for a specified value of single mission reliability or service life reliability, contingent on the existence of a "worst-case" value of β. For a given nonfailure data set, e.g., that of *Figure 1-6*, the specified value of reliability must be below a threshold value in order for the "worst-case" β to exist. At high confidence, this threshold value of reliability, which may be specified as either single mission reliability or service life reliability, is too low to be useful as a criterion for failure risk management.

For example, single mission reliability at 90% confidence must be specified to be no greater than .9965 in order for a "worst-case" β to exist for the data set used in *Figure 1-6*. If reliability is specified higher than the threshold value, no "worst-case" value of β will exist. The service life limit corresponding to a mission reliability of .995 that can be demonstrated by this approach is about 22 missions. A single mission reliability no greater than .995 for each of 22 missions is approximately equivalent to a service life reliability of .95, which implies a demonstrated failure risk of 5% or one in twenty over the 22 missions. This is an unacceptably high demonstrated failure risk, but it only illuminates the arbitrariness of this approach because the true failure risk can be higher or lower (most likely it is very much lower) depending on the actual values of the parameters of the failure probability distribution. This approach requires that high demonstrated failure risk be accepted in order to have reasonable service lifetime limits for components considered to be conservatively designed and for which there are no indications of problems.

The mathematical results in **[7]** are consistent with the fact that acceptable service life reliabilities cannot be demonstrated using a feasible amount of nonfailure data. The examples given in **[7]** are inappropriate for applications where failure risk must be stringently controlled, since they focus either on cases where 50% confidence levels are acceptable or on single mission reliabilities which are so low that they imply unacceptable service life reliabilities.

A risk control procedure based only on nonfailure operating experience cannot establish service lifetime limits that are commensurate with a component's capability. Such a procedure cannot set appropriately low service lives for components of low capability nor use a reasonable fraction of the capability of longer life components. From a feasible amount of nonfailure testing alone, it is not possible to distinguish between components with low failure risk and components with high failure risk which

have not yet failed. Relying on nonfailure data alone to establish lifetime limits results in ineffective risk control and in hardware replacement costs that are higher than necessary.

It is usually infeasible to design testing programs for the purpose of demonstrating high reliability at high confidence for flight configuration systems using only nonfailure operating experience. The primary purposes of a testing program should be: (1) to reveal failure modes not identified and to provide information to aid in uncovering analysis oversights or errors; and (2) by means of instrumented tests, to adequately characterize those parameters which drive the results of an engineering analysis of failure modes. Useful reliability statements result from probabilistic analysis which incorporates all available information, including engineering analysis as well as operating experience.

1.1.2.2 Deterministic Engineering Analysis

Consistently and verifiably conservative deterministic analyses to predict failure can provide assurance that the conditions under which a critical failure mode could occur do not intersect conditions that exist during mission operation. Such analyses are appropriate for most of the failure modes identified in an FMEA. In that situation, the deterministic approach serves to establish that the occurrence of the failure mode in question is extremely unlikely, although no quantitative estimate of the probability of failure is available from such analyses. When constraints and requirements for performance, weight, or cost force a departure from consistently conservative deterministic analyses for certain failure modes, worst-case or limiting values for parameters that govern failure are not always employed.

When worst-case values for the parameters that govern failure cannot be consistently used, deterministic analysis methods are credible only if they are calibrated by experience that is directly relevant in terms of knowledge of governing parameters, the stochastic nature of materials behavior, the accuracy of engineering models under the conditions of application, and the variability of manufacturing processes. Where there exists an extensive, directly relevant base of experience to guide the selection of less conservative safety factors and values for governing parameters, deterministic analyses can provide failure predictions that are generally consistent with the experience base, although the extent of conservatism is not known. An example of this is the use of an assumed initial crack size of .05 inches for most structures in the USAF damage tolerant design criteria **[8]**.

Spaceflight systems are typically subject to some significant number of failure modes for which important governing parameters may not be well known, e.g., knowledge of structural loads or a local environment may be highly uncertain, and the accuracy of engineering models used to characterize the failure phenomena may

be in question. When performance, weight, or cost requirements force the use of new design approaches, advanced materials, or a more severe operating environment, a suitably extensive experience base is usually not available to calibrate deterministic analyses to predict failure.

Under the conditions of uncertainty described above, deterministic analyses become arbitrary and can yield results that are subject to serious misinterpretation **[1]**. In these situations, a formal procedure for quantitatively accounting for risk due to uncertain knowledge is required if consistent criteria for flight readiness are to be established. In these cases, the consideration of risk by means of qualitative judgments based on deterministic analyses of failure modes and limited test experience can lead to erroneous or ineffective risk management decisions.

Section 1.2

An Improved Approach to Flight Readiness Assessment

1.2.1 Failure Risk Assessment

At any time in the design, development, or mission operation of a spaceflight system, the available information on which to base an assessment of flight readiness or failure risk comes from two fundamental sources: engineering analysis and operating experience. *Figure 1-2* shows how these two information sources can be used in a statistical framework to assess failure risk. The statistical framework used to combine information from engineering analysis with observed operating experience is a straightforward application of Bayes' Rule and is applied individually to certain failure modes identified for probabilistic analysis.

Engineering analysis can be used to characterize the conditions under which a specific failure mode may be expected to occur, e.g., pressure or accumulated time in service. As illustrated in *Figure 1-2*, engineering analysis provides information to establish the prior failure risk distribution which is modified to reflect the available success/failure data in a Bayesian statistical analysis **[9]**. Engineering analysis to predict failure is based on available knowledge of governing parameters, e.g., loads and material properties, that can be derived from measurements taken during tests or flights, from analyses to characterize parameter values, from applicable experience with similar systems, or from laboratory tests. Measurements of such physical parameters as temperatures or loads used in engineering analysis can be a strong information source in failure risk assessment.

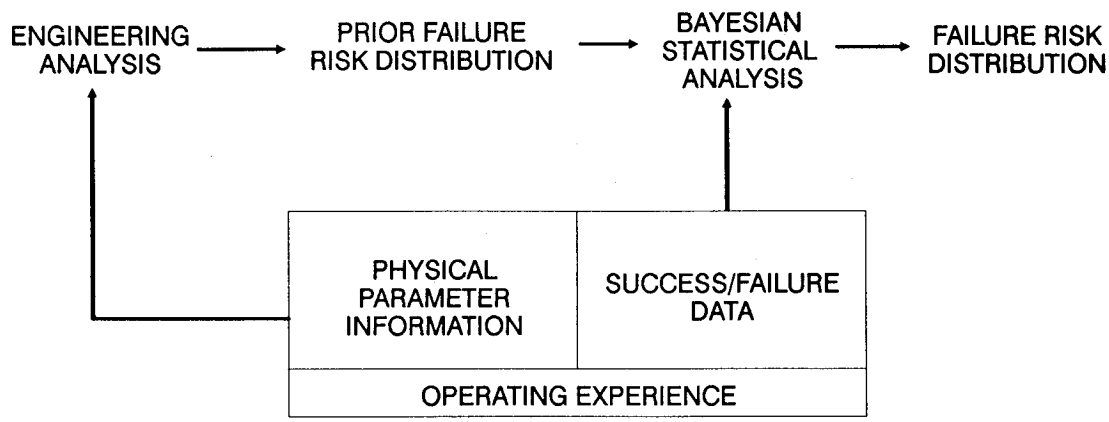

Figure 1-2 Information Sources for Failure Risk Assessment

As shown in *Figure 1-2*, operating experience consists of parameter information and success/failure data. Success/failure data can be acquired from development testing, certification testing, or flight operation. The failure risk distribution resulting from the combination of the prior distribution and the success/failure data is that which is warranted by the information available. As additional information regarding governing physical parameters becomes available it can be incorporated into the engineering analysis to obtain a revised prior failure risk distribution. Additional information in the form of success/failure data can be processed by the Bayesian statistical algorithm to update the failure risk distribution using procedures discussed later in this report.

When the success/failure data for flight configuration hardware consists of some number of trials with no failures, as is often the case for spaceflight systems, the data is usually a weak information source for reliability demonstration or failure risk assessment. In these cases, the failure risk distribution will be predominantly determined by the prior failure risk distribution of *Figure 1-2*. Consequently, the prior distribution based on the engineering analysis must accurately represent the available information.

Demonstrating high reliability at high confidence is equivalent to making statements about the extreme left-hand tail of a failure distribution. Nonfailure test data typically provides very conservative bounding information about location and variability of the failure distribution. Information about the failure distribution from engineering analysis can be extremely informative about the distribution's location. Thus, the inclusion of engineering analysis allows an improved description of the failure distribution, even with the conservatism about variability implied by uncertainty in engineering analysis due to sparse information.

1.2.2 The Probabilistic Failure Assessment Methodology

A formal stochastic structure for quantitatively assessing failure risk based on the available information about certain failure modes identified in an FMEA or other procedure is shown in *Figure 1-3*. This stochastic structure is called the Probabilistic Failure Assessment (PFA) methodology and is an implementation of the statistical framework of *Figure 1-2* in which information from engineering analysis is combined with success/failure data to obtain a quantitative failure risk estimate and a measure of its uncertainty as discussed in *Section 2.1.1* and in **[10]**. The available information pertinent to characterizing specific failure modes is used in the PFA methodology, not only to estimate the failure risk appropriate to the available information about failure modes, but also to characterize the sensitivity of failure to additional information about such parameters as structural loads, operating environment, and materials behavior.

The PFA methodology shown in *Figure 1-3* consists of three major steps: probabilistic failure modeling, a Bayesian statistical analysis to consider the success/failure

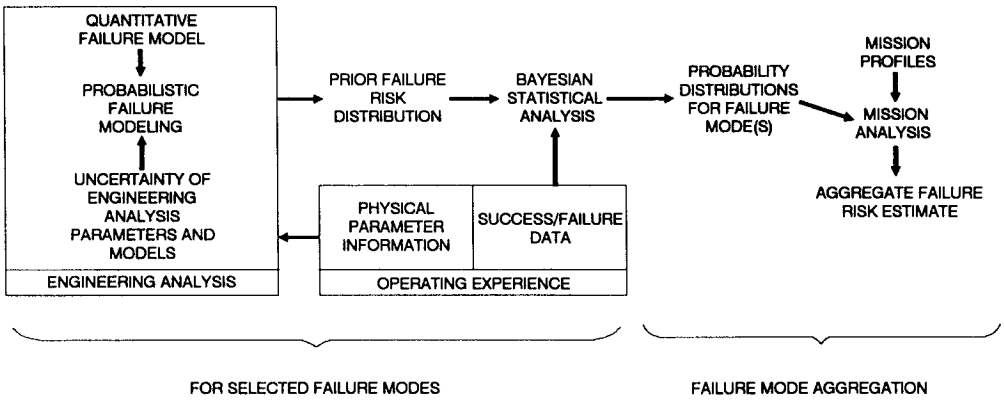

Figure 1-3 The Probabilistic Failure Assessment Methodology

data, and a mission analysis in which the failure probability distributions for a number of relevant failure modes can be aggregated. Probabilistic failure modeling and the Bayesian statistical analysis are performed for each failure mode identified for analysis. In the following sections of this report, the steps of the PFA methodology, with the exception of the mission analysis, are treated in detail. The results of applying the PFA methodology to a specific failure mode will include the left-hand tail of the failure probability distribution for that failure mode and a sensitivity analysis for drivers. Given such failure distributions for some limited number of critical failure modes, there exist several alternative approaches for aggregating the individual distributions that are thoroughly treated in the literature. In particular, Monte Carlo methods are discussed in **[6]**.

The features of the PFA methodology essential to the rational evaluation of failure risk are: (1) inclusion of information from engineering analysis and operating experience, (2) analytical modeling of failure phenomena based on mechanics or physics, (3) representation of the uncertainty about analytical models and their governing parameters, including uncertainty due to both intrinsic variation and limited information, and (4) consideration of failure risk over the service life.

Conventional engineering analysis models employed in component design and life prediction are used in the PFA methodology. Within the PFA structure, uncertainties due to sparse information about values of analysis parameters and uncertainties about the accuracy of the analysis models are quantitatively treated. For example, in addition to the intrinsic variability of materials fatigue life, the uncertainty resulting from basing a model of fatigue life on a limited amount of test data is treated in the stochastic materials fatigue life characterization model described in *Section 2.1.2* of this report.

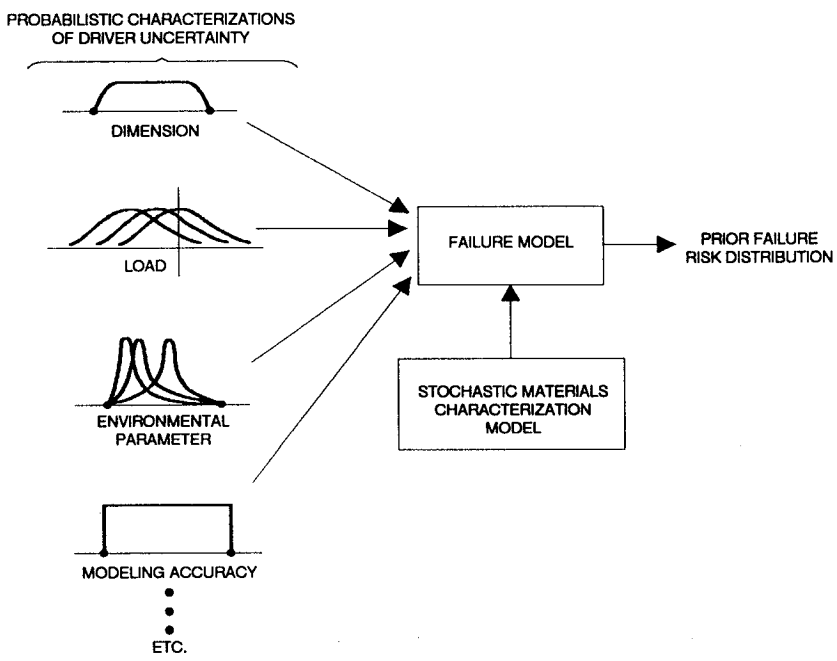

Figure 1-4 The Probabilistic Failure Modeling Procedure

1.2.3 Probabilistic Failure Modeling

The probabilistic failure modeling step of the PFA methodology is shown in greater detail in *Figure 1-4*. Here, uncertainties in engineering analysis parameters and models for the failure mode being analyzed are used in conjunction with a quantitative model of the failure phenomenon to predict failure probabilistically. Failure models are derived directly from engineering analyses of failure modes and express a failure parameter, such as burst pressure or fatigue life, as a function of governing parameters or *drivers*. For structural failure modes, drivers include dimensions, loads, materials characteristics, modeling accuracy, and such environmental parameters such as local temperatures.

For many failure modes of concern, the failure model of *Figure 1-4* involves the use of several engineering analysis procedures. State-of-the-art engineering models and analysis procedures used in the aerospace community to analyze failure modes have evolved through extensive experience. These models and procedures often are comprised of a series of steps, each of which may be complex. The PFA methodology can accommodate any engineering model. The accuracy of each engineering model and procedure is probabilistically characterized and treated as a driver. Characterizations of model accuracy are based on relevant experience with these engineering models and on specific calibrations of the models.

By calculating failure risk from an analysis based on a specification of failure models and drivers which incorporates their uncertainties, the PFA methodology enables the quantitative assessment of failure risk when failure data applicable to flight configuration hardware is sparse or does not exist.

1.2.4 Driver Characterization

A driver for which uncertainty is to be considered must be characterized by a probability distribution over the range of values it can assume. That distribution expresses uncertainty regarding specific driver values within the range of possible values. A driver probability distribution must represent both intrinsic variability of the driver and uncertainty due to limited information on which to base the driver characterization.

Stochastic drivers are responsible for the probabilistic character of the PFA methodology and their probability distributions are specified by using the information that exists at the time of analysis. Use of the PFA methodology does not imply a need for more information than would otherwise exist. If driver information is sparse, the probabilistic characterization of such a driver must reflect that sparseness. If extensive experimental measurements have been performed for a driver, its nominal value and characterization of its variability can be inferred directly from empirical data. However, if little or no directly applicable empirical data is available for a driver, engineering analysis and past experience with similar or related systems are used instead.

The information on which driver characterization is based can include measurements, related experience, and engineering analysis conducted to bound or characterize the driver. All sources of driver uncertainty must be considered to appropriately represent risk due to limited information, and driver distributions must meet the criterion of not overstating the available information. Drivers are fundamental in the sense that they are observable parameters for which additional information regarding their values can be obtained if necessary. Such parameters include temperatures, loads, materials behavior, and calibrations of model accuracy. If uncertainty due to lack of information on a driver is found to make a significant contribution to failure risk, then the desirability of acquiring additional driver information can be evaluated.

The need to represent a driver stochastically derives from two fundamental sources: intrinsic variability and specification error. Specification error refers to such model misspecification as the inaccurate specification of values of parameters of analytical models or probability distributions used to characterize such quantities as loads or fatigue life. The concept of specification error and its mathematical structure are discussed in **[11]** (*Chapter 1*). Specification error can be due to engineering model inaccuracy or to sparse information about physical parameters. Consider the ex-

ample of a finite element analysis used to characterize stresses. The finite element model itself is a source of specification error in the computation of stresses since the model will not match the hardware precisely. In many cases, loads and material properties are sources of specification error, in addition to having intrinsic variability. There are cases where engineers know that a certain load varies very little from flight to flight or part to part, but they may know the load magnitude only with a large uncertainty, say within a factor of two or four.

For many stochastic drivers, it is not possible to distinguish between intrinsic variation and variation due to specification error. In those cases, a stochastic driver is characterized by the compounded effect of both sources of variation without attempting to model each source separately. An example of this is the characterization of stress concentration factor presented in *Sections 3.2.2* and *3.A.2.3*. Uncertainty in stress concentration factor results from geometric variability induced by the manufacturing process and from an imperfect translation of geometric variability into stress concentration factor uncertainty.

Some general guidelines for characterizing stochastic drivers have emerged from case studies conducted to date. Information is typically provided by engineers experienced in the characterization of a particular driver. All sources of uncertainty must be considered, and the information used must be traceable and documented. Traceability and documentation assure that additional information can be consistently incorporated into driver distributions as it becomes available. For drivers which have physical bounds, such as temperature, controlled dimensions, and loads with physical upper limits, the Beta distribution parameterized with location, shape, and scale parameters has been successfully used in the application examples of *Section 3*. If only bounds are known, a Uniform distribution is appropriate. For a driver such as turbopump speed whose variation can be thought of as due to the combined influence of a large number of small independent effects, the Normal distribution is used. Also, past experience in characterizing a particular driver such as a material property may suggest the use of a particular distribution, for example, Weibull, Normal, or Lognormal. Characterization of stochastic drivers is discussed in more detail in *Sections 2.1.3, 2.3.2, 3.1.3, 3.2.2, 3.3.2, 3.A.2.3*, and *3.A.3.3* of this report.

The sparseness of the information typically available for characterizing a stochastic driver and the existence of significant specification error have often led to the use of a hyperparametric structure, which has proven useful in characterizing information provided by experienced engineers. For example, to characterize stress concentration factor uncertainty in a fatigue analysis example given in this report, engineering information was used to establish upper and lower bounds on the value for the stress concentration factor. In order to capture the fact that the most likely value of the stress concentration factor is not known with certainty, a Beta distribution with a Uniform

distribution on the location parameter was used. This Uniform distribution is the hyperdistribution associated with the stress concentration factor uncertainty, and its parameters are the associated hyperparameters. This driver distribution is given in *Figure 3-18*.

1.2.5 Computational Methods

The complexity of failure models and the need for a computational procedure capable of accuracy have led to the use of Monte Carlo simulation as the principal computational method in the probabilistic failure modeling step of *Figure 1-3*. Monte Carlo simulation is a general method for probabilistic analysis that can be used with failure models of any complexity. Continually increasing computer power due to improving hardware and software is steadily expanding the practical application of such computationally intensive methods as Monte Carlo simulation. Efficient Monte Carlo techniques can be used to reduce the number of simulation trials for those problems where computational time would be an issue if direct Monte Carlo simulation were used.

Alternatives to Monte Carlo simulation methods include FORM/SORM, **[12]** and **[13]**, and MVFO/AMVFO, **[14]** and **[15]**. These alternatives may fail to give demonstrably accurate results for realistic problems in which complex failure models are employed. Alternative computational methods can be used in probabilistic analyses which employ well-behaved failure models, particularly if the failure criterion is expressed explicitly in a closed form equation as opposed to a complex multistep algorithm. A comparison of FORM/SORM with direct Monte Carlo simulation for a crack growth example is given in **[16]**. Computational methods are also discussed in **[10]**.

Certain engineering analysis procedures sometimes employed in failure models, such as finite-element structural models, may appear to be too computationally intensive for practical use in a Monte Carlo simulation. However, when such procedures are used in a failure model for PFA, they can be represented as response surfaces over the range of variation of significant parameters. Response surface methods are discussed in **[17]**, **[18]**, **[19]**, **[20]**, **[21]**, and **[22]**. The uncertainties of engineering analysis procedures and of the response surface representation are treated as drivers.

Section 1.3
Implementing the PFA Methodology

In assessing failure risk, sound judgment is required to identify critical failure modes, to understand their origins and mechanisms, and to guide the implementation of the probabilistic analysis. This is an important role of FMEA and other qualitative procedures. The failure models required for meaningful probabilistic analysis must be developed in concert with a valid interpretation of relevant experience. Adjudging failure probabilities, even with the most sophisticated methods, does not imply that the origins, mechanisms, and consequences of known failure modes are understood and have been properly treated nor that unexpected test observations and indications of unanticipated failure modes have been pursued until they are understood. An understanding of the causes and mechanisms by which failures occur is the foundation on which valid failure models must be based.

The necessity for conducting an appropriate amount of testing for spaceflight systems is not eliminated through the use of the PFA methodology to assess failure risk. Testing programs, inspections, and careful analysis of experience are essential because they can reveal failure modes not identified and provide indications of analysis oversights or errors.

Application of the PFA methodology to a subset of failure modes selected by an FMEA and other screening procedures will identify failure modes whose risk of occurrence is unacceptable. Options for corrective action that could be taken to control risk are shown in *Figure 1-5*. The PFA methodology produces a risk assessment that is commensurate with the available information. Unacceptable risk could

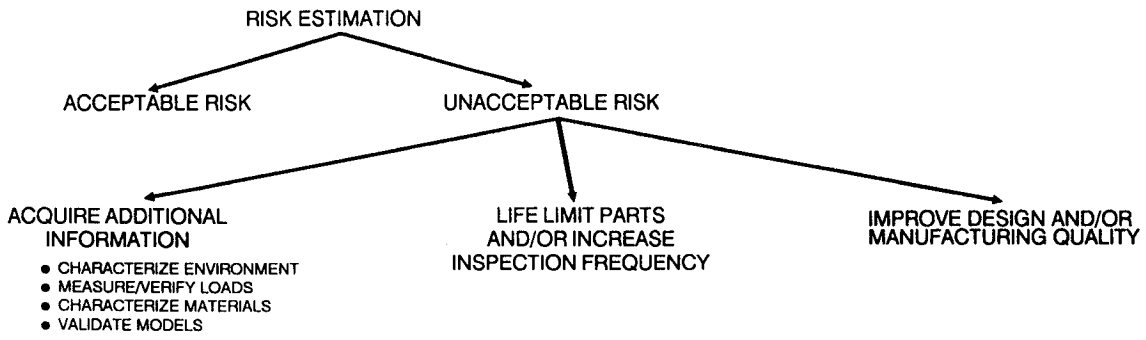

Figure 1-5 Options for Controlling Failure Risk

be reduced by changing the design or acquiring additional information to reduce the uncertainty of dominant drivers.

By conducting sensitivity analyses for selected failure modes with the PFA methodology, sources of unacceptable failure risk can be identified in terms of the responsible drivers, and corrective action can be delineated. Design changes, improvements in manufacturing processes, additional characterization of loads and environments, validation of analytical models, improved characterization of materials behavior, and additional testing are among the options for corrective action that can be quantitatively evaluated by PFA sensitivity analyses. The PFA methodology can be employed to identify risk sources and evaluate corrective actions during the design, development, and operational phases of a program, thereby enabling limited financial resources to be allocated more effectively to control failure risk.

Section 1.4
Report Organization

This report consists of three volumes in which an improved methodology for assessing the risk of occurrence of specific failure modes of spaceflight systems is presented. Volume I presents the PFA methodology and examples of its application to HCF and LCF failure modes. Volume II consists of the documentation of the computer software for implementing the methodology in the application examples, including user's guides and code execution examples. Volume III contains additional documentation of the software and listings of computer programs.

These three volumes constitute a thorough and comprehensive documentation of the methods, procedures, and software used in applying the PFA methodology to four failure modes of the SSME: HCF failure of the HPOTP Main Discharge Duct, HCF failure of the LPFTP Turbine Drive Duct, HCF Failure of the HPOTP Heat Exchanger Coil, and LCF failure of the ATD-HPFTP Second Stage Turbine Disk. Abbreviated presentations of the application of the PFA methodology to the heat exchanger coil and turbine disk failure modes are given in **[23]** and **[24]**, respectively. In a report to follow, the application of the PFA methodology to a flaw growth failure mode, an LCF failure mode of a turbine blade, and an HCF failure mode of a turbine blade will be covered in similar detail. A summary of the application of the PFA methodology to a flaw growth failure mode is presented in **[25]**.

In *Section 2.1*, the statistical methods used in applying the PFA methodology to fatigue failure modes are described in detail, including the methods used to stochastically represent materials fatigue life. In *Section 2.2*, the engineering analysis procedures used in the driver transformation steps of the application examples are discussed and the HCF and LCF analysis methods used in the application examples are described. The results for the four application examples are presented in *Section 3*. *Appendix 3.A* gives a detailed description of the application of the analysis procedures described in *Section 2.3* to the heat exchanger coil and turbine disk examples. The computer software used to implement the PFA methodology for the application examples is documented in *Sections 4*, *5*, *6*, and *7*.

An index of topics covered in this report is presented in *Tables 1-1* and *1-2*. The report sections wherein a particular topic is discussed are given in the index. Report sections which discuss the topics generically or with respect to an application example are listed separately. Sections dealing with the two duct application examples are listed together. This index enables all the report sections in which a particular topic is discussed to be located readily.

Table 1-1 Index of Topics Contained in the Report

TOPIC	GENERIC	APPLICATION		
		HCF		LCF
		DUCTS	HEAT EXCHANGER	TURBINE DISK
Analysis Procedures	2.3	–	3.A.2	3.A.3
Application Examples	–	3.1	3.2 3.A.2	3.3 3.A.3
Bayesian Updating	1.2.1 1.2.2 2.1.1 2.3.11 4.3 6.5 7.5	–	–	–
Computational Methods	1.2.5 2.1.1	–	–	–
Damage Modeling	2.2.1.4 2.2.2.2 2.A	2.2.1.4	2.2.1.4	2.2.2.2
Deterministic Analysis	1.1.2.2 2.3.3	2.2.1.2 2.2.1.5	2.2.1.2 2.2.1.5 3.A.2.2	2.2.2.2 3.A.3.2
Driver Distributions (Probability Distributions for Governing Parameters)	2.1.3 2.3.2	3.1.3	3.2.2 3.A.2.3	3.3.2 3.A.3.3
Driver Transformation (Stress Analysis)	2.3.4	2.2.1.3 3.1.4	2.2.1.3 3.2.3 3.A.2.2	2.2.2.2 3.3.3 3.A.3.2
Duty Cycle Effects (Mission Duty Cycle)	2.1.5	–	–	–
Failure Mode Identification	1.1.1 1.1.2.2	3.1.1 3.1.2	3.2.1 3.A.2.1	3.3.1 3.A.3.1
Load Characterization Load History Synthesis Load Scale Factors	2.1.3.2 2.1.4 2.3.7 2.3.8 2.A 3.1.3 3.2.2 4.5 6.6 7.7	2.2.1.2	2.2.1.2 3.A.2.5 3.A.2.6	3.2.2.2 3.A.3.5
Material Fatigue Life Characterization	2.1.2 2.3.6 4.1 6.3 7.3	3.1.1 3.1.2	3.2.1 3.A.2.4	3.3.1 3.A.3.4
Multiple Failure Locations	2.1.6	–	–	2.2.2.2

Table 1-1 Index of Topics Contained in the Report (Cont'd)

TOPIC	GENERIC	APPLICATION		
		HCF		LCF
		DUCTS	HEAT EXCHANGER	TURBINE DISK
Prior Distributions Probability of Failure Curve Prior Failure Risk Distribution	1.2.1 1.2.2 2.1.1 2.3.9 2.3.12 4.2 6.4 7.4	3.1.5 3.1.7	3.2.4 3.A.2.7 3.A.2.9	3.3.4 3.A.3.6 3.A.3.8
Probabilistic Approach	1.2	2.2.1.1	2.2.1.1	2.2.2.1
Random Number Generation	2.1.3.1 4.4 7.6	–	–	–
Reliability Demonstration by Testing	1.1.2.1 1.A	–	–	–
Sensitivity Analysis	1.2.2 1.3 2.3.10	3.1.5 3.1.7 6.1.4	3.2.4 3.A.2.8 6.1.11	3.3.4 3.A.3.7 6.2.4
Software Documentation Flowcharts	5.B	5.1.2	5.1.3	5.2
Software Documentation Program Listing/Structure	–	7.1.1	7.1.2	7.2
Software Documentation User's Guide	–	6.1.1-6.1.7	6.1.8-6.1.14	6.2

Table 1-2 Index of Software Documentation Contained in the Report

TOPIC	METHODOLOGY	SOFTWARE DOCUMENTATION		
		FLOWCHARTS	USER'S GUIDE	STRUCTURE /LISTING
Bayesian Updating	2.1.1	4.3	6.5	7.5
Ducts	2.2.1	5.1.2	6.1.1-6.1.7	7.1.1
Heat Exchanger	2.2.1	5.1.3	6.1.8-6.1.14	7.1.2
Materials Fatigue Life Characterization	2.1.2	4.1	6.3	7.3
Prior Distributions	2.1.1	4.2	6.4	7.4
Random Number Generation	2.1.3.1	4.4	–	7.6
Time History Generation	2.1.4	4.5	6.6	7.7
Turbine Disk	2.2.2	5.2	6.2	7.2

References

[1] Feynman, R. P., "Personal Observations on Reliability of Shuttle," Report of the Presidential Commission on the Space Shuttle Challenger Accident, Appendix F, 1986.

[2] "Post Challenger Evaluation of Space Shuttle Risk Assessment and Management," Committee on Shuttle Criticality Review and Hazards Analysis Audit, National Research Council, Washington, D.C., 1988.

[3] Moore, N., et al., A Review of Certification Practices Potentially Applicable to Man-Rated Reusable Rocket Engines – Certification Process Assessment Task, JPL D-7969, Jet Propulsion Laboratory, California Institute of Technology, Pasadena, California, February, 1986 (internal document).

[4] Ebbeler, D. H., "The Role of Testing in the Certification of Launch Vehicle Propulsion Systems," JPL D-7936, Jet Propulsion Laboratory, California Institute of Technology, Pasadena, California, February, 1991 (internal document).

[5] Mann, Nancy R., Schafter, Ray E., and Singpurwalla, Nozer D., Methods for Statistical Analysis of Reliability and Life Data, John Wiley & Sons, New York, New York, 1974.

[6] Abernethy, R. B., Breneman, J. E., Medlin C. H., and Reinman, G. L., Weibull Analysis Handbook, AFWAL-TR-83-2079, Aero Propulsion Laboratory, Air Force Wright Aeronautical Laboratories, Wright-Patterson AFB, Ohio, 1983.

[7] Huang, Zhaofeng, and Porter, Albert A., "Lower Bound On Reliability For Weibull Distribution When Shape Parameter Is Not Estimated Accurately," 1991 Proceedings Annual Reliability and Maintainability Symposium, IEEE, 1991.

[8] AFGS-87-221A, Aircraft Structures, General Guidelines for, Section 312, June 8, 1990.

[9] Martz, H. F., and Waller, R. A., Bayesian Reliability Analysis, John Wiley & Sons, New York, N.Y., 1982.

[10] Moore, N., Ebbeler, D., and Creager, M., "A Methodology for Probabilistic Prediction of Structural Failures of Launch Vehicle Propulsion Systems," Proceedings of the AIAA/ASME/ASCE/AHS/ASC 31st Annual Structures, Structural Dynamics, and Materials Conference, 1990, part 2, pp. 1092-1104.

[11] Ramsey, J. B., "Classical Model Selection Through Specification Error Tests," Frontiers in Econometrics, Edited by P. Zarembka, Academic Press, New York, N. Y., 1974.

[12] Madsen, H. O., Krenk, S., and Lind, N. C., Methods of Structural Safety, Prentice-Hall, 1986.

[13] Der Kiureghian, A., and Liu, P.-L., "First and Second-Order Finite Element Reliability Methods," to appear in Computational Mechanics of Probabilistic and Reliability Analysis edited by W.-K. Liu and T. Belytschko.

[14] Wirsching, P. H., et al., "An Overview of Reliability Methods in Mechanical and Structural Systems," 28th Annual Structures, Structural Dynamics and Materials Conference, April, 1987.

[15] Wu, Y. T., "Demonstration of a New, Fast, Probability Integration for Reliability Analysis," Journal of Engineering for Industry, Transactions of the ASME, Vol. 109, February, 1987, pp. 24-28.

[16] Sutharshana, S., Grigoriu, M., Moore, N., and Fox, E., "Computational Methods for Probabilistic Flaw Propagation Analyses," Structures Congress '91, American Society of Civil Engineers, Indianapolis, IN, April, 1991.

[17] Box, George E. P., Hunter, William G., and Hunter, J. Stuart, Statistics for Experimenters, John Wiley & Sons, New York, New York, 1978.

[18] Cornell, John A., "How to Apply Response Surface Methodology," The ASQC Basic References in Quality Control: Statistical Techniques, Vol. 8, American Society for Quality Control, Milwaukee, Wisconsin, 1990.

[19] Hicks, Charles R., Fundamental Concepts in the Design of Experiments, Third Edition, Saunders College Publishing, Fort Worth, Texas, 1982.

[20] Khuri, Andre I., and Cornell, John A., Response Surfaces, Marcel Dekker, Inc., New York, New York, 1987.

[21] Montgomery, Douglas C., Design and Analysis of Experiments, Third Edition, John Wiley & Sons, New York, New York, 1991.

[22] Snee, Ronald D., Hare, Lynne B., and Trout, J. Richard, Experiments in Industry, American Society for Quality Control, Milwaukee, Wisconsin, 1985.

[23] Sutharshana, S., et al., "Probabilistic High Cycle Fatigue Failure Analysis Applicable to Liquid Propellant Rocket Engines," Proceedings of the AIAA/ASME /ASCE/AHS/ASC 31st Annual Structures, Structural Dynamics, and Materials Conference, 1990, part 2, pp. 1105-1114.

[24] Newlin, L., et al., "Probabilistic Low Cycle Fatigue Failure Analysis Applicable to Liquid Propellant Rocket Engines," Proceedings of the AIAA/ASME/ASCE/AHS /ASC 31st Annual Structures, Structural Dynamics, and Materials Conference, 1990, part 2, pp. 1115-1123.

[25] Sutharshana, S., et al., "A Probabilistic Fracture Mechanics Approach for Structural Reliability Assessment of Space Flight Systems," Advances in Fatigue Lifetime Predictive Techniques, Special Technical Publication 1122, American Society for Testing and Materials, 1991.

Appendix 1.A

The Limitations of Testing for Reliability Demonstration

Certification of flight readiness of a spaceflight system should encompass an assessment of the risk of occurrence of critical structural failure modes. The impact of nonfailure tests and any tests to failure in establishing or contributing to that risk assessment can be considered for dominant critical failure modes. If all operating experience for spaceflight systems consists of nonfailures, it will be a weak information source for demonstrating the extremely high levels of reliability desired. That is because nonfailure data available for such systems typically provides very conservative bounding information about the location/variability of the failure distribution. Demonstrating extremely high levels of desired reliability is equivalent to making statements about the extreme left-hand tail of the failure distribution. The location/variability information available from nonfailures alone is usually inadequate for demonstrating levels of desired reliability.

Information about the failure distribution from an engineering analysis which avoids nonconservatisms is typically so extremely informative about location that, even with the conservatism on variability implied by uncertainty in engineering analysis due to lack of knowledge, useful probabilistic statements about reliability can be derived. By avoiding nonconservatisms when engineering analysis is incorporated, the true reliability will be bounded from below and that bound, typically, will be very much larger than what can be established by reliability demonstration with feasible nonfailure testing alone.

In the consideration of tests to failure, it is useful to consider two leading generic types of failure modes. Failure modes such as high cycle fatigue crack initiation, low cycle fatigue crack initiation or crack growth to fracture are damage accumulation failure modes; i.e., failure is a consequence of the cumulation of aging effects produced by the repeated exposure of a component to operating conditions. In contrast, a failure mode such as case rupture can be considered to be an event consequent failure mode; i.e., failure is a consequence of an event such as load pressure exceeding burst pressure, which is independent of the extent of previous exposure of a component to operating conditions.

Tests to failure are a much stronger source of information about reliability than nonfailures if they are a consequence of the failures occurring by intent; i.e., the failures occur because the operating conditions are consonant with a perceived significant likelihood of failure. However, spaceflight systems are so expensive that

test conditions are usually set so that the perceived likelihood of failure is extremely remote whenever flight configuration hardware is at risk. Any component failure is then viewed as the result of an anomaly in that perception and corrective actions such as redesign or procedural changes renders the failure immaterial to reliability demonstration. For damage accumulation failure modes, the component may be tested only as part of a system so it is unlikely that operating experience relevant for reliability demonstration will include failures. For event consequent failure modes, if the component can be tested meaningfully in isolation without risking system failure, a small number of failures (typically one) may be relevant to reliability demonstration. Also, nonfailure tests may be much more informative in this circumstance if test operating conditions are set so that the perceived likelihood of failure is much higher than for flight operating conditions.

It is unrealistic to believe that testing programs can be feasibly structured for the purpose of reliability demonstration using only operating experience. The ability to make reliability statements of interest will almost always depend on a probabilistic analysis framework which facilitates the use of all available information sources, in particular engineering analysis as well as operating experience, as discussed in *Section 1* of this report. The primary purposes of a testing program should be: (1) to uncover failure modes not analyzed, analysis oversights or errors, and anomalous conditions; and (2) by means of instrumented test, to accurately characterize those parameters which drive the results of an engineering analysis of each critical structural failure mode. Both (1) and (2) are aspects of assuring that engineering analyses are adequately characterized. Some detailed numerical examples illustrating the limitations of testing for reliability demonstration are presented in **[4]**.

Figures 1-6 through *1-9* illustrate reliability demonstration for reusable SSME components based on the Weibull probability distribution using *Equation 1-1*. Values of β between 1 and 3.5 are common for Weibull distributions for fatigue failure modes. From those figures it can be seen that .9999 reliability is typically demonstrated for a service life of only 3 to 4 missions and .999 for a service life of only 5 to 8 missions. We can conclude from these examples that acceptable service life reliability demonstration is impractical due to the infeasibility of acquiring the required amount of nonfailure data. As illustrated in *Section 3* of this report, the inclusion of knowledge gained from engineering analysis in risk assessment typically leads to acceptable service life reliability with respect to failure modes analyzed.

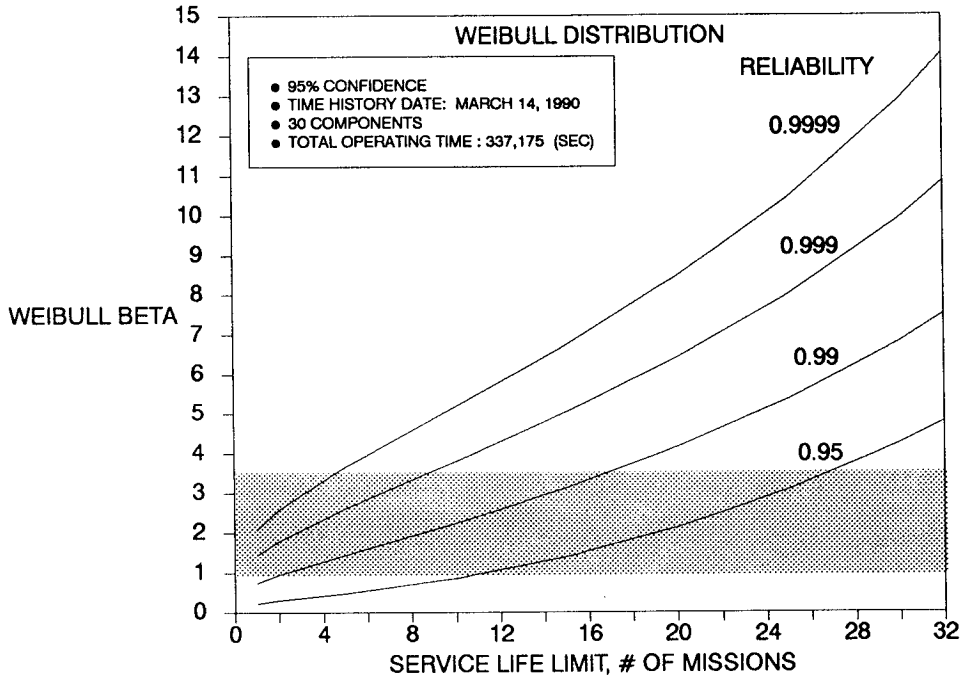

Figure 1-6 Reliability Demonstrated By Nonfailure Operating Experience for the Powerhead Assembly

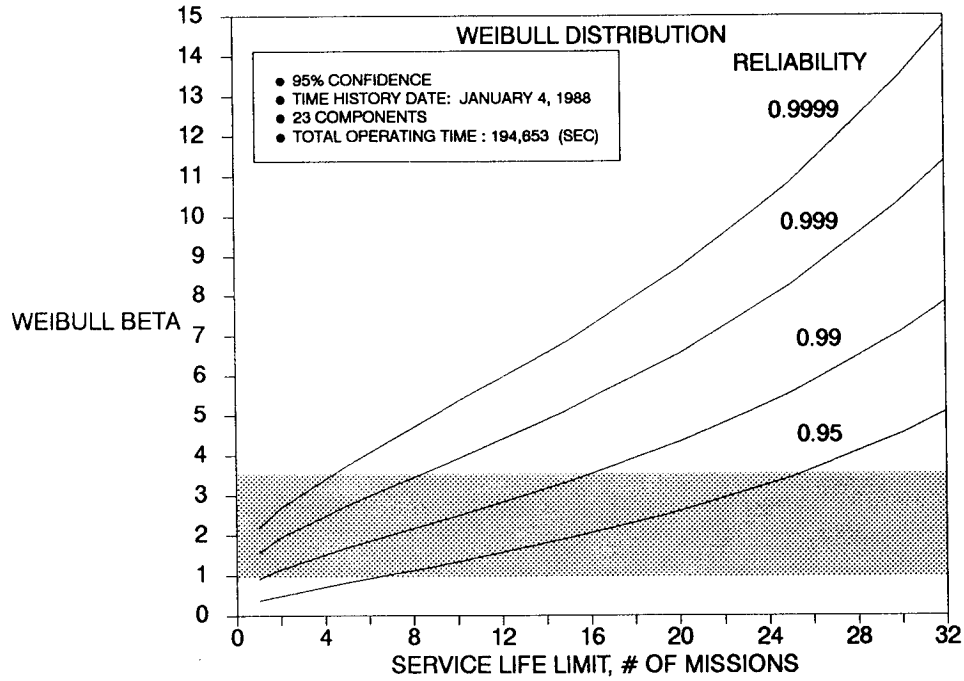

Figure 1-7 Reliability Demonstrated By Nonfailure Operating Experience for the HPOTP Main Discharge Duct

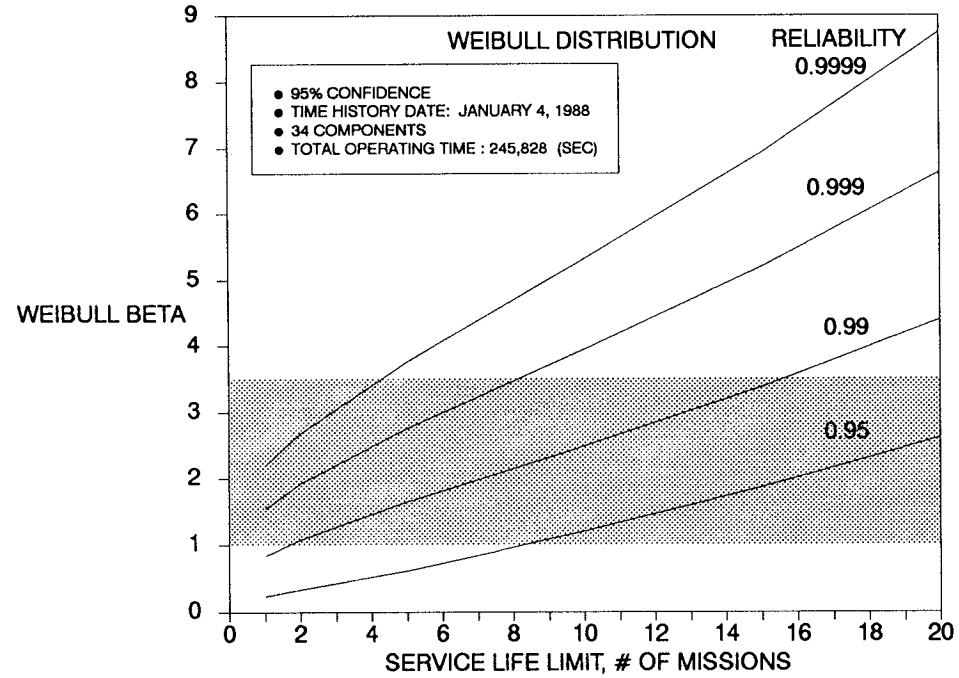

Figure 1-8 Reliability Demonstrated By Nonfailure Operating Experience for the LPFTP Turbine Drive Duct

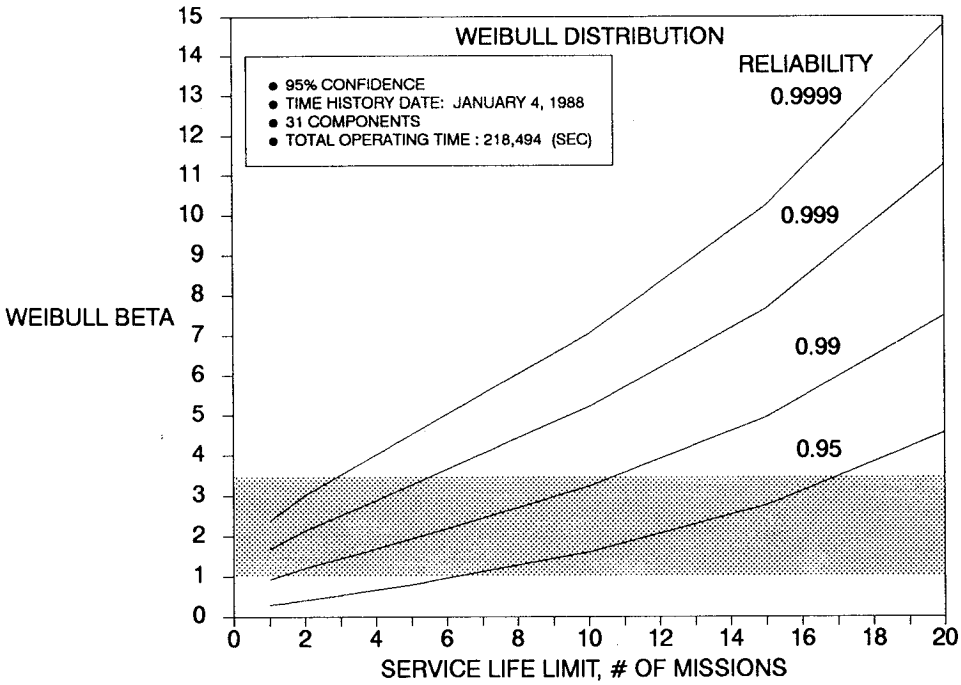

Figure 1-9 Reliability Demonstrated By Nonfailure Operating Experience for the HPOTP Heat Exchanger

Appendix 1.B
List of Acronyms

AR	Autoregressive
ATD-HPFTP	Alternate Turbopump Development Program – High Pressure Fuel Turbopump
BPVC	Boiler Pressure Vessel Code
FE	Finite Element
FFT	Fast Fourier Transform
FMEA	Failure Modes and Effects Analysis
FORM/SORM	First Order Reliability Method/Second Order Reliability Method
FR	Frequency Response
HCF	High Cycle Fatigue
HEX	Heat Exchanger
HPOTP	High Pressure Oxidizer Turbopump
JPL	Jet Propulsion Laboratory
LCF	Low Cycle Fatigue
LPFTP	Low Pressure Fuel Turbopump
MC	Monte Carlo
MRB	Material Review Board
MSFC	Marshall Space Flight Center
MVFO/AMVFO	Mean Value First Order/Advanced Mean Value First Order
NASA	National Aeronautics and Space Administration
PFA	Probabilistic Failure Assessment
PFM	Probabilistic Failure Model
PSD	Power Spectral Density
RA	Reduction of Area
RMS	Root Mean Square
RV	Random Vibration
S/N	Stress/LIfe
SSME	Space Shuttle Main Engine

2.0 Methodology

Section 2.1
Statistical Analysis

2.1.1 Failure Simulation Statistics

A failure mode specific Monte Carlo simulation is used to generate a set of failure data. That collection of failure data summarizes the information which engineering analysis provides us concerning service life with respect to the indicated failure mode. It is used both by itself and, by means of Bayesian methods, in combination with component operating history to generate estimates of the probability of occurrence of specific failure modes.

As currently implemented, for High Cycle Fatigue (HCF) or Low Cycle Fatigue (LCF) failure modes, the structure of the Monte Carlo simulation is given in *Figure 2-1*. The double-loop structure indicated in *Figure 2-1* is not an essential part of the simulation. It has been included in order to facilitate runs of the order $Nn = 200{,}000$ which have been used to validate the use of smaller size single-loop runs, i.e., runs in which all passes through the calculation procedure include only the outer loop by setting $n = 1$. The size of the simulation is user-selected. The required simulation size is a function of the failure probability at which a life estimate is desired and is also a function of the precision desired. For applications to date, single-loop runs of size 20,000 have been sufficient for characterizing component reliability and single-loop runs of size

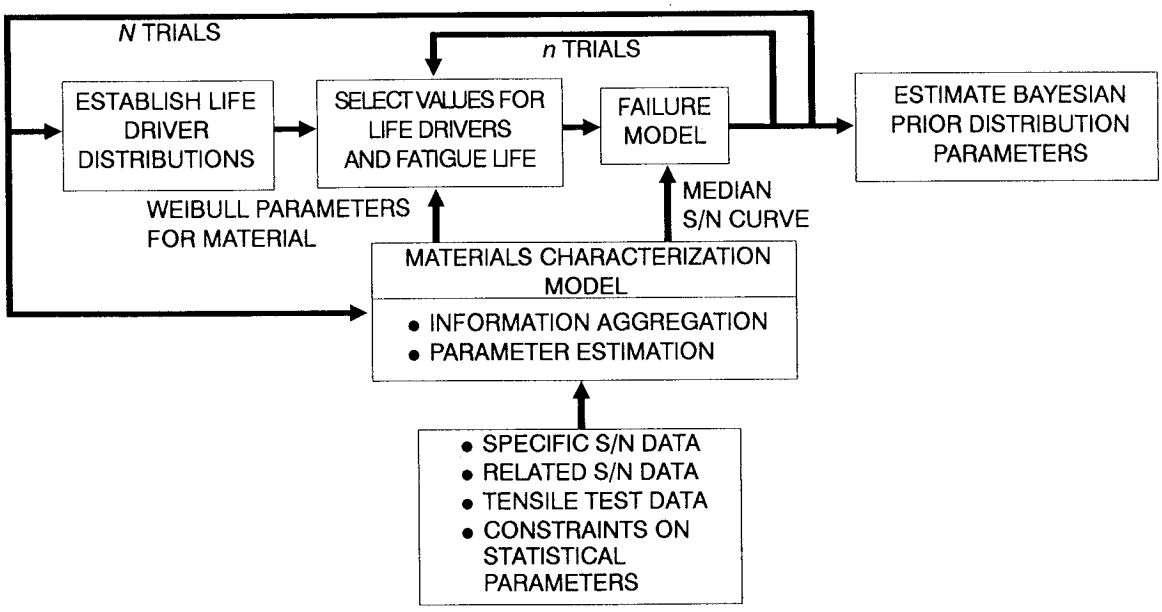

Figure 2-1 Component Failure Mode Monte Carlo Simulation Structure

1000 have been sufficient for marginal analysis to assess the importance of individual life drivers.

Variation in simulated failure data results from two fundamental sources. The first source of variation is the intrinsic stochastic nature of the physical processes modeled which produce component failure. The second source of variation is lack of knowledge regarding the parameters of those physical processes that significantly affect the failure prediction, the drivers. In general, the nature of the experience-based judgment used to describe individual drivers does not allow for accurately specifying those sources of variation separately for all drivers.

In order to assess failure probability based on all the information available, the left-hand tail distribution of the simulated failures will be represented in an analytical form which allows for the use of Bayesian updating in order to combine simulation results with operating experience. The chosen analytical form for the tail distribution also allows the assurance or confidence with which a reliability statement is made to be modeled, and that form matches the simulation result that the left-hand tail of the distribution of simulated failures is approximately linear in log–log space. A set of assumptions for an analytical form with these attributes is

$$F(N|\lambda) = 1 - \exp\left(-\lambda N^{\beta}\right) \qquad \text{(Weibull)} \tag{2-1}$$

$$f(\lambda) = \frac{(\theta)^{\alpha}\lambda^{\alpha-1}}{\Gamma(\alpha)} \exp(-\theta\lambda) \qquad \text{(Gamma)}$$

with β constant.

Operating experience consists of n tests with s failures and $n - s$ successes. Data is then in the form of s failure times and $n - s$ suspension times, t_i. Combining that data with *Equation 2-1* by Bayes' rule yields the updated distribution of λ

$$f(\lambda) = \frac{(\theta')^{\alpha'}\lambda^{\alpha'-1}}{\Gamma(\alpha')} \exp(-\theta'\lambda) \qquad \text{(Gamma)} \tag{2-2}$$

$$\alpha' = \alpha + s$$

$$\theta' = \theta + \sum_{i=1}^{n} t_i^{\beta}$$

[1], p. 399.

Component reliability is given by

$$R\left(N|\lambda\right) = 1 - F\left(N|\lambda\right) = \exp\left(-\lambda N^{\beta}\right) \tag{2-3}$$

Since λ is a random variable, variation in λ translates into variation in reliability as defined by *Equation 2-3*. A reliability/assurance pair, (R_o, A), defined by

$$Pr\left[R\left(N|\lambda\right) > R_o\right] = A \tag{2-4}$$

is thus equivalent to

$$Pr\ [\lambda < \lambda_o\ ] = A \tag{2-5}$$

where $R_o = \exp\ (-\lambda_o N^{\beta})$. If A is specified, λ_o and hence R_o can be found from *Equation 2-5* since $f(\lambda)$ is known, providing that a procedure for estimating α, θ, and β can be found. There are, of course, an infinity of (R_o, A) pairs satisfying *Equation 2-4*, which are equivalent in the sense that they represent the available information. For a given assurance, A, either the reliability satisfying *Equation 2-4* at each life level or the life satisfying *Equation 2-4* at each level of reliability can be found. The results are identical.

The procedure for finding α, θ and β follows: from *Equation 2-1*, we can derive

$$F\left(N\right) = 1 - \left(1 + N^{\beta}/\theta\right)^{-\alpha} \tag{2-6}$$

Component reliability is thus given by

$$R\left(N\right) = \left(1 + N^{\beta}/\theta\right)^{-\alpha} \tag{2-7}$$

The simulated failure times are treated as if each one corresponds to a Weibull failure with λ varying over components.The failure time distribution in *Equation 2-6* can be written equivalently as

$$Y = \ln\{-\ln[1 - F(N)]\} = \ln(\alpha) + \ln\{\ln[1 + N^{\beta}/\theta]\} \tag{2-8}$$

which reduces to

$$Y \approx \ln[F(N)] \approx \ln(\alpha/\theta) + \beta \ln(N) \tag{2-9}$$

for sufficiently small N.

A least squares regression of Y on $\ln(N)$ can be used to estimate β by b. When the materials data covers a single life region, the data base used should be from a failure simulation which considers variation in those drivers which reflect the state of knowledge concerning component capability, e.g., dimensions and materials properties. It should correspond to the portion of the left-hand tail of the simulated failure distribution which is approximately linear in log space. For multiple life region materials data, β should correspond to that associated with the variation in life resulting from the leftmost life region from which damage is calculated. Imposing the constraint $\beta = b$, *Equation 2-6* can be written as

$$y = -\ln\left[1 - F(N)\right] = \alpha \ln\left[1 + N^b/\theta\right] \tag{2-10}$$

with

$$\frac{\partial y}{\partial \alpha} = \ln\left[1 + N^b/\theta\right]$$

$$\frac{\partial y}{\partial \theta} = \frac{-\alpha N^b}{\theta^2\left[1 + N^b/\theta\right]}$$

Using these analytical gradients, a nonlinear least squares fit of *Equation 2-10* over the range of $F(N)$ of interest lets us estimate α by a and θ by c. Initial guesses for a and c can be found by choosing $c_o = N_{.001}^b$ and, supposing that the fitted curve is near the B.1 value, $N_{.001}$, initializing a at $a_o = -\ln .999/\ln 2$. The data base used should be from a failure simulation which considers variation in all drivers.

Reference

[1] Martz, H. F., and R. A. Waller, Bayesian Reliability Analysis, John Wiley & Sons, 1982.

2.1.2 Materials Fatigue Life Characterization

2.1.2.1 Stress/Life Characterization of Fatigue Failure of Materials

When stress/life test data is available, the knowledge of the fatigue properties of a component material is represented by uncertainty in the appropriate Stress/Life (S/N) curve for the material. That uncertainty will be characterized both by an intrinsically stochastic S/N curve and by uncertainty in S/N curve parameters. In order to represent the latter uncertainty, the alternatives of using either Uniform or truncated Normal distributions based on estimates of S/N curve shape parameters are provided.

Information which can be used to characterize the S/N curve will be classified as follows:

Necessary Information

- Specific failure data of size N_o. The subscript "o" will denote reference to this data set.

Optional Information

- Related failure data of size N_j, $j = 1, ..., P$. The subscript "j" will denote reference to the jth related data set.
- An upper bound on the coefficient of variation of material fatigue strength and/or explicit constraints on the shape parameters of the S/N curve.

Specific failure data refers to laboratory data generated by fatigue tests on material specimens under specifications appropriate for that component, including such elements as environment, specimen geometry, specimen finish, etc. Related failure data refers to laboratory data generated by fatigue tests on specimens of the same material, but under specifications which are in some respect different from those appropriate for specific failure data. In order for data to be a suitable related data set for a given life range, it is required that, after transformation to an equivalent zero-mean alternating stress, the coefficient of variation of fatigue strength and the S/N curve shape parameters for that life range be the same within the populations from which the specific and related data are samples.

The methodology developed will be designed for characterizing component material uncertainty when the specific failure data set is sparse, but it will also accommodate cases where that data set is extensive.

In formulating an S/N curve model, the empirical phenomenon that the variance of log life tends to increase as stress decreases must be taken into account. Also, the intrinsic stochastic character of the S/N curve must be represented in such a way that the notion of a random fatigue strength has meaning. Since fatigue tests are executed at fixed nominal stress levels, a sensible interpretation of random fatigue strength expressed as a stress at a fixed life can be achieved by assuming that there exists some median S/N curve, and that the appropriate lives for individual tests are derived from the curves which result from random shifts of the median S/N curve in the log stress direction. For a physical rationalization of this assumption in terms of sizes of defects at the origin of the failure see Spindel and Haibach [3] p. 103.

A simple model which encompasses both the notion of random fatigue strength and increasing variance of log life with decreasing stress is as follows:

$$S = K_j N^{-1/m_j} \varphi \qquad j = 1, ..., R \tag{2-11}$$

$$\varphi \sim W(\eta_o, \beta_o)$$

$W(\bullet)$ denotes a Weibull probability distribution, and R is the number of life regions into which the life axis is divided. The S/N curve is linear in the log S/log N space within each life region. The value of this piecewise linear parameterization as opposed to a nonlinear parameterization over the entire range of life is that, for the case of sparse specific data, it facilitates the information aggregation process involved in combining specific data, related data and other information used to determine the shape of the median S/N curve.

Equivalently, *Equation 2-11* can be rewritten as

$$N = A_j S^{-m_j} \varepsilon_j \qquad j = 1, \ldots, R \tag{2-12}$$

$$\varepsilon_j \sim W\left(\eta_o^{m_j},\ \beta_o / m_j\right)$$

where $A_j = K_j^{m_j}$ and $\varepsilon_j = \varphi^{m_j}$.

The value of η_o is a function of β_o determined by requiring the median S/N curve to be

$$MED\,(S|N) = K_j N^{-1/m_j}$$

which implies that

$$MED\,(\varphi|N) = 1 = \eta_o\,(\ln 2)^{\beta_o^{-1}}.$$

The distribution of ε_j follows by noting that the cumulative distribution function of φ can be written as

$$F(\varphi) = 1 - \exp\left[- \left(\frac{\varphi}{\eta_o}\right)^{\beta_o} \right] \tag{2-13}$$

$$= 1 - \exp\left[- \left(\frac{\varphi^{m_j}}{\eta_o^{m_j}}\right)^{\beta_o/m_j} \right] .$$

Note also that the distribution of lives given S in *Equation 2-12* is <u>not</u> Weibull. For a fixed value of S, the assumption that $\varphi \sim W(\bullet)$ in *Equation 2-11* leads to a Weibull distribution on lives in *Equation 2-12* **<u>conditional</u> on** A_j, m_j, β_o. Since we are also characterizing uncertainty in A_j, m_j, and β_o, the unconditional distribution on lives for a fixed value of S will not be Weibull.

To the extent that the median S/N curve is concave to the origin in the log S/log N space, V [ln $N|S$] tends to increase as S decreases, since m_j will tend to increase as S decreases.

In *Equation 2-11* the coefficient of variation of fatigue strength, C, is approximated by the scatter in log stress about the mean S/N curve. That can be seen by considering a Taylor's Series expansion of ln S about $E(S|N)$.

$$\ln S \approx \ln E(S|N) + \frac{S - E(S|N)}{E(S|N)} \tag{2-14}$$

From *Equation 2-14*, we have

$$V(\ln S|N) \approx \frac{V(S|N)}{E^2(S|N)} \equiv C^2. \tag{2-15}$$

C can also be related to the Weibull parameter β_o by observing that, under the transformation $\xi = -\beta_o \ln(\varphi/\eta_o)$, $E(\xi) = \gamma =$ *Euler's constant* and $V(\xi) = \pi^2/6$, Johnson and Kotz **[2]**, pp. 266, 277-78. Then *Equation 2-11* can be written as

$$\ln S = k_j - \frac{1}{m_j} \ln N + u \tag{2-16}$$

where

$$k_j = \ln K_j + \ln \eta_o - \gamma/\beta_o$$

$$u = -\frac{1}{\beta_o}(\xi - \gamma)$$

with the moment generating function of u given by

$$M_u(t) = \exp\left(\frac{\gamma t}{\beta_o}\right) \Gamma(1 + t/\beta_o) \tag{2-17}$$

$E[u] = 0$, $V[u] = \pi^2/6\,\beta_o^2$ and, by using asymptotic expansions provided by Abramowitz and Stegun **[1]**, pp. 68, 256, we find that *Equation 2-17* can be approximated by

$$\ln M_u(t) \approx \frac{1}{2}\left(\frac{\pi^2}{6\beta_o^2}\right) t^2 \tag{2-18}$$

which implies that $u \sim N(0, \pi^2/6\,\beta_o^2)$ approximately. From *Equation 2-15* and *Equation 2-16,* we have

$$V(\ln S|N) = V(u) = \frac{\pi^2}{6\,\beta_o^2} \approx C^2 \tag{2-19}$$

$$V(\ln N|S) = m_j^2\, V(u) = \frac{m_j^2 \pi^2}{6\,\beta_o^2} \approx m_j^2\, C^2$$

Thus, in this model, C is approximately constant and $V[\ln N|S]$ is proportional to m_j^2.

This model will be estimated by a two-step procedure. Within each life region we will characterize uncertainty in the S/N curve shape parameter, m, by combining specific failure data with related failure data and any constraints on C or m. Then, conditional on selected values of the shape parameters for all life regions, $\{m_j\}$, the specific failure data alone will be used to determine the remaining S/N curve parameters.

Let $x = \ln S$ and $y = \ln N$. Specific data and related data, after transformation to an equivalent alternating stress, are combined by life region as follows to produce a credibility range for C and for m:

First, find $S_{\hat{w}}^2$ from combined data bases for $j = 0, 1, \ldots, P$ by estimating

$$y_j = \gamma_j + \delta\, x_j + w_j = c_j + d x_j + \hat{w}_j \tag{2-20}$$

where

$$d = S_{xy}/S_x^2 \text{ and } c_j = \bar{y}_j - d\,\bar{x}_j$$

$$N = \sum_{j=0}^{P} \left(N_j - 1 \right) - 1$$

$$N\, S_{\hat{w}}{}^2 = \sum_{j=0}^{P} \sum_{i=1}^{N_j} \hat{w}_{ji}{}^2$$

Next, find $S_{\hat{u}}^2$ from combined data bases for $j = 0, 1, \ldots, P$ by estimating

$$x_j = \alpha_j + \beta y_j + u_j = a_j + b y_j + \hat{u}_j \tag{2-21}$$

where

$$b = S_{xy} / S_y^2 \quad \text{and} \quad a_j = \bar{x}_j - b\bar{y}_j$$

$$N S_{\hat{u}}^2 = \sum_{j=0}^{P} \sum_{i=1}^{N_j} \hat{u}_{ji}^2 .$$

From *Equations 2-19, 2-20*, and *2-21*, we find point estimates of C and m based on life region-specific information,

$$\hat{C} = S_{\hat{u}} \tag{2-22}$$

$$\hat{m} = -d$$

Since $u \sim N(0, C^2)$ approximately, from *Equation 2-18* and *Equation 2-19,* a 95% confidence interval for C, I_o, can be based on the approximation

$$\frac{N \hat{C}^2}{C^2} \sim \chi^2(N) \tag{2-23}$$

$$Pr\left[\hat{C} \left(N / \chi^2_{.975}(N) \right)^{1/2} \leq C \leq \hat{C} \left(N / \chi^2_{.025}(N) \right)^{1/2} \right] = .95.$$

From *Equation 2-23,* we have

$$I_o \equiv \left[\hat{C} \left(N / \chi^2_{.975}(N) \right)^{1/2}, \ \hat{C} \left(N / \chi^2_{.025}(N) \right)^{1/2} \right]. \tag{2-24}$$

The life region-specific credibility range for C will be called I_o. An analogous credibility range for m is defined by J_o. Since, to an approximation, $\hat{m}$ and $S_{\hat{w}}$ are independently distributed, with

$$\frac{\hat{m} - m}{\left(m^2 C^2 / N S_x^2 \right)^{1/2}} \sim N(0, 1)$$

$$\frac{N S_{\hat{w}}^2}{m^2 C^2} \sim \chi^2(N)$$

we have,

$$\frac{\hat{m} - m}{\left(S_{\hat{w}}^2 / N S_x^2\right)^{1/2}} \sim t(N) \tag{2-25}$$

From *Equation 2-25*, we obtain

$$Pr\left[\hat{m} - t_{.025}(N)\frac{S_{\hat{w}}}{\left(N S_x^2\right)^{1/2}} \leq m \leq \hat{m} + t_{.025}(N)\frac{S_{\hat{w}}}{\left(N S_x^2\right)^{1/2}}\right] = .95$$

so that

$$J_o \equiv \left[\hat{m} - t_{.025}(N)\frac{S_{\hat{w}}}{\left(N S_x^2\right)^{1/2}}, \quad \hat{m} + t_{.025}(N)\frac{S_{\hat{w}}}{\left(N S_x^2\right)^{1/2}}\right] \tag{2-26}$$

I_o provides, for each life region, an interval estimate of C based on fatigue data alone. Similarly, J_o provides, for each life region, an interval estimate of m based on fatigue data alone.

If there are explicit constraints on the shape parameters of the S/N curve, they are of the form

$$\underline{m} \leq m \leq \overline{m} \tag{2-27}$$

Implicit constraints on the shape parameters are provided if an upper bound is specified for the coefficient of variation of material fatigue strength,

$$C^2 < C_o^2 .$$

From *Equations 2-16* and *2-19,* with $x = \ln S$ and $y = \ln N$, we derive

$$S_x^2 + \frac{2}{m} S_{xy} + \frac{1}{m^2} S_y^2 = C^2 < C_o^2 \tag{2-28}$$

which can be written as

$$m^2(S_x^2 - C_o^2) + 2m\, S_{xy} + S_y^2 < 0. \tag{2-29}$$

Thus, $C^2 < C_o^2$ implies constraints on the shape parameters of the S/N curve.

The sign of S_{xy} should be tested; if S_{xy} is not negative then the data is inadequate for analysis since this implies life increasing with increasing stress.

If $S_x^2 = C_o^2$, *Equation 2-29* reduces to

$$m > -S_y^2/2S_{xy} \tag{2-30}$$

If $S_x^2 < C_o^2$, *Equation 2-29* reduces to

$$m > \frac{-S_{xy} - \left(S_{xy}^2 - S_y^2(S_x^2 - C_o^2)\right)^{1/2}}{S_x^2 - C_o^2} \tag{2-31}$$

If $S_x^2 > C_o^2$ with $S_{xy}^2 - S_y^2(S_x^2 - C_o^2) \geq 0$, then *Equation 2-29* reduces to

$$\frac{-S_{xy} - \left(S_{xy}^2 - S_y^2(S_x^2 - C_o^2)\right)^{1/2}}{S_x^2 - C_o^2} < m < \frac{-S_{xy} + \left(S_{xy}^2 - S_y^2(S_x^2 - C_o^2)\right)^{1/2}}{S_x^2 - C_o^2} \tag{2-32}$$

If $S_x^2 > C_o^2$ with $S_{xy}^2 - S_y^2(S_x^2 - C_o^2) < 0$, then the specification $C^2 < C_o^2$ is inconsistent with observed data since the constraint cannot be met by an adjustment to a shape parameter.

A posterior credibility range for each of the shape parameters is then established by taking the intersections of the ranges defined by *Equations 2-26*, *2-27* and *Equations 2-30*, *2-31* or *2-32*.

Uncertainty in m is incorporated into the S/N failure simulation by forming a probability distribution on m, $\pi(m)$. One alternative provided is to use a Uniform distribution over the posterior credibility range for m. Note that defining the addition of information in the form of constraints on m and/or C is motivated by the notion that for N small, the posterior credibility range for m should be dominated by the constraints, but that as N increases, it should approach J_o.

The S/N curves obtained by this procedure are required to be concave to the origin with positive shape parameters, i.e., $0 < m_1 < m_2 < \ldots < m_R$. To ensure that, we will impose the additional constraints that the upper bound of the ith posterior credibility range be no larger than the upper bound of the $(i+1)st$ and that the lower bound of the $(i+1)st$ be no larger than the sampled value of m_i, with $m_1 > 0$.

Calculation of the median values of the shape parameters under concavity constraints is equivalent to calculating mean values when Uniform distributions are used to represent shape parameter uncertainty; i.e., $MED(m_i) = E(m_i)$.

$$m_1 \sim U(L_1, U_1) \tag{2-33}$$

$$m_{i+1} \sim U\left[\max(m_i, L_{i+1}), U_{i+1}\right] \quad i = 1, \ldots, R-1$$

From *Equation 2-33* we derive the recursive relationship

$$E(m_1) = \frac{L_1 + U_1}{2} \tag{2-34}$$

$$E(m_{i+1}) = \max\left[\frac{E(m_i) + U_{i+1}}{2}, \frac{L_{i+1} + U_{i+1}}{2}\right] \quad i = 1, \ldots, R-1$$

The other alternative provided is to represent $\pi(m)$ as a truncated Normal distribution derived from a Bayesian analysis of *Equation 2-20*. Within a given life-region, suppose $V(\ln N | \ln S) = V(y|x) = \sigma^2$ is known. Then, based on the approximate Normality of w,

$$L(m) \propto \exp\left[\frac{-N S_x^2}{2\sigma^2}(m - \hat{m})^2\right]$$

This suggests a Bayesian prior on m of the form

$$P(m) \propto \exp\left[\frac{-\delta}{2\sigma^2}(m - m_o)^2\right] \quad \delta > 0$$

The posterior density is then $N(m_*, \sigma_*^2)$

$$m_* = \frac{\hat{m}\, N S_x^2 + m_o\, \delta}{N S_x^2 + \delta}$$

$$\sigma_*^2 = \sigma^2/(N S_x^2 + \delta)$$

Constraints of the form given in *Equation 2-27* will always be required for this representation of $\pi(m)$ in order to preclude inconsistent extreme values of m, δ must also always be specified. $\delta = 0$ corresponds to a diffuse prior so that sample information alone determines the posterior distribution. If m_o is not user-specified, $m_o = \hat{m}$ and $\delta = 0$ will be assumed. If σ^2 is not user-specified, $\sigma^2 = S_{\hat{w}}^2$ will be assumed and the uncertainty associated with that estimate will be ignored for the purpose of representing $\pi(m)$.

Again, the S/N curves obtained using the truncated Normal $\pi(m)$ are required to be concave to the origin. However, it will not be possible to calculate the median S/N curve analytically. That median curve is estimated by saving the realized values of m for each life-region from the simulation run and finding the corresponding sample medians.

Within each life region we establish a value for the S/N curve shape parameter by a draw from the $\pi(m)$ for that region. Conditional on this set of shape parameters, $\{m_j\}, j = 1, \ldots, R$, we then use the specific failure data to determine the remaining S/N curve parameters.

In order for the S/N curve to be continuous, we need to impose continuity constraints at the life region boundaries. The ith life region, R_i, is defined by

$$R_i \equiv \left\{N \ni N^*_{i-1,i} \leq N < N^*_{i,i+1}, i = 1, \ldots, R\right\} \tag{2-35}$$

with $N^*_{01} \equiv 0$ and $N^*_{R,R+1} \equiv \infty$. The continuity constants are then given by

$$K_i \left(N^*_{i,i+1}\right)^{\frac{-1}{m_i}} = K_{i+1} \left(N^*_{i,i+1}\right)^{\frac{-1}{m_{i+1}}} \qquad i = 1, \ldots, R-1 \tag{2-36}$$

From *Equation 2-35*, $K_2, \ldots, K_R$ can be found as a function of K_1.

$$K_i = K_1 \prod_{j=1}^{i-1} \left(N^*_{j,j+1}\right)^{\left(\frac{1}{m_{j+1}} - \frac{1}{m_j}\right)} \qquad i = 2, \ldots, R \tag{2-37}$$

In the ith life region, the S/N curve is defined by *Equation 2-11*, or equivalently

$$S\,N^{\frac{1}{m_i}} = K_i\,\varphi \qquad i = 1, \ldots, R \tag{2-38}$$

Combining *Equations 2-37* and *2-38*, we have

$$S\,N^{\frac{1}{m_1}} = K_1\,\varphi \qquad N \in R_1 \tag{2-39}$$

$$S\,N^{\frac{1}{m_i}} \prod_{j=1}^{i-1} \left(N^*_{j,j+1}\right)^{\left(\frac{1}{m_j} - \frac{1}{m_{j+1}}\right)} = K_1\,\varphi \qquad N \in R_i, i = 2, \ldots, R$$

The transformation given by *Equation 2-39* is of the form $X = K_1 \varphi$ which lets us parameterize the S/N curve, conditional on $\{m_j\}$ by

$$\ln X = k + u \tag{2-40}$$

where

$$k = \ln K_1 + \ln \eta_o - \frac{\gamma}{\beta_o}$$

$$u = -\frac{1}{\beta_o}(\xi - \gamma)$$

$$\xi = -\beta_o \ln\left(\frac{\varphi}{\eta_o}\right)$$

with $u \sim N\left(0, C^2\right)$, approximately.

Since $\eta_o^{-1} = (\ln 2)^{\beta_o^{-1}}$

$$K_1 = (\ln 2)^{\beta_o^{-1}} \exp\left(k + \frac{\gamma}{\beta_o}\right) \tag{2-41}$$

with K_i defined by *Equation 2-37* for $i = 2, \ldots, R$

Let

$$Z = \ln X = k + u \text{ and } N_o = \sum_{i=1}^{R} N_{oi}\,.$$

Under this parameterization, the S/N curve is specified by estimating the parameters k and C. But from *Equation 2-40*, we have point estimates

$$\hat{k} = \bar{Z} \tag{2-42}$$

$$\hat{C} = S_Z$$

where

$$\bar{Z} = \frac{1}{N_o} \sum_{i=1}^{N_o} Z_i$$

$$S_Z^2 = \frac{1}{N_o - 1} \sum_{i=1}^{N_o} \left(Z_i - \bar{Z}\right)^2$$

These estimates of k and C are life region independent estimates conditional on $\{m_j\}$. Given an estimate of C, we estimate β_o using the relationship in *Equation 2-19*, $C^2 \approx \pi^2/6\,\beta_o^2$. The S/N curve location parameters $\{K_i\}$ are then determined from *Equations 2-37* and *2-41*.

In addition to life regions with some fatigue data, for HCF applications we may also need to represent the S/N curve in the ultra-HCF region, typically above 10^7 cycles where there may well be no data. In the absence of data, the structure of the materials model accommodates a number of alternative assumptions:

1. If it is desired to posit a quasi-endurance limit, the shape parameter for the ultra-HCF region is set to an arbitrarily large fixed value, say $m = 20$.

2. If it is desired to err conservatively, the ultra-HCF region can simply be added to the highest life region for which m is determined by data and any applicable constraints.

3. Another option, which is less conservative than *Option 2* but not as non-conservative as *Option 1* is to extrapolate to the ultra-HCF region an S/N curve estimated from data under environmental conditions such that the unknown S/N curve should be strictly above the extrapolated estimated curve. For example, in some applications, if operating conditions are cryogenic and we have no data above 10^7 cycles, we can use room temperature data to estimate an S/N curve which would be used only in the ultra-HCF region. These options are illustrated in *Figure 2-2*.

For LCF applications, we may also need to represent the S/N curve in a region between 1 cycle and the smallest observed value of N. The materials model can represent an S/N curve in such a region by simulating the curve as before for the higher life-regions and then tying a calculated tensile test stress-life value to the simulated S/N curve subject to the constraint $m_1 \geq 0$. In general $MED(m_1) > MED(m_2)$ so that concavity to the origin is only required above the first life

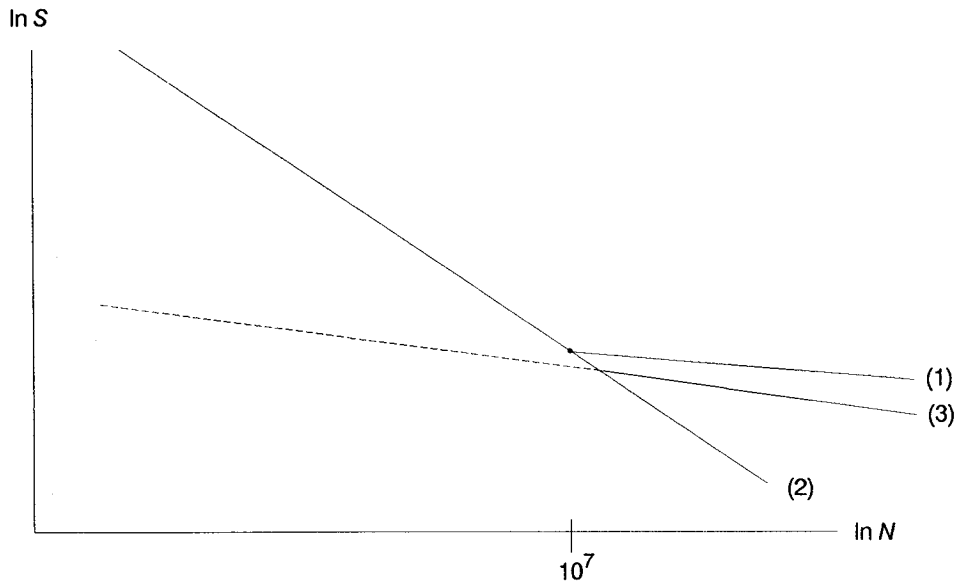

Figure 2-2 S/N Curves

region. Note also that this procedure is consistent with the notion that C would not be constant over life-regions down to 1 cycle.

Variation in the S/N curve parameters $\{m_j\}$, k, β_o leads to a set of stochastic S/N curves, represented equivalently by *Equation 2-11* or *Equation 2-12*. The random variable φ plays the role of a materials life driver. It models intrinsic S/N curve uncertainty in the Monte Carlo Component Stress/Life Failure simulation. The parameters of the probability distribution of φ are a function of the S/N curve parameters $\{m_j\}$, k, β_o.

References

[1] Abramowitz, M., and Stegun, I. A., editors, Handbook of Mathematical Functions, National Bureau of Standards, Applied Mathematics Series 55, Issued June 1964, Ninth Printing, November 1970 with corrections.

[2] Johnson, N. L., and Kotz, S., Distributions in Statistics: Continuous Univariate Distributions - 1, Houghton Mifflin Company, 1970.

[3] Spindel, J. E., and Haibach, E., "Some Considerations in the Statistical Determination of the Shape of S-N Curves," Statistical Analysis of Fatigue Data, edited by R. E. Little and J. C. Ekvall, ASTM Publication STP 744, 1981.

2.1.2.2 Strain/Life Characterization of Fatigue Failure of Materials

LCF applications, when strain/life rather than stress/life test data is available, our knowledge of the fatigue properties of a component material is represented by uncertainty in the appropriate Strain/Life curve for the material. Our model is analogous to the stress/life fatigue model at the level of total strain data decomposed into plastic and elastic strain components with no life region partitions.

Information which can be used to characterize the plastic and elastic components of the Strain/Life curve will be classified as follows:

Necessary Information

- Specific plastic and elastic strain component failure data.

Optional Information

- Specific total strain failure data.
- Related failure data.
- Tensile test data.
- Explicit constraints on the plastic and/or elastic component shape parameters.

The Strain/Life curve is defined by

$$S_P = K_P N^{-1/m_P} \varphi \tag{2-43}$$

$$S_E = K_E N^{-1/m_E} \varphi$$

$$\varphi \sim W(\eta_o, \beta_o)$$

$$S \equiv S_P + S_E$$

Where S is total strain, S_E is the elastic strain component and S_P is the plastic strain component. Requiring $MED(\varphi) = 1$ implies

$$\eta_o = (\ln 2)^{-1/\beta_o} \tag{2-44}$$

From *Equation 2-43* and *Equation 2-44*, using only specific plastic and elastic strain component failure data, the procedures developed for the stress/life model can be used to find median values for K_P, K_E, m_P and m_E. Some specific or related optional information may be available only as total strain failure data. Also, tensile test data can be used to derive a value of plastic strain at one cycle, given a value for specimen reduction of area (R.A.), according to

$$S_P = \frac{1}{2} D N^{-1/2} \tag{2-45}$$

$$D = -\ln (1 - R.A.)$$

If we assume that all data sets under consideration follow

$$S_{P_i} = \lambda_i S_i \tag{2-46}$$

$$S_{E_i} = (1 - \lambda_i) S_i$$

then we can generate both component strain failure data and the elastic component corresponding to *Equation 2-45* by deriving

$$\frac{S_{P_i}}{S_{E_i}} = \frac{\lambda_i}{1 - \lambda_i} = \left(\frac{K_p}{K_E}\right) N_i^{-\left(\frac{1}{m_P} - \frac{1}{m_E}\right)} \tag{2-47}$$

from *Equations 2-43*, *2-44* and *2-46*.

Once *Equation 2-47* has been used to augment the necessary strain component failure data with any optional strain component failure data, we consider any shape parameter constraints and apply the stress/life methodology directly to each set of strain component failure data.

In the strain/life methodology, since $V(\ln \varphi) = \pi^2/6\,\beta_o^2$, each strain component analysis provides an estimate of $V(\ln \varphi)$. We will specify a unique estimate for β_o by defining the estimate of $V(\ln \varphi)$ to be the average of those derived from the plastic and elastic strain component analyses.

The strain/life and stress/life characterizations differ significantly only in how life is calculated. To solve *Equation 2-43* for life, *N*, given total strain, *S*, we require a numerical procedure such as Newton's method in order to perform the computation.

2.1.2.3 Process Variation in Materials

Materials test data which is available to characterize fatigue properties in a component operating environment is typically from a single heat of the material. The structure of the materials characterization models has been extended to allow for consideration of the impact of heat-to-heat or process variation on component reliability.

In the case of stress/life test data, process variation is represented by the stochastic shift factor, $\lambda_K^* Z$ in *Equation 2-48*

$$S = K N^{-1/m} \varphi \left[\lambda_K^* Z\right] \tag{2-48}$$

with λ_K^* and Z defined by

$$\lambda_K^* = MED\ K^* / MED\ K$$

$$Z \sim \Lambda(\mu, \sigma^2)$$

$$MED\ Z = 1 \Rightarrow \mu = 0$$

λ_K^* can be interpreted as a location shift parameter used to account for the fact that the location of the median S/N curve constructed from data for a single heat may vary from the location of a median S/N curve constructed by considering data from multiple heats. σ^2 represents the extent of departures from the multiple heat median S/N curve warranted by the information available.

From *Equation 2-48*,

$$VAR\left[\ln N | S, multiple\ heats\right] = m^2\left(C^2 + \sigma^2\right) \tag{2-49}$$

$$VAR\left[\ln N | S, single\ heat\right] = m^2 C^2$$

From *Equation 2-49*,

$$\lambda_N = \frac{VAR\ [\ln N | S, multiple\ heats]}{VAR\ [\ln N | S, single\ heat]} = 1 + \sigma^2 / C^2$$

so that

$$\sigma^2 = (\lambda_N - 1)\, C^2$$

where C is the coefficient of variation of material fatigue strength.

λ_N is a measure of the increase in intrinsic material fatigue life variation for multiple heats relative to single heat fatigue life variation.

In the case of strain/life test data, analogous results are obtained for the extension of the materials model given by *Equation 2-50*.

$$S = \left[K_P N^{-1/m_P} + K_E N^{-1/m_E}\right] \varphi \left[\lambda_K^* Z\right] \tag{2-50}$$

where

$$\lambda_K^* = MED\ K_P^* / MED\ K_P = MED\ K_E^* / MED\ K_E$$

$$\lambda_N = 1 + \sigma^2 / VAR\left(\ln \varphi\right)$$

so that

$$\sigma^2 = \left(\lambda_N - 1\right) VAR\left(\ln \varphi\right)$$

Thus, whenever λ_K^* and λ_N can be specified, we can account for process variation in materials characterization.

2.1.3 Driver Characterization

2.1.3.1 Driver Probability Distributions

Probabilistic characterization of a component failure mode utilizes an engineering failure model which determines component failure as a function of both fixed parameters and stochastic parameters, called drivers. The purpose of this section is to provide some guidelines for specification of driver distributions.

It is necessary to identify the portion of the driver space critical to accurate simulation of the left-hand tail of the failure probability curve based on the information available. With that goal in mind, prior to any exogenous specification of driver distributions, a failure probability curve based on nominal values of life drivers with a stochastic materials curve estimated from materials data should be simulated. The sensitivity of that failure probability curve's left-hand tail to the specification of life driver distributions should then be investigated in the following way. For each life driver, define a worst-case value based on available information and re-simulate a corresponding failure probability curve with other drivers fixed at nominal values. Single-loop simulations of size 1000 should be adequate for this procedure. Concern for the detail of driver distribution specification should focus on those drivers whose worst-case values correspond to extreme shifts of the left-hand tail of the simulated failure probability curve. If those worst-case values are due to lack of knowledge rather than intrinsic variability, then these results also provide an indication of the value of increasing knowledge about those life drivers. It is important to realize that accurately specifying the life driver distributions over that part of the life driver space which corresponds to simulated failures outside the left-hand tail of the failure distribution function is not necessary.

Driver distributions should be specified to reflect both intrinsic variability and variation due to lack of knowledge. For high cycle fatigue and low cycle fatigue applications to date, three families of distributions have been found sufficient for characterizing driver distributions.

$$UNIFORM : X \sim U(a, b) \tag{2-51}$$

$$NORMAL : X \sim N(\mu, \sigma^2)$$

$$BETA : X \sim Be(a, b, \rho, \theta)$$

Uniform Distribution

The Uniform distribution is illustrated in *Figure 2-3* and is given by *Equation 2-52*.

$$f(x) = \begin{cases} \dfrac{1}{b-a} & a \le x \le b \\ 0 & otherwise \end{cases} \tag{2-52}$$

It is appropriate to use the Uniform distribution to characterize driver variability whenever finite bounds, a and b, can be established on the range of a variable and the probability that the driver falls in the interval (x_1, x_2), where $a \le x_1 \le x_2 \le b$, can be considered to be proportional to $(x_2 - x_1)$. That is the case when all the information that is available about a driver consists of its finite bounds, or the Uniform distribution may be a useful conservative approximation when the nominal sensitivity analysis shows that the driver under consideration is not important in determining the left-hand tail of the simulated failure probability curve.

Normal Distribution

The Normal distribution is illustrated in *Figure 2-4* and is given by *Equation 2-53*.

$$f(x) = \left(2\pi\sigma^2\right)^{-1/2} \exp\left[-(x-\mu)^2 / 2\sigma^2\right] \tag{2-53}$$

The Normal distribution is used to characterize a driver in two leading situations. First, there may be measurements available which suggest that the value of the driver is distributed symmetrically about some central value, μ, and there is sufficient data to calculate a measure of deviation, σ. Additionally, if the underlying physical processes which produce the value of the driver can be considered to operate so that it is the resultant sum of many small independent effects, then the driver distribution is approximately Normal as a consequence of the Central Limit Theorem. In the second situation, the Normal distribution is essentially used as a convenient approximation where there is additional uncertainty as to appropriate values for μ and σ. Then, hyperdistributions on μ and σ are formed based on the information available.

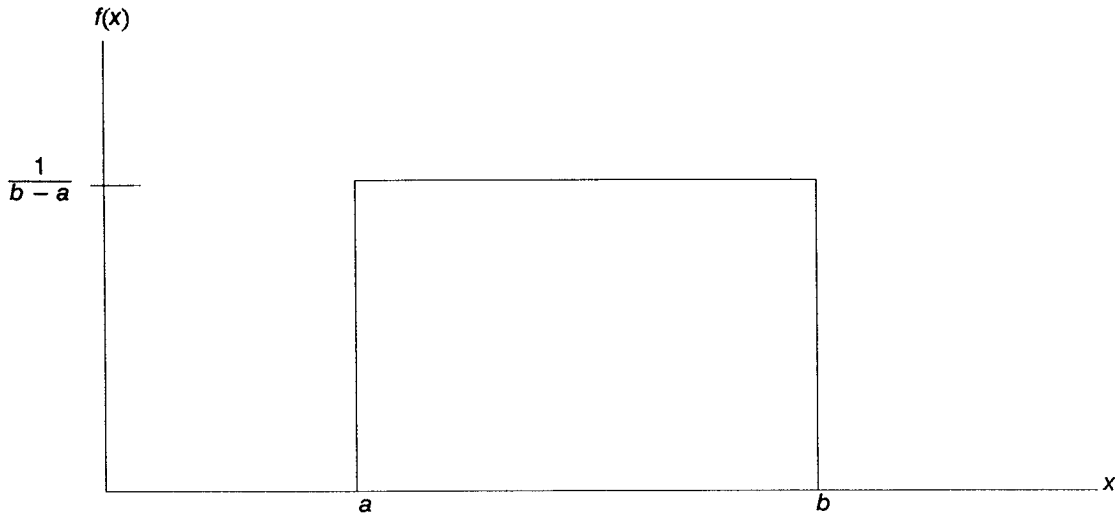

Figure 2-3 Uniform Distribution

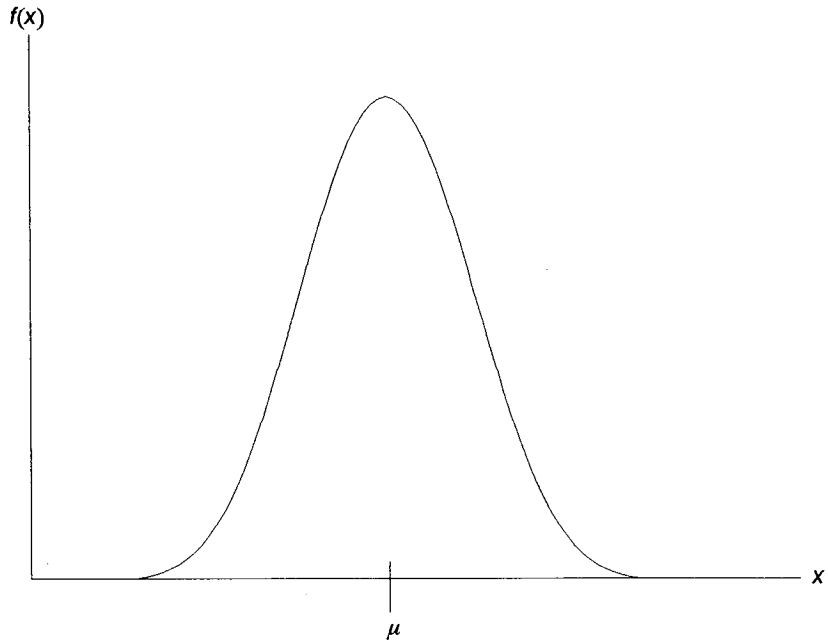

Figure 2-4 Normal Distribution

Beta Distribution

Beta distributions are illustrated in *Figure 2-5* and *Figure 2-6* and are given by *Equation 2-54.*

$$f(x) = Be\,(x; a, b, \rho, \theta) \tag{2-54}$$

$$f(x) \propto (x - a)^{\rho\,\theta}\,(b - x)^{(1-\rho)\theta}$$

$$a \le x \le b \qquad 0 \le \rho \le 1 \qquad \theta \ge 0$$

The Beta distribution family is very useful for characterizing driver variation because in the (a, b, ρ, θ) parameterization it provides a framework for experience-based judgment on driver variability to be translated into shape and location parameters of a probability distribution. The peak of the distribution occurs at $\pi = a + \rho(b - a)$ where a and b are the finite bounds on the range of life driver values. Thus, ρ parameterizes the peak of the distribution. θ characterizes the variability of the distribution. As $\theta \to 0$, the variability is maximized at $(b - a)^2/12$ since the distribution converges to $U(a, b)$. As $\theta \to \infty$, the variability is minimized at 0, since x approaches the peak location, π, with probability 1.

The Beta distribution can be used as follows if warranted by the available information. Let a, b and θ be specified from experience-based judgment on the bounds and shape of the distribution function. Bounds on the peak value π, π_1 and π_2, imply

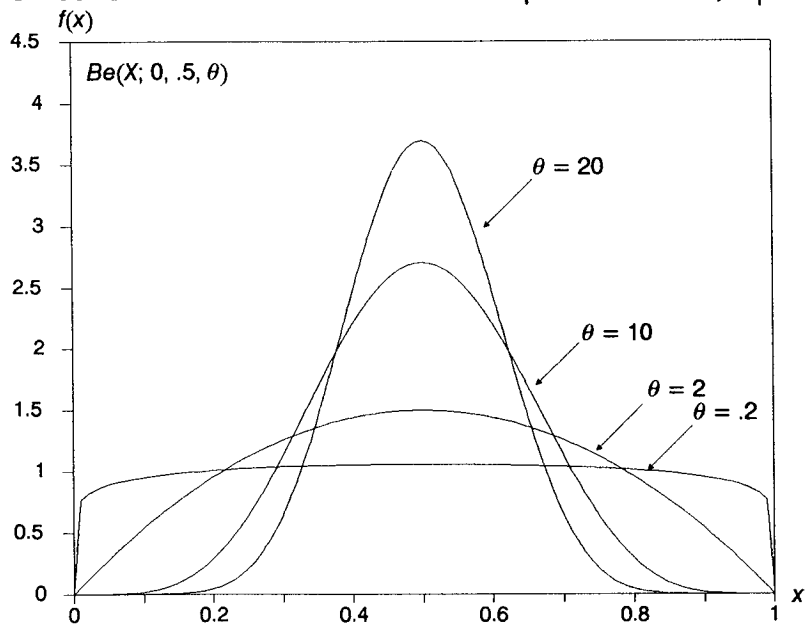

Figure 2-5 Beta Distributions with $\rho = 0.5$ and Different Values of θ

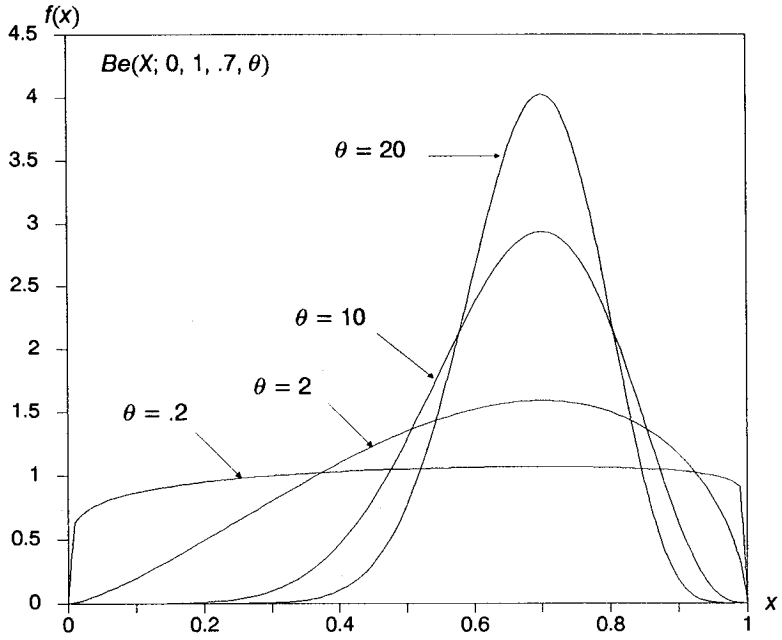

Figure 2-6 Beta Distributions with $\rho = 0.7$ and Different Values of θ

bounds, μ_1 and μ_2 on the mean of the corresponding Beta distribution. We will use Uniform distributions to represent uncertainty in ρ and take $\overline{\mu} = (\mu_2 - \mu_1)/2$ to be the nominal value of the driver. Note that only two of the three parameters $(\pi_1, \pi_2, \overline{\mu})$ can be uniquely specified from experience-based judgment. The resulting procedure for finding bounds on ρ, ρ_1 and ρ_2, is illustrated in *Figure 2-7*.

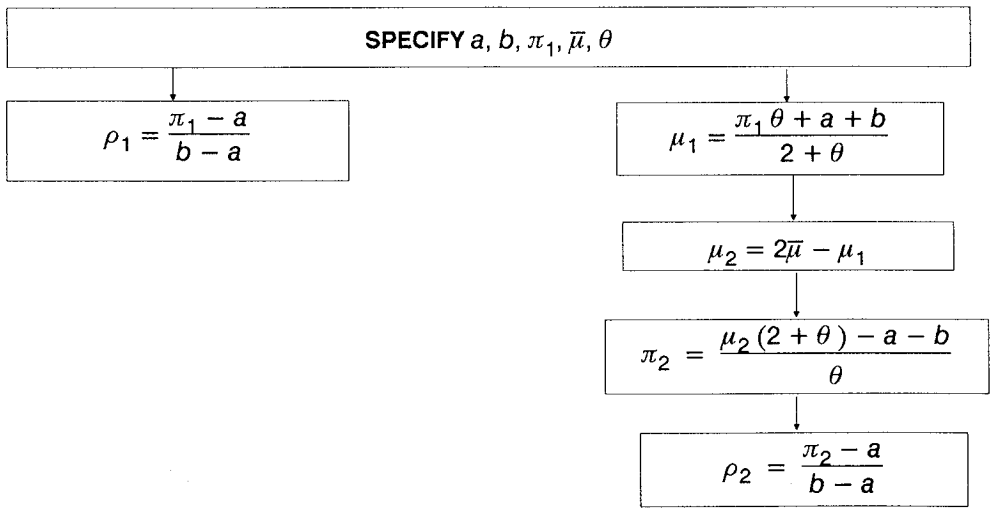

Figure 2-7 Procedure for Specifying Beta Distribution

When the information being represented is more diffuse, we can also introduce variation in θ by specifying bounds, θ_1, θ_2, and simply represent peak variation by specifying bounds π_1, and π_2.

These procedures for forming life driver distributions are illustrated in the case studies of *Section 3.0*.

2.1.3.2 Load Scale Factors

The design reference values of loads are extreme values of loads derived from power spectral density enveloping procedures. Load scale factors are stochastic multipliers which are derived from knowledge of the design reference values, the procedures used to generate them, and a requirement that the resulting load scale factors be consistent with any available strain gage stress measurements.

A load scale factor, λ, can be represented as a Normally distributed random variable, $\lambda \sim N(\mu, \sigma^2)$, where λ is the ratio of load to the reference value of load. Since $\lambda = 1$ represents the design reference value of the load, the problem of statistically characterizing the load can be posed in terms of finding the parameters μ and σ^2 based on the available information, where $\mu + k\sigma = 1$. Load scale factor density functions are represented in *Figure 2-8* as a function of alternative values of *k*.

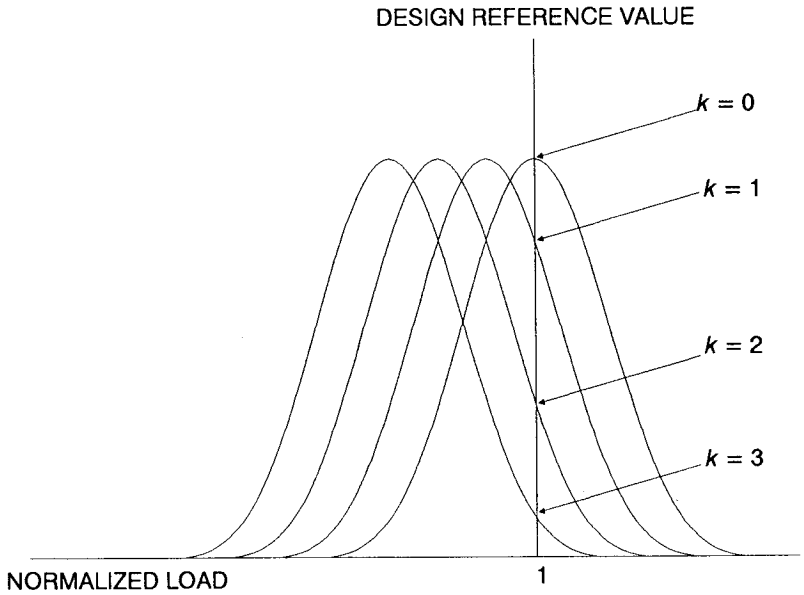

Figure 2-8 Load Scale Factors

The available information regarding loads is assumed to allow the coefficient of variation, C, to be approximated, so we have $\sigma/\mu = C$. Then μ and σ^2 are given by

$$\mu = \frac{1}{1 + kC} \qquad (2\text{-}55)$$

$$\sigma^2 = \left(\frac{C}{1 + kC}\right)^2$$

To account for the requirement of consistency of *Equation 2-55* with measurements from which loads are obtained, *Equation 2-55* will be modified to obtain

$$\mu = \frac{d}{1 + kC} \qquad (2\text{-}56)$$

$$\sigma^2 = \left(\frac{C}{1 + kC}\right)^2$$

where

$$d = \begin{cases} 1 & \text{No Strain Gage Data} \\ (1 + kC)\mu_G & \text{Strain Gage Data} \end{cases}$$

and μ_G represents the average value of λ indicated by strain gage data.

We will let $k \sim U(a, b)$ in order to account for uncertainty in the appropriate value for k. An approach to setting a value or range of values for k can be derived by considering the impact of sample size on the enveloping procedures used to arrive at a design reference value. In general, design reference values will exceed "3σ" points as measured by means of estimates of μ and σ. To account for the precision of those estimates we will use the concept of an expected coverage tolerance limit, described in **[1]**. The computed coverage in *Table 2-1* is the expected fraction of the population bounded by a "3σ" envelope, based on a sample of size N. The corresponding value of k is that k required to shift the load scale factor density function so that the probability of being below the design reference value is the same as the coverage.

Since the design reference values are typically based on sample sizes of 10-15, these results provide a guide to selecting a value or range of values for k.

Table 2-1 The Required Values of k and the Computed Coverage for Sample Sizes of N

N	COVERAGE	k
2	.855	1.06
5	.974	1.94
10	.990	2.33
15	.992	2.41
80	.997	2.75

Reference

[1] Owen, D. B., Factors for One-Sided Tolerance Limits and for Variables Sampling Plans, SCR-607: Sandia Corporation Monograph, March 1963 (Available through National Technical Information Service, Department of Commerce).

2.1.4 Composite Stresses in High Cycle Fatigue Analysis

Fatigue failure can be the result of a combination of stresses induced by random vibration and periodic loads. Structural components often exhibit narrow-band response to a broad-band vibration environment. The narrow-band response frequencies of such components will be near a modal frequency. Periodic loads, such as those due to constant speed rotation of turbopump components, may be superimposed onto the narrow-band response of some structures, producing a complex stress-time history. In an analytical model representing such cases, narrow-band Gaussian stresses resulting from the stimulus of broad-band Gaussian loads are superimposed on sinusoidal stresses generated by the stimulus of sinusoidal loads to produce a composite stress-time history. In general, that composite stress-time history will be formed from the superposition of multiple narrow-band Gaussian stress-time histories, each at a different frequency, and multiple sinusoidal stress-time histories, each at a different frequency and phase angle. Such a superposition is illustrated in *Figure 2-9* for one narrow-band Gaussian stress-time history superimposed on one sinusoidal stress-time history.

A procedure for determining the magnitude and frequency of peak stresses in the composite process from knowledge about the individual processes is given as follows. If peaks result from one or more sinusoidal stress-time histories with no random stresses, the analytical solution is straightforward. If peaks result from a single narrow-band Gaussian stress-time history with no sinusoidal stress, the analytical solution is again straightforward. In that case, the peaks follow a Rayleigh distribution with associated frequency equal to the narrow-band frequency, **[1]**, p. 498. A method is presented which will accurately describe the magnitude and frequency of peak stresses for the composite process in the cases where there is at least one random

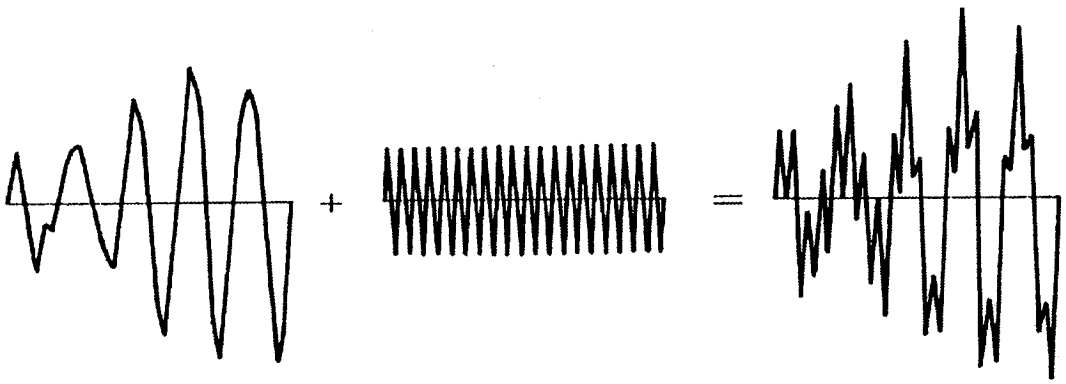

Figure 2-9 Superposition of Narrow-Band Gaussian and Sinusoidal Stress-Time Histories

and one other stress-time history, but will also be valid in all other cases which can define the composite process presented here.

The procedure is to generate a pseudo-time history of the composite process from knowledge of the properties of the individual processes, i.e., narrow-band frequencies, variances, and damping coefficients for the narrow-band Gaussian processes and sinusoidal amplitudes, frequencies and phase angles for the sinusoidal processes. By generating a pseudo-time history which captures this input information, the rainflow cycle counting methodology discussed in *Section 2.2.1.4* can be used to compute the magnitude and frequency of peak stresses just as they would be computed from observations on the composite processes.

Some terms which are used in representing the pseudo-time history are defined as follows:

σ_N = standard deviation of narrow-band stresses

f_o = a modal frequency of the component: $\omega_o = 2\pi f_o$

f_c = sinusoidal frequency: $\omega_c = 2\pi f_c$

f = frequency used to determine time increment; usually $\max(f_o, f_c)$

ξ = damping coefficient

N = number of points per cycle of frequency f

T = length of generated stress-time history

A narrow-band Gaussian process $\{N(t)\}$ can be written in the form

$$N(t) = N_c(t) \cos \omega_o t + N_s(t) \sin \omega_o t \tag{2-57}$$

with spectral density

$$S(f) = \frac{2 \sigma_N^2 \xi}{\pi f_o} \left[\frac{1}{1 + (4 \xi^2 - 2) (f/f_o)^2 + (f/f_o)^4} \right] \tag{2-58}$$

[1], p. 495.

There are computer intensive methods which can be used to generate a narrow-band Gaussian time history directly by a numerical inverse Fourier transform of a given spectral density. A simpler procedure which approximates $\{N(t)\}$ results if we consider *Equation 2-58* in the neighborhood of f_o. Then, linear and quadratic deviation terms can be used to approximate $S(f)$ by

$$S(f) \doteq \sigma_N^2 \left[\frac{\omega_o \xi}{\left(\omega_o \xi\right)^2 + 4\pi^2 \left(f - f_o\right)^2} + \frac{\omega_o \xi}{\left(\omega_o \xi\right)^2 + 4\pi^2 \left(f + f_o\right)^2} \right] \tag{2-59}$$

But *Equation 2-59* is the spectral density which results when $\{N_c(t)\}$ and $\{N_s(t)\}$ are independently generated from the AR(1) process (autoregressive process of order one) specified by *Equation 2-60.*

$$x(t) = \rho\, x(t - \Delta t) + u(t) \tag{2-60}$$

$$\rho = \exp \left[- 2 \pi \xi f_o / N f \right]$$

$$\Delta t = 1/N f$$

$$VAR[u(t)] = \sigma_N^2 \left(1 - \rho^2\right)$$

Thus, each narrow-band Gaussian stress-time history is generated using *Equation 2-60* and the composite stress-time history is formed by their superposition with sinusoidal stress-time histories defined by their frequencies, amplitudes and phase angles. For a discussion of the procedure used to eliminate insignificant contributors to the composite process and the procedure used to establish an adequate length of the composite history, see *Sections 2.2.1.5* and *2.3.7.*

Reference

[1] Clough, R. W., and J. Penzien, Dynamics of Structures, McGraw-Hill, 1975.

2.1.5 Duty Cycle Effects in Reliability Estimation

For some components subject to an LCF failure mode there may be some significant drivers which exhibit intrinsic variation from mission to mission. In such a case, the failure to model mission-to-mission variation will result in a conservative estimate of reliability, i.e., reliability will be understated. That conservatism can be seen by considering the following analysis.

Let X be the fraction of life consumed in a given time period. $f(x)$ describes the variation in damage possible during a time period. If we do not model mission-to-mission variation, then the life distribution simulated is constructed from

$$1/x_1,\ 1/x_2,\ \ldots,\ 1/x_T \tag{2-61}$$

where $x_1, \ldots, x_T$ are random draws from $f(x)$. If we do model mission-to-mission variation, then life, L, is defined by

$$\sum_{j=1}^{L} x_j \geq 1 \tag{2-62}$$

For a fixed integer j, let

$$y_j = \begin{cases} 1 & \text{if } L \geq j \\ 0 & \text{if } L < j \end{cases} \tag{2-63}$$

Then *Equation 2-63* can be used to represent *Equation 2-62* equivalently as

$$\sum_{j=1}^{\infty} y_j x_j \geq 1 \tag{2-64}$$

$$\sum_{j=1}^{\infty} y_j = L$$

In turn, *Equation 2-64* can be written as

$$L \sum_{j=1}^{\infty} (y_j / L)\, x_j = L\bar{X} \geq 1 \tag{2-65}$$

Thus, from *Equation 2-65*, the life distribution simulated is constructed from

$$\left(1/\bar{x}_1,\ 1/\bar{x}_2,\ \ldots,\ 1/\bar{x}_T\right) \tag{2-66}$$

ignoring the truncation effects implied by the inequality in *Equation 2-65.* For a simulated life set of size T, the effect of modeling mission-to-mission variation on the life distribution is thus to shift the tails toward the central part of the distribution. Thus, for high reliability, which corresponds to left-hand tail probabilities, the failure to model mission-to-mission variation will result in a conservative estimate of reliability.

However, it is also important to note that it is essential that it be possible to accurately partition driver variation into intrinsic variation and lack of knowledge components for all drivers whose intrinsic variation is a determinant of mission-to-mission variation. That is essential because, if we erroneously include variation due to lack of knowledge in the simulation of the life distribution indicated by *Equation 2-66,* the effect of modeling mission-to-mission variation on the life distribution will be to over-shift the tails toward the central part of the distribution, resulting in a nonconservative estimate of reliability, i.e., reliability will be overstated.

Mission-to-mission variation has not been implemented in the current computer code because, for SSME components subject to an LCF failure mode for which the analysis has been completed, either drivers which do vary mission-to-mission have an insignificant impact on life or it was not possible to separate intrinsic variation from variation due to lack of knowledge. The general procedure for adding mission-to-mission variation to the existing computer code is as follows.

For each iteration of the simulation, a stress or strain time history should be generated which incorporates driver variation due to mission-to-mission variation for fixed values of other drivers. The history length should be sufficient to capture the statistical properties of mission-to-mission variation. A damage histogram on a mission by mission basis can then be constructed for each iteration and represented in cumulative distribution form. For example, iteration 1 might correspond to *Figure 2-10*, a situation with a lot of small damage effects, whereas iteration 2 might correspond to *Figure 2-11*, a situation with a rare large damage effect. In order to simulate component life, we then draw M times from a given damage distribution function, where M is sufficiently small that the cumulative damage (sum of the variation drawn) is less than one. The life of the component on that iteration is then taken to be (*M/Cumulative Damage*) measured in missions. Note that basing the simulated life at each iteration on more than one draw is an attempt to capture the likelihood of experiencing any extremely damaging cycles during a given component's exposure to risk.

2.1.6 Modeling Spatially Symmetric Components

For those SSME components with spatial symmetry, such as turbine disks and impellers, engineering analysis is conducted at the level of a symmetric element of the component. That situation is illustrated in *Figure 2-12.*

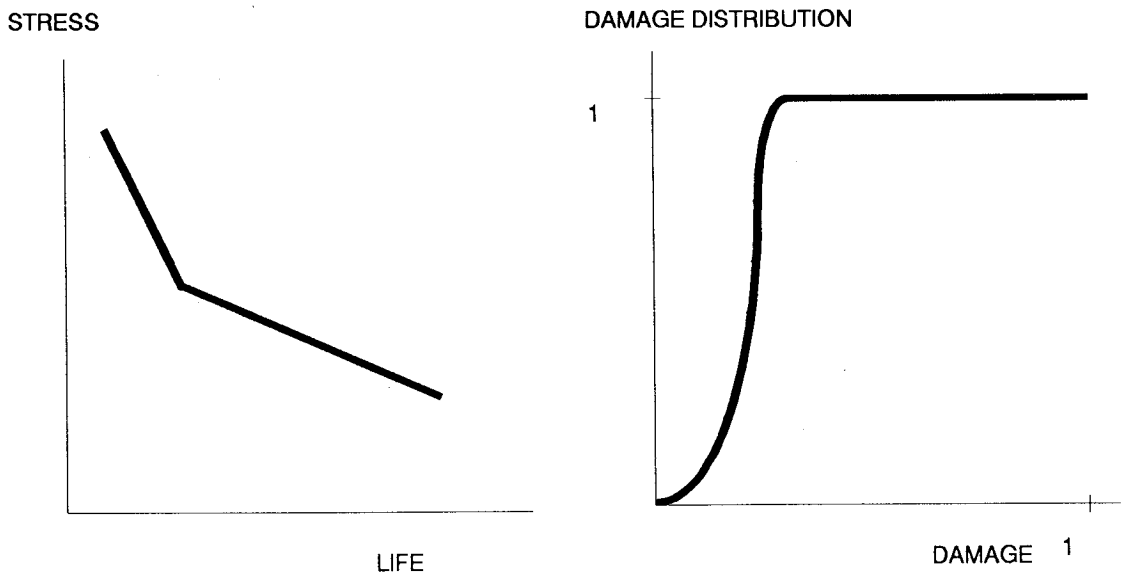

Figure 2-10 Cumulative Distribution for a Situation with a Lot of Small Damage Effects

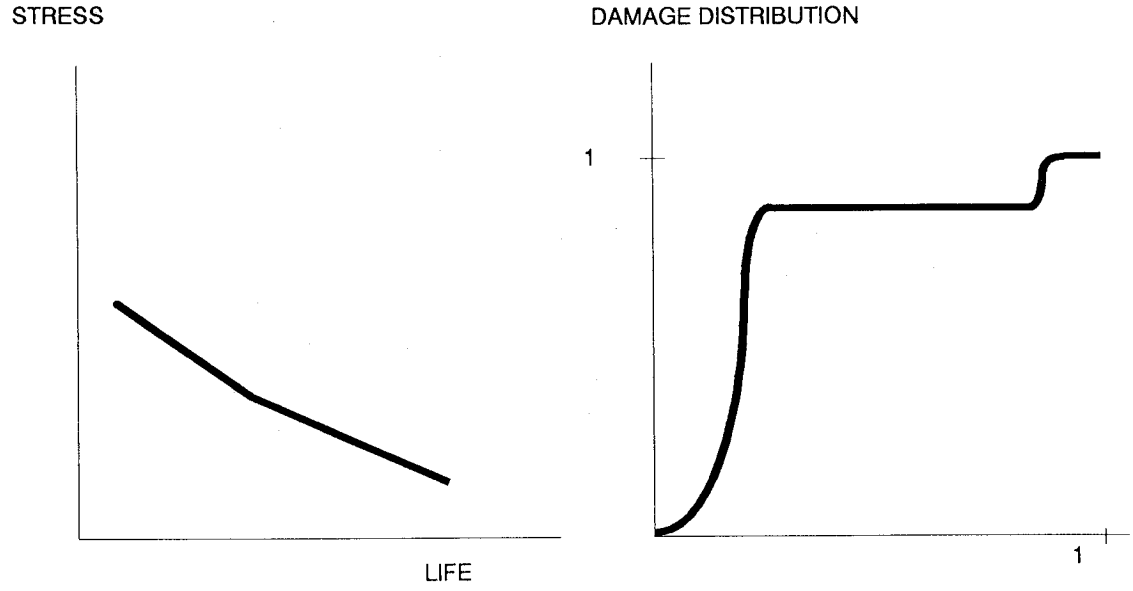

Figure 2-11 Cumulative Distribution for a Situation with a Rare Large Damage Effect

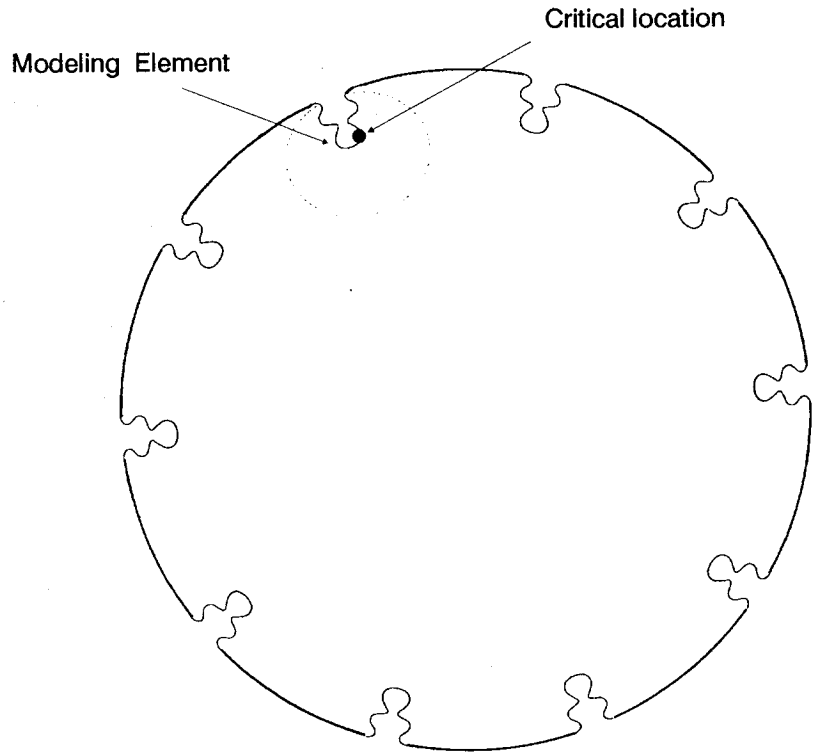

Figure 2-12 Component with 10-element Symmetry

Materials characterization is based on test data presumed to be representative of the component. The scatter in failure times indicated by test data can be used to model the scatter in failure times over the symmetric elements of a component when that scatter is due only to intrinsic materials variability.

In stochastic failure modeling a component with N-element symmetry fails, in a given environment, at the minimum of N failure times simulated to represent the scatter in lives due to intrinsic materials variability.

There is a negligible cost in simulation time to modeling spatial symmetry since it is not actually necessary to simulate N lives to find the minimum life. The Stress/Life or Strain/Life model is of the form $S = f(N)\varphi$, and when scatter in life, for a given environment, is due to intrinsic material variability, that scatter is simulated by N draws of φ. The minimum life calculated will correspond to min φ, so finding the life of an element for the materials curve with $\varphi_o = \min \varphi$ is equivalent to finding the life of the component.

For any component we analyze, we wish to specify both stress behavior and materials behavior as accurately as possible. In the following we want to consider the potential impact on simulated failure distribution curves of two kinds of specifica-

tion errors: (i) neglecting to model load-sharing and (ii) systematic materials variation attributed to random variation. Load-sharing consists of a redistribution of the stresses encountered at critical locations of the component.

For a component having a single critical location (i) is not an issue, by definition. However, once we begin to consider a component having multiple nominally identical critical locations, such as the attachment slots on a disk, it becomes important to determine, for the failure mode under consideration, (1) whether or not there exist interaction effects which induce load-sharing so that critical location life correlation effects need to be captured in the model as well as (2) whether or not there exists systematic materials variation which should be accounted for in modeling materials behavior so that it is not falsely attributed to random materials variation. The load-sharing specification error given by (i) will shift the lower tail of the simulated failure distribution for a disk toward zero whereas the impact of the systematic materials variation specification error given by (ii) depends on the particular misspecification.

If interaction effects exist which induce load-sharing, an upper bound on a particular B-life[1] of a disk could be found by considering the limiting case where all critical locations fail simultaneously. For the LCF crack initiation failure model which we have postulated, load-sharing has not been included; however, work is currently in progress to validate or refute that feature of the model specification. That work is motivated by the fact that, since one disk being modeled has fifty attachment slots, a specification bias as large as an order of magnitude shift of B-lives toward zero can result if load-sharing is erroneously excluded.

On the other hand, suppose there exists systematic materials variation which is misspecified as random variation. Also, let that misspecification assign a significant probability to materials life being much less than that under a correct specification. Then the lower tail of the distribution of disk failures predicted by a model incorporating such a misspecification will be shifted toward zero and away from the distribution of observed component failures. The magnitude of that shift will be an increasing function of the number of critical locations. Since one disk being modeled has fifty attachment slots, if there is a materials specification error under the conditions set out above, there might be a very significant impact on the lower tail of the distribution of disk failures. We presently have no evidence of the existence of such systematic variation in the materials data used for our analysis of LCF crack initiation disk failures.

---

[1] A B-life is the value of accumulated operating time to failure at a failure probability specified as a percent; e.g., B.1 is the failure time at a probability of 0.001 or 0.1%.

Under the criteria stated in *Section 1*, our objective is to present analysis based on the characterization of a failure distribution warranted by the existing state-of-knowledge, subject to the constraint never to be nonconservative; i.e., specification biases are to be avoided, but if it is necessary to introduce those biases in the course of characterizing the state-of-knowledge, they must be conservative. Therefore, we will present all our computational results under the condition that neither of the specification issues discussed is included in our analysis, and with the realization that if either exclusion is erroneous, our results could be conservative.

Section 2.2
Engineering Analysis

2.2.1 High Cycle Fatigue Failure Modeling

2.2.1.1 Introduction

The High Cycle Fatigue (HCF) failure model computes the life of a structure subjected to a relatively large number of small amplitude load cycles. For many spaceflight systems components, these loads are primarily due to structural vibration. The additional loads from temperature gradients, aerodynamic effects, and internal and external pressures combine with the vibrating stresses to cause fatigue failure. Typically, fatigue crack initiation at a single critical location will determine fatigue life of a component.

A schematic diagram of the HCF modeling approach is given in *Figure 2-13.* A major element in this approach is the transformation of the loads and other driver parameters, such as geometry and material properties, to synthesize an equivalent stress history. The details of the stress analysis are given in the next section. A description of the driver transformation and the inclusion of the driver uncertainties are found in *Section 2.2.1.3.* This is followed by a description of the damage calculations. Computer implementation of the HCF failure model is described in *Section 2.2.1.5*. The HCF failure model as developed is generic in nature. Specific details pertaining to the HCF analyses of three Space Shuttle Main Engine components are given in *Section 2.2.1.5*.

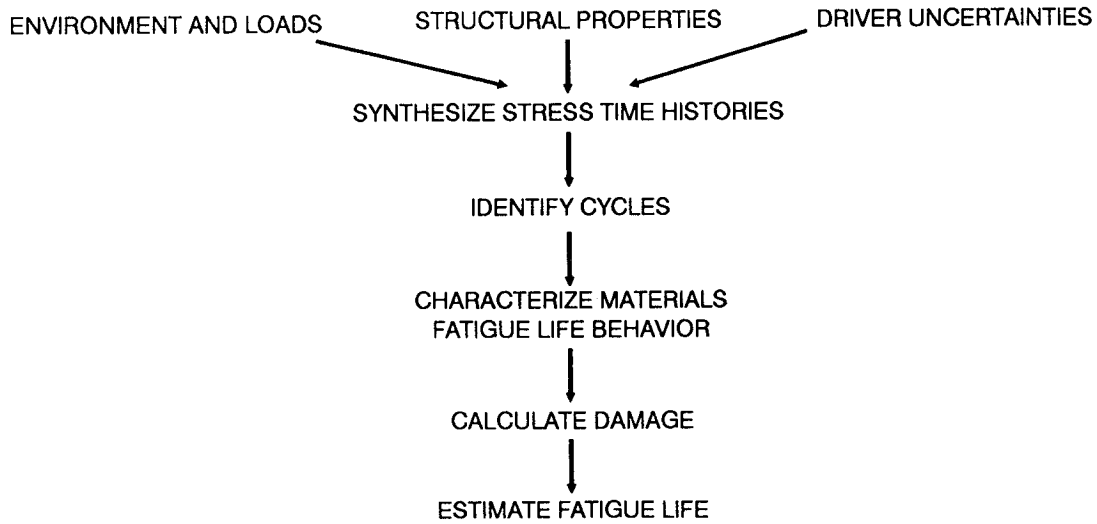

Figure 2-13 High Cycle Fatigue Failure Modeling Approach

2.2.1.2 Load Description and Stress Analysis

In the cases considered herein, vibration loads are primarily responsible for HCF failure, and the load environment is characterized by power spectral density (PSD) envelopes for the different vibration zones. A finite element (FE) model of the component is employed for the stress analysis. The FE analysis response, near the location of interest, is then used for a detailed stress analysis.

Vibration Environment Characterization

In the procedures employed by Rocketdyne and NASA/MSFC, data for characterizing the SSME vibration environment are obtained from engine hot fire tests. Accelerometers are attached at various locations and acceleration response time histories are recorded in one, two or all three of the global directions. The time signals are converted to PSDs by fast Fourier transform (FFT). A typical time signal is 3 seconds long, and a stationary PSD is determined by ergodically averaging 0.5 sec time slices. A bandwidth (i.e., frequency discretization interval) of 2.5 Hz is used in most cases. The vibration environment was separated into sinusoidal and random vibration components. These environments were used respectively for frequency response (FR) and random vibration (RV) dynamic analyses. An FR analysis derives the steady state dynamic response of the structure for a sinusoidal load input. An RV analysis derives the statistics of the dynamic response of the structure for a stationary random input process. The response stresses from these analyses are combined to calculate the fatigue life. The procedure for arriving at the composite stresses and the method for fatigue life calculation differ from those used by Rocketdyne. A detailed description of composite stress generation and the justification for the alternative procedure are given in *Section 2.1.4.*

The acceleration PSDs are processed by Rocketdyne to derive design envelopes which are a part of their current R5 vibration load criteria **[1]**. First, the spikes in the PSD which correspond to sinusoidal load components are identified and filtered from each PSD. The square root of the height of the spike is multiplied by the bandwidth to estimate the magnitude of the sinusoidal load. The filtered PSD with the spikes removed is the "random" component of the load. Envelope PSDs for each vibration zone and global direction x, y, z are constructed by adjusting the envelope curve such that all the filtered PSD curves corresponding to that zone and direction lie below the envelope. Similarly, the envelope sinusoidal loads are derived based on the highest peak from among the spikes for the given zone and direction.

The envelopes reflect extreme loads. Thus, in the procedure used by JPL, the envelope loads (i.e., Rocketdyne's design values) were adjusted to derive the unbiased nominal loads. Scale factors used to adjust the load distribution were derived based on information such as coefficients of variation and coverage factors of the raw PSD sample population. If strain gage measurements were available, the

mean of the scale factor was further adjusted to reflect the acquisition of this additional information. A detailed discussion on the load factors is given in *Section 2.1.3.2.*

Finite Element Stress Analyses

The static and dynamic analyses to determine forces at various locations in the ducts were performed using finite element numerical models. In these models the ducts were represented by line finite elements (e.g., beams, pipes, elbows) which do not provide accurate estimates of stress. Thus, the approach adopted was to extract the beam-end forces at a node close to the location of interest and employ the beam bending and cylindrical pressure vessel equations to derive the stresses. The beam-force-to-stress mapping is described in *Section 2.2.1.3. Figure 2-14* depicts the approach to the duct structural analysis used by Rocketdyne and followed in this publication. The FE analysis to determine beam end forces was performed by Rocketdyne. These beam end forces were used as input to the probabilistic HCF duct analysis programs developed by JPL.

The commercial software package STARDYNE was used by Rocketdyne for the FE analysis **[2]**. Modal dynamic analysis procedures were used to perform RV and FR analyses. The first step prior to modal analyses requires the extraction of the

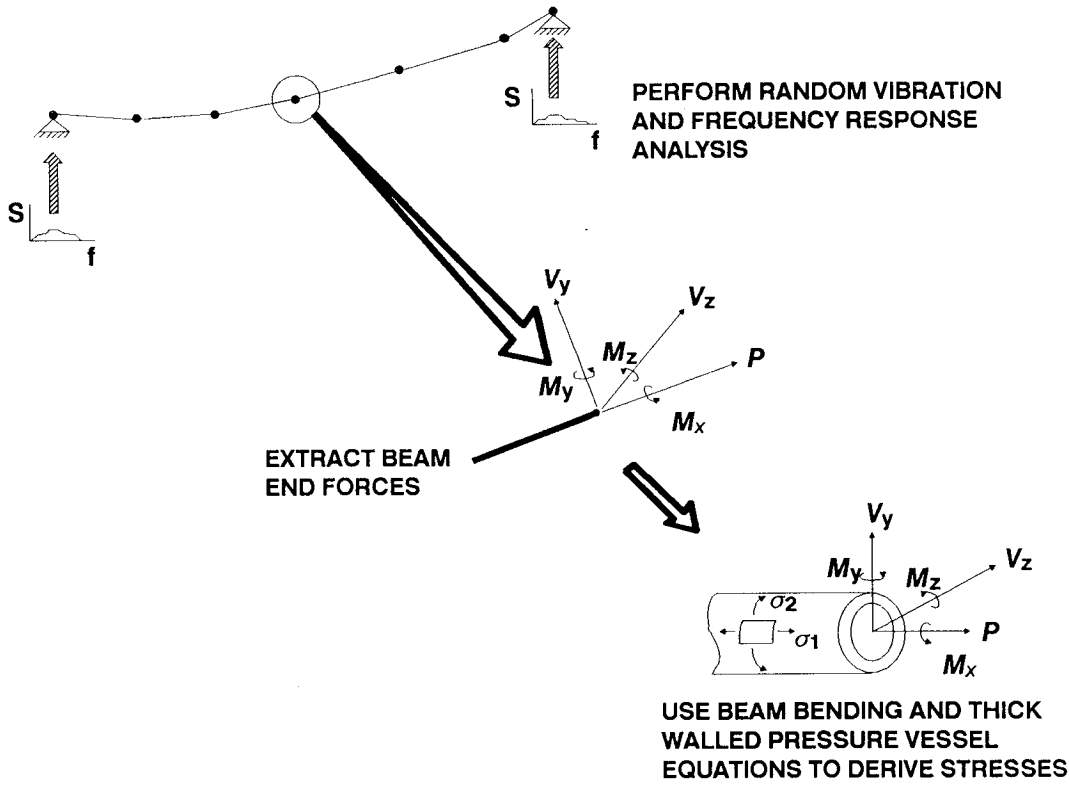

Figure 2-14 Duct Structural Analysis Procedure

eigenvalues of the system. Typically, the lowest twenty modes in the system were included in the modal analyses.

A linear RV analysis was performed using the acceleration PSDs for the component's vibration zone. The excitation was applied along one of the global directions at the supports of the structure. The analysis was performed separately for excitation in each of the three global x, y, z directions. Two quantities, namely the root mean square (RMS) beam-end force F_i and the force velocity F_i', are extracted for the critical node from the Rocketdyne RV analysis output. The force and the force velocity at a node are taken as the average of the absolute values of the forces and force velocities at the ends of line elements that are connected to that node. The force velocity is used to calculate the expected frequency for each force component i as follows:

$$f_i = \frac{1}{2\pi} \left(\frac{F_i'}{F_i} \right)^{1/2} \tag{2-67}$$

This procedure of calculating a frequency for each force component is different from an approach previously used where a single *representative* beam frequency was employed for the fatigue calculation. In the present approach, the RMS value and the expected frequency for each force component (P, M_z, T, etc.) are used to generate their respective narrow-band force time-histories.

The procedure for the Rocketdyne FR analysis was similar to their RV analyses. However, two passes of the FR analysis were performed. In the first pass, the maximum displacements and the associated phase angles were calculated for all the sinusoidal frequencies. In the second pass, these phase angles were assigned to each sinusoidal load and the responses were calculated. For the critical node, the beam-end force amplitudes for each sinusoidal exciting frequency are extracted. As in the case for the RV analyses, the absolute values of the element force amplitude are averaged across the node.

2.2.1.3 Duct Stress Analysis

As mentioned above, stresses at the location of interest in a duct are calculated using the beam-end forces derived from the FE analyses, thermal gradient, and internal and external pressures. The 1989 ASME Boiler and Pressure Vessel Code (BPVC) **[3]** was the basis for the elbow stress equations used in the probabilistic HCF duct analysis computer programs developed by JPL. The stress coefficients for moment loading and pressure, given in *Section NB-3685.1* of the BPVC, are used here. These coefficients modify the standard straight-pipe longitudinal and circumferential stress equations. The elbow effects on the radial and shear stresses are neglected both in BPVC and in this publication.

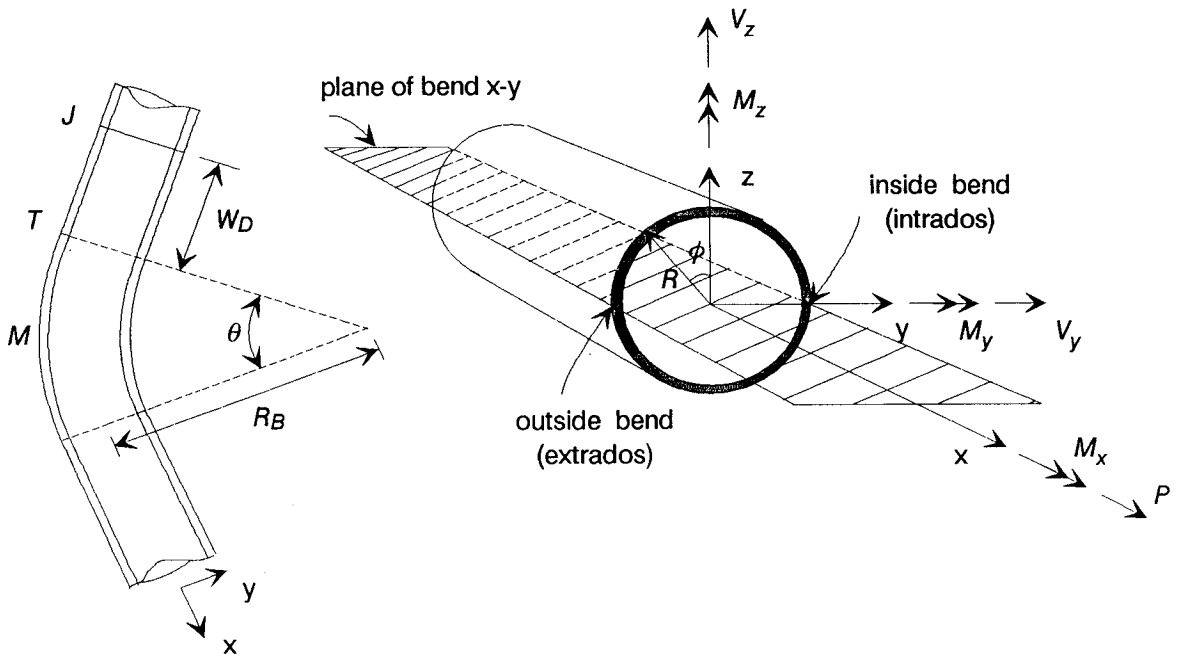

(a) Plane of Bend

(b) Cross Section

Figure 2-15 Geometry of an Elbow Duct

Figure 2-15 describes the geometry and the nomenclature for an elbow duct. The plane of the bend contains axes x and y, and the location of the axes in the elbow are consistent with those used in BPVC and in the STARDYNE program. The stresses in the elbow are given as modifications due to the *ovality effect* and the *torus effect.*

The longitudinal (axial) stress in an elbow is:

$$\sigma_1 = K_{T1}\,K_{OFF}\left\{\frac{P}{A} + \gamma_{Iy}\frac{M_y R}{I} + \gamma_{Iz}\frac{M_z R}{I} + \left(p_i - p_o\right)\frac{R_i^2}{R_o^2 - R_i^2}\right\} + \sigma_{TH} \tag{2-68}$$

in which γ_{Iz}, γ_{Iy} are longitudinal stress coefficients for ovality effect, defined in *Equations 2-74* and *2-76*, due to in-plane and out-of-plane moments. The circumferential (hoop) stress in an elbow is:

$$\sigma_2 = K_{T2}\left\{\beta\left(p_i\frac{R_i^2(R_o^2+R^2)}{R^2(R_o^2-R_i^2)} - p_o\frac{R_o^2(R_i^2+R^2)}{R^2(R_o^2-R_i^2)}\right) + \gamma_{cy}\frac{M_y R}{I} + \gamma_{cz}\frac{M_z R}{I}\right\} + \sigma_{TH} \tag{2-69}$$

C-2

in which γ_{cz}, γ_{cy} are circumferential stress coefficients for ovality effect, defined in *Equations 2-75* and *2-77* due to in-plane and out-of-plane moments, and β is the stress coefficient, defined in *Equation 2-79*, for the torus effect. In the above equations, the thermal stresses at the inside and outside wall are:

$$\sigma_{TH} = \frac{\Delta T\, \alpha\, E}{2\,(1-\nu)\ln\frac{R_o}{R_i}} \left(1 - \frac{\frac{2R_i^2 R_o^2}{R^2}}{\left(R_o^2 - R_i^2\right)} \ln\frac{R_o}{R_i} \right) \tag{2-70}$$

A positive ΔT will result in tension in the outer wall and compression in the inner wall. The radial stress is:

$$\sigma_3 = -\,p_i \frac{R_i^2(R_o^2-R^2)}{R^2(R_o^2-R_i^2)} + p_o \frac{R_o^2(R_i^2-R^2)}{R^2(R_o^2-R_i^2)} \tag{2-71}$$

and the only non-zero shear stress component is in the yz plane and is

$$\sigma_4 = \frac{M_x R}{2I} - \frac{2\,V_y}{A}\cos\phi - \frac{2\,V_z}{A}\sin\phi \tag{2-72}$$

The notation for the above equations is as follows:

p_i, p_o	= internal and external pressure
R	= radius where the stress is to be found
R_i, R_o	= internal and external radii
P	= axial force along axis x
M_y, M_z	= moment about axes y (out-of-plane) and z (in-plane)
V_y, V_z	= shear forces along axes y and z
M_x	= torque about axis x
K_{T1}, K_{T2}, K_{OFF}	= stress concentration factors
ΔT	= temperature difference across wall $T_{in} - T_{out}$
E	= Young's modulus
α	= thermal coefficient of expansion
ν	= Poisson's ratio
ϕ	= angle between z-axis and critical location on the circumference
A	= cross-sectional area
I	= cross-sectional moment of inertia

For a straight pipe, the ovality effect coefficients become $\gamma_{lz} = \sin\phi$, $\gamma_{ly} = \cos\phi$, $\gamma_{cz} = \gamma_{cy} = 0$, and the torus effect coefficient $\beta = 1$, in which case *Equations 2-68* through *2-72* would reduce to the standard multi-axial bending and pressure vessel equations.

The factors K_{T1} and K_{T2} are stress concentrations along the axial and hoop directions of the duct, respectively. They are functions of the duct geometry, welding process, and the reaming or polishing procedure used after welding. The factor K_{OFF} is an additional stress concentration due to weld offset. Assuming the joint to have zero weld dimensions, it can be shown that $(1 + 3\,W_{OFF})$ is a good approximation for the stress concentration due to a weld offset W_{OFF} **[4]**. This stress increase is conservative for weld thickness and length that is greater than the wall thickness. The empirical relation used in this study to estimate the stress concentration factor is

$$K_{OFF} = \lambda_{OFF}\left[1 + 3F_k\,W_{OFF}\right] \qquad (2\text{-}73)$$

in which λ_{OFF} is the weld offset accuracy factor and F_k is a stress reduction factor **[5]** which is based on the ratio R/t. A piecewise linear F_k vs. R/t curve was used to obtain F_k for a given value of R/t.

In **[6]**, F_k factors are presented for different R/t ratios based on FE stress analysis of detailed models of weld regions. Many F_k vs. R/t curves have been generated based on such analyses in the last few years, e.g., **[5,6]**. The F_k values from these studies vary since they are sensitive to the weld bead size and shape. In the application examples of this study, an F_k vs. R/t curve was used along with a λ_{OFF} factor which accounted for the uncertainty in F_k. This F_k curve and the distribution for λ_{OFF} are given in *Section 3.A.2.3*.

Ovality Effect

In a curved beam, the neutral axis for bending in the plane of the curve does not pass through the centroid of the beam, due to fibers of different lengths in the inner and outer sides of the bend. The normal stress due to bending moments and longitudinal force, and shear stresses due to shear forces, are different from straight pipe stresses. Also, due to components of the normal stresses in the radial direction, radial stresses are present. For tubular cross sections, these radial stresses attempt to make the circular sections in elbows become oval in shape. This *ovality effect* reduces the stiffness of the elbow and modifies the stresses. Also, internal and external pressures affect the elbow flexibility and stresses. In this publication, the *ovality effect* refers not only to the consequence of tubular sections going oval, but also it includes the curved beam effect which is present in non-tubular sections.

The 1957 paper by Rodabaugh and George **[7]** was an important contribution towards understanding the *ovality effect*, and it gave expressions for accurately calculating stresses in elbows subject to in-plane and out-of-plane bending and internal pressure. Since then, various papers have been written extending Rodabaugh's 1957 solutions to include effects due to elbow-to-straight-pipe transitions, flanges, and flexibility of joints. Most notable among them is the series of papers by Whatham, et al. **[8,9]**; an outcome of their work was an elbow analysis software package called BENDPAC. As mentioned above, the expressions from BPVC were used in this publication.

The ovality stress effect coefficients in *Equations 2-68* and *2-69* γ_{lz}, γ_{ly}, γ_{cz}, and γ_{cy} are given as follows:

$$\gamma_{lz} = \lambda_{oval} \left[\sin\phi + Q_o \left(C_{lz}\, \gamma_{lz}' - \sin\phi \right) \right] \tag{2-74}$$

$$\gamma_{cz} = \lambda_{oval}\, Q_o\, C_{cz}\, \gamma_{cz}' \tag{2-75}$$

$$\gamma_{ly} = \lambda_{oval} \left[\cos\phi + Q_o \left(C_{ly}\, \gamma_{ly}' - \cos\phi \right) \right] \tag{2-76}$$

$$\gamma_{cy} = \lambda_{oval}\, Q_o\, C_{cy}\, \gamma_{cy}' \tag{2-77}$$

in which λ_{oval} is the accuracy factor on the ovality effect calculations; Q_o is the ovality stress decay factor; C_{lz}, C_{cz}, C_{ly}, and C_{cy} are the stress carryover factors; and γ_{lz}', γ_{ly}', γ_{cz}', and γ_{cy}' are as follows (from *Table NB3685.1-2* in **[3]**):

$$\gamma_{lz}' = \gamma_{tmi} \pm \nu\gamma_{nbi}$$

$$\gamma_{cz}' = \nu\gamma_{tmi} \pm \gamma_{nbi}$$

$$\gamma_{ly}' = \gamma_{tmo} \pm \nu\gamma_{nbo}$$

$$\gamma_{cy}' = \nu\gamma_{tmo} \pm \gamma_{nbo}$$

in which

$$\gamma_{tmi} = \sin\phi + \left[(1.5X_2 - 18.75) \sin 3\phi + 11.25 \sin 5\phi \right] / X_4$$

$$\gamma_{nbi} = \lambda(9X_2 \cos 2\phi + 225 \cos 4\phi) / X_4$$

$$\gamma_{tmo} = \cos\phi + \left[(1.5X_2 - 18.75) \cos 3\phi + 11.25 \cos 5\phi \right] / X_4$$

$$\gamma_{nbo} = \lambda(9X_2 \sin 2\phi + 225 \sin 4\phi) / X_4$$

$$X_1 = 5 + 6\lambda^2 + 24\psi$$

$$X_2 = 17 + 600\lambda^2 + 480\psi$$

$$X_3 = X_1 X_2 - 6.25$$

$$X_4 = \left(1 - \nu^2\right)\left(X_3 - 4.5 X_2\right)$$

$$\lambda = \frac{t_m R_B}{R_m^{\,2}\sqrt{1 - \nu^2}}, \quad \lambda \geq 0.16$$

$$\psi = \frac{p_i R_B}{E R_m t_m}$$

and

R_B = radius of bend

R_m = mean duct radius $\left(\frac{R_i + R_o}{2}\right)$

t_m = mean wall thickness

The coefficients γ_{lz}', γ_{ly}', γ_{cz}', and γ_{cy}' used in this publication and given in the BPVC, are from Rodabaugh's paper **[7]**, and they are the second-order approximations of series solutions for stresses in an elbow. The approximations are valid for values of $\lambda > 0.16$. The derivation assumes that the elbow is continuous with a constant radius and that it has no *end effects* due to elbow-to-straight-pipe transitions or flanges. *Figure 2-15a* shows a typical elbow and, as per the assumptions, the stresses calculated from the BPVC are applicable at the midpoint *M* of the elbow. In this publication, the stresses at the straight-pipe transition point *T* are estimated by modifying the mid-elbow stresses via carryover factors C_{lz}, C_{cz}, C_{ly}, and C_{cy}. Often the weld (i.e., critical location) is at the transition point *T*.

The carryover factors depend on relative stiffness between the straight pipe and elbow, distance to straight-pipe transition point, existence of flanges, and rigidity of the weld. They may be estimated using a program such as BENDPAC **[8]**. If joint flexibility and relative stiffnesses are not known accurately, experiments will have to be performed to determine the carryover factors. In this publication, to account for

uncertainty in the carryover factors, they were specified as probability distributions. The range of the distributions is assigned based on elbow stress analysis and experiments in the literature **[8,9,10]**.

If the weld J joining the segments is a distance W_D from T, then stresses at the weld are estimated via an ovality stress decay factor Q_o, as suggested in **[11]**. This factor decays the stress at T linearly to the straight-pipe stress value at a distance of two diameters ($4R_m$) away from T. The decay factor for the ovality effect is given by

$$Q_o = \left(1 - \frac{W_D}{4R_m}\right) \tag{2-78}$$

Torus Effect

The *torus effect* is the result of pressure in the elbow causing unbalanced shell forces perpendicular to the plane of the bend. The circumferential (hoop) stress due to internal or external pressure in an elbow, unlike in a straight pipe, is no longer a constant value but is a function of the circumferential location and the bend radius. The torus effect is given by

$$\beta = 1 + Q_T [\beta' - 1] \tag{2-79}$$

in which Q_T is the torus stress decay factor and β' is the stress effect for a continuous torus with no end effect and is given as follows (*Table NB-3685.1-1* of **[3]**):

$$\beta' = \frac{(2R_B + R_m \sin\phi)}{2\,(R_B + R_m \sin\phi)}$$

The torus effect similar to the ovality effect, is assumed to decay linearly to the straight pipe value of unity at a distance of half the diameter (R_m) from T. The decay factor is given by

$$Q_T = 1 - \frac{W_D}{R_m} \tag{2-80}$$

Stress Summation

The stress components due to static and dynamic load sources are combined to derive the history for each stress component. That is,

$$\sigma_k(t) = \lambda_{ST}\,\lambda_{ST_{str}}\,\sigma_{STk} + \sum_{i=1}^{NLOAD} \lambda_{Di}\,\lambda_{DYN_{str}}\,\sigma_{Dki}(t) \tag{2-81}$$

in which

λ_{ST} = accuracy factor on the static load source

$\lambda_{ST_{str}}$ = static stress analysis accuracy factor

σ_{STk} = kth stress component due to static loads

λ_{Di} = accuracy factor on the ith dynamic load source

$\lambda_{DYN_{str}}$ = dynamic stress analysis accuracy factor

$\sigma_{Dki}(t)$ = time history for kth stress component due to ith dynamic load source

NLOAD = total number of dynamic load sources

The static stresses σ_{STk} are due to pressures p_i and p_o, temperature difference ΔT, and secondary static loads. The secondary static loads are from misalignment, gimbal displacement, fluid momentum, acceleration loads and the non-vibrating component of the aerodynamic loads and are specified as concentrated nodal forces P, M_y, M_z, etc., for the stress calculation. The dynamic load sources are due to random vibration, superimposed sinusoidal forces, and the vibrating component of the aerodynamic load.

An efficient form of the calculation given by *Equation 2-81* was implemented for summing the stresses from dynamic loads. First, reference time histories are derived for each dynamic load source. The reference histories due to a random load are generated for a standard deviation of unity. The sinusoidal reference time histories were generated having a maximum amplitude of unity. The reference histories are generated in a separate computer program and are used as input for the probabilistic HCF duct analysis programs. Then, the non-time varying stress amplitudes $\overline{\sigma_{Dki}}$ are used to scale the reference histories. The $\overline{\sigma_{Dki}}$ are the stress components derived due to the RMS values and maximum amplitudes of the beam-end forces obtained from the RV and FR analyses, respectively. The implementation of *Equation 2-81* may be written as

$$\sigma_k(t) = \lambda_{ST}\,\lambda_{ST_{str}}\,\sigma_{STk} + \sum_{i=1}^{NLOAD} \lambda_{Di}\,\lambda_{DYN_{str}}\,\overline{\sigma_{Dki}}\;\sigma_i(t) \qquad (2\text{-}82)$$

in which $\sigma_i(t)$ is the reference time history for the ith dynamic load source.

As mentioned above, separate RV and FR analyses were performed by applying the excitation along each global direction x, y and z. Thus, the total stress response is the summation from responses in each direction. The dynamic stresses in *Equation 2-82* for the three directions are given by

$$\overline{\sigma_{Dki}}\;\sigma_i(t) = \overline{\sigma_{Dkix}}\;\sigma_{ix}(t) + \overline{\sigma_{Dkiy}}\;\sigma_{iy}(t) + \overline{\sigma_{Dkiz}}\;\sigma_{iz}(t) \qquad (2\text{-}83)$$

The reference time histories for the different load sources in a given direction were generated by assuming that they were fully correlated. However, across the three directions x, y, z, the histories were assumed to be uncorrelated.

The loads-to-stress mapping for an elbow duct is shown schematically in *Figure 2-16.* The injection of uncertainty at the different stages of the calculation is shown. The von Mises criterion is used to combine the individual stress components $\sigma_k(t)$ to derive a single equivalent stress history. There are four non-zero components of stress in this case. The equivalent stress

$$\sigma(t)=\text{sign}[\sigma_1(t)]\frac{1}{\sqrt{2}}\left[\left(\sigma_1(t)-\sigma_2(t)\right)^2+\left(\sigma_2(t)-\sigma_3(t)\right)^2+\left(\sigma_3(t)-\sigma_1(t)\right)^2+6\,\sigma_4^2(t)\right]^{\frac{1}{2}} \qquad (2\text{-}84)$$

The equivalent stress is assigned the algebraic sign of the maximum principal stress – in this case, it is of the axial stress component $\sigma_1(t)$.

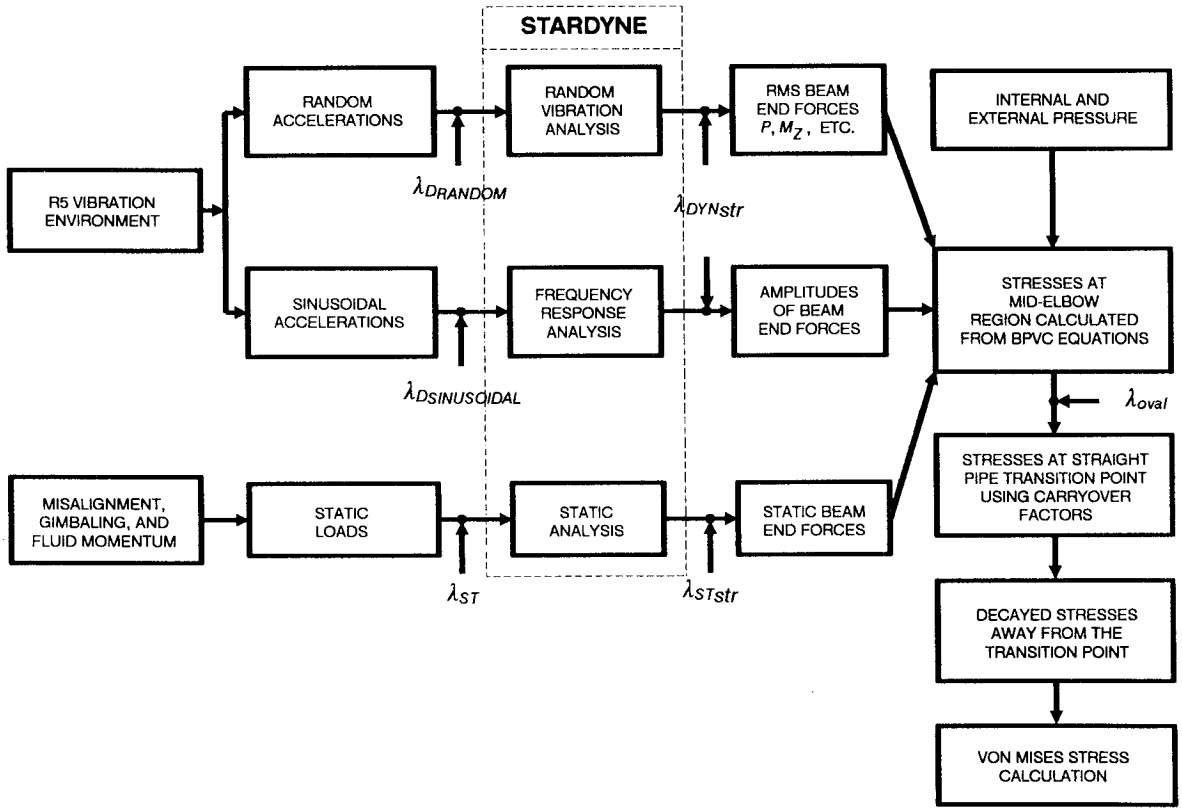

Figure 2-16 Schematic of Duct Stress Analysis

2.2.1.4 Damage Calculations

A common approach for HCF analysis involves the use of an *endurance limit.* This is based on the notion that a material has a safe stress below which fatigue failure never occurs (i.e., infinite life). It is now known that many materials do not exhibit a clearly defined endurance limit. In such cases, design and life prediction methods have shifted to the concept of finite fatigue life. Here failure is considered to be due to damage accumulation from a finite number of cycles at different stress levels.

The finite life approach employing a stress time history is used here. A key step in damage calculations is to identify the magnitudes and the number of the stress cycles in the stress time history. A cycle counting method called the *rainflow technique* has been implemented to calculate the number of cycles at different stress levels in the stress history.

A procedure for computing the cycles vs. stress level information directly from the PSD in the frequency domain has often been used for HCF analysis. However, this procedure is valid only when stress is a narrow-band Gaussian process such that the peaks may be represented by a Rayleigh distribution **[12]**. For a given SSME component, the stress may not be a narrow-band process. It is usually a composite process of a number of narrow-band and sinusoidal processes. Thus, a general approach was adopted in the JPL methodology for generating each narrow-band and sinusoidal process as a time history and correctly combining them in the time domain. The number and amplitude of stress cycles needed for fatigue calculation is obtained by performing a rainflow count on the combined stress time history.

Rainflow Cycle Counting

The objective of cycle counting is to reduce an irregular stress history to a number-of-cycles versus stress-level table so that a stress/life (S/N) curve obtained with uniformly repeated simple load cycles may be used for estimating the fatigue life of the component. The rainflow method **[13]** used here is an accepted technique.

The rainflow algorithm initially resequences the data such that the largest cycle occurs first. The portion of the stress history prior to the largest stress is shifted as a block to the end of the stress history. Thus, the largest stress is at the beginning and at the end of the stress history, while the cyclic shape of the history is unchanged. Next, all the non-extrema points are filtered out since the cycles depend only on the peak and trough points. Then the identification of the cycles begins. A schematic of the rainflow algorithm is given in *Figure 2-17.*

A cycle is a closed loop on a cyclic stress-strain diagram. The algorithm is based on the idea that a cycle has been closed if the stress difference between a peak-valley pair is less than the stress difference of the neighboring pairs. Once a closed cycle is

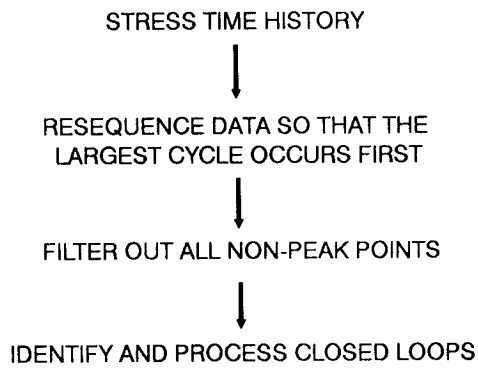

Figure 2-17 Procedure for Rainflow Counting

identified having a maximum stress of σ_{PEAK} and a minimum stress of σ_{VALLEY}, then the alternating stress and mean stress are calculated as follows:

$$\sigma_{ALT} = \frac{\sigma_{PEAK} - \sigma_{VALLEY}}{2} \tag{2-85}$$

$$\sigma_{MEAN} = \frac{\sigma_{PEAK} + \sigma_{VALLEY}}{2} \tag{2-86}$$

Then the closed cycle is deleted and the process is repeated. A pictorial walk-through example of rainflow counting is given in *Appendix 2.A*.

Mean Stress Effects

The mean stress can have a substantial influence on fatigue behavior. In general, tensile mean stresses are detrimental and compressive mean stresses are beneficial. In the components analyzed for HCF failure, the mean stresses are the result of static loads due to pressure and temperature. Although the alternating stresses due to dynamic loads alone were elastic, there were instances where the combined stresses from static and dynamic loads resulted in plasticity at the critical location.

As described above, the equivalent stress time history is derived based on elastic material behavior. Thus, when the elastic stresses exceed the linear portion of the material stress-strain curve, the stresses had to be adjusted. Two approaches were employed to approximate these stresses.

The first approach was used when the stress vs. strain diagram were elastic perfectly plastic. The total stress $\sigma_{MEAN} + \sigma_{ALT}$ cannot exceed the yield stress σ_y. There are three cases to calculate the adjusted mean stress. They are:

case 1 if $\sigma_{ALT} + \sigma_{MEAN} < \sigma_y$

$$\sigma'_{MEAN} = \sigma_{MEAN}$$

case 2 if $\sigma_{ALT} + \sigma_{MEAN} > \sigma_y$ and $\sigma_{ALT} < \sigma_y$ (2-87)

$$\sigma'_{MEAN} = \sigma_y - \sigma_{ALT}$$

case 3 if $\sigma_{ALT} > \sigma_y$

$$\sigma'_{MEAN} = 0$$

The mean calculation for *case 2* is shown in *Figure 2-18.*

The second approach was based on the Neuber's rule **[13]**. Here, the stress vs. strain curve may be a general shape—a piecewise linear definition of a curve was employed here. Neuber's rule states that the product of stress and strain is the same for elastic regions and small regions of plastic deformation. That is

$$\sigma \varepsilon = C \tag{2-88}$$

in which C is a constant. *Equation 2-88* is a hyperbola, and its intersection of the stress-strain curve defines the desired σ_N value. *Figure 2-19* shows the application of the Neuber's rule to estimate the mean stress.

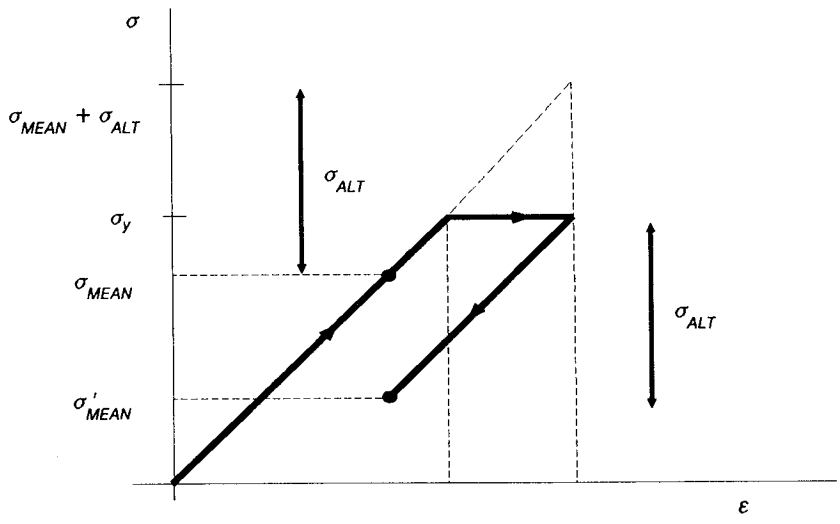

Figure 2-18 Mean Stress Calculation Assuming an Elastic Perfectly Plastic Stress-Strain Curve

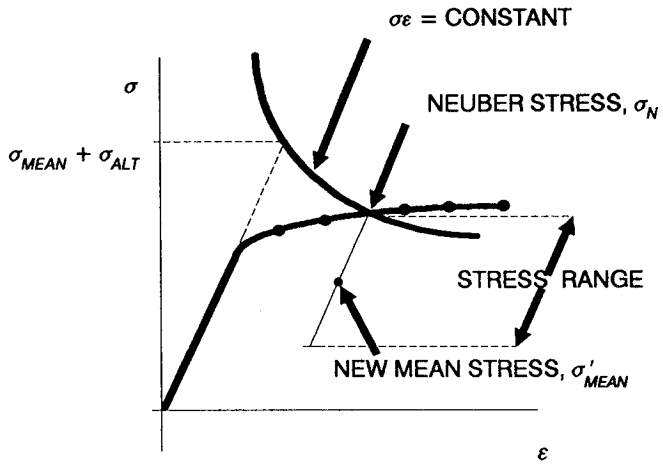

Figure 2-19 Mean Stress Calculation Using Neuber's Rule

The new mean stress based on the adjusted stress σ_N is given by

$$\sigma'_{MEAN} = \lambda_{neu}\,\sigma_N - \sigma_{ALT} \tag{2-89}$$

in which λ_{neu} is the accuracy factor on Neuber's rule calculation. All cycles due to dynamic loads lie in the elastic region around σ'_{MEAN}. It may be seen that this approach would reduce to the first approach if the stress vs. strain diagram were elastic perfectly plastic. The mean stress for the history is taken as the mean of the largest stress cycle from the rainflow count.

The analysis is conducted using S/N curves which are based on a zero mean stress. Thus, the stress cycles from rainflow are adjusted to equivalent zero-mean amplitudes using the Goodman relation **[13]**. The equivalent stress amplitude given by the Goodman relation is:

$$\sigma_{EQ} = \frac{\sigma_{ALT}}{1 - \left(\dfrac{\sigma'_{MEAN}}{\sigma_{ULT}}\right)} \tag{2-90}$$

in which σ_{ULT} is the ultimate strength for the material. Also, if the available S/N information was for non-zero mean, the same Goodman relation is employed to convert the data to zero-mean S/N curves. The fatigue life is calculated by accumulating the damage due to the stress cycles utilizing Miner's rule. The life in seconds is

$$L = \lambda_{dam}\left[\frac{T}{\sum_{j=1}^{n}\dfrac{1}{N_j}}\right] \tag{2-91}$$

in which N_j are the cycles to failure given by *Equation 2-12* corresponding to a stress level σ_j; T is the length of the reference stress time histories in seconds; n is the number of stress cycles after rainflow counting; and λ_{dam} is the accuracy factor on damage accumulation.

2.2.1.5 Component Analyses

A flowchart for the damage calculations of the HCF failure model is given in *Figure 2-20.* The failure model computation is embedded within the simulation loops of the Monte Carlo (MC) procedure, as shown in *Figure 2-1.* For every MC simulation, the driver values are perturbed by randomly drawing from their respective probability distributions. The outcome of the simulation is a list of lives of the component. Since the failure probabilities of interest are of the order 10^{-3}, only the smallest one percent of these failure times is saved and used to calculate the Bayesian Prior Distribution parameters. A more detailed description of the MC procedure can be found in *Section 2.1.1.* Specific details of the software are given in *Section 5.1.*

Three SSME components were analyzed using the HCF failure model. Static and dynamic analyses to determine beam-end forces (see *Section 2.2.1.2*) were conducted by Rocketdyne on 3-D finite element models of the components. The bend segments of the elbow ducts were modeled using STARDYNE elbow finite elements. These elbow elements accounted for the ovality effect via a flexibility reduction factor. STARDYNE had an option to calculate this factor internally, as specified by the BPVC (NB-3686.2). As mentioned above, the BPVC expressions did not account for the end effects. Thus, in some cases an estimate of the flexibility factor based on end effects was used in the FE analysis.

The static analyses took account of the loads due to misalignment, gimbaling, acceleration, and fluid momentum. Static beam-end forces were obtained at a node closest to the critical location from these analyses. Similarly, the RV analyses provided the RMS beam-end forces and the expected frequencies, and the FR analyses gave the beam-end force amplitudes at the critical locations. The beam-end forces from the static and dynamic analyses were used in the HCF analysis performed at JPL. Before performing HCF analyses, preliminary analyses were made to identify the worst circumferential location, to choose a suitable load history length and a random number seed for the stochastic reference time histories, and to identify significant beam-end force components.

In general, the worst circumferential location on a pipe does not necessarily lie on the bending axes (such as the extrados, intrados, or crown for elbows), since multi-axial moments and shear forces and, for the elbow ducts, ovality and torus effects can cause the highest stresses to occur anywhere around the circumference of the pipe. Thus, the worst location was identified by computing single fatigue life

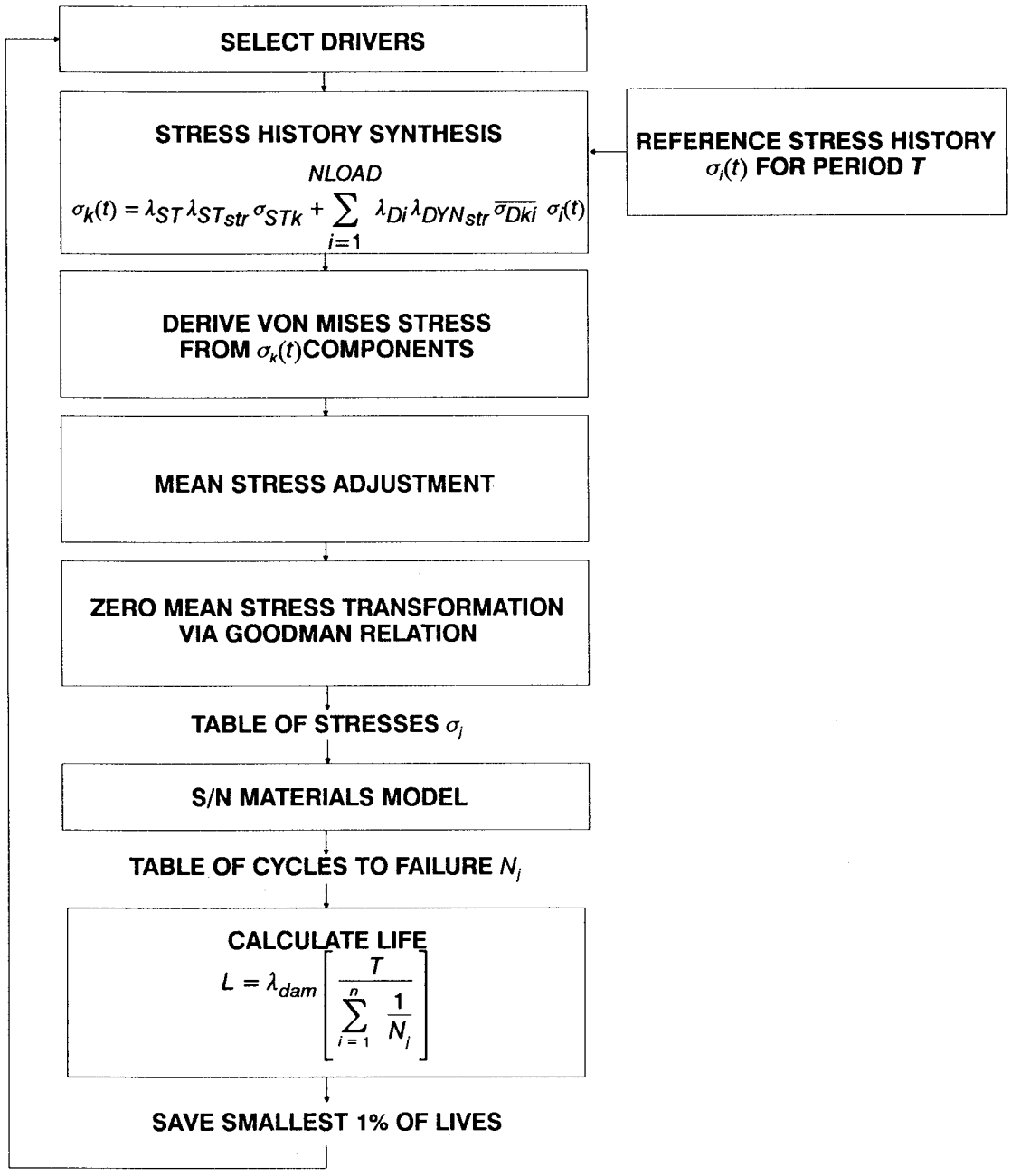

Figure 2-20 Calculation Procedure for the High Cycle Fatigue Failure Simulation

values (i.e., a deterministic run with nominal values) for different circumferential positions on the duct. This involved repeating the analyses and varying angle ϕ in *Equations 2-68, 2-69* and *2-72*. The critical circumferential angle corresponds to the analysis with minimum life.

The stochastic reference histories are generated for a given length (in seconds) of load history. The suitable length for a specific problem is determined by calculating single fatigue lives, each time increasing history lengths, until the change in the lives becomes negligible. The histories are generated using a random number stream as described in *Section 2.1.4*. Since finite length histories are employed to keep computational costs down, the occurrence of peaks in the histories will vary with different random number streams. The random number stream is based on the random number seed input for the analysis. The suitable random number seed is selected by generating reference time-histories for 21 seeds and calculating a single fatigue life for each history. The chosen seed is the one that gave the median life from among the 21 lives calculated.

The next set of preliminary analyses involved identifying significant random beam-end forces such as P, M_z, etc., and sinusoidal load frequencies. Reducing the number of force components can decrease the effort involved in input/output and processing of their respective force histories. First, the life was calculated when all the forces were present. Then the analyses were repeated, starting with the force components which were most likely to be significant, each time adding back the forces. The goal was to get a good estimate of the life by using as few force components as possible. The outcome of these force identification analyses for the three components is summarized in *Table 2-2*. This initial step saved considerable computing time, with no significant loss in accuracy of the result.

The applications of HCF probabilistic failure models to three SSME components are presented in *Section 3*. They are the High Pressure Oxygen Turbo Pump (HPOTP) main discharge duct, Low Pressure Fuel Turbo Pump (LPFTP) turbine drive duct, and the HPOTP heat exchanger coil small tube outlet. The critical location on each duct was identified as that having stresses sufficiently high to control HCF life for the component. The input, rationale for driver specification, and the results of the probabilistic failure assessment are given in *Sections 3.1* and *3.2*.

References

[1] SSME Structural Loads Criteria, Rockwell International, RSS-8561-22, October 1987.

[2] STARDYNE User Information Manual, MRI, 1984.

[3] ASME Boiler and Pressure Vessel Code, Division 1, NB-3600, 1989.

Table 2-2 Summary of Load Sources, Critical Locations and Significant Force Components

ITEM	HPOTP MAIN DISCHARGE DUCT	LPTFP TURBINE DRIVE DUCT	HEAT EXCHANGER COIL
LOAD SOURCES	RANDOM VIBRATION SUPERIMPOSED SINUSOIDAL INTERNAL PRESSURE SECONDARY STATIC LOADS*	RANDOM VIBRATION SUPERIMPOSED SINUSOIDAL INTERNAL PRESSURE SECONDARY STATIC LOADS *	RANDOM VIBRATION SUPERIMPOSED SINUSOIDAL INTERNAL PRESSURE EXTERNAL PRESSURE AERODYNAMIC LOAD THERMAL GRADIENT
CRITICAL LOCATION	WELD 6 OUTSIDE WALL ANGLE ϕ : 20°	WELD 32 OUTSIDE WALL ANGLE ϕ : 25°	WELD 3 INSIDE WALL ANGLE ϕ : 85°
SIGNIFICANT RANDOM FORCE COMPONENTS AND SINUSOIDAL LOAD FREQUENCIES	RANDOM: P, M_y, M_z, V_y SINUSOIDAL : 500 Hz, 1000 Hz, 1500 Hz, 2000 Hz	RANDOM: P, M_x, M_y, M_z, V_y SINUSOIDAL: 270 Hz, 500 Hz, 540 Hz, 600 Hz, 810 Hz, 1000 Hz, 1080 Hz, 2000 Hz	RANDOM: P, M_z SINUSOIDAL: 500 Hz AERODYNAMIC LOAD

* These include loads from misalignment, gimbaling, acceleration, and fluid flow.

[4] Johns, R. H., "Mismatch Stresses in Pressure Vessels," AIAA Journal, Vol. 2, No. 10, Oct. 1964, pp. 1827-1828.

[5] Gunay, M. H., "Elastic Mismatch Stresses in Circumferentially Welded Cylindrical Shells Under Moment Loading," ASME Pressure Vessel and Piping Conference, Nashville, TN, 1990.

[6] Naugel, F. V., "Review of Duct Program," Internal Letter, IL8126-3145, Rocketdyne, Rockwell International, May, 1988.

[7] Rodabaugh, E. C., and George, H. H., "Effect of Internal Pressure on Flexibility and Stress-Intensification Factors of Curved Pipe or Welding Elbows," Transactions of the ASME, May 1957, pp. 939-948.

[8] Whatham, J. F., "Pipe Bend Analysis by Thin Shell Theory," Journal of Applied Mechanics, ASME, Vol. 53, March 1986 pp. 173-180.

[9] Karabin, M. E., Rodabaugh, E. C., and Whatham, J. F., "Stress Component Indices for Elbow-Straight Pipe Junctions Subjected to In-Plane Bending," Journal of Pressure Vessel Technology, ASME, Vol. 108, February 1986, pp. 86-91.

[10] Thomson, G., and Spence, J., "Maximum Stresses and Flexibility Factors of Smooth Pipe Bends with Tangent Pipe Terminations Under In-Plane Bending," Journal of Pressure Vessel Technology, ASME, Vol. 105, November 1983, pp. 329-336.

[11] O'Hara, K., "Analytical Methods & Theory of Structural Analysis – DUCT," Internal Letter, No. 9113-3042, Rocketdyne, May 14, 1979.

[12] Crandall, S. H., and Mark, W. D., Random Vibration in Mechanical Systems, Academic Press, 1963.

[13] Fuchs, F. O., and Stevens, R. I., Metal Fatigue in Engineering, John Wiley, 1980.

2.2.2 Low Cycle Fatigue Failure Modeling

2.2.2.1 Introduction

A Low Cycle Fatigue (LCF) Failure Model calculates the crack initiation life of a structure subjected to a small number of high amplitude load cycles. In the ATD-Turbopump, these loads result from start-up, throttling, and shutdown. As shown in *Figure 2-21*, the driver information used in LCF failure modeling, includes environmental parameters, loads, material properties, structural parameters, and model specification uncertainties. The available information about the drivers, including their uncertainties, is used to generate stress or strain histories. Individual cycles of the stress or strain histories are identified and characterized by a value of equivalent stress or strain range that accounts for the mean and extrema of each cycle. The materials characterization model establishes a value of fatigue life for the equivalent stress or strain range of each cycle. The fatigue life for a stress or strain history is computed from the accumulated damage due to a sequence of individual cycles.

Figure 2-22 shows the life calculation procedure in more detail. The major elements of the life calculation procedure are driver selection, driver transformation, rainflow cycle counting for multiple cycle histories, the materials model, and the damage accumulation algorithm which is used for multiple cycle histories. In the driver transformation, stress or strain is defined as a function of the drivers.

The driver transformation can be performed in two ways. A rigorous structural analysis can be incorporated within the Monte Carlo simulation, or the driver trans-

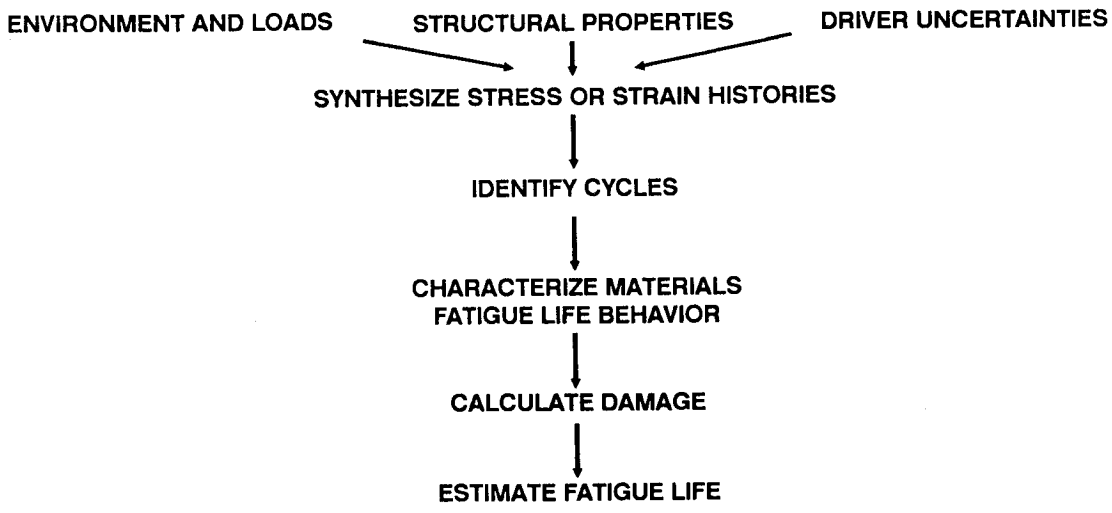

Figure 2-21 Low Cycle Fatigue Failure Modeling Approach

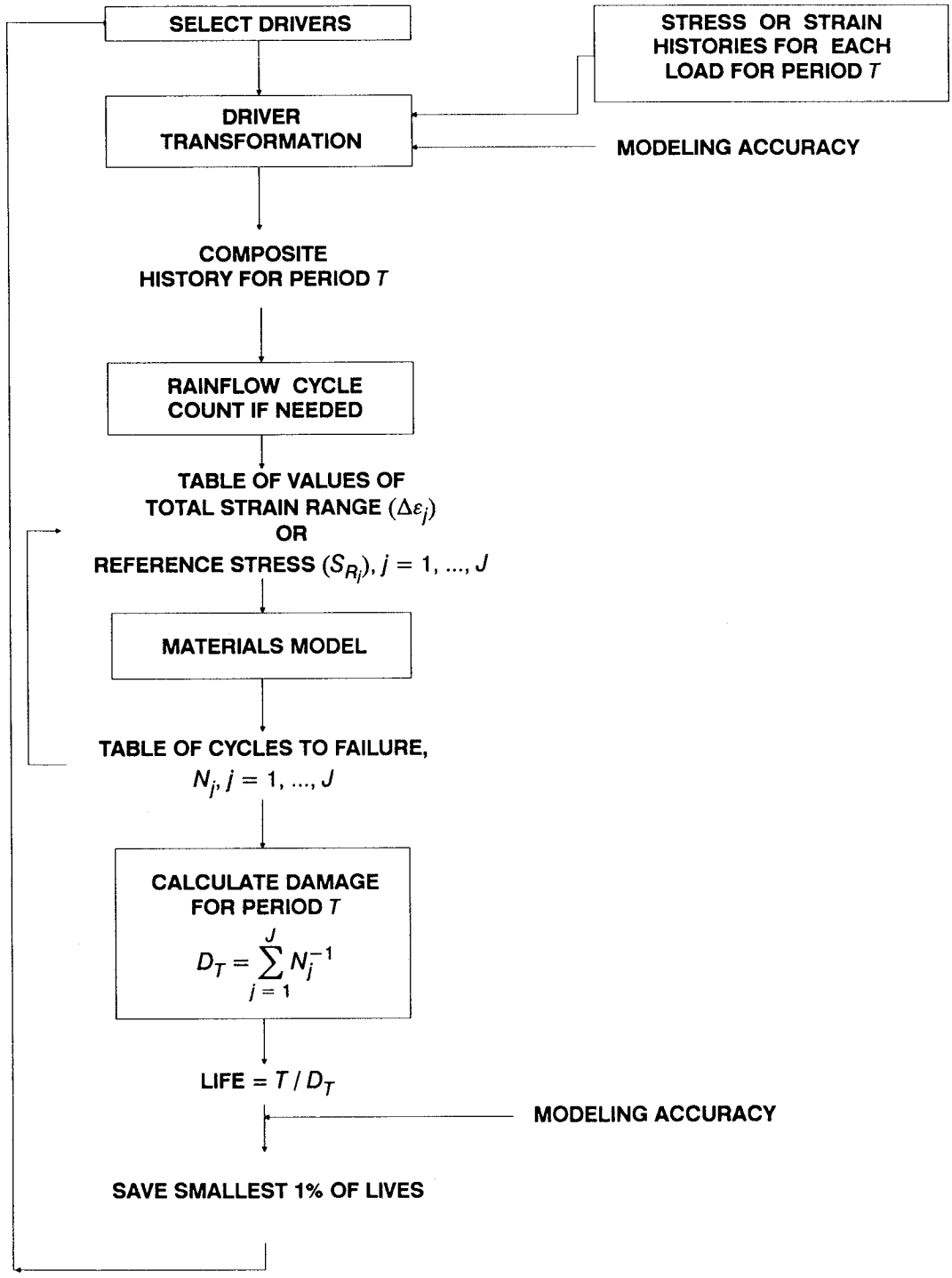

Figure 2-22 Calculation Procedure for the Low Cycle Fatigue Failure Simulation

formation can be accomplished by a parametric representation of the rigorous structural analysis, i.e., by a response surface. The latter approach was chosen because response surface methods gave accurate answers and were computationally efficient. A parametric representation of the structural analysis is obtained by performing a sensitivity analysis using structural finite element models. The results of the sensitivity analysis are then expressed as a functional relationship of stress or strain with respect to the relevant drivers.

Factors to account for uncertainties, such as that of modeling accuracy, are inserted as appropriate, at the steps of the life calculation procedure of *Figure 2-22.* When multiple cycle histories are analyzed, rainflow cycle counting is used to identify individual cycles. The fatigue life corresponding to each cycle is provided by the materials model. The failure time for multiple cycles is obtained from the damage accumulation calculation using Miner's rule. Details on rainflow cycle counting, the materials characterization model, and the damage accumulation algorithm can be found in *Sections 2.2.1.4, 2.1.2,* and *2.2.1.4,* respectively.

The ATD-HPFTP Turbine Disk low cycle fatigue analysis is described below. The engineering analysis and driver transformation are presented, followed by a discussion of the implementation of the failure simulation model for the Disk.

2.2.2.2 ATD-HPFTP Second Stage Turbine Disk LCF Analysis

Component Description

The ATD-HPFTP Turbine Disk is a monolithic forging with two rows of turbine blades attached to its outer circumference. *Figure 2-23* shows an axial cross section of the monolithic disk with both rows of blades. *Figure 2-24* illustrates the face of a stylized disk and its blade attachment areas. The actual ATD Disk has fifty blade attachment areas. The turbine is driven by high temperature, high pressure steam (H_2O) and gaseous hydrogen (H_2). The Disk is surrounded by flowing hydrogen coolant to control the temperature and thermal gradient at critical locations.

Low Cycle Fatigue Failure Modeling Approach

The LCF analysis for the ATD Disk is performed at the location identified as having the largest local total strain range and as the controlling location for LCF crack initiation life. This critical location is in the blade attachment area, and the fact that there are fifty such locations is taken into account in the failure simulation. The position of the critical location is indicated in the axial and radial cross sections in *Figures 2-23* and *2-24,* respectively. The critical location is on the downstream face and in the lower lobe.

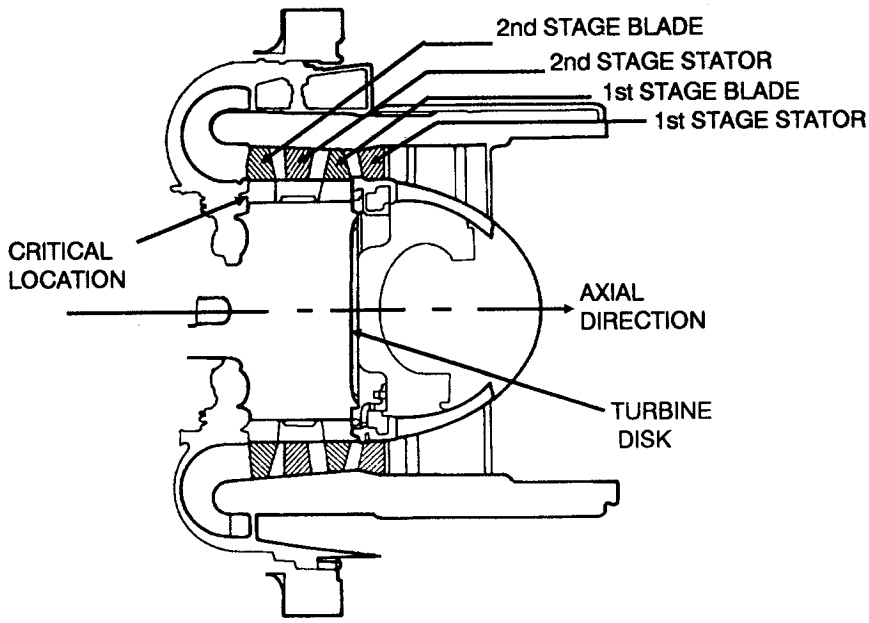

Figure 2-23 Axial Cross Section of the ATD-HPFTP Turbine Showing the Monolithic Disk

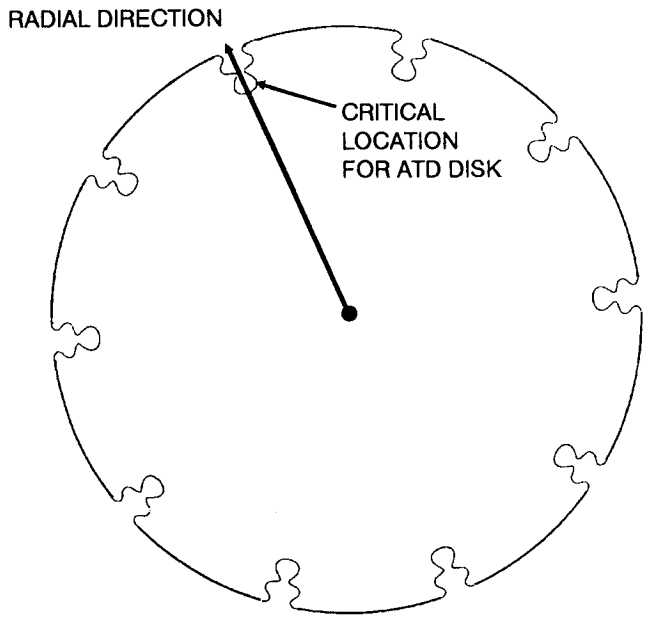

Figure 2-24 Stylized Radial Cross Section of a Turbine Disk

The strains in the disk at the critical locations are produced by mechanical and thermal stresses. The mechanical stress is due to centrifugal effects caused by blade pull and the mass of the disk itself. The thermal stress is primarily due to the radial and axial thermal gradients in the attachment area. The results of sensitivity analyses with the finite element structural and thermal models show that thermal stress is also dependent on the temperature of the disk in the attachment area.

The location of highest local total strain range is that having the largest "equivalent" elastic stress. The term "equivalent" is used because the actual material yields locally, so the peak stress is not within the elastic range. The LCF life analysis was based on a reference stress that, for a given notch stress concentration, determines the strain at the critical location. This approach is illustrated in *Figure 2-25* and will be referred to as the reference stress method. In this approach, fatigue life materials data are taken in the form of stress controlled tests of notched specimens in which the stress concentration factor at the notch of the test specimen approximately matches that of the component location being analyzed. The reference stress S_R used to relate the specimen fatigue data to the critical location of the disk is given by

$$S_R = \frac{S_E}{K_t} \tag{2-92}$$

where S_E is the equivalent elastic stress at the critical location and K_t is the local stress concentration factor. S_R corresponds to the average stress across the specimen cross

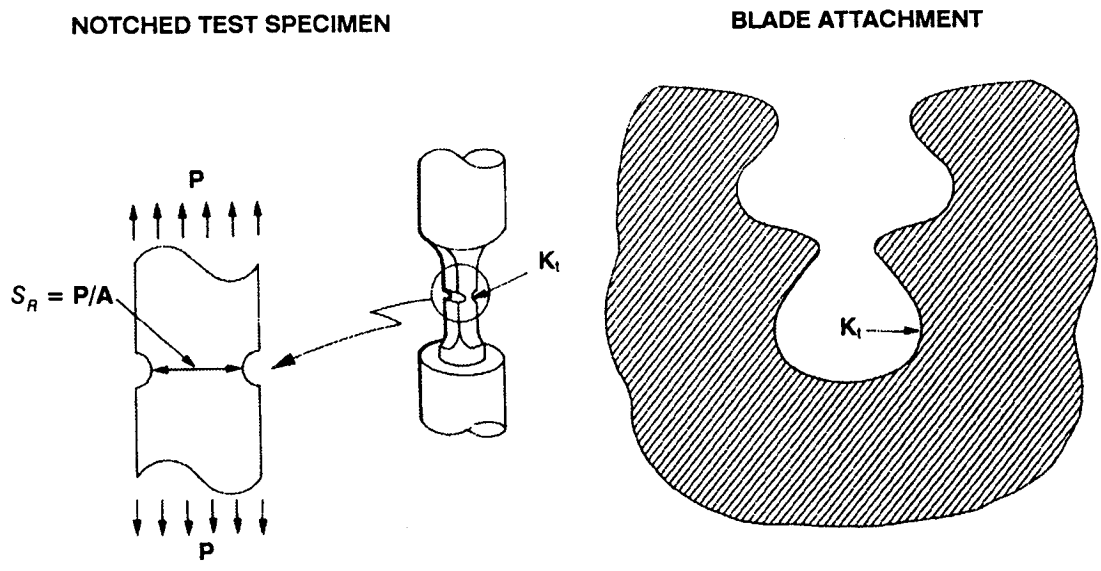

Figure 2-25 Reference Stress Method for ATD Disk LCF Life

section, as indicated in *Figure 2-25.* With fatigue data thus characterized, an elastic stress analysis can be used to predict failure at a notched location of a component.

The test specimens of the ATD Disk material were subjected to stress controlled cyclic loading with a stress ratio of $R = 0.05$. The fatigue tests were performed in 5000 psig hydrogen at room temperature. The stress field of the ATD Disk is elastic, except for a small region of plasticity at the critical location. Consequently, a linear elastic analysis can be used to determine the equivalent elastic stress. The reference stress at the critical location is then given by *Equation 2-92.*

Driver Transformation

The equivalent elastic stress can be written as the sum of mechanical and thermal components

$$S_E = S_M + S_T \tag{2-93}$$

where S_M is the total mechanical stress due to both rotor mass and blade pull, and S_T is the total thermal stress due to both thermal gradient and metal temperature.

The variation in mechanical stresses due to rotor mass S_{MM} and blade pull S_{MP} is expressed as a function of rotor speed only. This allows the combined stresses S_M due to rotor mass and blade pull to be adjusted for rotor speed variation as follows:

$$S_M(\omega) = \left(\frac{\omega}{\omega_o}\right)^2 \left[S_{MM}(\omega_o) + S_{MP}(\omega_o)\right] \tag{2-94}$$

$$= C_S(\omega)\, S_{M_o}$$

where

ω	= actual rotor speed;
ω_o	= nominal rotor speed;
$S_M(\bullet)$	= total mechanical stress;
$S_{MM}(\bullet)$	= nominal mechanical stress due to rotor mass;
$S_{MP}(\bullet)$	= nominal mechanical stress due to blade pull;
$C_S(\bullet)$	= speed variability correction factor $(\omega/\omega_o)^2$;
S_{M_o}	= nominal mechanical stress, equal to the sum of the stresses due to rotor mass $S_{MM}(\omega_o)$ and blade pull $S_{MP}(\omega_o)$.

The thermal stresses due to metal temperature and thermal gradient were found to be primarily dependent on the temperature of the hydrogen coolant supplied to the disk. Thermal sensitivity analyses were performed for three different temperature and coolant flow combinations. A coolant flow model was used to establish boundary conditions for a two-dimensional (2-D) thermal analysis to characterize the disk internal temperature field. This thermal analysis provided the two important parameters necessary to characterize the thermal stresses: the thermal gradient and the metal temperature at the critical location. Both parameters can be expressed as a function of the coolant fluid temperature. Uncertainty in both parameters is due to uncertainty in the coolant fluid temperature. The functions relating these parameters to coolant temperature are conveniently expressed in terms of deviation of the parameters from their nominal values and a coefficient derived from the sensitivity analysis. Hence, the deviation from nominal metal temperature ΔT_m, can be expressed as a function of the deviation from nominal coolant fluid temperature ΔT_f, that is,

$$\Delta T_m = C_{mf}\ \Delta T_f \tag{2-95}$$

where C_{mf} is the sensitivity of metal temperature to deviation from nominal coolant fluid temperature. Similarly, ΔG_T, the deviation from the nominal thermal gradient is also expressed as a function of the deviation from coolant fluid temperature ΔT_f, as follows

$$\Delta G_T = \begin{cases} C_{G1}\,\Delta T_f, & \Delta T_f < 0 \\ C_{G2}\,\Delta T_f, & \Delta T_f \geq 0 \end{cases} \tag{2-96}$$

where C_{G1} and C_{G2} characterize the sensitivity of thermal gradient to deviation from nominal coolant fluid temperature.

The disk internal temperature field obtained from the thermal analysis was also used to provide boundary conditions to a 2-D finite element stress analysis carried out to obtain thermal stress sensitivities. The stress due to metal temperature S_m may be related to its nominal value S_{m_o} by the parameter λ_m

$$\lambda_m = S_m / S_{m_o}.$$

And the difference $S_m - S_{m_o}$ is conveniently expressed in terms of ΔT_m by

$$S_m - S_{m_o} = C_m\,\Delta T_m$$

where C_m is the sensitivity of S_m to ΔT_m as determined by the finite element structural analysis. That is,

$$C_m = \frac{S_m - S_{m_o}}{T_m - T_{m_o}}.$$

Thus, the sensitivity of stress due to metal temperature variation is

$$\lambda_m = 1 + C_m \Delta T_m / S_{m_o}. \tag{2-97}$$

Analogously, the sensitivity of stress due to thermal gradient variation is then expressed as

$$\lambda_G = 1 + C_G \Delta G_T / S_{G_o} \tag{2-98}$$

where C_G is the variation in stress due to thermal gradient and S_{G_o} is the nominal thermal stress due to the nominal thermal gradient. The thermal gradient at the critical location is defined as the difference in metal temperatures between lobe center lines as illustrated in *Figure 2-26.*

The effects of stresses due to metal temperature S_{m_o} and thermal gradient S_{G_o} on the total thermal stress S_T are given by

$$S_T = \lambda_m S_{m_o} + \lambda_G S_{G_o} \tag{2-99}$$

Combining *Equations 2-93*, *2-94* and *2-99*, the total equivalent elastic stress becomes

$$S_E = C_S S_{M_o} + \lambda_m S_{m_o} + \lambda_G S_{G_o}. \tag{2-100}$$

The values for the nominal stresses, S_{M_o}, S_{m_o} and S_{G_o} were obtained from a NASTRAN finite element (FE) stress analysis. The blade attachment area shown in *Figure 2-26* was discretized using a finely meshed 2-D FE model. Stress was treated only as a function of disk radius r and angular position θ. However, the location of maximum S_E is not the actual critical location, since stress also depends on axial position within the disk. Thus, a second 2-D coarse mesh finite element stress analysis was performed to characterize stress in the blade attachment area with respect to radius r and axial location z, as shown in *Figure 2-27.* This second analysis was used to determine the variation with respect to axial position of stress at the radial location of maximum S_E; that is, to determine $S_d = f(z)$. A stress adjustment factor K_d was defined as the ratio of the maximum value of $S_d(z)$ to the value S_{d_o} which corresponds to the axial location at which the analysis to determine S_E was performed, thus

$$K_d = \frac{\max_z S_d(z)}{S_{d_o}}. \tag{2-101}$$

$\nabla T = (T_o - T_1)/(r_o - r_1)$
WHERE
T_o = TEMPERATURE AT CRITICAL LOCATION
T_1 = TEMPERATURE IN ADJACENT LOBE
r_o = POSTION OF CRITICAL LOCATION
r_1 = POSTION OF ADJACENT LOBE

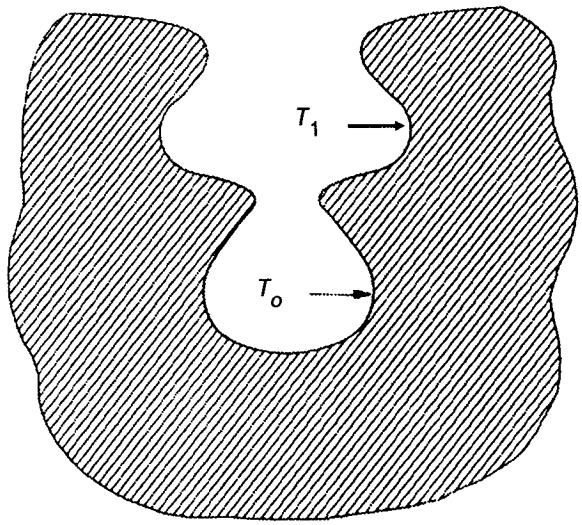

Figure 2-26 Radial Cross Section of the Disk Blade Attachment Area Illustrating the Thermal Gradient Between the Lobes

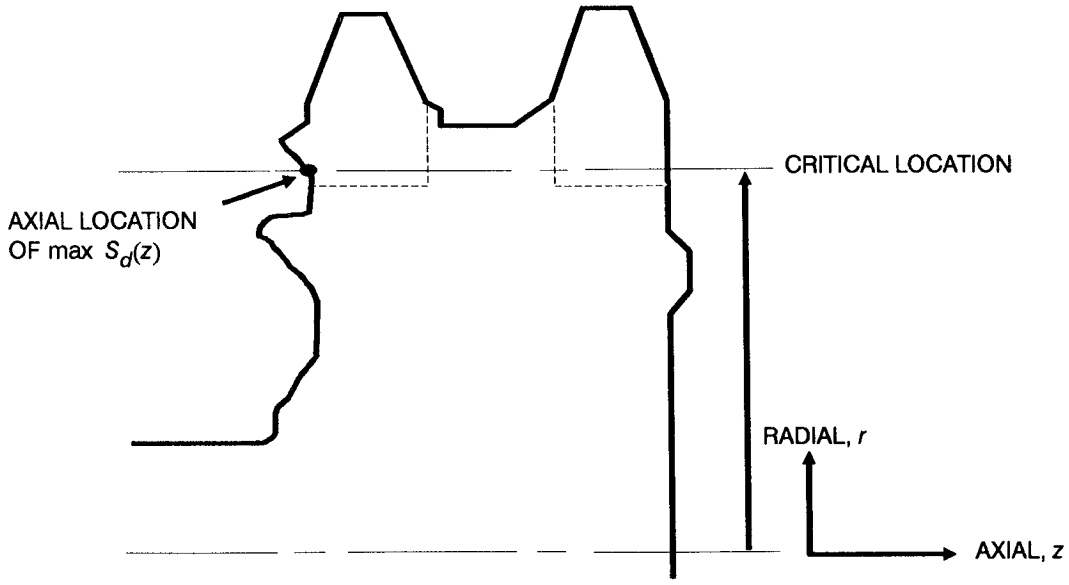

Figure 2-27 Axial Cross Section of the Disk Illustrating K_d, the Stress Factor to Adjust Axially for Two-Dimensional Analyses

The maximum value of S_d was found to occur at the downstream face of the disk. The equivalent elastic stress at the critical location is then $S_E K_d$. An uncertainty factor, λ_{K_d}, has been included in the LCF model to account for uncertainty of the K_d value.

The stress concentration factor at the critical location was determined in a separate effort using established engineering methods. According to *Equation 2-92*, the reference stress at the critical location then becomes

$$S_R = \frac{S_E K_d}{K_t} . \tag{2-102}$$

An uncertainty factor, λ_{K_t}, has been included in the LCF model to account for uncertainty of the K_t value.

The driver transformation equation for the ATD Disk can now be obtained by combining *Equations 2-100* and *2-102*, and applying the uncertainty factors for K_d and K_t. The result is the reference stress S_R given by

$$S_R = \lambda_{K_d} \lambda_{K_t} \left[C_S S_{M_o} + \lambda_m S_{m_o} + \lambda_G S_{G_o} \right] K_d / K_t \tag{2-103}$$

Mission Stress History for the ATD Disk

A representative stress-time history for the ATD Disk is shown in *Figure 2-28.* The start-up–shutdown cycle dominates the mission duty cycle because the minor throt-

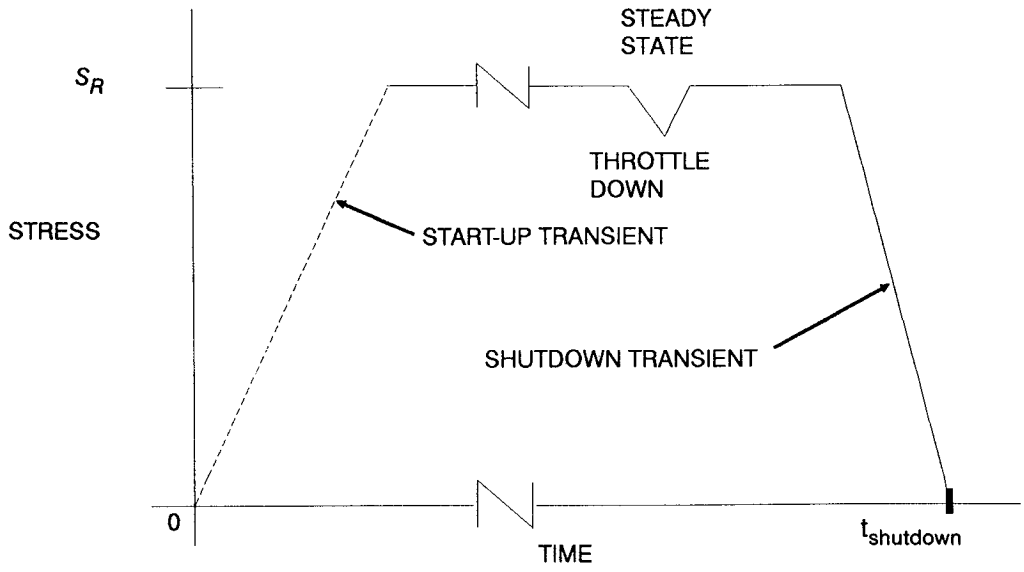

Figure 2-28 Illustration of the Stress-Time History for the ATD Disk

tle-down cycle contributes negligible damage. Note that the stress reached during steady state operation is the "peak" value of the start-up–shutdown cycle. No significant minor cycles occur during the start-up–shutdown transients. Consequently, the history can be reduced to a single stress cycle characterized by S_R. Since the fatigue life is due to one cycle only, rainflow cycle counting and Miner's rule are not required to calculate damage.

Modeling Multiple Critical Locations

The fact that only one blade attachment area is modeled by the engineering analysis while there are fifty identical blade attachment areas around the circumference of the disk must be considered. The procedure for modeling LCF failure in this case is discussed in *Section 2.1.6* and is used in the ATD Disk LCF Model.

Probabilistic Failure Model Implementation

The probabilistic failure model (PFM) for low cycle fatigue (LCF) failure of the ATD Disk generates a distribution of failure times that results from the probabilistic characterization of drivers. As shown in *Figure 2-29*, the PFM model for the ATD Disk consists of the materials model, the LCF failure simulation, the structure for selection of drivers, and the procedure for characterizing the simulated failures as a Bayesian prior failure distribution for the purpose of allowing the impact of any available disk success/failure data to be included in our characterization of the disk failure distribution. Since the current analysis is for a candidate disk, no test data is available to use Bayesian updating.

In the PFM model shown in *Figure 2-29*, ΔT_f is characterized by two Beta distributions, while ω, λ_{K_t} and λ_{K_d} are each characterized by a single distribution. The materials model provides a family of stochastic curves relating fatigue life to stress. In the outer loop, to be executed N times, the Beta distribution for ΔT_f is selected, and the materials model parameters are established. Then, in the inner loop, to be carried out n times, values of $\Delta T_f, \omega, \lambda_{K_t}$ and λ_{K_d} are drawn from their respective distributions.

Since the ATD Disk has fifty attachment areas, the appropriate realization of the stochastic stress-life curve to use in computing component life for each inner loop iteration will be that corresponding to the minimum of fifty selections of the materials model parameter, φ. See *Section 2.1.6* for further explanation. Since a Disk LCF life is calculated for each inner loop iteration, a total of Nn simulated failure times will be calculated. The disk results presented in *Section 3* were obtained using $N = 20{,}000$. Since the failure probabilities of interest are of the order 10^{-3}, only the smallest one percent of these failure times is saved and used to calculate the Bayesian Prior Distribution parameters α, β, θ. The procedure for calculating α, β, and θ is discussed in *Section 2.1.1.*

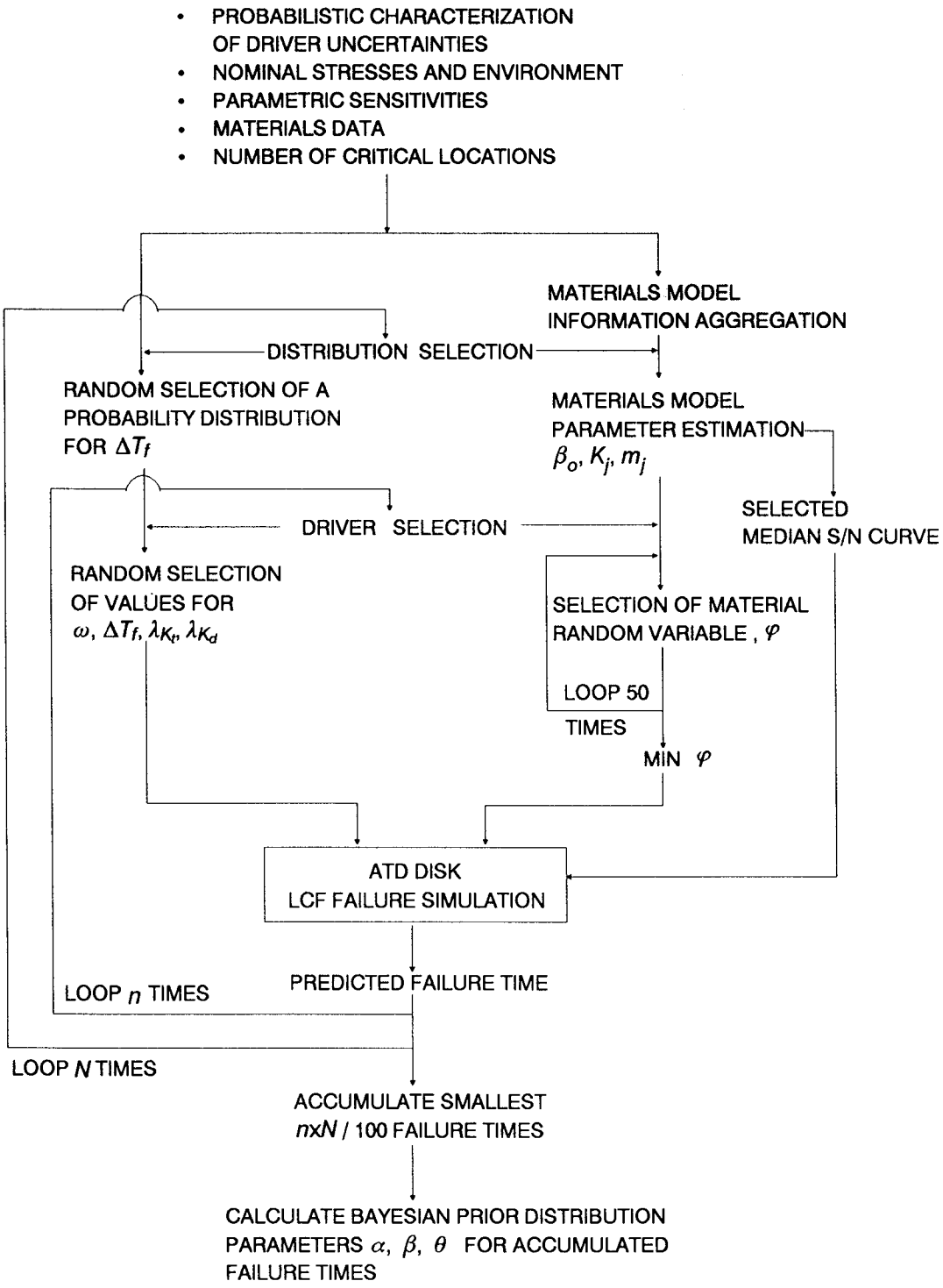

Figure 2-29 Structure of the Probabilistic Failure Model for the ATD-HPFTP Second Stage Turbine Disk

The double-loop structure allows the user to improve computing efficiency for large sample sizes. The simulation may be run in a single loop rather than a double loop by specifying a value of 1 for n. It was found that, for the driver variation used in the ATD Disk analysis with $N = 200$ and $n = 100$, the left-hand tail distribution of simulated failures was essentially the same as for a single-loop simulation with $N = 20{,}000$ and $n = 1$. The ATD Disk results presented in *Section 3.3* were obtained using $N = 20{,}000$ and $n = 1$.

The driver transformation and the fatigue life calculation used in the ATD Disk LCF failure simulation are shown in *Figure 2-30*. The driver transformation, shown in *Equation 2-103*, is performed in several steps. The first step is to calculate C_S, λ_m, and λ_G using the parametric relationships of *Equations 2-94* through *2-98*, and the values of ω and ΔT_f. Then C_S, λ_m, λ_G, the nominal stresses and the model accuracy factors λ_{K_t} and λ_{K_d} are combined using *Equation 2-103*. The result is the reference stress for the single-cycle stress history. The predicted failure time N_f is then obtained using the randomly selected S/N curve from the materials characterization model.

The probability distributions characterizing driver uncertainty in the ATD Disk PFM are summarized in *Table 2-3*. ΔT_f is characterized by two Beta distributions with the capability for assigning Uniform distributions on the hyperparameters, ρ and θ. In the ATD Disk simulation, ρ and θ were fixed at specific values, so no hyperdistributions were used. Turbopump speed is considered to be Normally distributed with fixed mean and variance. The model accuracy factors, λ_{K_t} and λ_{K_d}, are represented by Uniform distributions with fixed endpoints. The specific distributions for all drivers are discussed in *Section 3.3*.

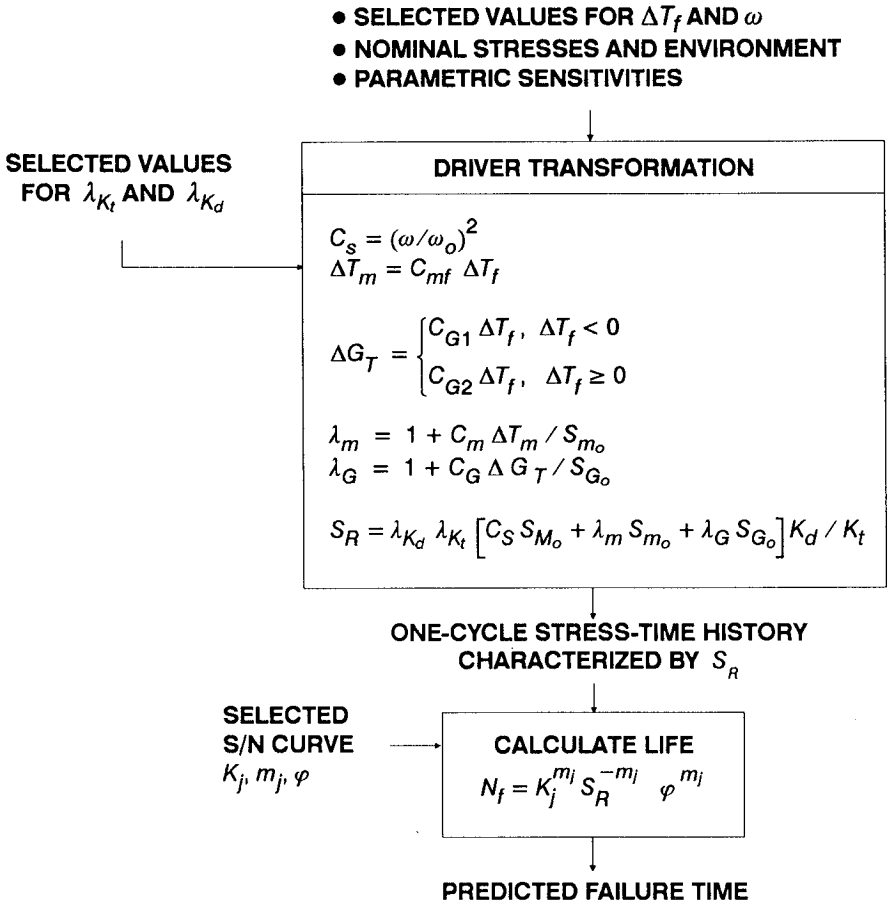

Figure 2-30 Structure of the LCF Failure Simulation for the ATD-HPTFP Second Stage Turbine Disk

Table 2-3 Driver Distributions for the ATD-HPFTP Second Stage Turbine Disk

DRIVER	DISTRIBUTION	HYPERDISTRIBUTION
ΔT_f	Two Betas	Fixed
ω	Normal	N/A
λ_{K_t}	Uniform	N/A
λ_{K_d}	Uniform	N/A

Section 2.3
Analysis Procedures

2.3.1 Introduction

The procedure for conducting a probabilistic analysis of fatigue failure modes is described here. The relevant statistical and engineering theory is given in *Sections 2.1* and *2.2*. Although the procedure is described for high and low cycle fatigue failures, the approach is general, and the procedure for analyzing other failure modes will be similar. Case studies were conducted for four SSME components to demonstrate the application of the methodology. The results of the application examples are given in *Section 3*.

The overall procedure is schematically described in *Figure 2-31*. The driver characterization and preliminary deterministic analysis steps, described in *Sections 2.3.2* and *2.3.3*, are carried out in parallel. This information is then utilized in the driver transformation step described in *Section 2.3.4*. For fatigue failure modes, the driver transformation is the mapping of the applied loads to stress or strain at the critical location.

The key step in the procedure is the formulation of the probabilistic failure model and it is described in *Section 2.3.5*. This step incorporates the driver transformation, stress or strain history, materials characterization and the damage accumulation model in a stochastic simulation structure. The failure models are often unique for a specific component geometry and failure mode, although the procedure for formulating the model and performing the failure assessment are the same. In this work, a separate program was developed for each failure model instead of developing a single general purpose program. *Sections 4, 5, 6* and *7* give a description of the programs, their user's guides, and the listings. The materials characterization and time history definition are described in *Sections 2.3.6* and *2.3.7*.

Once the probabilistic model is in place a set of abbreviated probabilistic analyses are often employed to identify and eliminate non-life controlling parameters (e.g., insignificant load components) as described in *Section 2.3.8*. This step is optional although it can save significant computational time. The calculation of the probability of failure vs. fatigue life curve is described in *Section 2.3.9*, and the driver sensitivity analysis is described in *Section 2.3.10*. The inclusion of operating experience by Bayesian updating is described in *Section 2.3.11*. Standardization of the probability of failure curve to a desired assurance level is described in *Section 2.3.12*.

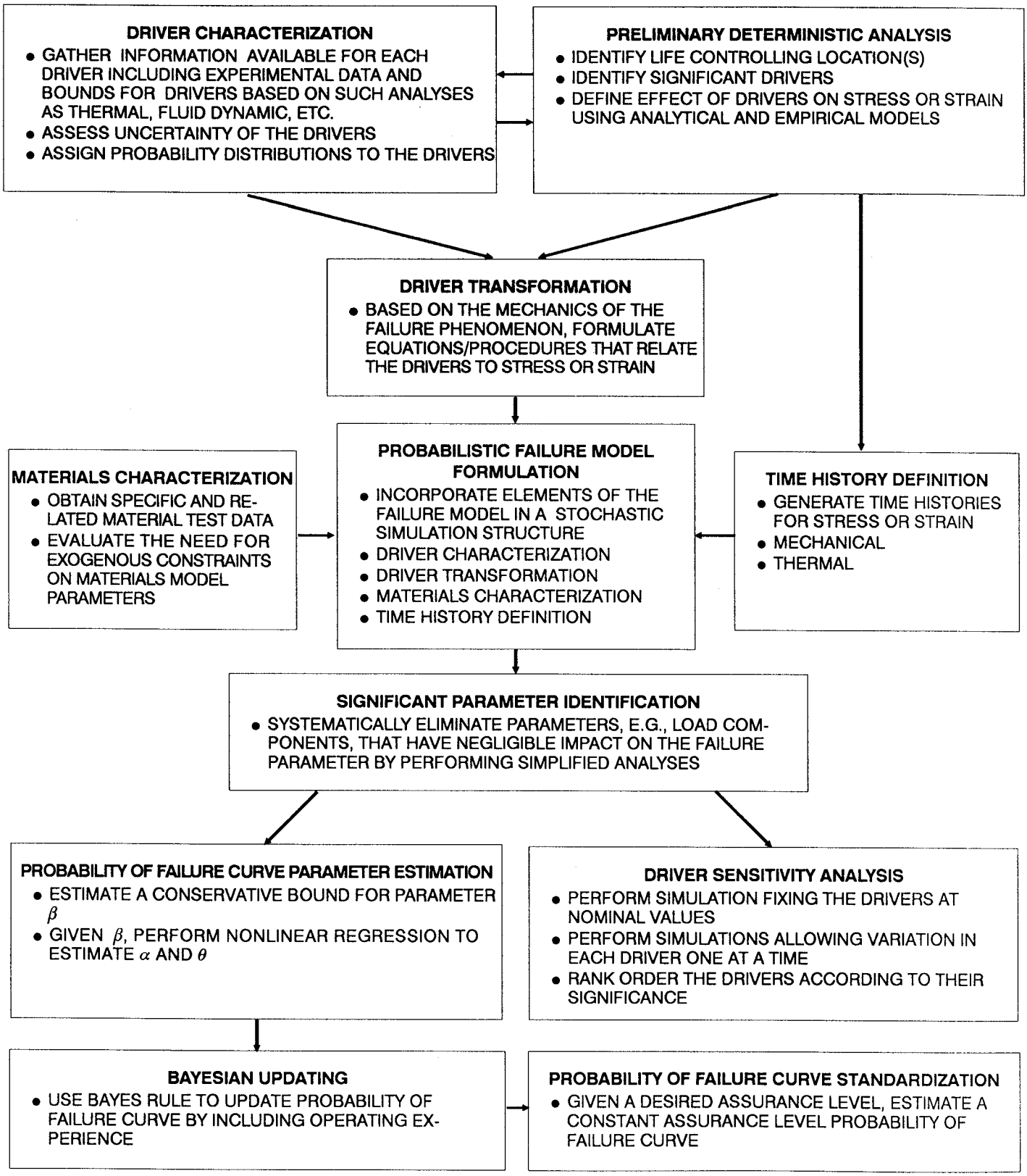

Figure 2-31 Overall Procedure for Fatigue Failure Modes

2.3.2 Driver Characterization

Deterministic engineering failure models are used to compute a failure parameter as a function of a set of inputs which are called "drivers." Those drivers which are stochastic are responsible for the probabilistic character of the PFA methodology. The need to represent a driver stochastically derives from two fundamental sources: intrinsic variability and specification error. Some stochastic drivers have intrinsic stochastic components, and drivers may have stochastic components because specification error is being represented. Specification error can be further divided into that due to engineering model accuracy and into that due to limited information and incomplete knowledge about physical parameters.

Consider the example of a finite element model used to compute stresses given input loads, material properties, and other drivers. Material properties and input loads are possible sources of intrinsic variation. The finite element model itself is a source of specification error in the computation of stresses since the model will not match the hardware precisely. Loads are often sources of specification error. There are cases where engineers know that a certain load varies very little from flight to flight or part to part, but they may only know the load magnitude within a factor of four. If such a load is computed from a phenomenological model, specification error in the load model itself and limited information about its inputs account for the need to characterize the load stochastically. Examples such as this have been encountered in case studies conducted for SSME components presented in *Section 3*.

For many stochastic drivers it is not possible to distinguish between intrinsic variation and variation due to specification error. In those cases, a stochastic driver is characterized by the compounded effect of both sources of variation without attempting to model each source separately. Examples of this are the characterization of stress concentration factors presented in *Sections 3.1.3* and *3.2.2*. There may exist heterogeneity due to manufacturing variability and that heterogeneity will also be imperfectly translated into stress concentration factor variability.

In the PFA methodology, a stochastic driver is characterized by a probability distribution over the range of values it can assume. That distribution expresses uncertainty regarding specific driver values within the range of possible values. The stochastic characterizations of drivers are inputs to the PFA simulation so that there is no restriction on specifying explicit driver probability distributions or defining a process which generates an implicit driver probability distribution.

There is no specific or required information for any driver. Drivers are characterized using the information that exists at the time of analysis. If driver information is very sparse, then the probabilistic characterization of such a driver must reflect that sparseness. If extensive experimental measurements have been performed for a

driver, its nominal value and characterization of its variability can be inferred directly from empirical data. However, if little or no directly applicable empirical data is available for a driver, engineering analysis and past experience with similar or related systems must serve for that characterization.

Drivers are fundamental in the sense that they represent parameters of direct experience for which information regarding their values can be empirically obtained. All sources of driver uncertainty must be represented in order to appropriately represent risk due to limited information. By inferring failure risk from an analysis based on the specification of failure models, drivers, and operating experience, the PFA methodology permits the assessment of reliability when the relevant data base does not exist at the higher level of direct knowledge about component reliability itself. In the PFA methodology, driver characterization is carried out according to the criterion of never overstating the available information.

Some general guidelines for characterizing stochastic drivers have emerged from case studies conducted to date. Information is typically provided by engineers experienced in the characterization of a particular driver. All sources of uncertainty must be considered, and the information used must be traceable and documented. Such information includes available driver data, related past experience, and engineering analysis. For drivers which have physical bounds such as temperature, controlled dimensions, and loads with physical upper limits, the Beta distribution parameterized with location, shape and scale parameters has been used. If only scale information is available, applying our characterization criterion results in the special case of the Beta distribution called the Uniform distribution. For a driver such as turbopump speed whose variation can be thought of as due to the combined influence of a large number of small independent effects, the Normal distribution can be used. Also, past experience in characterizing a particular driver such as a materials property may suggest the use of a particular distribution, Weibull, Normal, Lognormal, etc.

The sparseness of the information typically available for characterizing a stochastic driver and the existence of significant specification error has often led to the use of a hyperparametric structure, which is a natural format for extracting information from experienced engineers. For example, to characterize stress concentration factor uncertainty, engineering information was used to establish upper and lower bounds on the value for the stress concentration factor. In order to capture the fact that the most likely value of the stress concentration factor is not known with certainty, a Beta distribution with a Uniform distribution on the location parameter was used. This Uniform distribution is the hyperdistribution associated with the stress concentration factor uncertainty, and its parameters are the associated hyperparameters. Examples of driver characterization are given in *Sections 3.A.2.3* and *3.A.3.3*

2.3.3 Preliminary Deterministic Analysis

The component and the failure mode are selected for probabilistic failure assessment based on the criteria outlined in *Section 1*. The criteria call for preliminary deterministic analyses to identify the critical components that warrant a probabilistic failure assessment. Also, in most cases a recent deterministic stress analysis or even a deterministic fatigue analysis used for conventional design is available. Such deterministic analyses form the basis for the probabilistic failure model.

Results from deterministic stress, thermal, and fluid flow analyses may be used for driver characterization and the formulation of the driver transformation. Stress analysis including static and dynamic finite element analysis may be used to identify the high stress locations and the significant drivers that control life. Thermal and fluid flow analyses may provide bounds on temperatures, temperature gradients, pressures, etc.

Development of the probabilistic failure model may be tested by running the embedded deterministic module as a stand-alone program. Deterministic modules of the duct stress analysis software were used to identify the critical circumferential location on the tube (angle ϕ in *Equations 2-68* through *2-72*) and to rank order the force components based on their contribution to the von Mises stress and damage indices as described in *Section 2.3.8*. Examples of deterministic analysis are given in *Sections 3.A.2.2* and *3.A.3.2*.

2.3.4 Driver Transformation

The driver transformation is the mapping of the external loads to the stress or strain at the location of interest. It can be in the form of a set of analytical equations (e.g., beam bending and pressure vessel *Equations 2-68* through *2-72* for ducts), a finite element stress analysis code, or empirical relationships which relate loads to stresses (e.g., stresses from blade pull and temperature gradient in a disk given by *Equations 2-93* through *2-103*).

It is computationally inefficient and often unnecessary to include a complete finite element stress analysis procedure within a driver transformation. Instead empirical relationships or *response surfaces* may be established off-line, by performing a few finite element stress analyses with input forces, temperatures, and other drivers carefully chosen to ensure that the stress or strain responses are in the domain of interest. The response surface will be a multi-variable function; the unknown coefficients may be determined by a statistical fit of the data points generated from the finite element stress analyses. A driver may be specified to capture the level of approximation in the generated response surface.

The driver transformation may also include expressions for local stress concentration due to geometric discontinuities. For example, empirical expressions given by *Equation 2-73* were used to account for stress concentration due to weld offset in ducts. Information from relevant experimental data may be used to generate the response surface or merely to calibrate the analytical stress equations. The latter is achieved for duct stress analyses via a strain gage factor *d* in *Equation 2-56*.

2.3.5 Probabilistic Failure Model Formulation

The formulation of the probabilistic failure model is a key step in the procedure for conducting a probabilistic analysis of fatigue failure modes. This step incorporates the driver characterization, driver transformation, materials characterization, time history definition, and the damage accumulation model in a stochastic simulation structure. Failure models are often formulated for a specific component geometry and failure mode, although the procedures for formulating the models and performing the failure risk assessment are the same. Computer programs were developed for each of the three failure models presented in this publication.

The first step in formulating the probabilistic failure model is driver characterization and it includes the identification of the appropriate random number generation software modules. Modules for Uniform, Normal/Lognormal, Beta, Gamma and Weibull distributions are described in *Sections 4.4* and *7.6*. *Section 4.4* contains references to literature which gives algorithms for generating random numbers from other distributions.

The driver transformation step is described in *Section 2.3.4*. This step usually requires some computer code development, since this is where the engineering analysis for specific failure modes is used.

Materials characterization, *Section 2.3.6*, is performed using the software described in *Sections 4.1, 6.3* and *7.3*. After the materials model parameters have been established and the appropriate exogenous information has been incorporated, the appropriate code modules for materials characterization are selected. *Section 7.3.1.4* guides the analyst in this step.

Time history generation, *Section 2.3.7*, is typically performed independently of the fatigue model code by program NBSIN. Also the time histories can be obtained from test data. The failure model code must be set up to read and save the history data.

Finally, a damage accumulation model, *Section 2.2.1.4*, is incorporated if needed. Usually a module from an existing failure model program can be used with few modifications. *Section 7.1* contains the damage accumulation modules included in this publication.

2.3.6 Materials Characterization

Materials characterization is the process of using the information available to provide a probabilistic representation of materials behavior. For the HCF and LCF applications in this report, the materials characterization models described in *Sections 2.1.2.1* and *2.1.2.2* have been used. *Sections 4.1, 6.3,* and *7.3* give a description of the program, the user's guide, and the program listing. Using the stress/life formulation of the materials model, materials characterization is accomplished by means of fatigue data from tests on material specimens and by exogenous constraints on materials model parameters. Using the strain/life formulation of the materials model, materials characterization is accomplished by means of plastic and elastic strain component data from fatigue testing to failure, total strain fatigue failure data, tensile test data and, if warranted, by explicit constraints on plastic or elastic component shape parameters.

In order to implement the stress/life formulation of materials characterization, it is necessary to specify the number of life regions. That is accomplished by plotting the stress/life data on log-log paper and making a visual assessment of the number of life regions required to capture any nonlinearity in the plot. With the sparse data sets typical for these applications, no more than two life regions covering the data are feasible, and most often a single region will be adequate. If more than one life region covers the data, it is necessary to assign data to a region. While most data naturally corresponds to a particular life region, there may be a few data points near life region boundaries where the choice of assignment should be made so as to err on the side of conservatism by selecting the lower life region when a question of appropriate life region exists.

The value of exogenous constraints on materials model parameters results from the situation where there is a limited amount of usable test data. There are such cases where the procedure used to assign uncertainty to materials model parameters can allow materials curves in the simulation which violate known materials properties. Those properties, expressed as exogenous constraints, can be imposed on the model with the result that such improper materials curves will be precluded from the simulation. Examples of materials characterization are given in *Sections 3.A.2.4* and *3.A.3.4*.

2.3.7 Time History Definition

The composite stresses in HCF analysis result from a superposition of stresses induced by random vibration and periodic loads. The theoretical foundation for creating a composite stress-time history from a knowledge of the structural properties of individual processes is described in *Section 2.1.4.* A description of the program, the user's guide, and the program listing are given in *Sections 4.5, 6.6,* and *7.7.*

In order to implement the procedure in *Section 2.1.4* it is necessary to select f, the frequency used to determine the time increment; N, the number of generated values per cycle of frequency f; T, the length of the generated stress-time history; and the random number seed used to initiate the generation of the random processes described by *Equation 2-60.* Ideally, T and $f \cdot N$ are sufficiently large that the statistical properties of the stress-time history are captured by the generated values and the results of life calculations are invariant to the choice of random number seed. In practice, data storage and cost constraints require that the foregoing parameters be selected so as to meet practical constraints without sacrificing essential accuracy in life calculations.

The procedure which has been developed to accomplish this follows. $N = 10$ is sufficiently large to maintain accuracy in life calculations if f is taken to be the highest frequency associated with an individual process. If the highest frequency turns out to be associated with a process which is not significant according to the procedure described in *Section 2.3.8*, f should be taken to be the highest frequency associated with a significant individual process. The number of points generated is then given by $N \cdot f \cdot T$, so that storage constraints determine feasible values for T, given N and f. Suppose $T = 4$ seconds is the maximum value of T compatible with storage constraints. A number of stress-time histories of length 4 seconds are then generated, each based on a different initiating random number seed. It has been found to be sufficient to consider 21 alternative random number seeds. Fixing all drivers at their nominal values, the 21 corresponding values of life are calculated using the failure model for $T = 1, 2, 3$ and 4 seconds. If those lives are rank-ordered for each value of T, it is possible to select a random number seed which corresponds to a life near the median life for each value of T considered. T is then selected to be the smallest value considered for which the calculated life is close to those for higher values of T. This choice of random number seed and T minimizes the need to choose a very large value of T in order to wash out initializing effects. Although T and the random number seed have been selected on the basis of nominal driver values, their choice is robust to other decision rules, involving driver variation, which are much more costly to implement. An example of time history definition is given in *Sections 3.A.2.5*.

2.3.8 Significant Parameter Identification

This step in the procedure is optional. In some cases the identification and elimination of some insignificant input parameters may save considerable computational time. For example, in the HCF analysis of the ducts, the insignificant loads and associated reference histories were eliminated. The loads are eliminated if their contribution to damage is negligible. Calculation of the load histories and the von Mises stress, due to random and sinusoidal load sources present in SSME ducts, are given by *Equations 2-82* and *2-84*.

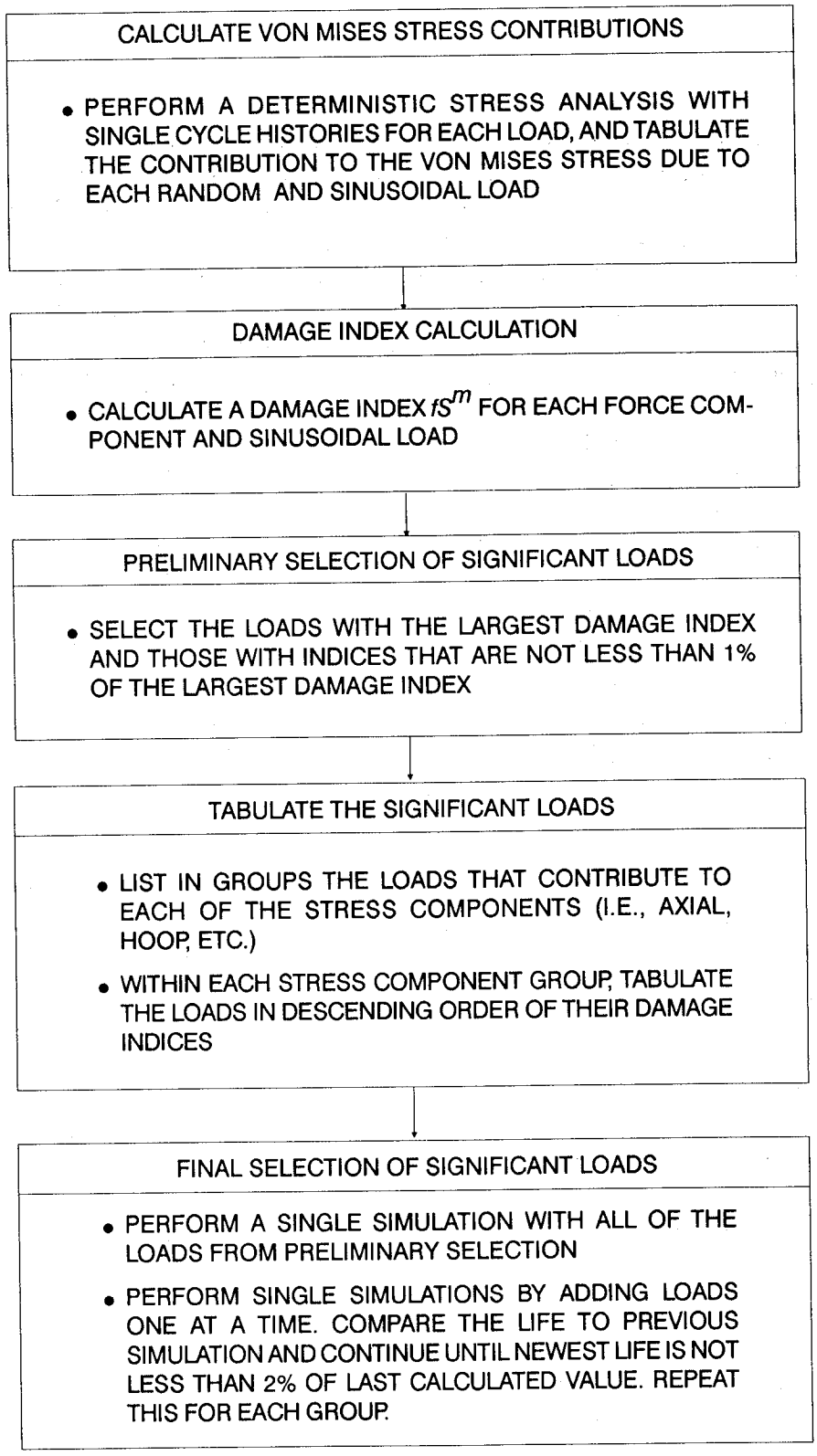

Figure 2-32 Procedure for Significant Load Identification

The significant load identification procedure is schematically shown in *Figure 2-32*. First, a deterministic stress analysis is performed with single cycle histories for the loads, and von Mises stresses due to each random and sinusoidal load are calculated. Next, a damage index fS^m is calculated for each load. The symbol f is the frequency of the load, S is the von Mises stress, and the value m is the lower bound of the shape parameter of the S/N model given in *Equation 2-11*. Then a preliminary selection of the significant loads are made. The loads with the largest damage index and those with indices that are not larger than 1% of the largest damage index are selected.

Checks are then done to ensure that none of the loads that were eliminated are in fact significant. This is done by performing single life calculations with full length load histories and calculating their impact on life while adding back the eliminated loads one at a time. However, the choice of loads to be added back is based not only on the next highest value of the damage index but also on their contribution to the individual stress components (such as axial hoop, radial and shear). To perform the check, loads are first listed in groups that contribute to a certain stress component. For example, as seen from *Equation 2-68* and *2-69*, the moment M_z contributes to the axial and hoop stress components σ_1 and σ_2 but not to the radial and shear stress components σ_3 and σ_4. On the other hand the shear force V_z contributes to only the shear stress component σ_4. The loads from the preliminary selection would be at the top of the list in each group.

The final selection of the significant loads is conducted as follows. A single simulation is performed with all the loads from the preliminary selection included. Then, single simulations are performed by adding to the selection the loads from the list in each group, one at a time. The life is compared to the previous simulation and this procedure is continued until the change in life is not greater than 2%. This is repeated for the lists in each group, retaining all the loads that have been selected so far. When this has been done for all the stress component groups, the selected loads are deemed the significant ones. An example of significant parameter identification is given in *Section 3.A.2.6*.

2.3.9 Probability of Failure Curve Parameter Estimation

The model used to represent the probability of failure as a function of service life is described in *Section 2.1.1*. Descriptions of the software, the user's guides, and the program listings are given in *Sections 4.2*, *6.4*, and *7.4*. In principle, α, β and θ can be estimated simultaneously using *Equation 2-8*. However, since we are interested in the region of high reliability (low failure probability), *Equation 2-9* suggests that an identifiability problem may occur since only two parameters are required to specify the region of extremely high reliability. Therefore, we will attempt to bound one of the parameters conservatively and estimate the other two parameters from *Equation 2-8* under that bounding constraint.

From *Equation 2-9* it can be seen that the parameter β is the slope of the failure probability – life curve in the log – log space for sufficiently small values of failure probability and life. This simple physical interpretation of β lends itself to devising procedures for bounding it. For example, if the simulated failure curve is significantly nonlinear in log – log space in the failure probability range 10^{-3} to 10^{-2}, then a subset of that data extending from10^{-3} to some value below 10^{-2} can be used to estimate a bounding value of β. Another procedure, which is less conservative, is to generate failures from a failure simulation which only considers variation in those drivers which reflect the state of knowledge concerning component capability, e.g., dimensions and materials properties. The latter procedure is only operational when the "all driver" simulation and the "capability" simulation generate failures of interest from the same life region of the S/N curve. Once a bounding value for β has been established, α and θ can be estimated from *Equation 2-10*. Examples of probability of failure curve parameter estimation are given in *Sections 3.A.2.7* and *3.A.3.6*.

2.3.10 Driver Sensitivity Analysis

The purpose of this analysis is to evaluate the drivers according to the impact of their uncertainty on the failure probability curve. The failure simulation capability provides a means to do this as desired by the analyst. We have used the following procedure for reporting on the importance of driver uncertainty across component failure modes.

A failure simulation is executed with all drivers except intrinsic materials variation set at nominal values. Then a series of simulations are performed, allowing the variation of one other driver at a time. Together with the failure simulation which was executed with all drivers simultaneously varying, these simulations provide an information set which allows for the quantification of the relative importance of individual driver variation. The impact of variation in a driver is a function of failure probability level, but the rank-order of drivers measured by that impact is independent of that level. The selection of a failure probability level is largely a matter of convenience. The impact of driver variation was measured at a failure probability level of 10^{-2} to accommodate the use of relatively small simulation sizes, of the order of 1000 replications, to accurately capture driver variation impacts.

For example, in *Figure 3-9*, variation in the driver "Damage Accumulation Accuracy" has the greatest impact on life, with the drivers "S/N Model Parameters" and "Stress Concentration Factor" having nearly the same impact. Jointly, those three drivers account for 93% of the difference between "nominal" life and "all driver" life at 10^{-2} failure probability level. Other examples of driver sensitivity analysis are given in *Sections 3.A.2.8* and *3.A.3.7*.

2.3.11 Bayesian Updating

In the region of interest, the probability of failure curve given by *Equation 2-6* is estimated by the procedures described in *Section 2.3.9* above. In order to include the impact of operating experience, we have used Bayes rule. Bayes rule changes the probability of failure curve by updating the parameters α and θ of the probability distribution of the Bayesian parameter, λ, in a Weibull failure process. The Bayesian model and consequent updating algorithms are given by *Equations 2-1* and *2-2*.

2.3.12 Probability of Failure Curve Standardization

It is desirable to standardize our results over component failure modes to a common measure of precision. The Bayesian confidence interval can be used to accomplish this. At any fixed value of life a one-sided Bayesian confidence interval on reliability can be constructed based on the distribution of λ given by *Equation 2-2*. A Bayesian confidence interval is a fixed interval which covers a random parameter. We will refer to the Bayesian confidence level as the assurance level to distinguish it from the term confidence level associated with sampling theory confidence intervals. The latter confidence intervals are random intervals which cover a fixed parameter. Both kinds of confidence levels are measures of precision for appropriate applications. The curve traced out by the Bayesian confidence interval endpoint as life varies will be called an assurance curve. Our results are reported at a 95% assurance level. That means that the probability is .95 that the reliability warranted by the information available is greater than that corresponding to the 95% assurance curve. The curve is constructed by using the known distribution of λ to find the value of λ_o in *Equation 2-5*. Given λ_o and the bounding value for β, the assurance curve is defined by $R_o = \exp(-\lambda_o N^{\beta})$. Standardized curves can be computed both before and after Bayesian updating, if desired. Examples of probability of failure curve standardization are given in *Sections 3.A.2.9* and *3.A.3.8*.

Appendix 2.A
Pictorial Example of Rainflow Counting

Preprocessing

1. Resequence

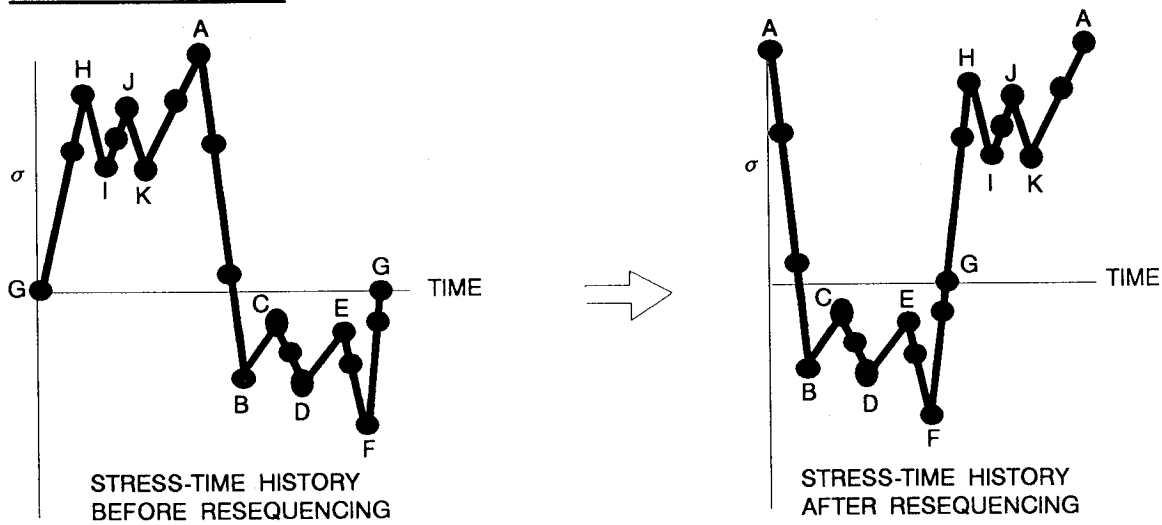

2. Filter

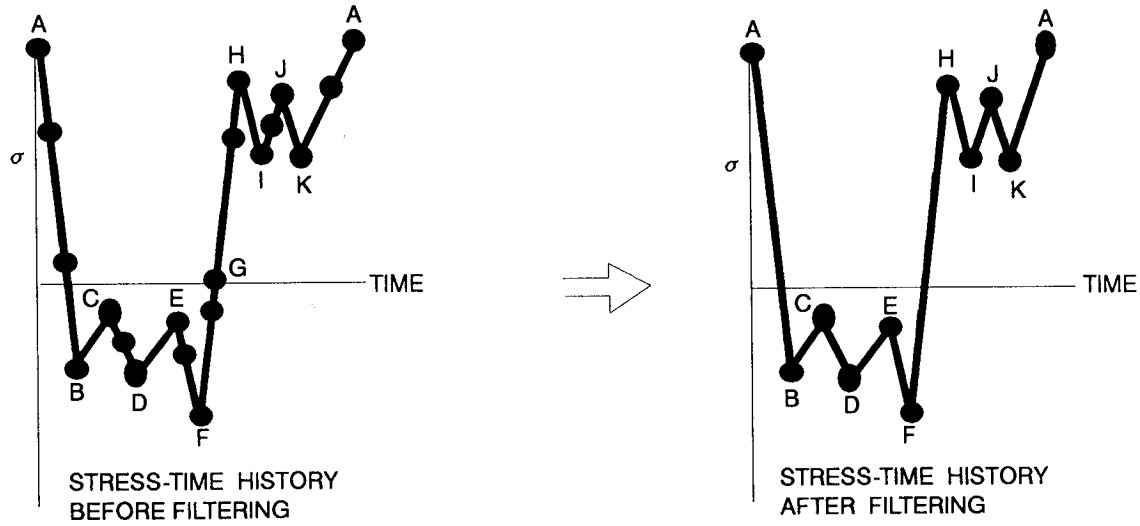

Figure 2-33 Preprocessing

Cycle Identification

3. Identify Cycle : DE

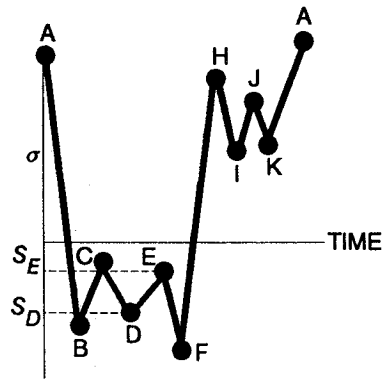

$$\text{ALTERNATING STRESS} = \frac{|S_D - S_E|}{2}$$

$$\text{MEAN STRESS} = \frac{|S_D + S_E|}{2}$$

DISCARD POINTS D AND E

4. Identify Cycle : BC

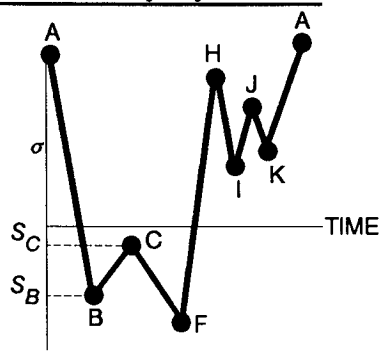

$$\text{ALTERNATING STRESS} = \frac{|S_B - S_C|}{2}$$

$$\text{MEAN STRESS} = \frac{|S_B + S_C|}{2}$$

DISCARD POINTS B AND C

5. Identify Cycle : JK

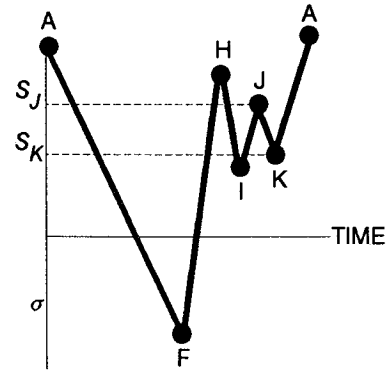

$$\text{ALTERNATING STRESS} = \frac{|S_J - S_K|}{2}$$

$$\text{MEAN STRESS} = \frac{|S_J + S_K|}{2}$$

DISCARD POINTS J AND K

Figure 2-34 Cycle Identification

6. Identify Cycle : HI

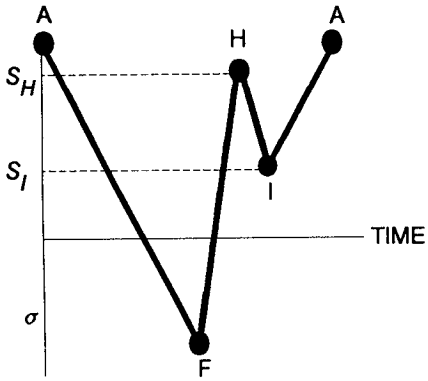

$$\text{ALTERNATING STRESS} = \frac{|S_H - S_I|}{2}$$

$$\text{MEAN STRESS} = \frac{|S_H + S_I|}{2}$$

DISCARD POINTS H AND I

7. Identify Cycle : AF

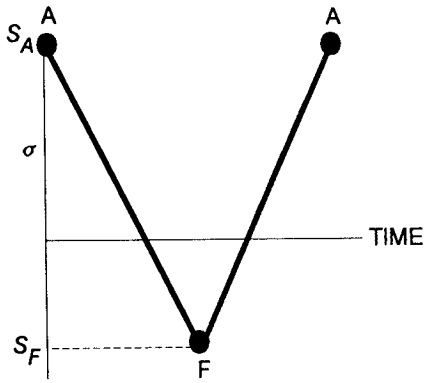

$$\text{ALTERNATING STRESS} = \frac{|S_A - S_F|}{2}$$

$$\text{MEAN STRESS} = \frac{|S_A + S_F|}{2}$$

DISCARD POINTS A AND F

Figure 2-34 Cycle Identification (Cont'd)

A total of 5 cycles were identified

Appendix 2.B
List of Symbols for Statistical Analysis

a	Beta distribution range parameter
a	Uniform distribution range parameter
A	statistical assurance that reliability is at least as large as stated
A_j	S/N curve location parameter
b	Beta distribution range parameter
b	Uniform distribution range parameter
$Be(\cdot)$	Beta distribution function
C	coefficient of variation
C, C_o	coefficient of variation of fatigue strength
f	frequency
$f(\cdot)$	probability density function
f_o	modal frequency
f_c	sinusoidal frequency
$F(\cdot)$	cumulative probability distribution function
I_o	credibility range for coefficient of variation of fatigue strength
J_o	credibility range for an S/N curve shape parameter
K_j, K^*	S/N curve location parameter
K_P	plastic strain/life curve location parameter
K_E	elastic strain/life curve location parameter
L	life of an SSME component
$L(\cdot)$	likelihood function
m_*	Bayesian posterior mean of S/N curve shape parameter

m_j	S/N curve shape parameter
m_o	Bayesian prior mean of S/N curve shape parameter
$\underline{m}$	lower bound S/N curve shape parameter constraint
$\overline{m}$	upper bound S/N curve shape parameter constraint
m_P	plastic strain/life curve shape parameter
m_E	elastic strain/life curve shape parameter
M	mission-to-mission variation damage distribution samples
$MED(\cdot)$	median value
n	inner loop simulation trials
n	number of tests
N	degrees of freedom parameter
N	outer loop simulation trials
N	fatigue life
N	number of points per cycle
$N_c(\cdot)$	random variable generated by an autoregressive process of order one
$N_s(\cdot)$	random variable generated by an autoregressive process of order one
N_j	size of the jth materials fatigue test data set
$N^*_{i,\,i+1}$	S/N curve life boundaries
$N(\cdot)$	Normal distribution function
$P(\cdot)$	Bayesian prior distribution function
R, R_o	component reliability
R	number of life regions used to represent an S/N curve
s	number of failures
$S(\cdot)$	spectral density function
S	stress
S	total strain range

S_x^2, S_y^2	sample variance
S_{xy}	sample covariance
S_P	plastic strain
S_E	elastic strain
S/N	stress/life
$t(\cdot)$	Student's *t*-distribution function
t_i	operating test duration
T	size of life distribution simulation
T	length of stress-time history
$U(\cdot)$	Uniform distribution function
$VAR(\cdot)$	Variance value
$W(\cdot)$	Weibull distribution function
x_i	fraction of life consumed in *i*th time period
x	ln (*stress*)
y	ln (*life*)
α, α'	Gamma distribution parameter
β, β_o	Weibull distribution shape parameter
γ	Euler's constant, .577....
δ	Bayesian prior distribution shape parameter for S/N curve shape parameter
η_o	Weibull distribution scale parameter
θ, θ'	Gamma distribution parameter
$\theta, \theta_1, \theta_2$	Beta distribution parameter
λ, λ_o	Weibull distribution parameter
λ	load scale factors
λ_K^*	materials process variation shift parameter
λ_N	materials process variation relative variability parameter

$\Lambda(\cdot)$	Lognormal distribution function
μ	Lognormal distribution parameter
μ	Normal distribution parameter
μ_1, μ_2	Beta distribution mean value
μ_G	average value of load scale factor indicated by strain gage data
ξ	damping coefficient
π	3.14159265 . . .
$\pi(\cdot)$	distribution function assigned to S/N curve shape parameters
π, π_1, π_2	Beta distribution peak values
ρ, ρ_1, ρ_2	Beta distribution parameters
ρ	autocorrelation coefficient
σ^2	Lognormal distribution parameter
σ^2	Normal distribution parameter
σ^2	known variance of ln (*fatigue life*) within a life-region
σ_N	standard deviation of narrow-band stresses
σ_*^2	Bayesian posterior variance of S/N curve shape parameter
$\chi^2(\cdot)$	Chi-square distribution function
ω_o	modal frequency
ω_c	sinusoidal frequency

Appendix 2.C
List of Symbols for Engineering Analysis

A	cross-sectional area of duct
C	sensitivity; C_G = sensitivity of stress due to thermal gradient; C_{G1}, C_{G2} = sensitivities of thermal gradient due to coolant fluid temperature; C_m = sensitivity of stress due to metal temperature; C_{mf} = sensitivity of metal temperature due to coolant fluid temperature
C	stress carryover factor; C_{lz} = in-plane axial stress carryover factor; C_{ly} = out-of-plane axial stress carryover factor; C_{cz} = in-plane circumferential stress carryover factor; C_{cy} = out-of-plane circumferential stress carryover factor
C_S	disk speed variability correction factor
E	Young's modulus
f_i	frequency of the ith force component
$\{F\}$	beam end force vector with elements F_i
I	cross-sectional moment of inertia of duct
K_d	2-D finite element analyses stress adjustment factor
K_t	local stress concentration factor
K_T	stress concentration factor; K_{T1} = stress concentration along axial direction; K_{T2} = stress concentration along hoop direction; K_{OFF} = stress concentration due to weld offset
L	high cycle fatigue life in seconds
M	moment; M_x = moment about x axis; M_y = moment about y axis; M_z = moment about z axis
$NLOAD$	total number of dynamic load sources
p	pressure; p_i = internal pressure; p_o = external pressure
P	axial force along x axis
Q_o	ovality stress decay factor
Q_T	torus stress decay factor
r	radial position

R	radius; R_B = elbow bend radius; R_i = internal duct radius; R_o = external duct radius; R_m = mean duct radius
R	stress ratio = $\sigma_{min} / \sigma_{max}$
S	stress; $S_d(z)$ = stress as a function of axial location z from the 2-D coarse mesh finite element stress analysis; $S_{d_o} = S_d$ at axial location of interest; S_E = equivalent elastic stress; S_G = stress due to thermal gradient; S_{G_o} = nominal stress due to thermal gradient; S_m = stress due to metal temperature; S_{m_o} = nominal stress due to metal temperature; S_M = total mechanical stress; S_{M_o} = nominal total mechanical stress; S_{MM} = mechanical stress due to rotor mass; S_{MP} = mechanical stress due to blade pull; S_R = reference stress; S_T = total thermal stress
T	length of reference time history in seconds
T_m	metal temperature; T_{m_o} = nominal metal temperature
t	wall thickness of duct; tw_1 = thickness at outside of bend; tw_2 = thickness at inside of bend; t_m = mean wall thickness
V	shear force; V_y = shear force along y axis; V_z = shear force along z axis
W_D	distance of weld from elbow tangent point
W_{OFF}	percentage weld offset for duct
z	axial position on disk
α	thermal coefficient of expansion
β	torus effect stress index
γ	stress indices for the ovality effect; γ_{lz} = longitudinal stress index due to in-plane moment; γ_{ly} = longitudinal stress index due to out-of-plane moment; γ_{cz} = circumferential stress index due to in-plane moment; γ_{cy} = circumferential stress index due to out-of-plane moment
ΔG_T	deviation from nominal thermal gradient
ΔT_f	deviation from nominal coolant fluid temperature
ΔT_m	deviation from nominal metal temperature
ΔT	temperature difference across duct wall
ε	strain

λ accuracy or uncertainty factor; λ_{OFF} = weld offset accuracy factor for duct; λ_{ST} = accuracy factor on the static load source; λ_{Di} = accuracy factor on the *i*th dynamic load source: λ_{K_d} = stress adjustment factor K_d uncertainty; λ_{K_t} = stress concentration factor K_t uncertainty; λ_{DYNstr} = dynamic stress analysis accuracy; λ_{STstr} = static stress analysis accuracy; λ_{oval} = ovality effect calculation accuracy; λ_{neu} = Neuber's rule accuracy factor; λ_{dam} = damage accumulation accuracy factor

λ sensitivity; λ_G = sensitivity of stress due to thermal gradient variation; λ_m = sensitivity of stress due to metal temperature variation

ν Poisson's ratio

ϕ angle between z axis and critical location on the circumference of the tube

σ stress; σ_1 = axial stress; σ_2 = hoop stress; σ_3 = radial stress; σ_4 = shear stress; σ_{ALT} = alternating stress amplitude; $\sigma_{Dki}(t)$ = time history for *k*th stress component due to *i*th dynamic load source; $\overline{\sigma_{Dki}}$ = non-time varying stress amplitude; σ_{EQ} = equivalent zero-mean alternating stress amplitude; $\sigma_i(t)$ = reference time history for *i*th load source; σ_k = *k*th stress component; σ_{MEAN} = mean stress; σ'_{MEAN} = adjusted mean stress; σ_N = adjusted total stress from using Neuber's rule; σ_{STk} = *k*th stress component due to static loads; σ_{TH} = thermal stress; σ_{ULT} = ultimate strength; σ_y = yield stress

θ bend angle

ω rotor speed; ω_o = nominal rotor speed

3.0 Application Examples

Section 3.1
Elbow Duct HCF Analysis

3.1.1 HPOTP Main Discharge Duct Description

The HPOTP main discharge duct supplies liquid oxygen from the high pressure oxidizer turbo-pump (HPOTP) to the main oxidizer valve and main injector oxidizer supply. *Figure 3-1* shows how the duct fits into the assembled engine. Deterministic structural analyses of the main discharge duct, performed by Rocketdyne, showed that the stresses at weld 6 are sufficiently high to control the HCF life for the component. The weld is 0.112 inches from the tangency line of the elbow. The bend radius for the elbow is 6.00 inches. The minimum wall thickness is 0.1115 inches, and the wall thickness at the bend is 0.1378 inches. The duct inside diameter is 4.00 inches. *Figure 3-2* shows this component in detail.

The HPOTP discharge duct is made of Inconel 718. The welded Inconel 718 **[1]** fatigue test data used in the JPL analysis is given in *Figure 3-3*. Twenty fatigue failure tests at – 320°F with straight and hourglass specimens were used.

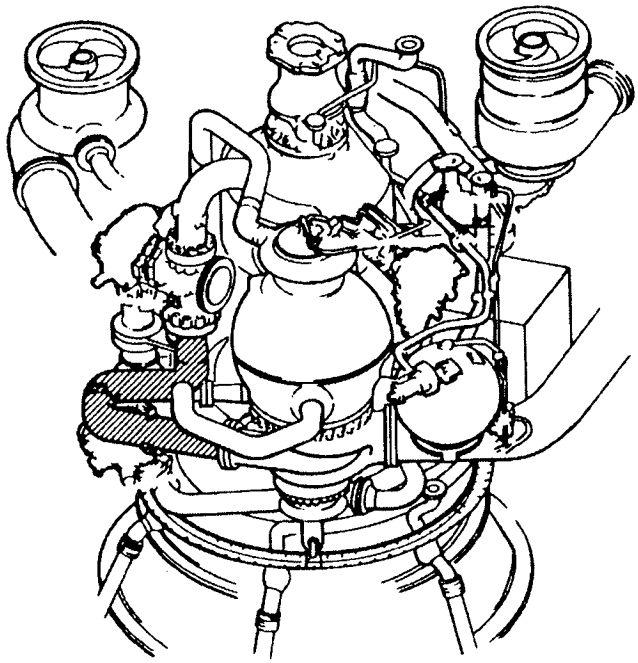

Figure 3-1 Location of the HPOTP Main Discharge Duct

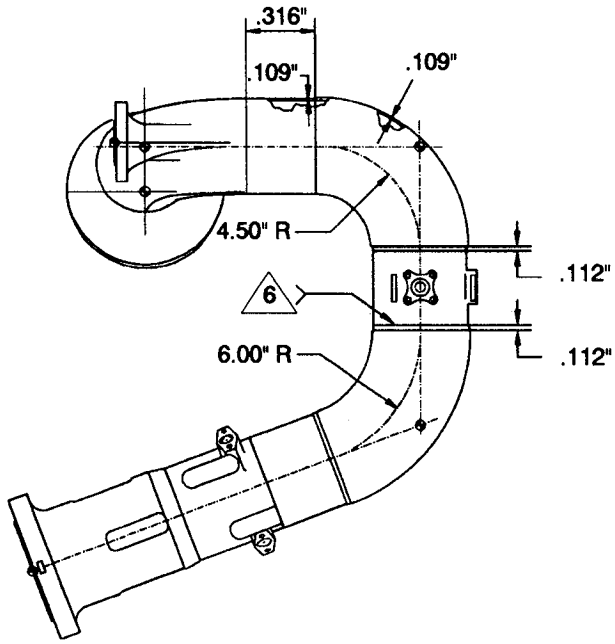

Figure 3-2 Detail of HPOTP Main Discharge Duct Near Weld 6

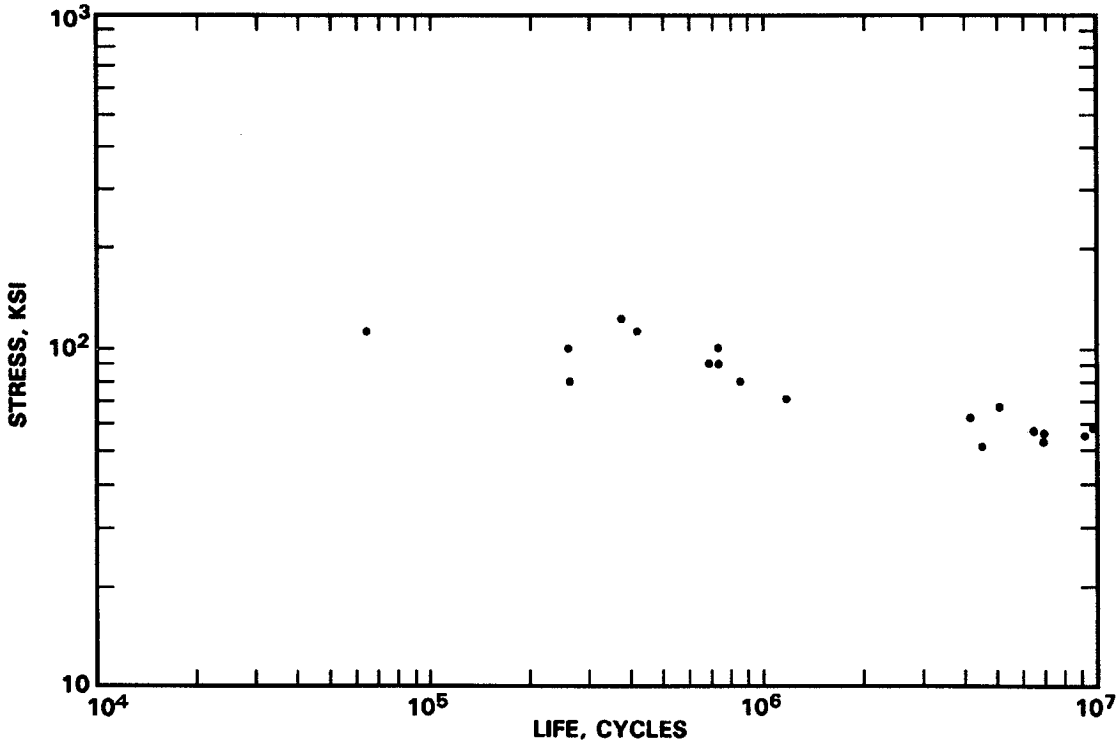

Figure 3-3 Inconel 718 Weld Data **[1]**

3.1.2 LPFTP Turbine Drive Duct Description

The LPFTP turbine drive duct carries gaseous hydrogen from the main combustion chamber coolant jacket to the turbine inlet of the low pressure fuel turbopump (LPFTP). *Figure 3-4* shows how the duct fits into the assembled engine. The life-controlling location for the drive duct was identified as weld 32 by Rocketdyne's deterministic analyses. The weld is 0.700 inches from the tangency line of the elbow. The bend radius for the elbow is 6.00 inches. The minimum wall thickness is 0.1180 inches, and wall thickness at the bend is 0.1660 inches. The duct inside diameter is 2.00 inches. *Figure 3-5* shows this component in detail.

The LPFTP drive duct is made of Incoloy 903. The welded Incoloy 903 **[2]** fatigue test data used in the JPL analysis is given in *Figure 3-6*. Twenty fatigue failure tests at 75°F, with ten smooth specimens and ten rough specimens, were used **[2]**. Two life regions divided at 10^6 cycles were used in the materials characterization model described in *Section 2.1.2.1*.

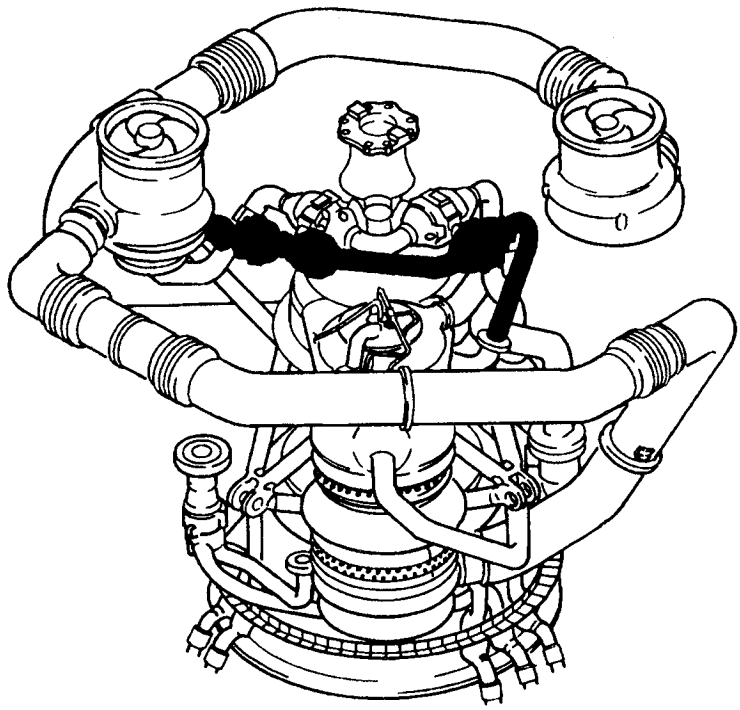

Figure 3-4 Location of the LPFTP Turbine Drive Duct

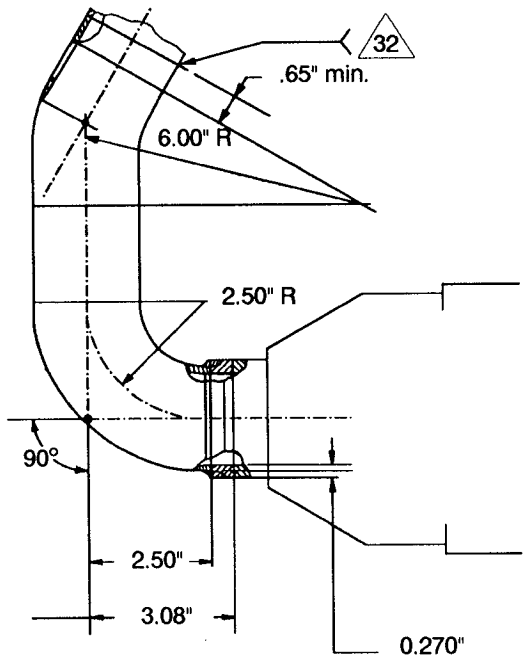

Figure 3-5 Detail of the LPFTP Turbine Drive Duct Near Weld 32

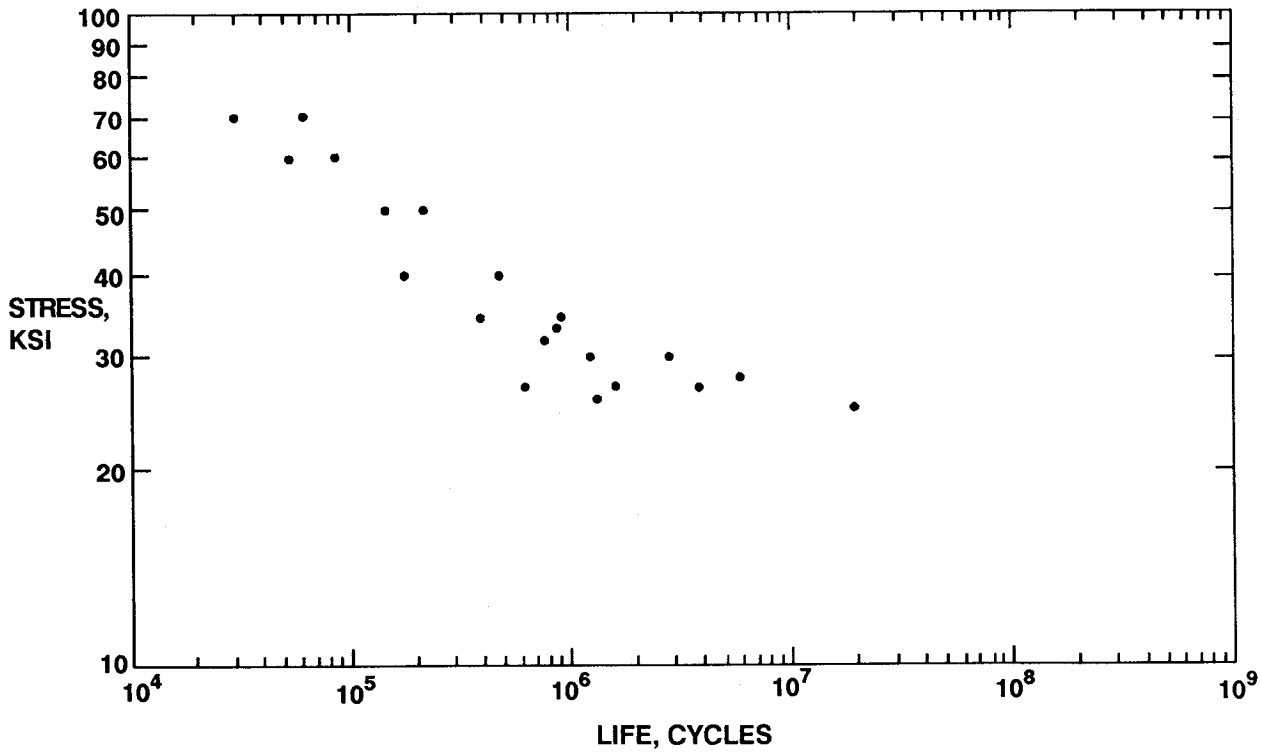

Figure 3-6 Incoloy 903 Weld Data **[2]**

3.1.3 Driver Description for Elbow Ducts

Fifteen drivers, in addition to the materials model, were used in the probabilistic HCF model for elbow ducts. The same drivers were used for the HPOTP main discharge duct and the LPFTP turbine drive duct. However, the parameters for the driver probability distributions, including the range of the driver values, differ in some cases. In particular, the loads are different for the two ducts and they are given in *Tables 3-3* and *3-4*. *Tables 3-1* and *3-2* give the drivers, their distributions, and parameters for the discharge duct and the drive duct, respectively.

Stress concentration factors due to weld surface finish and geometry effects were treated separately. The distribution for the weld stress concentration factor $K_{T_{weld}}$, which accounts for surface finish effects, was based on a consideration of the condition of the welded surface. The range of $K_{T_{weld}}$ was established from analyses of bounding expectations of the weld condition. The location analyzed on the HPOTP main discharge duct had an unflushed weld; hence, the range of the stress concentration factor $K_{T_{weld}}$ was assessed to be 1.2 to 3.5. The weld analyzed on the LPFTP turbine drive duct was flushed; hence, the range of $K_{T_{weld}}$ was assessed to be 1.05 to 1.45. The Beta distribution was used to characterize $K_{T_{weld}}$, and the Beta distribution parameter ρ was considered to be Uniformly distributed. The geometry stress concentration factor $K_{T_{geom}}$ accounts for the radius transition in the vicinity of the critical location. The range of $K_{T_{geom}}$ used in the failure simulation was 1.20 to 1.35 for both the discharge duct and the drive duct.

As discussed in *Sections 2.1.3.2* and *2.2.1.2*, the design reference loads are obtained from PSD enveloping procedures. The random and sinusoidal dynamic load adjustment factors $\lambda_{D_{RANDOM}}$, $\lambda_{D_{SINUSOIDAL}}$ were represented by Normally distributed random variables, where λ_Ds are the ratios of load to design reference load. The parameters of the distribution are the mean $\mu = 1/(1+kC)$ and the standard deviation $\sigma = C/(1+kC)$ where C is the coefficient of variation. The value of k was derived by considering the raw PSD population used in the enveloping procedure and by accounting for sample size effects using the concept of an expected coverage tolerance limit. That is, k is the value required to shift the load factor density functions so that the probability of being below the reference value is the same as the coverage. A value of $k = 2$ was used here, and *Figure 2-8* shows the probability density function for alternative values of k. The strain gage adjustment factor d was based on comparisons of the strain gage measurements from hot fire tests with the dynamic stresses from Rocketdyne's finite element (FE) analysis. The measured stresses for the discharge duct and the drive duct near welds 6 and 32, respectively, were a factor of 0.67 of the values of the predicted dynamic stresses. In order for $d/(1 + kC)$ to be 0.67 given the values for k and C, the d was set to 0.87 for random loads and 0.93 for sinusoidal loads. The static loads due to gimbaling, misalignment, and quasi-static

Table 3-1 Driver Distributions for the HPOTP Main Discharge Duct

DRIVER	DISTRIBUTION	RANGE
Weld Offset W_{OFF}	Fixed	13%, 20%, 50%
Weld Stress Concentration Factor $K_{T_{weld}}$	$\left\{\begin{array}{l}\text{Beta } (\rho, \theta) \\ \rho \sim \text{Uniform } (.087,.35) \\ \theta = 10\end{array}\right\}$	1.2 to 3.5
Geometry Stress Concentration Factor $K_{T_{geom}}$	$\left\{\begin{array}{l}\text{Beta } (\rho, \theta) \\ \rho \sim \text{Uniform } (.3,.7) \\ \theta \sim \text{Uniform } (.5,10)\end{array}\right\}$	1.2 to 1.34
Random Load Adjustment Factor $\lambda_{D_{RANDOM}}$	$\left\{\begin{array}{l}\text{Normal} \\ k = 2.0,\ C = 0.15 \\ d = 0.87\end{array}\right\}$	—
Sinusoidal Load Adjustment Factor $\lambda_{D_{SINUSOIDAL}}$	$\left\{\begin{array}{l}\text{Normal} \\ k = 2.0,\ C = 0.20 \\ d = 0.93\end{array}\right\}$	—
Static Load Adjustment Factor λ_{ST}	Uniform (.9, 1.1)	.9 to 1.1
Dynamic Stress Analysis Accuracy Factor $\lambda_{DYN_{str}}$	Uniform (.8, 1.2)	.8 to 1.2
Static Stress Analysis Accuracy Factor $\lambda_{ST_{str}}$	Uniform (.9, 1.1)	.9 to 1.1
In-plane Axial Stress Carryover Factor C_{lz}	Uniform (0.4, 0.6)	.4 to .6
Out-of-plane Axial Stress Carryover Factor C_{ly}	Uniform (0.4, 0.6)	.4 to .6
In-plane Circumferential Stress Carryover Factor C_{cz}	Uniform (0.4, 0.6)	.4 to .6
Out-of-plane Circumferential Stress Carryover Factor C_{cy}	Uniform (0.4, 0.6)	.4 to .6
Ovality Analysis Accuracy Factor λ_{oval}	Uniform (.85, 1.15)	.85 to 1.15
Weld Offset Stress Concentration Accuracy Factor λ_{OFF}	Uniform (.8, 1.2)	.8 to 1.2
Damage Accumulation Accuracy Factor λ_{dam}	Uniform (ln ¼, ln 2.59)	ln ¼ to ln 2.59

Table 3-2 Driver Distributions for the LPFTP Turbine Drive Duct

DRIVER	DISTRIBUTION	RANGE
Weld Offset W_{OFF}	Fixed	22%, 40%
Weld Stress Concentration Factor $K_{T_{weld}}$	$\left\{\begin{matrix}\text{Beta } (\rho, \theta) \\ \rho = .5, \theta = 10\end{matrix}\right\}$	1.05 to 1.45
Geometry Stress Concentration Factor $K_{T_{geom}}$	$\left\{\begin{matrix}\text{Beta } (\rho, \theta) \\ \rho \sim \text{Uniform } (.3,.7) \\ \theta \sim \text{Uniform } (.5,10)\end{matrix}\right\}$	1.21 to 1.35
Random Load Adjustment Factor $\lambda_{D_{RANDOM}}$	$\left\{\begin{matrix}\text{Normal} \\ k = 2.0, C = 0.15 \\ d = 0.87\end{matrix}\right\}$	—
Sinusoidal Load Adjustment Factor $\lambda_{D_{SINUSOIDAL}}$	$\left\{\begin{matrix}\text{Normal} \\ k = 2.0, C = 0.20 \\ d = 0.93\end{matrix}\right\}$	—
Static Load Adjustment Factor λ_{ST}	Uniform (.9, 1.1)	.9 to 1.1
Dynamic Stress Analysis Accuracy Factor $\lambda_{DYN_{str}}$	Uniform (.8, 1.2)	.8 to 1.2
Static Stress Analysis Accuracy Factor $\lambda_{ST_{str}}$	Uniform (.9, 1.1)	.9 to 1.1
In-plane Axial Stress Carryover Factor C_{lz}	Uniform (0.4, 0.6)	.4 to .6
Out-of-plane Axial Stress Carryover Factor C_{ly}	Uniform (0.4, 0.6)	.4 to .6
In-plane Circumferential Stress Carryover Factor C_{cz}	Uniform (0.4, 0.6)	.4 to .6
Out-of-plane Circumferential Stress Carryover Factor C_{cy}	Uniform (0.4, 0.6)	.4 to .6
Ovality Analysis Accuracy Factor λ_{oval}	Uniform (.85, 1.15)	.85 to 1.15
Weld Offset Stress Concentration Accuracy Factor λ_{OFF}	Uniform (.8, 1.2)	.8 to 1.2
Damage Accumulation Accuracy Factor λ_{dam}	Uniform (ln 1/4, ln 2.59)	ln 1/4 to ln 2.59

fluid loads were estimated to be within 10% of their true value; hence λ_{ST} was assigned a Uniform distribution with a range of 0.9 to 1.1.

The stress analysis accuracy factors $\lambda_{ST_{str}}$ and $\lambda_{DYN_{str}}$ account for uncertainty in the static and dynamic FE analyses, respectively. A review of FE literature and discussions with stress analysts who have compared analysis and tests indicate that a correct static FE stress analysis would calculate stresses to within 10% of the true value. Thus, the $\lambda_{ST_{str}}$ was represented as a Uniform distribution between 0.9 and 1.1. The uncertainty in the dynamic FE stress analyses were estimated to be higher and to be within 20% of the true dynamic stresses.

The straight-pipe stress equations were modified using stress indices which account for the ovality and torus effects in the elbow, as described in *Section 2.2.1.3.* The accuracy of the ovality effect calculation is taken into account by λ_{oval}. The carryover factors C_{lz}, C_{ly}, C_{cz} and C_{cy} were used to estimate the stresses at the straight-pipe elbow transition point. The carryover factors depend on relative stiffness between the straight pipe and the elbow, existence of flanges, rigidity of the welds, etc. The range of 0.4 to 0.6 for the carryover factors was estimated from detailed elbow stress analysis and experiments reported in the literature **[3, 4]**.

The weld offset was treated parametrically, i.e., the analyses were run with the discharge duct weld offset fixed at 13%, 20%, and 50% and the drive duct weld offset fixed at 22% and 40%. For the discharge duct, the weld offset of 13% is estimated to be typical, 20% is the design specification, and 50% is the worst case from the Rocketdyne structural audit **[5]**. For the drive duct, a 22% weld offset was the average and 40% was the worst case from a study of five ducts in the structural audit. As described in *Section 2.2.1.3,* an empirical relationship derived from FE stress analysis of the weld region was employed to model the stress concentration due to the weld offset. The λ_{OFF} accounts for the uncertainty in the empirical relationship used for calculating the stress increase due to the offset.

The damage accumulation accuracy factor λ_{dam} accounts for uncertainties in the linear Miner's rule, transformation of a variable amplitude stress history to constant amplitude stress cycles using rainflow counting, and the transformation of cycles at different stress ratios to equivalent cycles at a common stress ratio via the Goodman relation. Evidence in literature indicates factors of up to four between the calculated HCF life and tests. Since the life prediction is made in log life space, the distribution on λ_{dam} was cast in log space. The distribution was Uniform, and the lower bound was set at ln(1/4). In order for its mean value to be 1.0, the upper bound was set at ln(2.59).

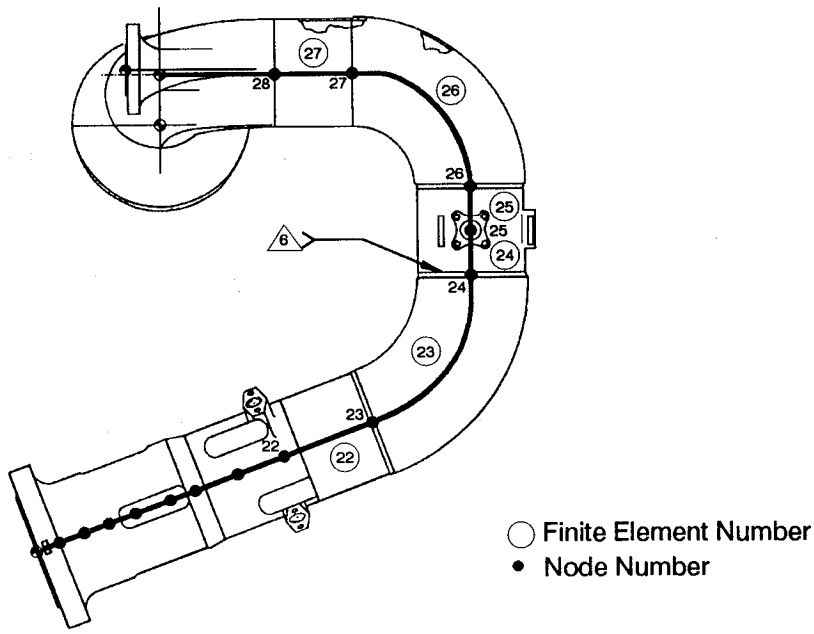

Figure 3-7 Finite Element Discretization of HPOTP Main Discharge Duct Forces Extracted from Node 24

3.1.4 HPOTP Main Discharge Duct Analysis

The program DCTHCF was used to perform the HCF analysis of the HPOTP main discharge duct. The overall description of the program is given in *Section 5.1*. The user's manual for DCTHCF, including the description of the input variables is given in *Section 6.1*. A source listing of DCTHCF is given in *Section 7.1.1*. The steps of the PFA analysis are given in *Section 2.3*.

As described in *Section 2.2.1.2*, the beam-end forces close to weld 6 were extracted from FE analyses conducted by Rocketdyne on a beam model of the discharge duct. The node and element numbers for the beam model are shown in *Figure 3-7*. The beam-end forces at node 24 are given in *Table 3-3*. The static forces were due to loads from misalignment, gimbaling, acceleration and fluid flow, and were provided by Rocketdyne as the maximum values on the duct circumference.

The R5 vibration environment given in **[6]** was employed in the random vibration (RV) and frequency response (FR) STARDYNE analyses performed by Rocketdyne. The HPOTP main discharge duct was primarily excited by R5 zone G vibration loads. Analyses were performed for excitations applied along the Y and Z directions. The RMS beam-end forces and the corresponding force velocities were extracted at node 24 from the RV analysis output. The root mean square (RMS) force magnitudes given in *Table 3-3b* are the averages of the two RMS values from element numbers 23 and 24 on both sides of node 24. The expected frequency for each force component is calculated using *Equation 2-67*. The beam-end force amplitudes were extracted for

Table 3-3 HPOTP Main Discharge Duct Beam-End Forces Near Weld 6

(a) BEAM-END FORCES FROM STATIC LOADS

P (lb)	M_X (in.-lb)	M_Y (in.-lb)	M_Z (in.-lb)	V_Y (lb)	V_Z (lb)
8120	20900	42010	42010	3805	3805

(b) BEAM-END FORCES FROM RANDOM VIBRATION ANALYSES

	P	M_X	M_Y	M_Z	V_Y	V_Z
Y-DIR						
RMS VALUE	237.7	103.4	181.2	626.2	147.5	34.08
FREQUENCY (Hz)	1306	323	420	498	1116	462
Z-DIR						
RMS VALUE	190.5	98.43	179.1	588.4	142.7	39.72
FREQUENCY (Hz)	1262	378	636	563	1197	707

(c) BEAM-END FORCES FROM FREQUENCY RESPONSE ANALYSES

FREQUENCY (Hz)	P	M_X	M_Y	M_Z	V_Y	V_Z
500	42.03	18.83	445.6	109.3	45.08	39.34
600	20.60	15.32	1.598	47.50	65.93	3.752
1000	25.71	28.35	23.27	218.1	45.83	34.09
1200	15.87	2.584	10.16	7.041	7.996	1.515
1500	63.31	1.881	4.905	57.73	30.37	79.57
2000	117.6	37.81	47.42	134.9	176.1	21.75

node 24 from the FR analyses output. The forces given in *Table 3-3c* are the sum of the amplitudes from Y and Z direction FR analyses. The force magnitudes are the averages of the absolute values of the forces on both sides of node 24.

The DCTHCF input for the HCF analysis of the discharge duct performed by JPL is given in *Appendix 3.B.1*. The input included narrow-band and sinusoidal reference time histories that were generated using the program NBSIN described in *Section 4.5*. Preliminary analyses described in *Section 2.2.1.5* were used to identify the critical circumferential position and the significant forces. The critical location was at a circumferential angle of 20° on the outside wall. The significant force components were P, M_y, M_z, and V_y, and the significant sinusoidal frequencies were 500Hz, 1000Hz, 1500Hz, and 2000Hz.

3.1.5 Results for HPOTP Main Discharge Duct

The results of failure simulations for the discharge duct are given in *Figure 3-8*. The graphs present the left-hand tails of the failure distributions for different simulations. The ordinate of these graphs is the failure probability. The abscissa of the graphs is the life of the component for HCF failure of the discharge duct. The life is given in seconds where approximately 500 seconds of exposure to this failure mode occurs during an SSME mission.

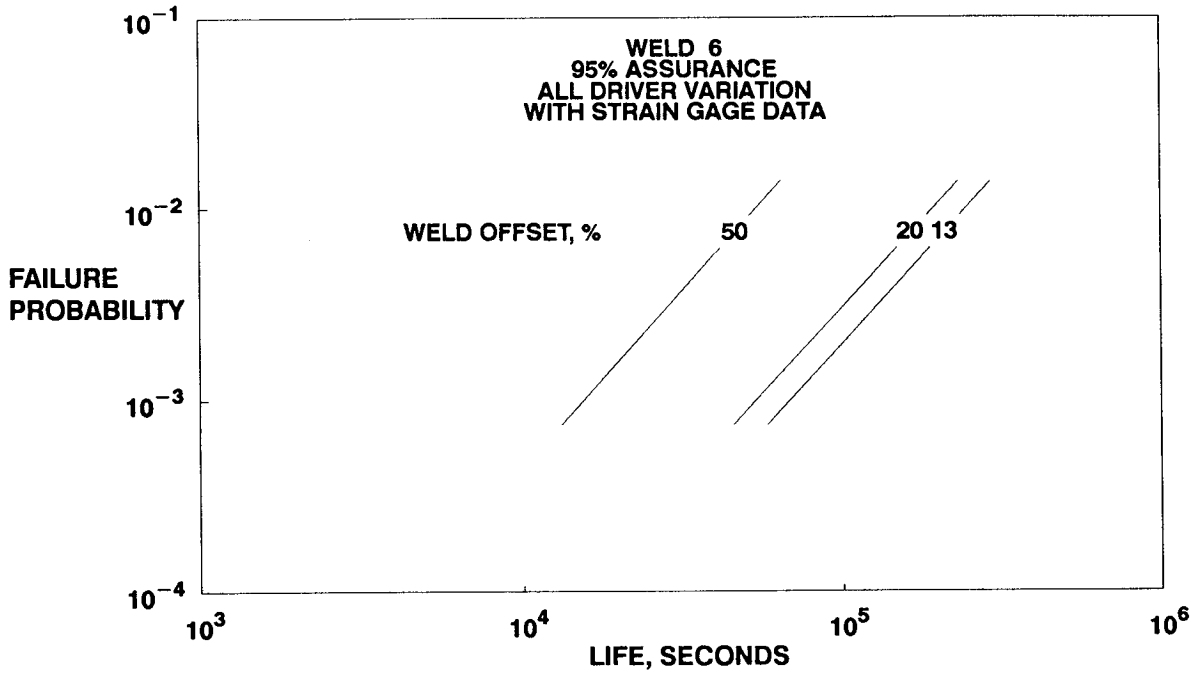

Figure 3-8 HPOTP Main Discharge Duct Impact of Weld Offset on Failure Life Distribution

Figure 3-8 shows the impact of 13%, 20%, and 50% weld offset on failure probability. The three curves are for a 95% assurance level. The meaning of a 95% assurance curve is that the failure probability at a given failure life will lie with 95% probability below that curve. For the maximum allowable weld offset of 50%, the B.1 life[1] at 95% assurance is about 30 missions. However, at a typical weld offset of 13%, the B.1 life is about 140 missions and the extrapolated B.01 life is about 40 missions.

Figure 3-9 provides the output of failure simulations for a 50% weld offset. These curves represent the direct output of the Monte Carlo simulation and are not given at a specified assurance. The right-most curve labeled "nominal" is for a simulation which included intrinsic materials variation only (see *Section 2.1.2.1*); all the other drivers were fixed at their nominal design values. The left-most curve in *Figure 3-9* is the "all driver variation" curve. The input and output files from the "all driver" analysis are given in *Appendix 3.B.1*. A measure of the relative importance of individual drivers is given in the upper left corner in *Figure 3-9*. These were obtained by finding the marginal effects of driver uncertainties on B1 lives using several sensitivity runs, where

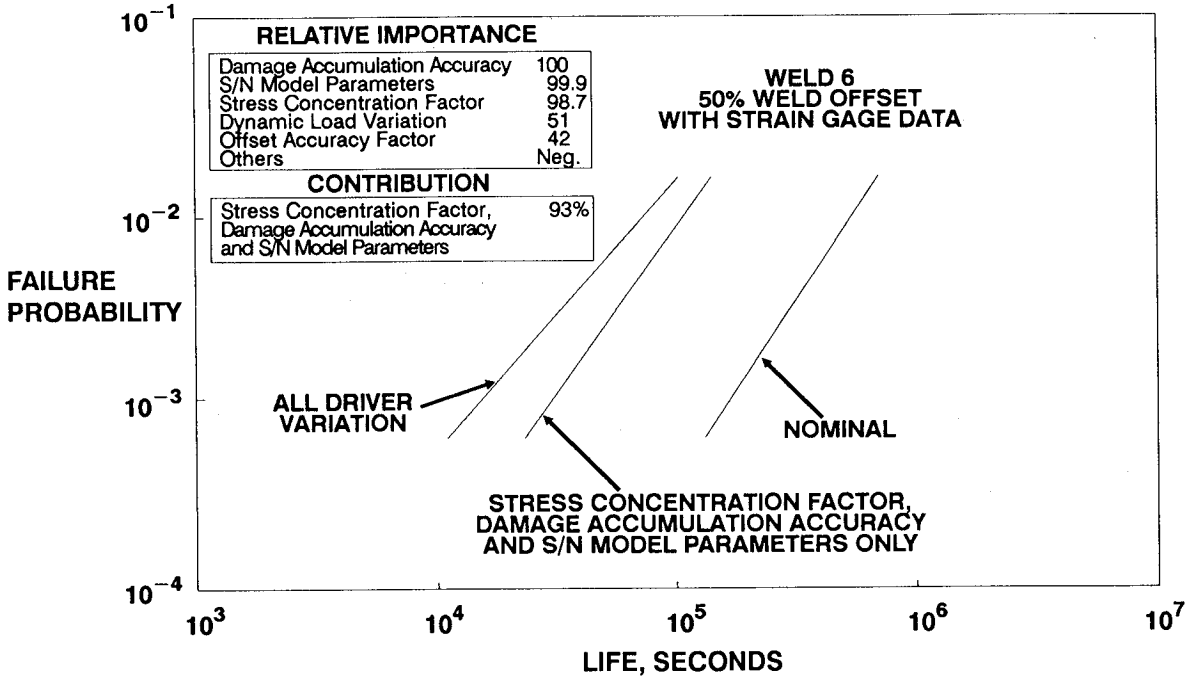

Figure 3-9 HPOTP Main Discharge Duct Failure Life Distribution and Driver Sensitivities

---

[1] A B-life is the value of accumulated operating time to failure at a failure probability specified as a percent; e.g., B.1 is the failure time at a probability of 0.001 or 0.1%.

one driver was allowed to vary while the rest were held at their nominal values. The S/N model parameters, stress concentration factor, and damage accumulation accuracy variation were the most significant drivers in this analysis, with a 93% contribution to the decrease in life. The middle curve in *Figure 3-9* shows the shift to the left due to variation only in the S/N model parameters, stress concentration factor, and damage accumulation accuracy.

Figure 3-10 may be used to demonstrate a risk-equivalent life-limiting procedure. The curves in *Figure 3-10* are the same as those in *Figure 3-8,* with the left-most curve at the 50% weld offset labeled MRB to represent a component with a weld offset that requires a material review board (MRB) action to establish a safe service life. This component may be life limited as a function of the weld offset. For example, in order to maintain reliability with 95% assurance the same for 200 missions at 13% weld offset, the MRB component must be limited to a service life of 45 missions.

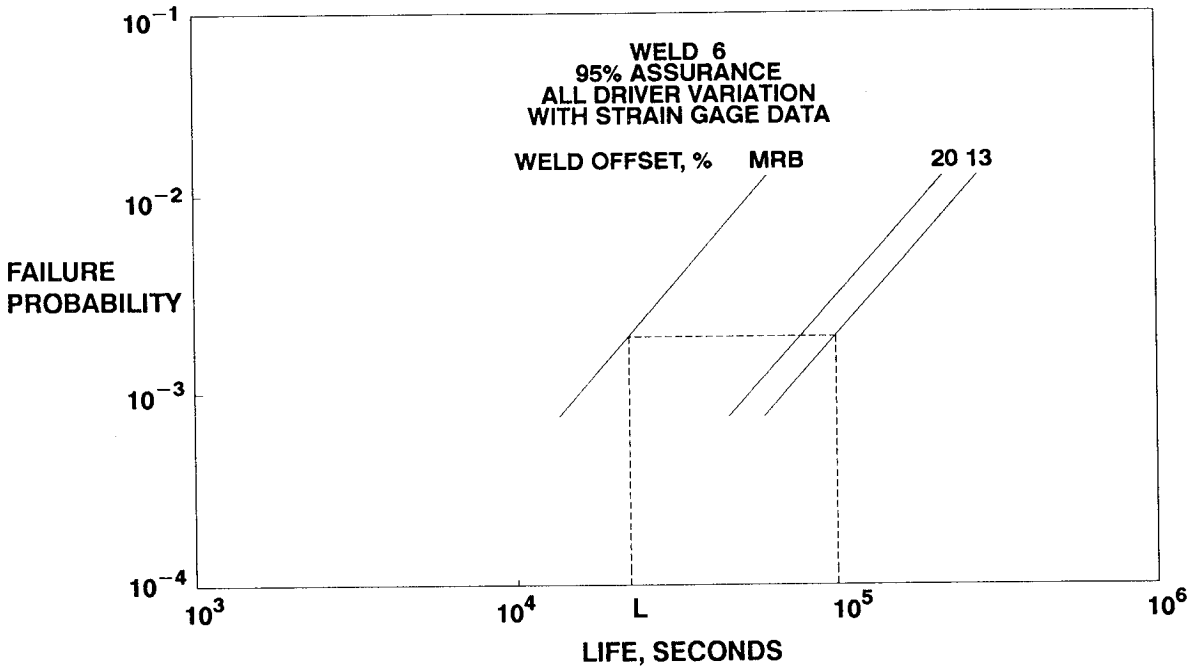

Figure 3-10 HPOTP Main Discharge Duct Risk Equivalent Life Limiting Procedure

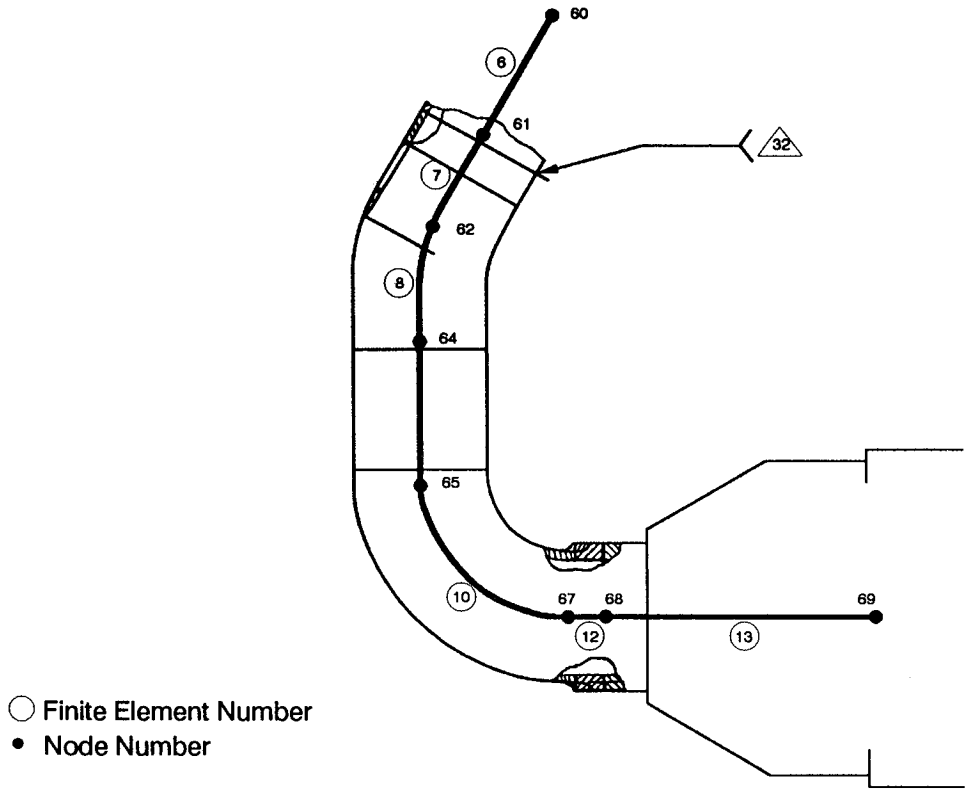

Figure 3-11 Finite Element Discretization of LPFTP Turbine Drive Duct Forces Extracted from Node 61

3.1.6 LPFTP Turbine Drive Duct Analysis

The program DCTHCF was also employed for analysis of the LPFTP turbine drive duct. The node and element numbers for the turbine drive duct beam FE model are shown in *Figure 3-11*. The beam-end forces at node 61 are given in *Table 3-4*.

The R5 vibration environment given in **[6]** was employed in the RV and FR STARDYNE analyses performed by Rocketdyne. The LPFTP turbine drive duct was primarily excited by the R5 zones A and H vibration loads. Analyses were performed for excitations applied along the X, Y, and Z directions. The RMS beam-end forces and the corresponding force velocities were extracted at nodes 61 and 62 from the RV analysis output. The P, M_x, V_y and V_z RMS force magnitudes given in *Table 3-4b* are the averages of the RMS values from element numbers 6 and 7 on both sides of node 61. However, the M_y and M_z RMS force magnitudes are the averages of the values from element numbers 7 and 8 on both sides of node 62. Similarly, the beam-end force amplitudes were extracted for nodes 61 and 62 from the FR analyses

Table 3-4 LPFTP Turbine Drive Duct Beam-End Forces Near Weld 32

(a) BEAM-END FORCES FROM STATIC LOADS

P (lb)	M_X (in.-lb)	M_Y (in.-lb)	M_Z (in.-lb)	V_Y (lb)	V_Z (lb)
2138	6820	16775	16775	1080	1080

(b) BEAM-END FORCES FROM RANDOM VIBRATION ANALYSES

	P	M_X	M_Y	M_Z	V_Y	V_Z
X-DIR						
RMS VALUE	42.74	145.4	41.68	202.7	57.69	20.30
FREQUENCY (Hz)	510	49	81	165	126	62
Y-DIR						
RMS VALUE	28.07	169.3	42.19	202.3	42.76	22.52
FREQUENCY (Hz)	910	51	96	226	365	75
Z-DIR						
RMS VALUE	16.24	152.3	68.54	126.8	28.64	26.08
FREQUENCY (Hz)	463	129	523	88	150	582

(c) BEAM-END FORCES FROM FREQUENCY RESPONSE ANALYSES

FREQUENCY (Hz)	P	M_X	M_Y	M_Z	V_Y	V_Z
270	21.91	43.91	39.48	60.54	14.91	12.88
500	78.55	1.609	0.974	73.77	4.589	0.265
540	19.62	3.359	1.339	32.92	7.498	0.721
600	166.4	0.548	4.250	189.1	22.33	0.100
810	24.16	1.043	0.753	18.55	1.769	0.285
1000	14.80	0.083	0.238	18.05	3.721	0.057
1080	11.16	1.619	6.061	8.034	2.633	0.586
1630	0.723	0.008	0.021	1.598	1.337	0.006
2000	6.768	0.137	0.395	17.00	1.566	0.200

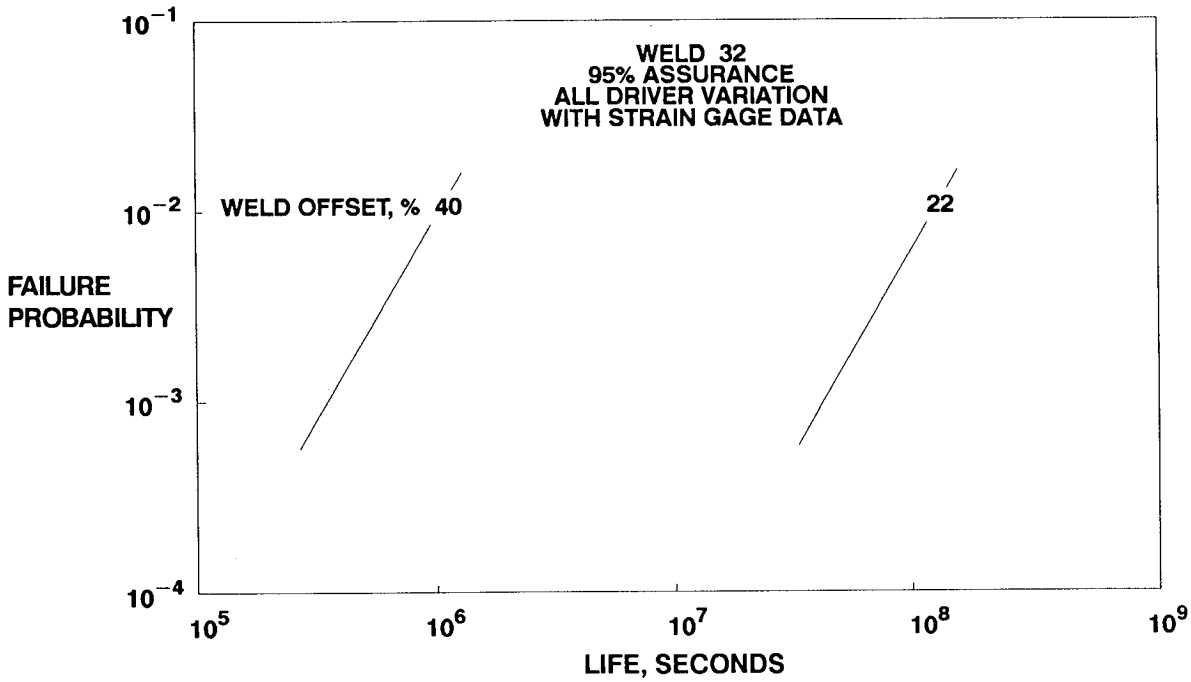

Figure 3-12 LPFTP Turbine Drive Duct Impact of Weld Offset on Failure Life Distribution

output. The forces given in *Table 3-4c* are the sum of the amplitudes from X, Y, and Z direction FR analyses.

The DCTHCF input for the HCF analysis of the turbine drive duct performed by JPL is given in *Appendix 3.B.2*. The input included narrow-band and sinusoidal reference time histories that were generated using the program NBSIN described in *Section 4.5*. Preliminary analyses described in *Section 2.2.1.5* were used to identify the critical circumferential position and the significant forces. The critical location was at a circumferential angle of 25° on the outside wall. The significant force components were P, M_x, M_y, M_z, and V_y, and the significant sinusoidal frequencies were 270Hz, 500Hz, 540Hz, 600Hz, 810Hz, 1000Hz, 1080Hz, and 2000Hz.

3.1.7 Results for LPFTP Turbine Drive Duct

The results of failure simulations for the turbine drive duct are given in *Figure 3-12*. *Figure 3-12* shows the impact of the 22% and 40% weld offset on failure probability. For a weld offset of 40%, the B.1 life[2] at 95% assurance is about 700 missions.

---

[2] A B-life is the value of accumulated operating time to failure at a failure probability specified as a percent; e.g., B.1 is the failure time at a probability of 0.001 or 0.1%.

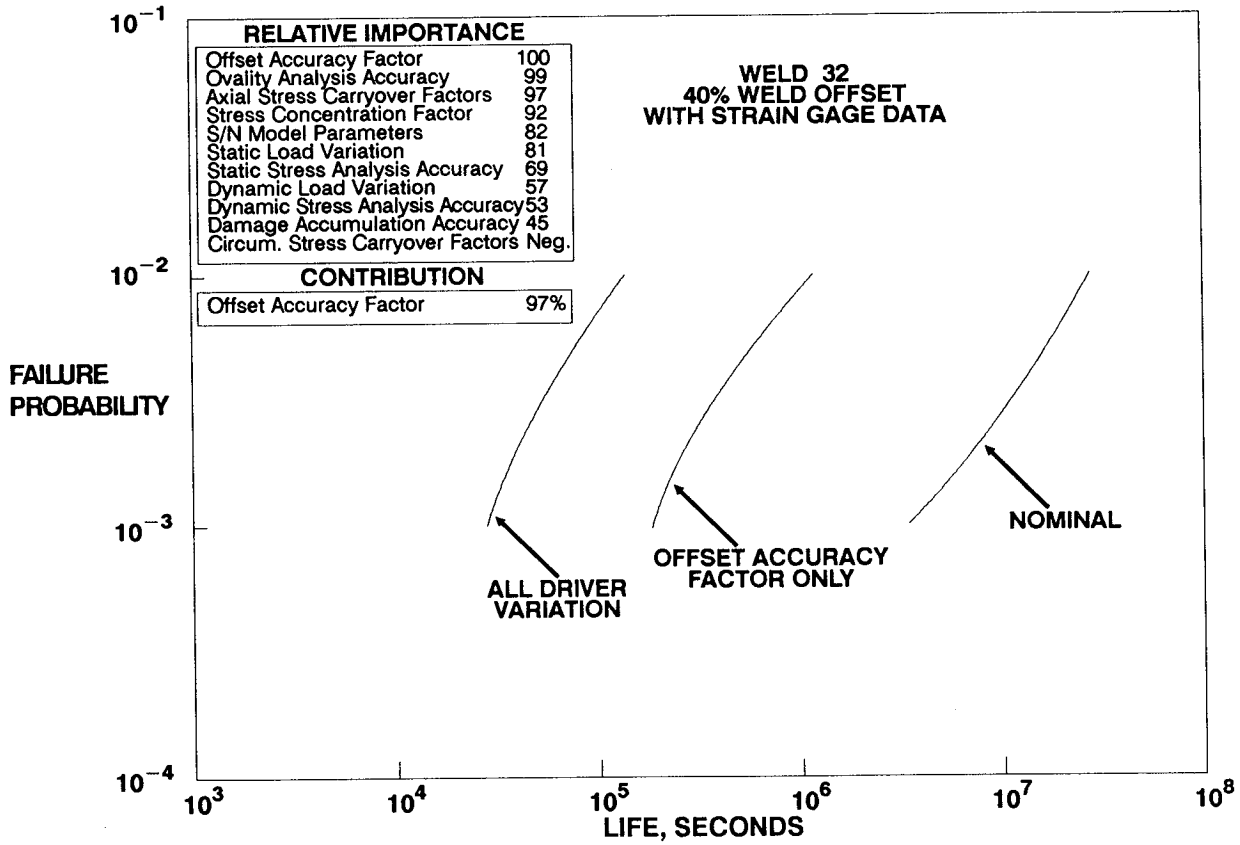

Figure 3-13 LPFTP Turbine Drive Duct Failure Life Distribution and Driver Sensitivities

However, at a weld offset of 22% the B.1 life is about 81,800 missions, and the extrapolated B.01 life is about 27,700 missions.

Figure 3-13 provides the output of failure simulations for a 40% weld offset. These curves represent the direct output of the Monte Carlo simulation and are not given at a specified assurance. The right-most curve, labeled "nominal," is for a simulation which included intrinsic materials variation only (see *Section 2.1.2.1*); all the other drivers were fixed at their nominal design values. The left-most curve in *Figure 3-13* is the "all driver variation" curve. The input and output files from the "all driver" analysis are given in *Appendix 3.B.2*. A measure of the relative importance of individual drivers is given in the upper left corner in *Figure 3-13*. These were obtained by finding the marginal effects of driver uncertainties on B1 lives using several sensitivity runs, where one driver was allowed to vary while the rest were held at their nominal values. The offset accuracy factor was the most significant driver in this analysis, with a 97% contribution to the decrease in life. The middle curve in *Figure 3-13* shows the shift to the left due to variation in offset accuracy factor alone.

Section 3.2
HPOTP Heat Exchanger Coil HCF Analysis

3.2.1 Component Description

The heat exchanger (HEX) is a coil pack installed in the oxidizer side of the hot gas manifold and is shown in *Figure 3-14*. It converts liquid oxygen tapped from the discharge of the high pressure oxygen turbopump (HPOTP) to gaseous oxygen for the vehicle oxygen tank and the POGO accumulator pressurization system. The crossflow of the hot turbine exhaust gases from the HPOTP provides the heat energy required to gasify the oxygen. The coil pack consists of a helically wound small tube approximately 30 inches long (primary tube) in series with two larger tubes, each approximately 300 inches long (secondary tubes). The tubes are made of 316L CRES stainless steel. The critical location is at weld 3 on the small tube outlet near the bifurcation joint, as shown in *Figure 3-15*. Analyses by Rocketdyne showed that weld 3 stresses control the HCF life for the HEX coil.

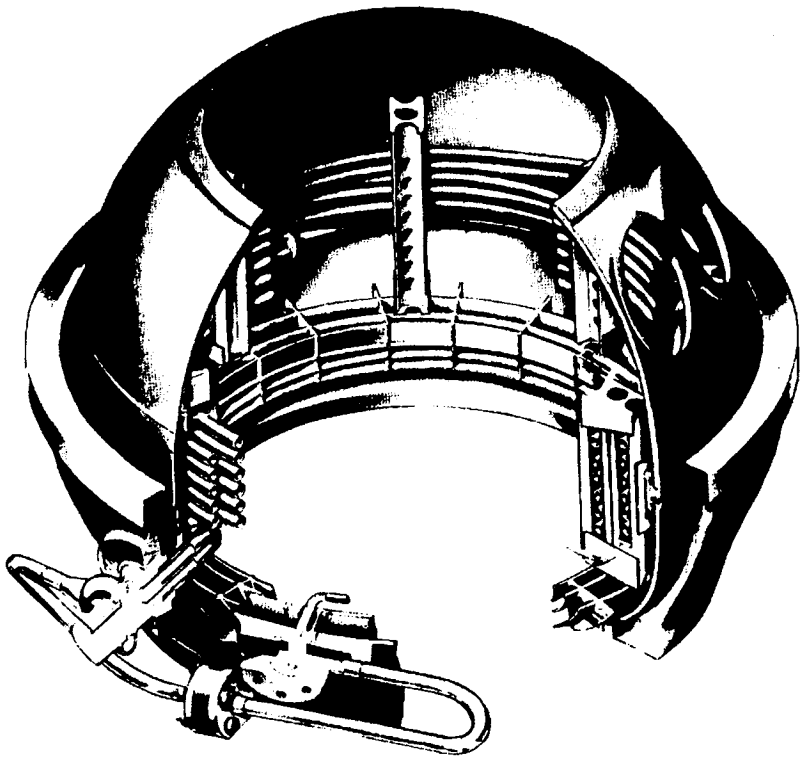

Figure 3-14 HPOTP Heat Exchanger

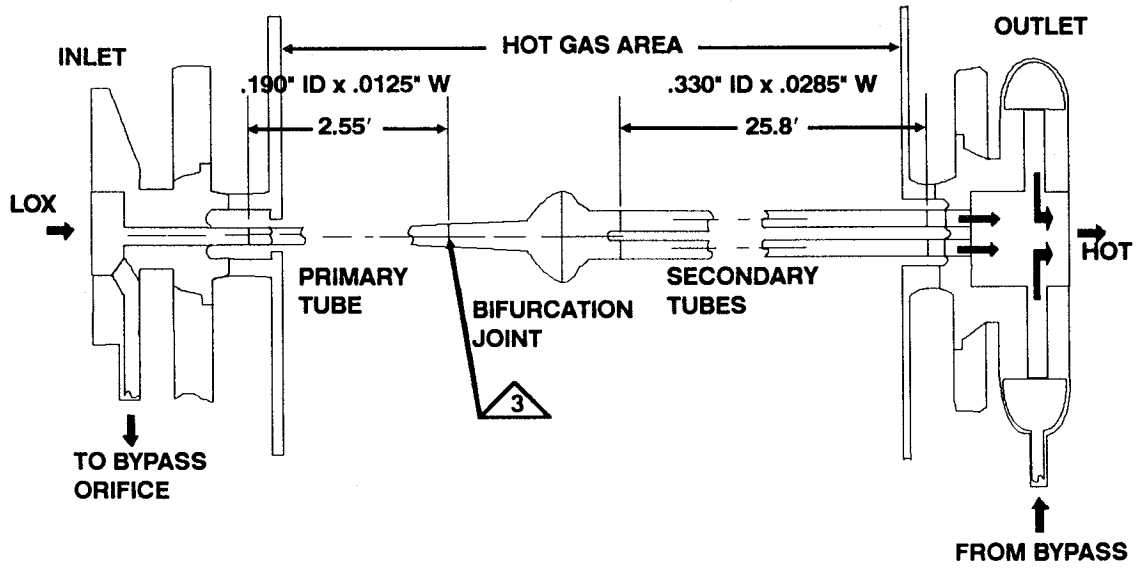

Figure 3-15 Detail of the HPOTP Heat Exchanger Coil Near Weld 3

Fatigue test data was not available for 316L CRES weld material. AISI 321 weld test data **[8]** was used in the PFA analysis as the best available proxy. *Figure 3-16* is a plot of 316L **[7]** and 321 parent material test data. The 321 weld material test data **[8]** used as a proxy is given in *Figure 3-17*. Thirteen tests to failure conducted at 70°F were used.

3.2.2 Driver Description

A total of sixteen drivers were identified which included five drivers to account for accuracy in the analyses. The list of drivers for the HEX coil HCF analysis, their distributions, and parameters are given in *Table 3-5*.

The distribution on the stress concentration factor K_T was based on the condition of the welded surface after finishing. Consideration of possible reamer gouges and the height of the offset that could remain after reaming gave K_T values in the range of 1.2 to 3.5, based on the behavior of welds determined by experiments reported in **[9]**. The driver K_T was described by a Beta distribution with a hyperdistribution for the "location" parameter ρ. The parameter ρ was assigned a Uniform distribution. This resulted in a family of Beta distributions for K_T, as illustrated in *Figure 3-18*.

The drivers may be uncorrelated or correlated with the correlation structure specified explicitly or implicitly. For many drivers there are physical reasons why they are uncorrelated. In the HEX analysis, all the drivers except the flow conditions (wall

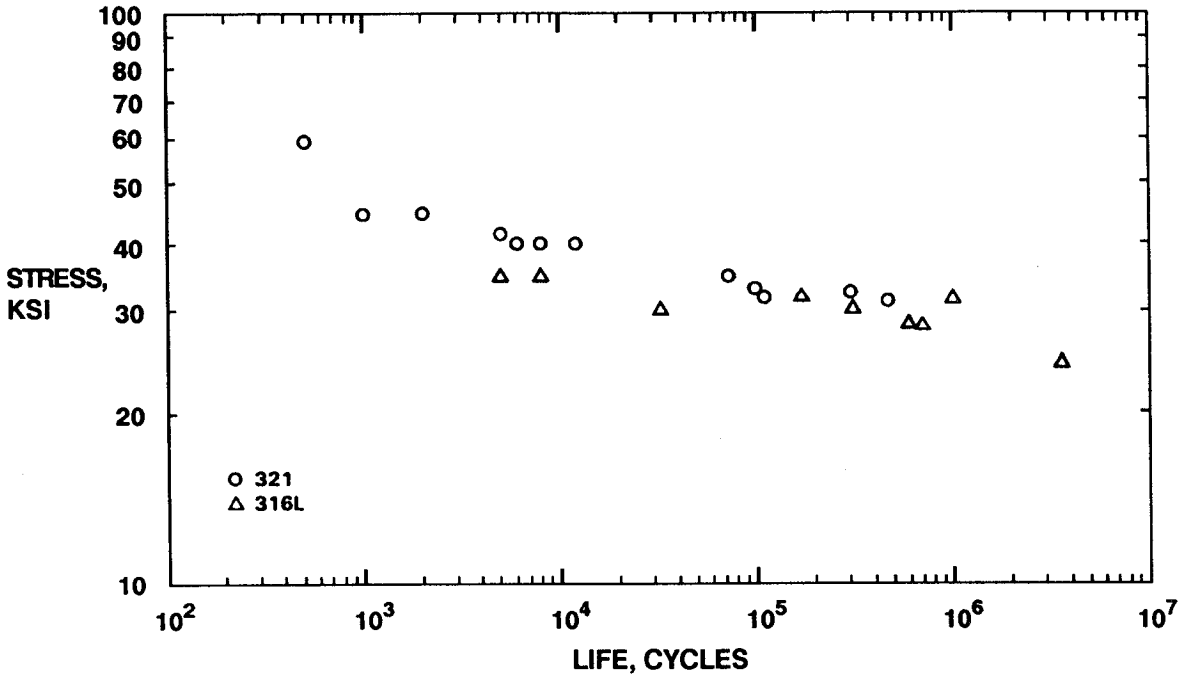

Figure 3-16 316L **[7]** and 321 **[8]** Stainless Steel Parent Material Test Data

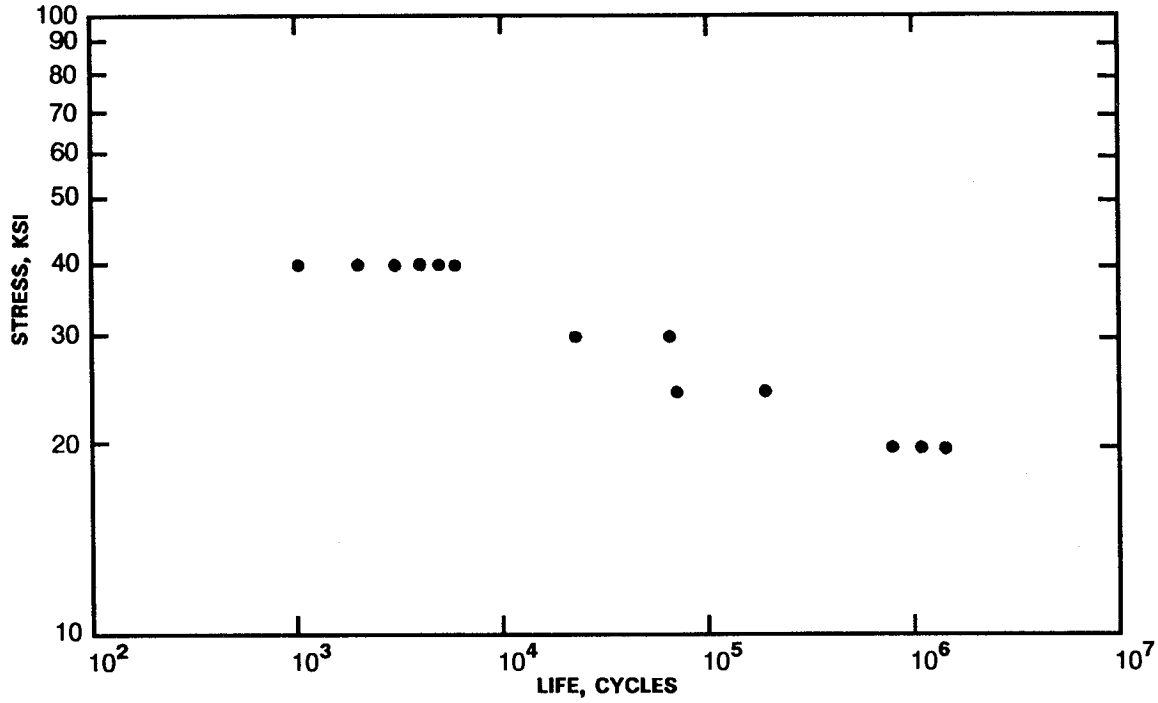

Figure 3-17 321 Weld Data Used as Proxy **[8]**

Table 3-5 Driver Distributions for the HPOTP Heat Exchanger Coil

DRIVER	DISTRIBUTION	RANGE
Weld Offset W_{OFF}	Fixed	6%, 10%, 20%
Weld Stress Concentration Factor K_T	Beta (ρ, θ) $\rho \sim$ Uniform (.13, .57) $\theta = 10$	1.2 to 3.5
Random Load Adjustment Factor $\lambda_{D_{RANDOM}}$	Normal $k = 2.0$ $C = 0.15$	—
Sinusoidal Load Adjustment Factor $\lambda_{D_{SINUSOIDAL}}$	Normal $k = 2.0$ $C = 0.20$	—
Buffeting Aero Load Factor	Uniform (.5, 1.5)	.5 to 1.5
Drag Aero Load Factor	Uniform (.8, 1.2)	.8 to 1.2
Inner Wall Temperature T_i	Normal (μ, σ^2) $\mu \sim$ Uniform (486, 666) $\sigma \sim$ Uniform (29, 56.5)	—
Outer Wall Temperature T_o	Normal (μ, σ^2) $\mu \sim$ Uniform (799, 908) $\sigma \sim$ Uniform (48, 49.5)	—
Internal Pressure p_i	Normal (μ, σ^2) $\mu \sim$ Uniform (3808, 4177) $\sigma = 69$	—
Inner Diameter D_i	Beta (ρ, θ) $\rho = .5$ $\theta \sim$ Uniform (.5, 20)	.1885 to .1915
Wall Thickness t_m	Beta (ρ, θ) $\rho = .27$ $\theta \sim$ Uniform (.5, 20)	.0113 to .0157
Dynamic Stress Analysis Accuracy Factor $\lambda_{DYN_{str}}$	Uniform (.8, 1.2)	.8 to 1.2
Static Stress Analysis Accuracy Factor $\lambda_{ST_{str}}$	Uniform (.9, 1.1)	.9 to 1.1
Damage Accumulation Accuracy Factor λ_{dam}	Uniform (ln ¼, ln 2.59)	ln ¼ to ln 2.59
Neuber's Rule Accuracy Factor λ_{neu}	Uniform (.6, 1.4)	.6 to 1.4
Weld Offset Stress Concentration Accuracy Factor λ_{OFF}	Uniform (.8, 1.2)	.8 to 1.2

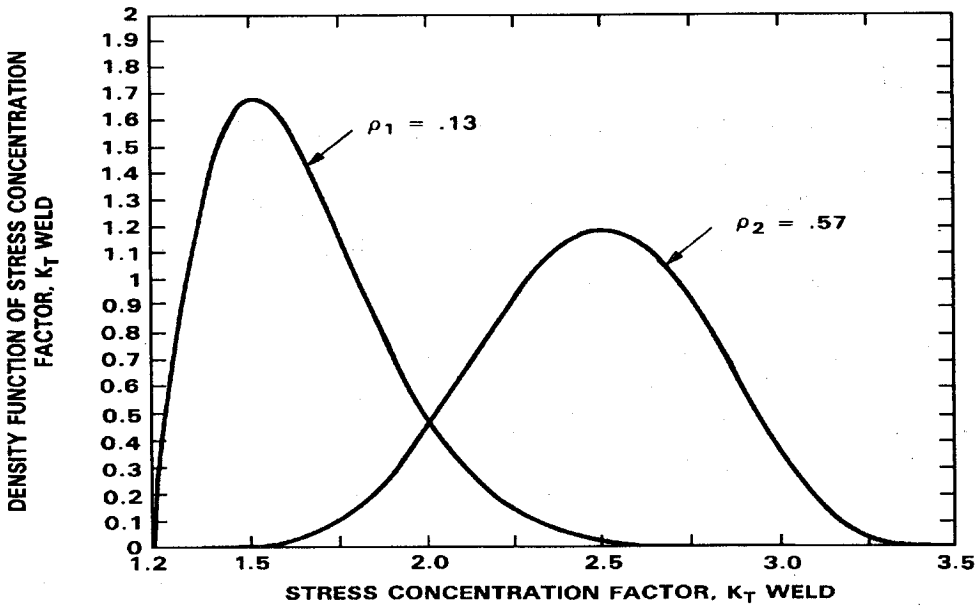

Figure 3-18 Stress Concentration Factor K_T Distribution

temperatures and internal pressure) are uncorrelated. The correlation in the flow conditions was implicitly specified in the driver transformation by requiring the inner and outer wall temperatures and internal pressure to increase and decrease according to governing physics. The inner and outer wall temperatures T_i, and T_o and the internal pressure p_i were represented by Normal distributions. The parameters of the Normal distributions were described by Uniform hyperdistributions. The ranges for the temperature and pressure drivers were derived from thermal and fluid dynamic analyses performed by Rocketdyne. The inner diameter and wall thickness were represented by Beta distributions. The ranges of these distributions were the specified manufacturing tolerances for the dimensions. The location parameter ρ ensures that the peaks of the distributions are at 0.1900 and 0.0125 for the diameter and the thickness, respectively. The Uniform hyperdistribution on θ captures the uncertainty in the shape of their Beta distributions.

The weld offset was treated parametrically, i.e., the analysis was run with the offset fixed at 6%, 10%, and 20%. The weld offset of 6% was the average from a Rocketdyne survey of ten coils, and the 10% offset was the design specification for this weld. The Neuber's rule accuracy factor accounts for the uncertainty in the calculation of the stresses when the stress vs. strain relationship is nonlinear. An accuracy range of 0.6 to 1.4 was estimated for λ_{neu}, based on energy consideration. The probability distributions for $\lambda_{ST_{str}}$, $\lambda_{DYN_{str}}$, λ_{OFF}, and λ_{dam} are the same as for the elbow ducts and are described above in *Section 3.1.3*. The parameters k and C for $\lambda_{D_{RANDOM}}$ and $\lambda_{D_{SINUSOIDAL}}$ distributions are the same as for the elbow ducts, but the strain gage factor d was set to unity for the HEX coil since available strain gage data was not applicable.

3.2.3 Analysis

The program HEXHCF was used to perform the probabilistic HCF analysis of the HPOTP heat exchange coil. The overall description of the program is given in *Section 5.1*. The user's manual for HEXHCF, including the description of the input variables, is given in *Section 6.1*. A source listing of HEXHCF is given in *Section 7.1.2*. The steps of the PFA analysis are given in *Section 2.3*.

The radius of bend for the coil was relatively large as compared with its cross-sectional dimensions. This allowed the tube to be considered as a straight pipe for the stress analysis. As described in *Section 2.2.1.2*, the beam-end forces close to weld 6 were extracted from FE analyses conducted by Rocketdyne on a beam model of the HEX coil. The node and element numbers for the beam model are shown in *Figure 3-19*. The beam-end forces at node 27 are given in *Table 3-6*. The aerodynamic loads on the coil due to flow past it were provided by Rocketdyne as the maximum static and dynamic stress values. The aerodynamic beam-end forces given in *Table 3-6a* were estimated from the stresses by assuming the coil to be a simple beam.

The R5 vibration environment **[6]** was employed for the RV and FR STARDYNE analyses performed by Rocketdyne. The HEX coil was primarily excited by the R5 zone G vibration environment. Analyses were performed for excitations applied along the X, Y, and Z directions. The RMS beam-end forces and the corresponding force velocities were extracted at node 27 from the RV analysis output. The RMS force magnitudes given in *Table 3-6b* are the averages of the RMS values from element numbers 25 and 26 on both sides of node 27. The expected frequency for each force component was calculated using *Equation 2-67*. The beam-end force amplitudes were extracted for node 27 from the FR analyses output. The forces given in *Table 3-6c* are the sum of the amplitudes from X, Y, and Z direction FR analyses.

The HEXHCF input for the probabilistic HCF analysis for the HEX coil is given in *Appendix 3.B.3*. The input included narrow-band and sinusoidal reference time histories, which were generated using the program NBSIN described in *Section 4.5*. Preliminary analyses, described in *Section 2.2.1.5*, were used to identify the critical circumferential position and the significant forces. The critical location was at a circumferential angle of 85°. The significant force components were P and M_z and the significant sinusoidal frequency was 500Hz. The aerodynamic load was also determined to be significant. The details of the HEX coil probabilistic failure assessment are given in *Section 3.A.2*.

3.2.4 HEX Coil Results

The results of the failure simulations for the HEX coil are given in *Figures 3-20* and *3-21*. The graphs present the left-hand tail of the failure distribution for different

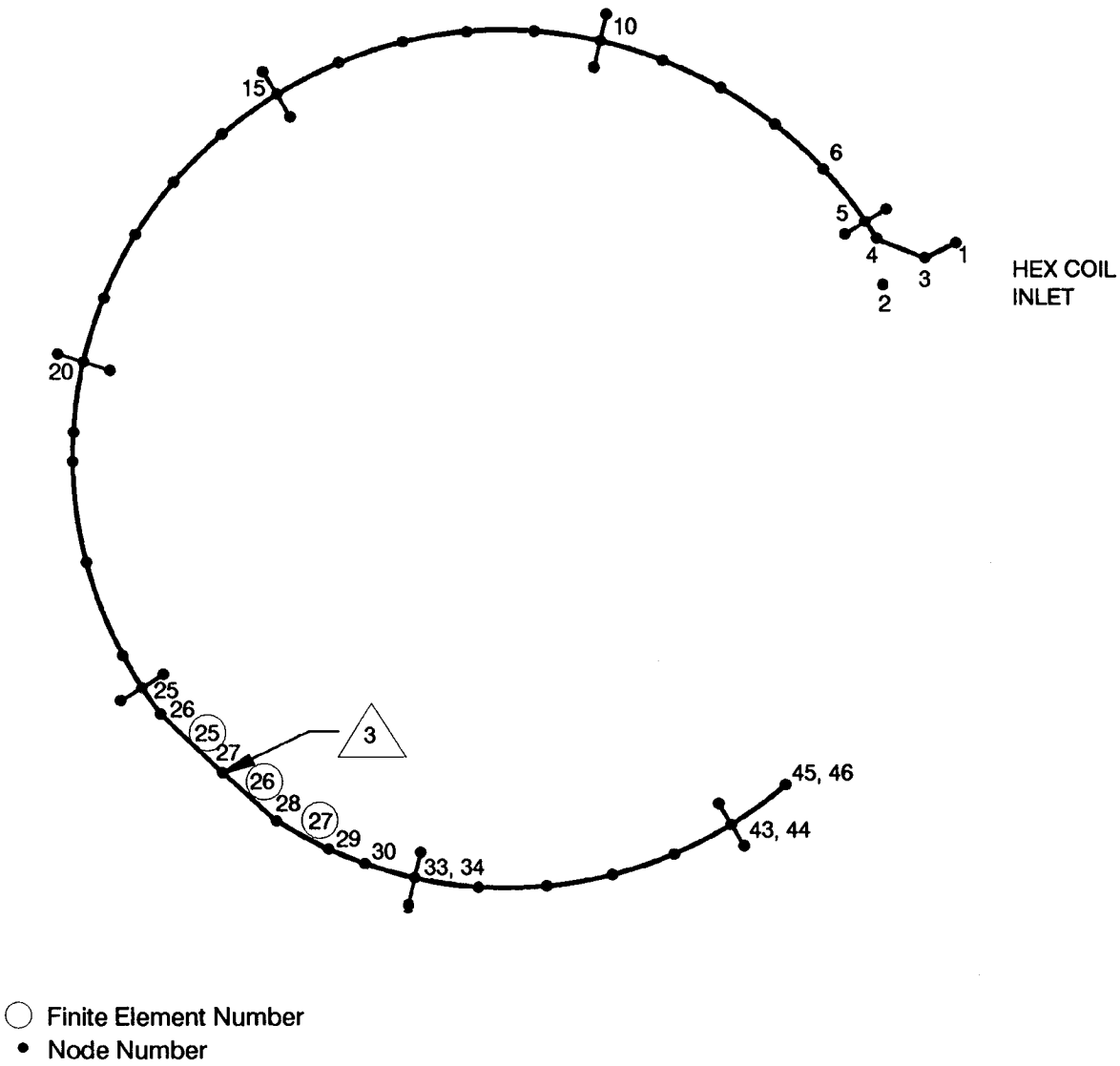

Figure 3-19 Finite Element Discretization of HPOTP Heat Exchanger Coil-Forces Extracted from Node 27

Table 3-6 HPOTP Heat Exchanger Coil Beam-End Forces Near Weld 3

(a) BEAM-END FORCES FROM AERO LOADS

	P (lb)	M_x (in.-lb)	M_y (in.-lb)	M_z (in.-lb)	V_y (lb)	V_z (lb)
STATIC	0.000	0.000	- 0.072	0.000	0.000	0.000
DYNAMIC 1780 Hz	0.000	0.000	0.000	0.072	0.000	0.000

(b) BEAM-END FORCES FROM RANDOM VIBRATION ANALYSES

	P	M_x	M_y	M_z	V_y	V_z
X-DIR						
RMS VALUE	0.857	0.001	0.004	0.141	0.259	0.019
FREQUENCY (Hz)	236	634	424	386	740	358
Y-DIR						
RMS VALUE	0.621	0.004	0.009	0.355	0.627	0.016
FREQUENCY (Hz)	840	800	275	320	1040	1011
Z-DIR						
RMS VALUE	0.041	0.014	0.050	0.007	0.049	0.643
FREQUENCY (Hz)	1404	1018	1224	1336	1392	1394

(c) BEAM-END FORCES FROM FREQUENCY RESPONSE ANALYSES

FREQUENCY (Hz)	P	M_x	M_y	M_z	V_y	V_z
500	0.270	0.003	0.010	0.205	0.348	0.052
600	0.070	0.002	0.005	0.015	0.035	0.038
1000	0.126	0.003	0.007	0.024	0.127	0.035
1500	0.077	0.003	0.019	0.019	0.144	0.307
1800	0.024	0.0003	0.0002	0.003	0.035	0.0007
2000	0.074	0.0009	0.003	0.009	0.099	0.077

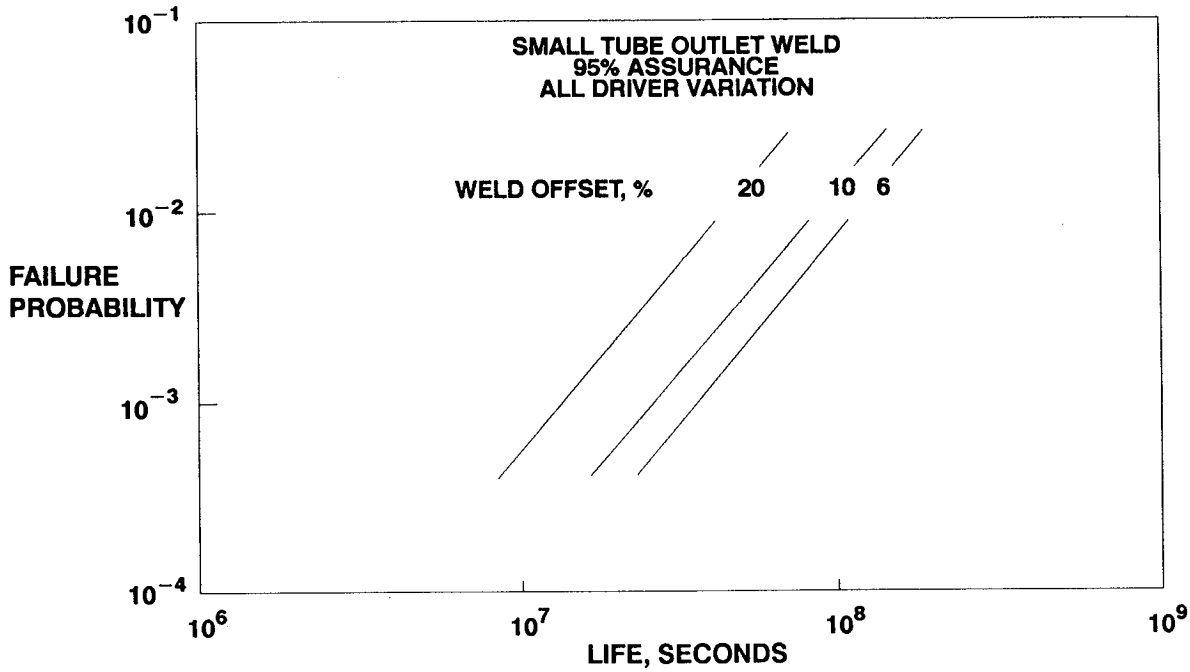

Figure 3-20 HPOTP Heat Exchanger Impact of Weld Offset on Failure Life Distribution

simulations. The weld offset was treated parametrically, and *Figure 3-20* shows results for 6%, 10%, and 20% weld offsets. For a weld offset of 20% the B.1 life[3] at 95% assurance is about 28,000 missions, and the extrapolated B.01 life is about 8,500 missions. At a weld offset of 6% the B.1 life is about 74,000 missions.

Figure 3-21 provides the output of failure simulations for a 10% weld offset. These curves represent the direct output of the Monte Carlo simulation and are given at a specified assurance. The left-most curve is the "all driver" variation curve and the input and output files for this analysis are given in *Section 3.B.3*. The right-most curve in *Figure 3-21* labeled "nominal" is for a simulation which included intrinsic materials variation only (see *Section 2.1.2.1*); all the other drivers were fixed at their nominal or most likely values. A measure of the relative importance of individual drivers is given in the upper left corner in *Figure 3-21*. These were obtained by finding the marginal effects of driver uncertainties on B1 lives using several sensitivity runs, where one driver was allowed to vary while the rest were held at their nominal values. The stress concentration factor and S/N model parameter variation were the most significant

---

[3] A B-life is the value of accumulated operating time to failure at a failure probability specified as a percent; e.g., B.1 is the failure time at a probability of 0.001 or 0.1%.

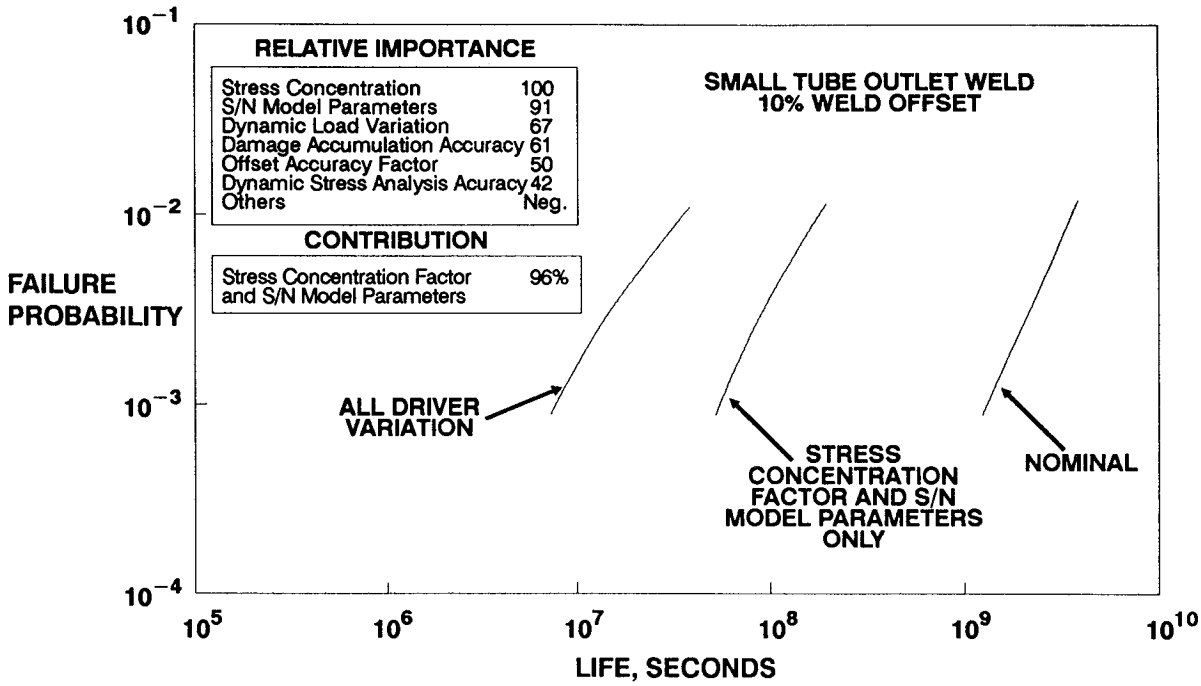

Figure 3-21 HPOTP Heat Exchanger Failure Life Distribution and Driver Sensitivities

drivers in this analysis with a 96% contribution to the decrease in life. The middle curve in *Figure 3-21* shows the shift to the left due to variation only in the stress concentration factor and S/N model parameters. The load variation, stress analysis accuracy, weld offset stress accuracy, and wall thickness were moderately important drivers. Flow parameters, inner diameter, and the Neuber's rule accuracy were not important drivers. It should be noted that the welded 321 material data may be a conservative or nonconservative representation of the behavior of welded 316L material.

Section 3.3

ATD-HPFTP Second Stage Turbine Disk LCF Analysis

3.3.1 Component Description

The ATD-HPFTP turbine disk is a monolithic forging with two rows of turbine blades attached to its outer circumference. *Figure 3-22* shows an axial cross section of the monolithic disk with both rows of blades. *Figure 3-23* illustrates the face of a stylized disk with blade attachment locations. The actual ATD disk has fifty blade attachment locations. The turbine is driven by high temperature, high pressure steam (H_2O) and hydrogen (H_2). The disk is surrounded by flowing hydrogen coolant to control the temperature and thermal gradient at critical locations.

As discussed in *Section 2.2.2.2*, the life-controlling location is in the blade attachment region of the disk. The radial and axial positions of this critical location are indicated in *Figures 3-23* and *Figures 3-24*, respectively. The axial position is on the downstream face and the radial position is in the lower lobe. The local strain range at this location is sufficiently high to control LCF crack initiation life.

The ATD-HPFTP turbine disk is made of Inconel 100. Inconel 100 notched fatigue test data used for the analysis is given in *Figure 3-25*. Nine test specimens of the material were subjected to stress-controlled cyclic loading with a stress ratio of $R = 0.05$. The fatigue tests were performed in 5000 psig hydrogen at room temperature **[10]**.

3.3.2 Driver Description

Four drivers, in addition to materials behavior, were characterized by probability distributions in the disk LCF analysis. Two of these drivers account for uncertainty of analysis methods. A list of the drivers, their distributions, and parameters are given in *Table 3-7*.

The stress concentration uncertainty factor λ_{K_t} was characterized by a Uniform distribution over the range (.95, 1.05). This relatively tight distribution was selected since the geometry and stress concentration factor of the fatigue test specimens were very close to those of the actual part. Experience has indicated that the error in the ratio of local stresses between the test specimens and actual parts is less than ±5%.

The stress analysis accuracy factor λ_{K_d} accounts for uncertainty in the FE analysis. A review of FE literature and discussions with stress analysts who have compared

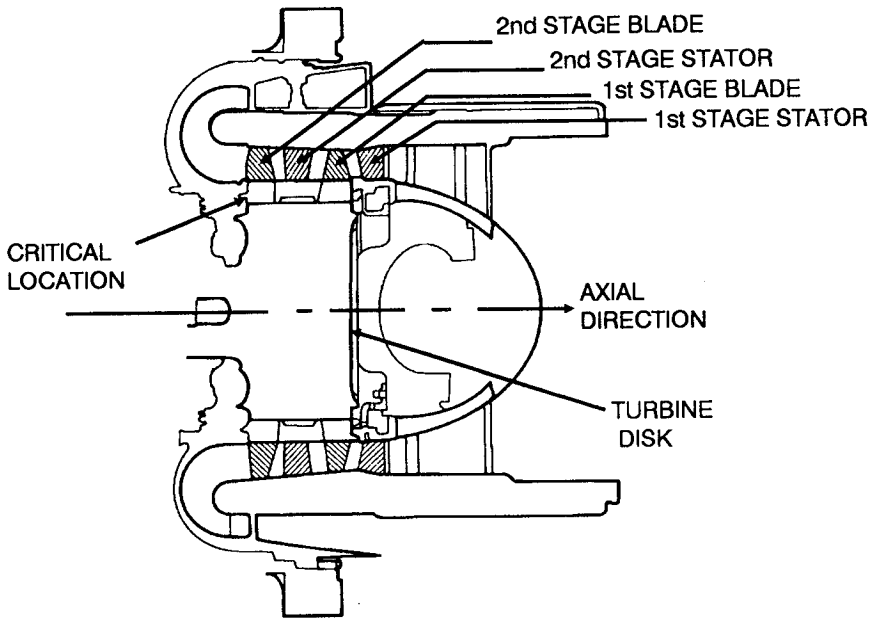

Figure 3-22 Axial Cross Section of the ATD-HPFTP Turbine Showing the Monolithic Disk

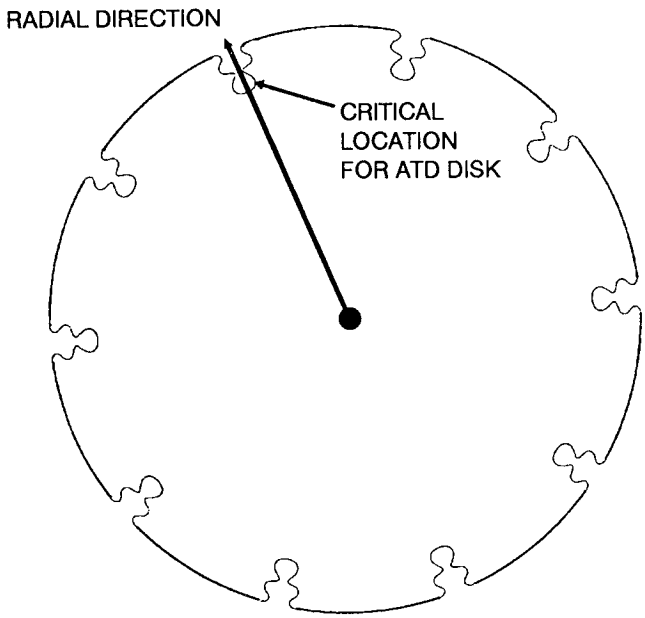

Figure 3-23 Stylized Radial Cross Section of a Turbine Disk

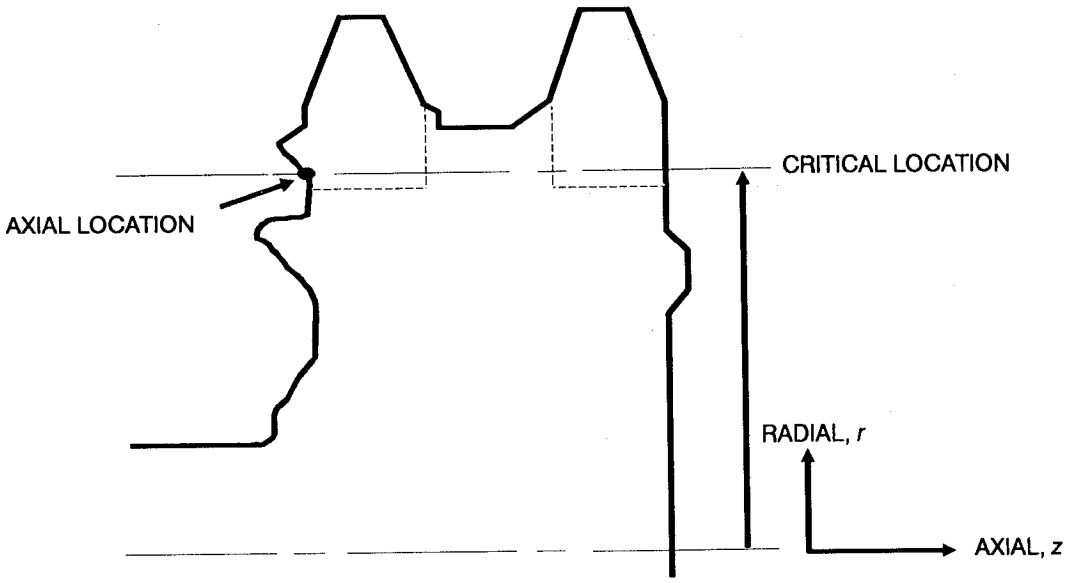

Figure 3-24 Axial Cross Section of the Disk

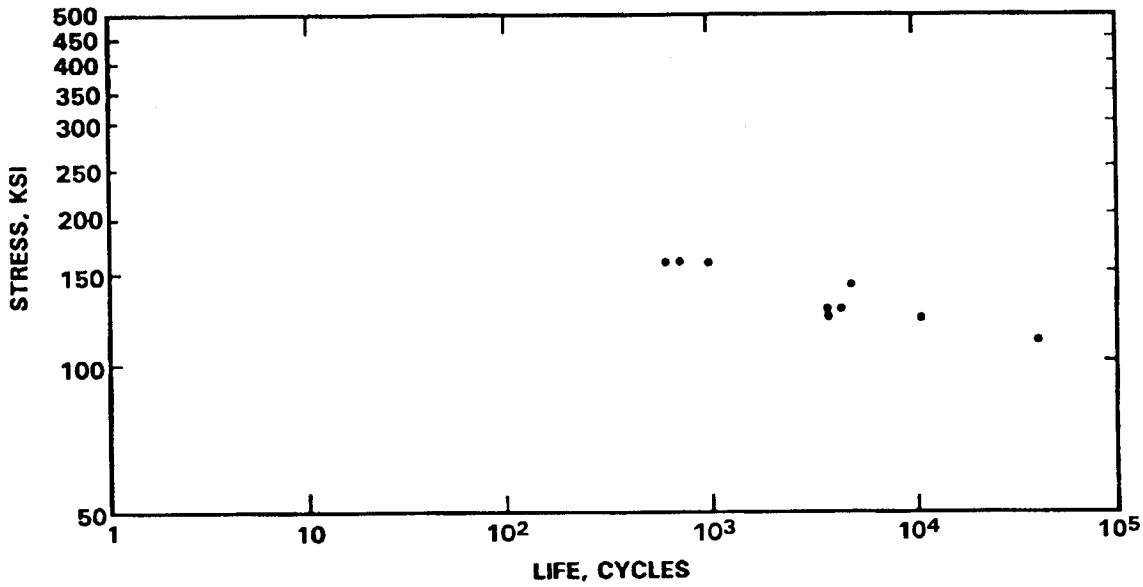

Figure 3-25 Inconel 100 Fatigue Life for Notched Specimens **[10]**

analysis and tests indicate that a correct FE stress analysis would calculate stresses to within 20% of the true value. Thus, λ_{K_d} was represented by a Uniform distribution over the range (.80, 1.20).

The rotor speed ω is distributed according to a Normal distribution about the nominal rotor speed with a standard deviation of 1.35% of the mean. This characterization is based on an analytical turbopump performance model.

Characterization of ΔT_f, the deviation from nominal coolant fluid temperature, is accomplished by means of Beta distributions. A Beta distribution can be parameterized as Beta(a, b, ρ, θ), where a and b are the lower and upper bounds of the range of the random variate, ρ is a location parameter, and θ is a shape parameter. See *Section 2.1.3.1* for a more detailed description of this parameterization of the Beta distribution.

ΔT_f was assigned the distribution

.95 Beta($-200°F$, $200°F$, .5, 0) + .05 Beta($200°F$, $500°F$, 0, 10).

This distribution is shown in *Table 3-7* and illustrated in *Figure 3-26*. The information available for characterizing the distribution of ΔT_f is that ΔT_f most likely lies between

Table 3-7 Driver Distributions for the Turbine Disk

DRIVER	DISTRIBUTION
λ_{K_t}	Uniform(0.95, 1.05)
λ_{K_d}	Uniform(0.80, 1.20)
ω	Normal(μ, σ^2) μ =37592 rpm σ = 1.35% of μ = 507 rpm
ΔT_f	Beta(a, b, ρ, θ) .95 Beta($-200°F$, $200°F$, 0.5, 0) +.05 Beta($200°F$, $500°F$, 0, 10)

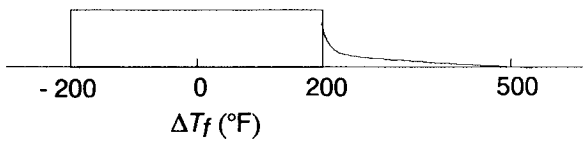

Figure 3-26 Driver Distribution for ΔT_f

$-200°F$ and $200°F$, with no information available to differentiate among values in that range, and that ΔT_f is much less likely to lie between $200°F$ and $500°F$. A probability of .95 was assigned to the $-200°F$ to $200°F$ interval and .05 was assigned to the $200°F$ to $500°F$ interval.

For the Beta distribution characterizing $-200°F \leq \Delta T_f \leq 200°F$, ρ is .5 and θ is 0, which is equivalent to assigning a Uniform distribution to ΔT_f in this interval. For the Beta distribution characterizing $200°F \leq \Delta T_f \leq 500°F$, ρ is 0 and θ is 10, which represents the higher likelihood of ΔT_f values closer to $200°F$ than to $500°F$.

3.3.3 Analysis

The program TRBPWA was used to perform the LCF analysis of the ATD-HPFTP second stage turbine disk. The overall description of the program is given in *Section 5.2*. The user's manual for TRBPWA, including the description of the input variables, is given in *Section 6.2*. A source listing of TRBPWA is given in *Section 7.2*.

As described in *Section 2.2.2.2*, the values for the nominal stresses and stress adjustment factor were obtained from a NASTRAN FE stress analysis performed by Pratt & Whitney. The FE analysis was performed at a nominal rotor speed ω_o of 38,600 rpm. The nominal mechanical stress S_{M_o} was 159,807 psi, the nominal stress due to metal temperature S_{m_o} was 1,915 psi, and the nominal stress due to thermal gradient S_{G_o} was 14,749 psi. The stress adjustment factor K_d was found to be 1.41, and the value of the stress concentration factor K_t was 2.18. The FE analysis also provided C_{mf}, the sensitivity of metal temperature to deviation from nominal coolant fluid temperature, and C_{G1}, C_{G2}, the sensitivity of thermal gradient to deviation from nominal coolant fluid temperature. The values were 0.91325 for C_{mf}, 0.04 for C_{G1}, and 0.07 for C_{G2}. The remaining sensitivities were obtained from the thermal analysis performed to provide boundary conditions for the FE analysis. The sensitivity of stress to change in metal temperature C_m was 4.44 psi/°F, and the sensitivity of stress to change in thermal gradient C_G was 101.72 psi/°F.

3.3.4 Results

The results of failure simulations for the disk are given in *Figure 3-27*. The graph presents the left-hand tail of the failure distribution derived from the simulations. The ordinate of this graph is failure probability and the abscissa is life of the disk to LCF

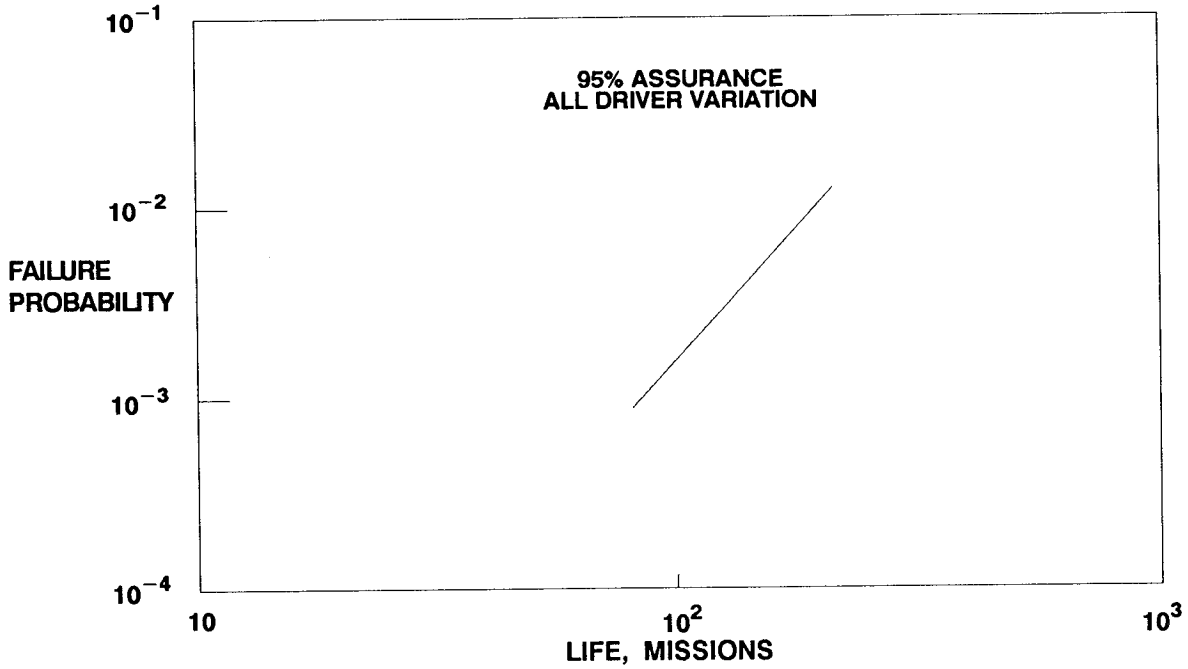

Figure 3-27 ATD-HPFTP Second Stage Turbine Disk Failure Life Distribution

failure. Life is given in missions and, for this analysis, a mission is one start-up–shut-down cycle. *Figure 3-27* shows disk LCF life at 95% assurance. The meaning of a 95% assurance curve is that the failure probability at a given life will lie with .95 probability below that curve. The B.1 life[4] at 95% assurance is 85 missions.

Figure 3-28 shows the output of failure simulations conducted to assess the sensitivity of the turbine disk failure life distribution to the drivers. The curves of *Figure 3-28* represent the direct output of the Monte Carlo simulation and are not given at specified assurance. The right curve, labeled "nominal" in *Figure 3-28*, is for a simulation which included intrinsic materials variation only (see *Section 2.1.2.1*); all the other drivers were fixed at their nominal or most likely values. The left-most curve in *Figure 3-28* is the "all driver variation" curve, which essentially coincides with the curve for the combination of variation in "S/N model parameters" and "stress adjustment factor." The input and output files from the "all driver" analysis are given in *Section 3.B.4*. A measure of the relative importance of individual drivers is given in the lower right corner in *Figure 3-28*. These were obtained by finding the marginal

---

[4] A B-life is the value of accumulated operating time to failure at a failure probability specified as a percent; e.g., B.1 is the failure time at a probability of 0.001 or 0.1%.

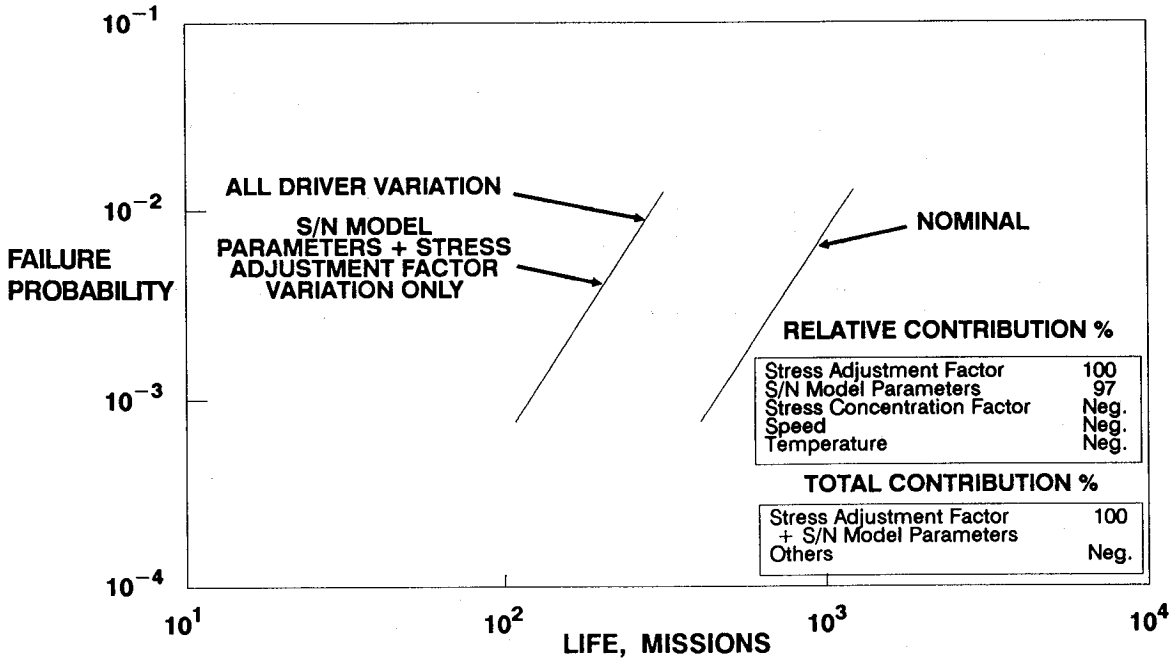

Figure 3-28 Driver Sensitivities for the ATD-HPFTP Second Stage Turbine Disk LCF Failure Life

effects of driver uncertainties on B.1 lives using several sensitivity runs, where one driver was allowed to vary while the rest were held at their nominal values. The S/N model parameters and stress adjustment factor λ_{K_d} were the most significant drivers in this analysis, with an essentially 100% contribution to the decrease in life. Variation in the stress concentration factor λ_{K_t}, deviation from nominal coolant fluid temperature ΔT_f, and rotor speed ω are not important drivers.

This analysis is for a 1988 design. The Pratt & Whitney designers decided to redesign for longer life because their analysis showed unacceptably high stresses. This probabilistic analysis is consistent with the need to redesign since the B.1 life for the nominal failure probability curve is below the design goal of the order of 1000 missions. Since additional information that would permit more accurate specification of the driver distributions could not shift the failure distribution sufficiently to make the design acceptable, it was concluded that this design is not information sensitive, providing that the nominal values of drivers have not been significantly misspecified. Thus, there is no need to acquire additional driver information. Stress must be reduced through a redesign in order to achieve the life goal.

References

[1] "High Cycle Fatigue Testing of Inconel 718 Straight and Hourglass Specimens," Report prepared by Metcut Research Associates for Rockwell International, No. 565-36153, April, 1984.

[2] Wong, T. T., "High Cycle Fatigue on GTA Welded Incoloy 903," Internal Letter No. MPR-87-0643, Rockwell International, August, 1987.

[3] Rodabaugh, E. C., and George, H. H., "Effect of Internal Pressure on Flexibility and Stress-Intensification Factors of Curved Pipe or Welding Elbows," Transactions of the ASME, May 1957, pp. 939-948.

[4] Whatham, J. F., "Pipe Bend Analysis by Thin Shell Theory," Journal of Applied Mechanics, ASME, Vol. 53, Mar., 1986, pp. 173-180.

[5] O'Connor, D., Personal Communication, Rocketdyne, Rockwell International, 1988.

[6] SSME Structural Loads Criteria, Rockwell International, RSS-8561-22, October 1987.

[7] "High Cycle Fatigue Testing of 316L SS Bar Specimens," Report prepared by Metcut Research Associates for Rockwell International, No. 565-37868-1, November, 1984.

[8] "Determination of Low-Temperature Fatigue Properties of Structural Metal Alloys," Prepared for NASA/MSFC by Martin Company, Contract NAS8-11300, Denver, Colorado, Oct., 1965.

[9] Reemsnyder, H. S., "Development and Application of Fatigue Data for Structural Steel Weldments," Fatigue Testing of Weldments, ASTM STP 648, 1978, p. 3.

[10] Internal Document ME&T No. 28872A, Pratt & Whitney, 6 May 1987, page 2.

[11] Peterson, R. E., Stress Concentration Factors, John Wiley & Sons, New York, 1974.

[12] Naugel, F. V., "Review of Duct Program," Internal Letter IL8126-3145, Rocketdyne, Rockwell International, May, 1988.

[13] Beer, R. F., "Structural Analysis of Mismatch Between Welded Ducts," Internal Letter IL4126-3008, Rocketdyne, Rockwell International, June 28, 1984.

[14] Gunay, M. H., and Newell, J. F., "Elastic Mismatch Stresses in Circumferentially Welded Cylindrical Shells Under Moment Loading," 1990 ASME PVP Conference, Nashville, TN, June, 1990.

Appendix 3.A
Probabilistic Failure Assessment Details

3.A.1 Introduction

The details of two Probabilistic Failure Assessment (PFA) application examples are given here. Every step of the procedure, including intermediate calculations and results, is presented. *Section 3.A.2* describes the HPOTP HEX Coil HCF analysis and *Section 3.A.3* describes the ATD-HPFTP turbine disk LCF analysis. The overall procedure for PFA is given in *Section 2.3*.

3.A.2 HPOTP Heat Exchanger Coil HCF Analysis Details

3.A.2.1 Selecting the Component, Failure Mode, and Critical Location

The HEX coil is a critical component since a leak in the coil carrying liquid oxygen can cause the liquid oxygen to mix with the hydrogen outside and cause a malfunction of the system. The failure mode and critical location for this study were based on the deterministic analyses that had been performed for the HEX coil. Since the HEX coil was already in operation at the time of this study, deterministic stress and fatigue analyses were available for the component. These deterministic analyses indicated that the stresses at the small tube outlet weld could approach the fatigue endurance limit for the component. Thus, it was deemed appropriate to apply the PFA methodology to evaluate its HCF failure risk.

3.A.2.2 Preliminary Deterministic Analysis

The stress, thermal, and fluid flow deterministic analyses performed by Rocketdyne were used for formulating the driver transformation and to identify and characterize driver distributions for the PFA. The Rocketdyne stress analyses included random vibration and frequency response dynamic analyses, and they are described in *Section 2.2.1.2*.

For the HEX coil, a deterministic module, which was a variation of the module embedded in the simulation loops, was used to test the driver transformation, scan the circumference of the duct to find the worst stress position, and to aid in significant load identification, as described in *Section 3.A.2.6*. The analysis for location of the worst stress position on the circumference were run with single cycle time histories – the amplitude of the random reference histories was three, and those for the sinusoidal reference histories was one. *Table 3-8* gives the outcome of the deterministic analysis for finding the critical location at the circumferential angle of 85° in the HEX coil.

Table 3-8 Scanning Circumference for Critical Angle Causing Minimum Life

ANGLE (deg)	LIFE (secs)
0	6.19×10^{14}
40	3.71×10^{10}
60	8.11×10^{9}
70	5.51×10^{9}
75	4.92×10^{9}
80	4.62×10^{9}
85	4.56×10^{9}
90	4.73×10^{9}
100	5.92×10^{9}
120	1.84×10^{10}
160	2.83×10^{13}
200	1.17×10^{14}
240	7.88×10^{10}
280	5.60×10^{10}
320	1.37×10^{13}

3.A.2.3 Driver Characterization

The list of drivers for the HEX coil, their distributions, and ranges are given in *Table 3-5*. The rationale for assigning the distributions for these drivers was presented in *Sections 3.1.3* and *3.2.2*. The information used to describe some of these distributions and the specification of the distribution parameters are given here.

Weld Offset

Weld offset measurements were available from ten coils at weld 3. *Table 3-9* gives the serial numbers of the coils and the weld offsets in inches. In cases when a low and high measurement were provided, the high value was used. This data was considered inadequate to assign a probability distribution for the weld offset, and as mentioned in *Section 3.2.2*, the weld offset was treated parametrically. The average weld offset for the ten coils was 0.00073 inches. The average percentage weld offset, obtained by dividing it by the nominal thickness of 0.00125, is 6%. In addition to the average weld offset of 6%, the HEX coil was analyzed for 10% and 20% weld offsets.

Table 3-9 Weld Offset Measurements

SERIAL NUMBER	WELD OFFSET (in.)
8674330	0.0005
8581654	0.0005*
8577498	0.0012*
8690140	0.0006*
8682049	0.0005*
8701217	0.0010*
8577501	0.0005
8577502	0.0005
8674328	0.0010
8577500	0.0010

*Highest of the low/high values

The 10% offset was the design specification for this weld, and 20% offset was the maximum weld offset that may be specified by MRB for weld 3.

Stress Concentration Factor

As mentioned in *Section 3.2.2*, the stress concentration factor K_T was based on the condition of the welded surface after finishing. The depth of the gouges made by the reamer was assumed to be equal to the radius of the reamer, which was 0.003 in. Also, the range of the positive and negative steps left after reaming and polishing was 0.001 to 0.003 in. The stress concentration factor K_T for a 0.003 in. deep gouge in a 0.125 in. thick tube is about 2.2 **[11]**. The stress concentration due to the step was inferred from fatigue failure data on weldments for different height to thickness ratios *h/t* reported by Reemsnyder **[9]** and is shown in *Figure 3-29*. The K_T for a step with *h/t* of 0.08 to 0.16 is between 1.50 to 3.50. The K_T values given by Peterson **[11]** for a trapezoidal step in tension was between 1.2 to 2.2. Based on all the above information, K_T was considered to be between 1.2 and 3.5. Since the value of K_T was bounded, it was decided to use the Beta distribution. The information, however, was inadequate to describe the shape of the distribution, except that the value was more likely to be closer to the lower bound. Thus, the uncertainty in the shape was modeled by varying the shape parameter ρ in the Beta distribution.

Wall Temperature and Internal Pressure

The ranges of temperatures and internal pressure obtained from an engine balance model were provided by Rocketdyne. These were the nominal, or mean, μ and the

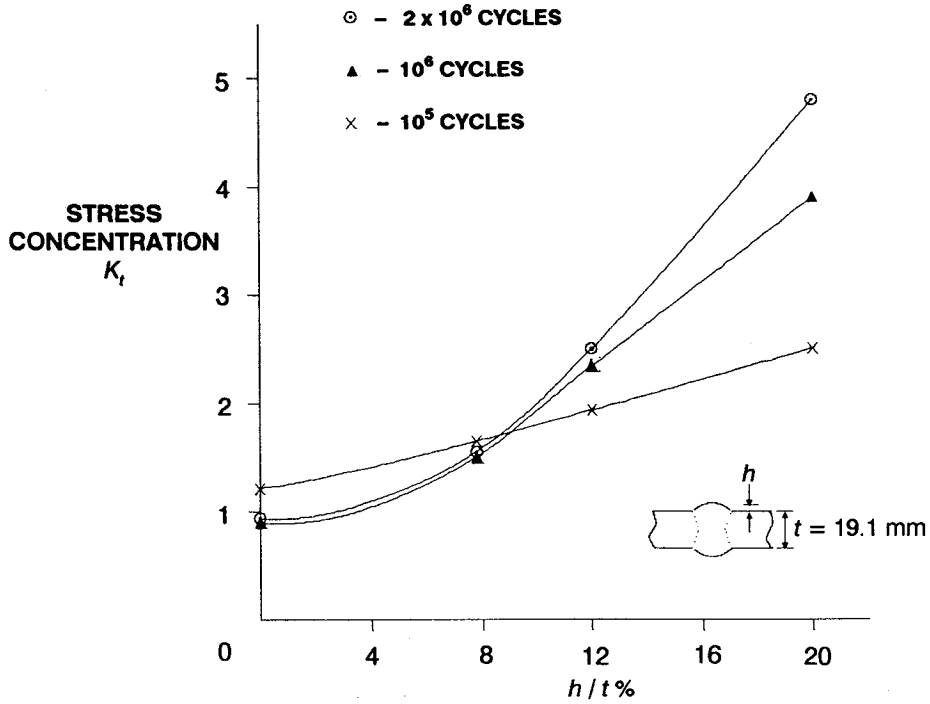

Figure 3-29 Stress Concentration Due to Different Height Welds **[9]**

$\mu + 2\sigma$ values of the temperatures and pressure for minimum and maximum flow conditions and they are given in *Table 3-10*. For the PFA, the temperatures and pressure were characterized with hyperparametric Normal distributions. That is, the mean and standard deviation of the Normal distributions themselves were characterized by Uniform distributions whose endpoints correspond to the driver values given in *Table 3-10* for the minimum and maximum flow conditions. The variation of the temperatures and pressure were correlated such that they assumed values that corresponded to the same flow condition, the correlation was specified implicitly in the HEXHCF program.

Weld Offset Stress Concentration Accuracy Factors

The weld offset stress concentration accuracy factor is given by *Equation 2-73*, and as mentioned in *Section 2.2.1.3*, the F_k factor in this equation was determined using finite element stress analyses of detailed models of the weld region **[12]**. The F_k factors were determined to be functions of the radius to thickness ratio *R/t*. *Figure 3-30* gives F_k vs. *R/t* curves from different studies. The curve used in the HCF application examples is shown in *Figure 3-30*, and the distribution on the uncertainty factor λ_{OFF} specified to account for uncertainty of this curve is also shown.

Table 3-10 Wall Temperature and Internal Pressure at Weld 3 From Engine Balance Model

	μ		$\mu + 2\sigma$		σ	
	MINIMUM FLOW	MAXIMUM FLOW	MINIMUM FLOW	MAXIMUM FLOW	MINIMUM FLOW	MAXIMUM FLOW
$T_{inner\ wall}$ (°R)	666	486	779	544	56.5	29
$T_{outer\ wall}$ (°R)	908	799	1004	898	48	49.5
$p_{internal}$ (psi)	4177	3808	4315	3946	69	69

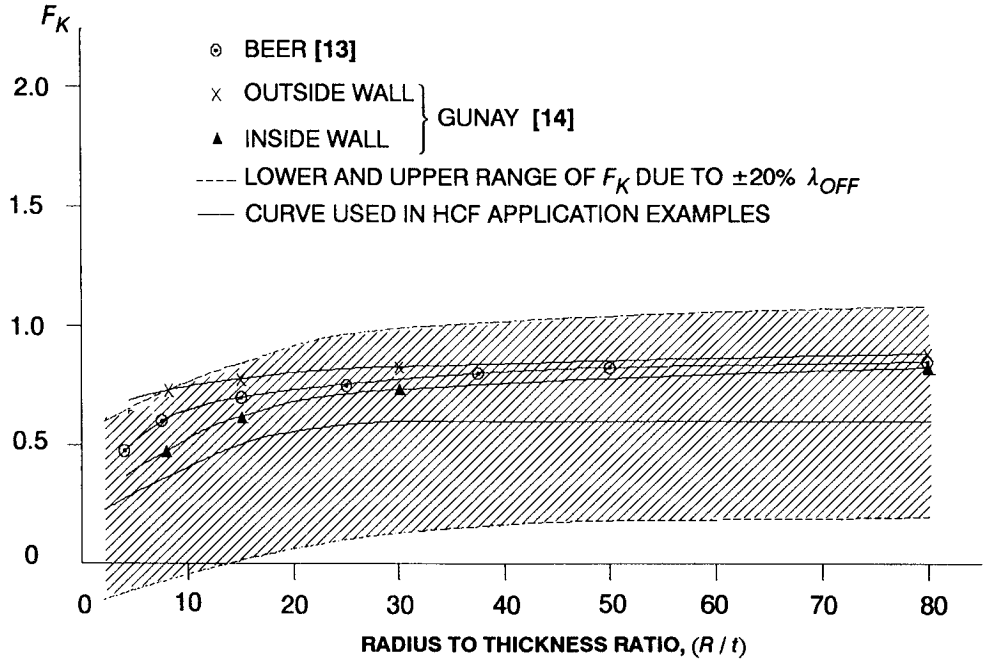

Figure 3-30 F_k Values From Different Sources, Comparison with Curve in Use and Accuracy Factor λ_{OFF} Impact

3.A.2.4 Materials Characterization

As described in *Section 3.2.1*, proxy 321 weld S/N material data had to be used for the HEX coil. The data is given in *Table 3-11* and is shown plotted in *Figure 3-17.* Based on the data points, a single data region was used since it was decided that the ln(*S*) vs. ln(*N*) behavior was linear in the life ranges of interest. Prior to using the S/N data for the HEX coil PFA, it was studied using the materials characterization program MATCHR (described in *Section 4.1*).

The 95% confidence intervals on the coefficient of variation *C* and the slope *m* denoted by I_o and J_o, respectively, in *Equations 2-24* and *2-26*, and generated by MATCHR for the 321 weld data, are given in *Table 3-12*. Point estimates for *C* and *m*

Table 3-11 321 SS Welded S/N Data **[8]**

STRESS S (psi)	LIFE N (cycles)
40,000	1000
40,000	2000
40,000	3000
40,000	5000
40,000	6000
30,000	23,000
30,000	66,000
25,000	72,000
25,000	190,000
20,000	789,000
20,000	1,070,000
20,000	1,450,000

Table 3-12 Summary of Materials Characterization Study of 321 Weld Data

	Coefficient of Variation C	Slope Parameter m
95% Confidence Interval	$I_O = \{0.047, 0.114\}$	$J_O = \{7.14, 9.60\}$
Point Estimates	0.067	8.37
Posterior Credibility Range Lower bound Upper bound	—	 7.14 9.60

are also given in the table. These point and interval estimates of C and m are consistent with any exogenous constraints on C and m, so there is no need to impose explicit constraints.

3.A.2.5 Time History Definition

The time histories were generated as described in *Sections 2.1.4* and *2.3.7*. The frequency f of the random and sinusoidal load components for the HEX coil are given in *Table 3-6*. If the highest frequency among the significant load components is f_{max}, then the number of points that will be generated is given by $N \cdot f_{max} \cdot T$, where T is the length of the history in seconds and N is the number of points within a single cycle of

Table 3-13 Lives for Different Random Number Seeds and History Length

SEED	$T = 1$	$T = 2$	$T = 3$	$T = 4$
175	$.7935 \times 10^{10}$	$.8229 \times 10^{10}$	1.054×10^{10}	1.281×10^{10}
275	1.853×10^{10}	1.765×10^{10}	1.869×10^{10}	1.872×10^{10}
375	3.015×10^{10}	2.842×10^{10}	2.853×10^{10}	2.992×10^{10}
475	2.162×10^{10}	2.056×10^{10}	2.312×10^{10}	2.233×10^{10}
575	3.167×10^{10}	3.250×10^{10}	3.082×10^{10}	2.900×10^{10}
675	2.270×10^{10}	2.604×10^{10}	2.472×10^{10}	2.215×10^{10}
775	2.674×10^{10}	2.906×10^{10}	3.238×10^{10}	3.232×10^{10}
875	1.241×10^{10}	1.268×10^{10}	1.672×10^{10}	2.037×10^{10}
975	2.554×10^{10}	2.779×10^{10}	3.049×10^{10}	2.689×10^{10}
1075	2.473×10^{10}	2.639×10^{10}	1.842×10^{10}	1.846×10^{10}
1175	2.174×10^{10}	2.070×10^{10}	1.668×10^{10}	1.853×10^{10}
1275	1.636×10^{10}	2.092×10^{10}	1.733×10^{10}	1.944×10^{10}
1375	1.948×10^{10}	2.167×10^{10}	2.468×10^{10}	2.513×10^{10}
1475	2.592×10^{10}	2.121×10^{10}	1.866×10^{10}	1.704×10^{10}
1575	1.531×10^{10}	2.037×10^{10}	1.839×10^{10}	2.026×10^{10}
1675	3.122×10^{10}	3.111×10^{10}	2.151×10^{10}	2.243×10^{10}
1775	3.432×10^{10}	3.131×10^{10}	2.783×10^{10}	2.866×10^{10}
1875	3.804×10^{10}	3.400×10^{10}	2.962×10^{10}	2.268×10^{10}
1975	2.977×10^{10}	2.745×10^{10}	2.447×10^{10}	2.074×10^{10}
2075	2.494×10^{10}	1.727×10^{10}	2.065×10^{10}	2.064×10^{10}
2175	2.114×10^{10}	2.937×10^{10}	3.009×10^{10}	2.773×10^{10}

the highest frequency history. The results of the significant load component selection is given below in *Section 3.A.2.6*. The length and the initiating random number seed for the reference time-histories were decided based on the lives calculated with 21 random number seeds and lengths of T = 1.0, 2.0, 3.0, 4.0 secs. The lives were calculated with nominal driver values and are given, for each value of T, in *Table 3-13*. The desired random number seed and history length are those which correspond to the life near the median life and the shortest value of T for which the calculated life is close to those for higher values of T. From *Table 3-13* the chosen seed was 675 and the optimum length was 1.0 sec.

3.A.2.6 Significant Load Identification

The significant load identification is carried out as described in *Section 2.3.8*. The von Mises stress and the damage index that were calculated for each load component are given *Table 3-14*. The random load components P, M_z, 500Hz sinusoidal load, and the aerodynamic load were identified as significant based on their damage indices. *Table 3-15* lists the load components that contribute to each stress component, rank ordered by their damage indices within each group. Analyses were performed by including the next significant load from the list in each stress component group. *Table 3-16* shows the outcome of these analyses.

3.A.2.7 Probability of Failure Curve Parameter Estimation

The steps required to carry out the probability of failure curve parameter estimation for this HEX example are given in *Figure 3-31*. This procedure was used to obtain the results discussed in *Section 3.2*. Only the calculations for the 10% weld offset case will be presented in this section.

The parameters of the prior distribution are estimated by determining a value for β, then estimating α and θ for fixed β. The first step in the procedure is to plot the failure simulation results contained in file LOWLIF for the "all drivers" run. That plot is shown in *Figure 3-21*. Since the all drivers run is nonlinear, the alternative procedure of *Section 2.3.9* was used. This run is called the "capability" run and was carried out by allowing variation in the stress concentration factors, inner diameter, wall thickness, and the S/N material properties. The other drivers were held at their nominal values.

The β estimate is based on an approximate linear portion of the left-hand tail (.001 to .005 on the ordinate) for this example. This probability range corresponds to simulated lives with index numbers 20 through 100, inclusive, in file LOWLIF. A value for β is estimated by program BFIT. The pertinent methodology is discussed in *Section 2.1.1*, the program description and flowcharts are presented in *Section 4.2.2*, the user's guide for running this program is given in *Sections 6.4.1-6.4.6*, and the code structure and listing are provided in *Section 7.4.1*. Program BFIT has provided the estimate $\beta = 1.951$ for this example.

The α and θ estimate must be based on the all driver run in order to fit a model which is nonlinear in log–log space. It is only necessary to consider points with probability in the range .001 to .01. α, θ are estimated by program ABTFIT. The pertinent methodology is discussed in *Section 2.1.1*, the program description and flowcharts are presented in *Section 4.2.3*, the user's guide for running this program

Table 3-14 Von Mises Stress and Damage Indices Due to Each Load Component

LOAD COMPONENT	FREQUENCY (Hz)	VON MISES STRESS	DAMAGE INDEX
$X - P$	236	193.8	5.06×10^{18}
$Y - P$	840	140.4	1.81×10^{18}
$Z - P$	1404	9.307	1.16×10^{10}
$X - M_x$	634	2.984	1.56×10^{6}
$Y - M_x$	800	7.772	1.83×10^{9}
$Z - M_x$	1018	28.73	2.63×10^{13}
$X - M_y$	424	1.456	6.21×10^{3}
$Y - M_y$	275	3.419	1.78×10^{6}
$Z - M_y$	1224	18.31	1.27×10^{12}
$X - M_z$	386	586.7	2.25×10^{22}
$Y - M_z$	320	1479	1.38×10^{25}
$Z - M_z$	1336	31.12	6.10×10^{13}
$X - V_y$	740	9.838	9.09×10^{9}
$Y - V_y$	1040	23.80	7.01×10^{12}
$Z - V_y$	1392	1.857	1.16×10^{5}
$X - V_z$	358	8.314	1.32×10^{9}
$Y - V_z$	1011	6.770	8.61×10^{8}
$Z - V_z$	1394	279.0	4.03×10^{20}
AERO	1780	298.7	8.38×10^{20}
SIN1	500	919.3	7.21×10^{23}
SIN2	600	80.81	2.50×10^{16}
SIN3	1000	132.6	1.43×10^{18}
SIN4	1500	167.0	1.11×10^{19}
SIN5	1800	17.48	1.34×10^{12}
SIN6	2000	66.84	2.15×10^{16}

Table 3-15 Load Components Rank Ordered by Damage Indices for Contributing Stress Components

RANDOM LOAD COMPONENTS

AXIAL STRESS	SHEAR STRESS
$Y - M_Z$	$Z - V_Z$
$X - M_Z$	$Z - M_X$
$X - P$	$Y - V_Y$
$Y - P$	$X - V_Y$
$Z - M_Z$	$X - V_Z$
$Z - M_Y$	$Y - M_X$
$Z - P$	$Y - V_Z$
$Y - M_Y$	$X - M_X$
$X - M_Y$	$Z - V_Y$

SINUSOIDAL LOADS

AXIAL STRESS	SHEAR STRESS
SIN1	SIN1
SIN3	SIN4
SIN4	SIN6
SIN2	SIN2
SIN6	SIN3
SIN5	SIN5

Table 3-16 Significant Load Identification Checks

LOADS INCLUDED	B.1 LIFE	B1 LIFE
$Y - M_Z$, SIN1	8.699×10^6	4.292×10^7
$Y - M_Z$, SIN1, AERO	6.474×10^6	3.249×10^7
$Y - M_Z$, SIN1, AERO, $X - M_Z$	4.506×10^6	2.276×10^7
$Y - M_Z$, SIN1, AERO, $X - M_Z$, $X - P$	4.199×10^6	2.108×10^7
$Y - M_Z$, SIN1, AERO, $X - M_Z$, $X - P$, $Y - P$	3.400×10^6	1.766×10^7
$Y - M_Z$, SIN1, AERO, $X - M_Z$, $X - P$, $Y - P$, $Z - M_Z$	3.387×10^6	1.760×10^7
$Y - M_Z$, SIN1, AERO, $X - M_Z$, $X - P$, $Y - P$, SIN3	3.312×10^6	1.715×10^7
ALL LOADS	3.277×10^6	1.687×10^7

C 3

1 Plot the failure simulation results contained in file LOWLIF in log–log space for both the "all driver" and "capability" runs.

2 Since the data for the capability run from .001 to .005, that is, point 20 to point 100 of file LOWLIF, is approximately linear, it can be used to estimate β.

3 Create file BFITD to indicate the indices of the LOWLIF data to be used in the β estimation. See *Section 6.4.3.1* for a detailed description of the contents of file BFITD.

4 Run program BFIT. The pertinent methodology is discussed in *Section 2.1.1*, the program description and flowcharts are presented in *Section 4.2.2*, the user's guide for running this program is given in *Sections 6.4.1-6.4.6*, and the code structure and listing are provided in *Section 7.4.1*. BFIT has two input files, LOWLIF and BFITD, and two output files, BFITO and IOUTPR.

5 Obtain β estimate from output files BFITO and IOUTPR. Program BFIT has provided the estimate of 1.951.

6 In order for α and θ to be uniquely determined, it is only necessary to consider the range .001 to .01, that is, point 20 to point 200 inclusive, of file LOWLIF (for the all driver run), for the estimated curve to be nonlinear in log–log space. Create file PARAMS to indicate the indices of the LOWLIF data to be used in the α, θ estimation, the initial values for α and θ, and any scaling factors required. See *Section 6.4.9.1* for a detailed description of the contents of file PARAMS.

7 Run program ABTFIT. The pertinent methodology is discussed in *Section 2.1.1*, the program description and flowcharts are presented in *Section 4.2.3*, the user's guide for running this program is given in *Sections 6.4.7-6.4.12*, and the code structure and listing are provided in *Section 7.4.2*. ABTFIT has two input files, LOWLIF and PARAMS, and three output files, ABTOUT, BAYESD and IOUTPR.

8 Obtain α, θ estimates from output files ABTOUT and BAYESD. Program ABTFIT has provided the values 2.08×10^{14} for θ and 0.00766 for α.

9 Calculate assurance based on estimates of α, β, θ. The assurance calculation is performed by program LZERO. The pertinent methodology is discussed in *Section 2.1.1*, the program description and flowcharts are presented in *Section 4.2.4*, the user's guide for running this program is given in *Sections 6.4.13-6.4.18*, and the code structure and listing are provided in *Section 7.4.3*.

Figure 3-31 Steps of the Probability of Failure Curve Parameter Estimation for the HEX HCF

Table 3-17 Probability of Failure Curve Parameter Estimates for 6%, 10% and 20% Weld Offset

	WELD OFFSET		
	6%	10%	20%
β	1.94555	1.95100	1.97183
α	0.007558	0.007657	0.007521
θ	3.33665×10^{14}	2.08238×10^{14}	7.27963×10^{13}
λ_o for 95% Assurance	1.91225×10^{-18}	3.34602×10^{-18}	8.47997×10^{-18}

is given in *Section 6.4.7-6.4.12*, and the code structure and listing are provided in *Section 7.4.2*.

PARAMS requires initial values[5] for α and θ that were obtained as follows:

B.1[6] = $.7718 \times 10^7$
B1 = 3.593×10^7

LSCALE[7] = $\left(1 \;/\; .7718 \times 10^7\right) \approx 10^{-7}$

$\theta_o = N_{.001}^{\beta} = \left(.7718 \times 10^7\right)^{1.951} = 2.7386 \times 10^{13}$

XGUESS(1)[8] = $\left(N_{.001} * \textbf{LSCALE}\right)^{\beta} = \left(.7718 \times 10^7 \times 10^{-7}\right)^{1.951} = .603$

XGUESS(2) = $\alpha_o = -\ln .999 \;/\; \ln 2 = .0014434$

Program ABTFIT has provided the estimates $\theta = 2.0824 \times 10^{14}$ and $\alpha = 0.007657$. *Table 3-17* gives the α, β, and θ values which define the left-hand tail of the probability–life distribution for weld offsets of 6%, 10%, and 20%.

---

5 The calculation of initial values is illustrated in *Section 6.4.11*.

6 B-lives were obtained from file LOWLIF. A B-life is the value of the failure parameter (e.g., failure time) at a failure probability specified as a percent: e.g., B.1 is the failure time at a probability of .001 or .1%.

7 Life scaling factor is described in *Section 6.4.9*.

8 Calculation of initial guesses is described in *Section 6.4.11*.

Table 3-18 Driver Sensitivity Analysis for 10% Weld Offset

DRIVER VARIATION IN ANALYSIS	B1 LIFE (seconds)	SHIFT IN LIFE FROM NOMINAL	% SHIFT IN LIFE FROM ALL DRIVERS	RELATIVE IMPORTANCE
NOMINAL	3.8547×10^9			
ALL DRIVERS	4.7195×10^7	3.8×10^9		
K_t	5.3093×10^8	3.3×10^9	87	100
S/N MODEL PARAMETERS	8.2609×10^8	3.0×10^9	80	91
$\lambda_{DRANDOM} + \lambda_{DSINUSOIDAL}$	1.6247×10^9	2.2×10^9	59	67
λ_{dam}	1.8380×10^9	2.0×10^9	53	61
λ_{OFF}	2.1833×10^9	1.7×10^9	44	50
$\lambda_{DYN_{str}}$	2.4667×10^9	1.4×10^9	36	42
λ_{neu}	3.5912×10^9	2.6×10^8	6.9	8
$T_i + T_o + P_i$	3.6199×10^9	2.3×10^8	6.2	7
BUFFETING AERO LOAD	3.6790×10^9	1.8×10^8	4.6	5
t_m	3.6927×10^9	1.6×10^8	4.3	5
D_i	3.7424×10^9	1.1×10^8	2.9	3
$\lambda_{ST_{str}}$	3.8299×10^9	2.5×10^7	.6	1
DRAG AERO LOAD	3.8570×10^9	-2.4×10^6	0	0

3.A.2.8 Driver Sensitivity Analysis

As described in *Section 2.3.10*, a set of simulations were executed to obtain the driver sensitivities. The first simulation was the nominal run, which included intrinsic materials variation only (see *Section 2.1.2.1*); all the other drivers were fixed at their nominal or most likely values. *Figure 3-21* shows the output of the nominal simulation for the HEX with a 10% weld offset. The next simulation was the "all driver" variation run, which was performed by allowing all the drivers to vary. *Figure 3-21* shows the output of the all-driver run for the HEX with a 10% weld offset.

Finally, the driver sensitivities were derived using simulations for which each driver (together with intrinsic material variation) was allowed to vary one at a time while all the other drivers were held at their nominal values. Some related drivers, such as the load adjustment factors (for random and sinusoidal loads) and the flow parameters (inner and outer wall temperatures and internal pressure), were allowed to vary together to estimate the sensitivity of the load factors or the flow parameter drivers as a group. The output from these simulations along with the results from the aforementioned all-driver variation and nominal runs allows the drivers to be rank ordered and allows their relative importance to be characterized. The impact of the drivers was calculated based on the failure lives at the .01 probability level, given in *Table 3-18*, for the all-driver, nominal, and driver sensitivity runs.

To calculate the relative importance of a driver, the change in life from the nominal analysis due to driver variation was first calculated as a percentage of the shift due to the all-driver variation, for each driver. The largest shift was caused by variation in the stress concentration factor, which is therefore the most important driver. The relative importance was derived by normalizing the percentage shifts due to variation of each driver with the percentage shift due to variation of the most important driver, in this case the stress concentration factor. *Table 3-18* gives the percentage shift in lives and the relative importance for each driver.

3.A.2.9 Probability of Failure Curve Standardization

In order to standardize the results, the probability of failure vs. life curves were generated for a given assurance level. The curve is constructed by first calculating λ_o in *Equation 2-5* for an assurance level of 95% by using the program LZERO. The pertinent methodology is discussed in *Section 2.1.1*, the program description and flowcharts are presented in *Section 4.2.4*, the user's guide for running this program is given in *Sections 6.4.13-6.4.18*, and the code structure and listing are provided in *Section 7.4.3*. The values of λ_o for 6%, 10%, and 20% weld offsets are given in *Table 3-17*. Given λ_o and the bounding value of β, the assurance curve may be defined as described in *Section 2.3.12*. The 95% assurance curves for the three weld offsets are given in *Figure 3-20*.

3.A.3 ATD-HPFTP Second Stage Turbine Disk LCF Analysis Details

3.A.3.1 Selecting the Component, Failure Mode, and Critical Location

The turbine disk was chosen for analysis since it is a CRIT I component and the deterministic analysis of the design resulted in an unacceptably low life. The failure mode and critical location for this study were based on the deterministic analyses that had been performed for the turbine disk during design. It was deemed appropriate to apply the PFA methodology to evaluate its LCF failure risk.

3.A.3.2 Preliminary Deterministic Analysis

The stress, thermal, and fluid flow deterministic analyses performed by Pratt & Whitney were used for formulating the driver transformation and to identify and characterize driver distributions for the PFA. The steps of the Pratt & Whitney stress analysis are as follows:

1. Perform coolant flow model to establish boundary conditions.
2. Perform 2-D thermal analysis to characterize the disk internal temperature field using the boundary conditions from (1). This thermal analysis will provide the thermal gradient and the metal temperature at the critical location
3. Perform 2-D FE stress analysis to obtain the mechanical stress due to rotor mass and blade pull. This FE model is a radial cross section of the blade attachment area with a fine mesh.

4 Perform 2-D finite element stress analysis using the model of (3) and the disk internal temperature field of (2) to obtain thermal stress sensitivities.

5 Perform 2-D FE stress analysis to obtain stress adjustment factor. This FE model is an axial cross section of half of the monolithic disk with a coarse mesh.

3.A.3.3 Driver Characterization

The list of drivers for the turbine disk, their distributions, and ranges are given in *Table 3-7*. The rationale for assigning the distributions for these drivers was presented in *Section 3.3.2*.

3.A.3.4 Materials Characterization

As described in *Section 3.3.1,* Inconel 100 notched S/N material data was used for the turbine disk. The data is given in *Table 3-19* and is shown plotted in *Figure 3-25*. Based on the data points, a single data region was used since it was decided that the ln(S) vs. ln(N) behavior was linear in the life ranges of interest. Prior to using the S/N data for the turbine disk PFA, it was studied using the materials characterization program MATCHR (described in *Section 4.1*).

The 95% confidence intervals on the coefficient of variation C and the slope m denoted by I_o and J_o, respectively, in *Equations 2-24* and *2-26*, and generated by MATCHR for the IN100 notched data, are given in *Table 3-20*. Point estimates for C and m are also given in the table. These point and interval estimates of C and m are consistent with any exogenous constraints on C and m, so there is no need to impose explicit constraints.

Table 3-19 Inconel 100 Notched S/N Data **[10]**

STRESS S (psi)	LIFE N (cycles)
160,000	636
160,000	677
160,000	1,019
140,000	4,743
130,000	3,824
130,000	4,163
120,000	3,749
120,000	11,349
110,000	39,600

Table 3-20 Summary of Materials Characterization Study of IN100 Notched Data

	Coefficient of Variation C	Slope Parameter m
95% Confidence Interval	$I_o = \{0.037, 0.113\}$	$J_o = \{5.73, 11.97\}$
Point Estimates	0.055	8.85
Posterior Credibility Range Lower bound Upper bound	—	 5.73 11.97

3.A.3.5 Time History Definition

The time history used for the turbine disk is described in *Section 2.2.2.2* and shown in *Figure 2-28*.

3.A.3.6 Probability of Failure Curve Parameter Estimation

The steps required to carry out the probability of failure curve parameter estimation for this disk example are given in *Figure 3-32*. This procedure was used to obtain the results discussed in *Section 3.3*.

The parameters of the prior distribution are estimated by determining a value for β, then estimating α and θ for fixed β. The first step in the procedure is to plot the failure simulation results contained in file LOWLIF for the "all drivers" run. That plot is shown in *Figure 3-28*.

The β estimate is based on an approximate linear portion of the left-hand tail (.001 to .003 on the ordinate) for this example. This probability range corresponds to simulated lives with index numbers 20 through 60, inclusive, in file LOWLIF. A value for β is estimated by program BFIT. The pertinent methodology is discussed in *Section 2.1.1*, the program description and flowcharts are presented in *Section 4.2.2*, the user's guide for running this program is given in *Sections 6.4.1-6.4.6*, and the code structure and listing are provided in *Section 7.4.1*. Program BFIT has provided the estimate $\beta = 2.7815$ for this example.

The α and θ estimate must be based on an extension of the data used to estimate β in order to fit a model which is nonlinear in log–log space. It is only necessary to consider points with probability in the range .001 to .01. α, θ are estimated by the program ABTFIT. The pertinent methodology is discussed in *Section 2.1.1*, the program description and flowcharts are presented in *Section 4.2.3*, the user's guide

1 Plot the failure simulation results contained in file LOWLIF in log–log space. That plot is shown in *Figure 3-28*.

2 Since the data in *Figure 3-28* from .001 to .003, that is, point 20 to point 60 of file LOWLIF, is approximately linear, it can be used to estimate β.

3 Create file BFITD to indicate the indices of the LOWLIF data to be used in the β estimation. See *Section 6.4.3.1* for a detailed description of the contents of file BFITD.

4 Run program BFIT. The pertinent methodology is discussed in *Section 2.1.1*, the program description and flowcharts are presented in *Section 4.2.2*, the user's guide for running this program is given in *Sections 6.4.1-6.4.6*, and the code structure and listing are provided in *Section 7.4.1*. BFIT has two input files, LOWLIF and BFITD, and two output files, BFITO and IOUTPR.

5 Obtain β estimate from output files BFITO and IOUTPR. Program BFIT has provided the estimate of 2.7815.

6 In order for α and θ to be uniquely determined, it is only necessary to consider the range .001 to .01, that is, point 20 to point 200 inclusive, of file LOWLIF, for the estimated curve to be nonlinear in log–log space. Create file PARAMS to indicate the indices of the LOWLIF data to be used in the α, θ estimation, the initial values for α and θ, and any scaling factors required. See *Section 6.4.9.1* for a detailed description of the contents of file PARAMS.

7 Run program ABTFIT. The pertinent methodology is discussed in *Section 2.1.1*, the program description and flowcharts are presented in *Section 4.2.3*, the user's guide for running this program is given in *Sections 6.4.7-6.4.12*, and the code structure and listing are provided in *Section 7.4.2*. ABTFIT has two input files, LOWLIF and PARAMS, and three output files, ABTOUT, BAYESD and IOUTPR.

8 Obtain α, θ estimates from output files ABTOUT and BAYESD. Program ABTFIT has provided the values 1.14×10^{7} for θ and 0.0204 for α.

9 Calculate assurance based on estimates of α, β, θ. The assurance calculation is performed by program LZERO. The pertinent methodology is discussed in *Section 2.1.1*, the program description and flowcharts are presented in *Section 4.2.4*, the user's guide for running this program is given in *Sections 6.4.13-6.4.18*, and the code structure and listing are provided in *Section 7.4.3*.

Figure 3-32 Steps of the Probability of Failure Curve Parameter Estimation for the ATD-HPFTP Second Stage Turbine Disk LCF Problem

for running this program is given in *Section 6.4.7-6.4.12*, and the code structure and listing are provided in *Section 7.4.2*.

PARAMS requires initial values[9] for α and θ that were obtained as follows:

B.1[10] = 121.108
B1 = 288.462

LSCALE[11] $= \left(1 / 121\right) \approx .01$

$\theta_o = N_{.001}^{\beta} = \left(121.108\right)^{2.7815} = 6.2280 \times 10^5$

XGUESS(1)[12] $= \left(N_{.001} * \textbf{LSCALE}\right)^{\beta} = \left(121.108 \times .01\right)^{2.7815} = 1.7$

XGUESS(2) $= \alpha_o = -\ln .999 / \ln 2 = .0014434$

Program ABTFIT has provided the estimates $\theta = 1.1360 \times 10^7$ and $\alpha = 0.020434$.

3.A.3.7 Driver Sensitivity Analysis

As described in *Section 2.3.10*, a set of simulations were executed to obtain the driver sensitivities. The first simulation was the nominal run, which included intrinsic materials variation only (see *Section 2.1.2.1*); all the other drivers were fixed at their nominal or most likely values. *Figure 3-28* shows the output of the nominal simulation for the turbine disk. The next analysis was the "all driver" variation analysis, which was performed allowing all the drivers to vary. *Figure 3-28* shows the output of the all-driver run for the turbine disk.

Finally, the driver sensitivities were derived using simulations for which each driver (together with intrinsic material variation) was allowed to vary one at a time while all the other drivers were held at their nominal values. The output from these simulations along with the results from the aforementioned all-driver variation and nominal runs allows the drivers to be rank ordered and allows their relative importance to be characterized. The impact of the drivers was calculated based on the failure lives at

---

[9] The calculation of initial values is illustrated in *Section 6.4.11*.

[10] B-lives were obtained from file LOWLIF. A B-life is the value of the failure parameter (e.g., failure time) at a failure probability specified as a percent: e.g., B.1 is the failure time at a probability of .001 or .1%.

[11] Life scaling factor is described in *Section 6.4.9*.

[12] Calculation of initial guesses is described in *Section 6.4.11*.

Table 3-21 Driver Sensitivity Analysis for the Turbine Disk

DRIVER VARIATION IN ANALYSIS	B1 LIFE (missions)	SHIFT IN LIFE FROM NOMINAL	% SHIFT IN LIFE FROM ALL DRIVERS	RELATIVE IMPORTANCE
NOMINAL	1116			
ALL DRIVERS	288	828		
λ_{K_d}	487	629	76	100
S/N MODEL PARAMETERS	568	549	66	87
λ_{K_t}	1037	79	10	13
ω	1070	46	6	7
ΔT_f	1100	15	2	3

the .01 probability level, given in *Table 3-21*, for the all-driver, nominal, and driver sensitivity runs.

To calculate the relative importance of a driver, the change in life from the nominal analysis due to driver variation was first calculated as a percentage of the shift due to the all driver variation for each driver. The largest shift was caused by variation in the stress adjustment factor, which is therefore the most important driver. The relative importance was derived by normalizing the percentage shifts due to variation of each driver with the percentage shift due to variation of the most important driver, in this case the stress adjustment factor. *Table 3-21* gives the percentage shift in lives and the relative importance for each driver.

3.A.3.8 Probability of Failure Curve Standardization

In order to standardize the results, the probability of failure vs. life curves were generated for a given assurance level. The curve is constructed by first calculating λ_o in *Equation 2-5* for an assurance level of 95% using the program LZERO. The pertinent methodology is discussed in *Section 2.1.1*, the program description and flowcharts are presented in *Section 4.2.4*, the user's guide for running this program is given in *Sections 6.4.13-6.4.18*, and the code structure and listing are provided in *Section 7.4.3*. The value of λ_o for the turbine disk was 4.2805×10^{-9}. Given λ_o and the bounding value of β the assurance curve may be defined as described in *Section 2.3.12*. The 95% assurance curve for the turbine disk is given in *Figure 3-27*.

Appendix 3.B
Input And Output Files

3.B.1 HPOTP Main Discharge Duct HCF Analysis Files

Selected input and output files for the HPOTP main discharge duct "all driver" analysis are given here. The analysis program DCTHCF requires two input files, DCTHCD and RELATD, along with the force history files. Annotated examples of the data file format for DCTHCD and RELATD input files are given in *Figures 6-1* and *6-2*. Related material data was not used for this component and hence the RELATD file was empty. The input file DCTHCD is given below. *Section 6.1.3.1* contains a description of the input variables and a user's guide for running DCTHCF.

The output files from a DCTHCF run are DCTHCO, LOWLIF, DUMP, RELATO, and IOUTPR. The DCTHCO, LOWLIF, and DUMP files are given below. The DCTHCO file contains an echo of the input data, output from the S/N material model, and the B lives. The LOWLIF file contains the lowest 200 (1% of total simulated) fatigue failure lives for the discharge duct, and are shown plotted in *Figure 3-10*. The DUMP file contains the results of the materials characterization calculations, including estimated values of the S/N curve parameters.

Input File - DCTHCD

```
675
0
1
20000
2
0
0
10
0.001
0.002
0.003
0.004
0.005
0.006
0.007
0.008
0.009
0.010
0.50  0.50  0.00  0.00  0.0   0.0
0.00  0.00  0.00  0.00  0.0   0.0
1.00
1.20  3.50  0.08696 0.3478 10. 10.
```

```
1.04  1.43  0.30  0.70  0.5  10.
1.20  1.34  0.30  0.70  0.5  10.
2.00  2.00  0.15  0.866667
2.00  2.00  0.20  0.933333
0.90      1.10
0.80      1.20
0.90      1.10
0.40      0.60
0.40      0.60
0.40      0.60
0.40      0.60
0.85      1.15
0.80      1.20
-1.38629  0.95166
12
8130    20900    42010    42010     3805     3805
'YNBP'  1  237.675     0.         0.         0.        0.         0.
'ZNBP'  1  190.53      0.         0.         0.        0.         0.
'YNBM2' 1    0.        0.       181.21       0.        0.         0.
'ZNBM2' 1    0.        0.       179.11       0.        0.         0.
'YNBM3' 1    0.        0.         0.       626.175     0.         0.
'ZNBM3' 1    0.        0.         0.       588.44      0.         0.
'YNBV2' 1    0.        0.         0.         0.      147.49       0.
'ZNBV2' 1    0.        0.         0.         0.      142.725      0.
'SIN1' 2  42.03382  18.83311  445.606    109.3303   45.0776    39.34468
'SIN3' 2  25.70783  28.35360   23.27139  218.0569   45.83069   34.09022
'SIN5' 2  63.3143    1.881339   4.904875  57.7348   30.37338   79.56984
'SIN6' 2 117.5516   37.80737   47.42376  134.9266  176.1129    21.75083
1.
1.
1.
4675.
6.0
.112
4.
0.1115
0.1378
3.01E+07
1
20.
1.0
0.00
20001
0.235     2.000000
0.300     4.800000
0.350     7.200001
0.400     9.600001
0.450    12.50000
0.500    15.80000
0.550    20.00000
```

```
0.580    24.00000
0.600    30.00000
0.600   200.0000
'-320 HOURGLASS + STRAIGHT'
178600.   220400.   1   20
20   0.05   1
150000.    65000.
140000.   261000.
120000.   265000.
160000.   377000.
130000.   694000.
110000.  2175000.
100000.  4198000.
105000.  5053000.
 92000.  9210000.
 95000.  9667000.
150000.   418000.
140000.   732000.
130000.   740000.
120000.   859000.
110000.  1181000.
100000.  4020000.
 92000.  5917000.
 94000.  6522000.
 90000.  6891000.
 86000.  4460000.
0.00
1  0
1.0E+36
0.00
0   0.00    0.00
```

Output File - DCTHCO

INPUT DATA

DRIVERS		PARAMETER DISTRIBUTIONS	
		RHO	THETA
WELD OFFSET (%)	Be(0.50, 0.50)	U(0.00000, 0.00000)	U(0.0, 0.0)
	Be(0.00, 0.00)	U(0.00000, 0.00000)	U(0.0, 0.0)
	TEST = 1.00		

K WELD (OD)	Be(1.20, 3.50)	U(0.08696, 0.34780)	U(10.0, 10.0)
K WELD (ID)	Be(1.04, 1.43)	U(0.30000, 0.70000)	U(0.5, 10.0)
K GEOM (OD)	Be(1.20, 1.34)	U(0.30000, 0.70000)	U(0.5, 10.0)

LAMBDA RANDOM
k: U(2.00000, 2.00000)
COEFFICIENT OF VARIATION: 0.150
STRAIN GAGE FACTOR: 0.8666670

LAMBDA SINE
k: U(2.00000, 2.00000)
COEFFICIENT OF VARIATION: 0.200
STRAIN GAGE FACTOR: 0.9333330

LAMBDA STATIC	U(0.90000, 1.10000)
DYNAMIC STRESS ANALYSIS	U(0.80000, 1.20000)
STATIC STRESS ANALYSIS	U(0.90000, 1.10000)
STRESS CARRYOVER FACTORS	
IN-PLANE AXIAL	U(0.40000, 0.60000)
OUT-OF-PLANE AXIAL	U(0.40000, 0.60000)
IN-PLANE CIRCUMFERENTIAL	U(0.40000, 0.60000)
OUT-OF-PLANE CIRCUMFERENTIAL	U(0.40000, 0.60000)
OVALITY ANALYSIS FACTOR	U(0.85000, 1.15000)
LAMBDA KOFF	U(0.80000, 1.20000)
DAMAGE MODEL ACCURACY	U(ln 0.25000, ln 2.59001)

LOADS INPUT

P LOADS (LBS)	T LOADS (IN.-LBS)	M2 LOADS (IN.-LBS)	M3 LOADS (IN.-LBS)	V2 LOADS (LBS)	V3 LOADS (LBS)
STATIC					
8130.0000	20900.0000	42010.0000	42010.0000	3805.0000	3805.0000
YNBP					
237.6750	0.0000	0.0000	0.0000	0.0000	0.0000
ZNBP					
190.5300	0.0000	0.0000	0.0000	0.0000	0.0000

YNBM2					
0.0000	0.0000	181.2100	0.0000	0.0000	0.0000
ZNBM2					
0.0000	0.0000	179.1100	0.0000	0.0000	0.0000
YNBM3					
0.0000	0.0000	0.0000	626.1750	0.0000	0.0000
ZNBM3					
0.0000	0.0000	0.0000	588.4400	0.0000	0.0000
YNBV2					
0.0000	0.0000	0.0000	0.0000	147.4900	0.0000
ZNBV2					
0.0000	0.0000	0.0000	0.0000	142.7250	0.0000
SIN1					
42.0338	18.8331	445.6060	109.3303	45.0776	39.3447
SIN3					
25.7078	28.3536	23.2714	218.0569	45.8307	34.0902
SIN5					
63.3143	1.8813	4.9049	57.7348	30.3734	79.5698
SIN6					
117.5516	37.8074	47.4238	134.9266	176.1129	21.7508

GEOMETRIC AND OTHER INPUT

K GEOM (ID)	1.00
K HOOP (OD)	1.00
K HOOP (ID)	1.00
LIMIT PRESSURE, PSI	4675.
BEND RADIUS, IN.	6.00
WELD DISTANCE FROM ELBOW TANGENCY LINE, IN.	0.112
DUCT INSIDE DIAMETER, IN.	4.00
MINIMUM WALL THICKNESS, IN.	0.1115
WALL THICKNESS AT BEND (ID), IN.	0.1378
ELASTIC MODULUS, PSI	0.301E+08
ANALYSIS LOCATION	1
ANGLE PHI (DEG)	20.0

STRESS-TIME HISTORY PERIOD, SEC 1.00

STRESS-TIME HISTORY NOISE FILTER, PSI 0.0

NUMBER OF TIME-VARYING LOADS 12

NUMBER OF POINTS IN HISTORIES 20001

MATERIAL INPUT

DESCRIPTION: -320 HOURGLASS + STRAIGHT

YIELD STRENGTH 0.17860E+06

ULTIMATE STRENGTH 0.22040E+06

NUMBER OF POINTS 20

ORIGINAL S/N STRESS	ORIGINAL S/N LIFE	STRESS RATIO	REGION	TRANSFORMED S/N STRESS	TRANSFORMED S/N LIFE
0.15000E+06	65000.	0.05	1	0.11086E+06	65000.
0.14000E+06	261000.	0.05	1	0.99773E+05	261000.
0.12000E+06	265000.	0.05	1	0.79814E+05	265000.
0.16000E+06	377000.	0.05	1	0.12280E+06	377000.
0.13000E+06	694000.	0.05	1	0.89449E+05	694000.
0.11000E+06	2175000.	0.05	1	0.70802E+05	2175000.
0.10000E+06	4198000.	0.05	1	0.62353E+05	4198000.
0.10500E+06	5053000.	0.05	1	0.66510E+05	5053000.
0.92000E+05	9210000.	0.05	1	0.55964E+05	9210000.
0.95000E+05	9667000.	0.05	1	0.58323E+05	9667000.
0.15000E+06	418000.	0.05	1	0.11086E+06	418000.
0.14000E+06	732000.	0.05	1	0.99773E+05	732000.
0.13000E+06	740000.	0.05	1	0.89449E+05	740000.
0.12000E+06	859000.	0.05	1	0.79814E+05	859000.
0.11000E+06	1181000.	0.05	1	0.70802E+05	1181000.
0.10000E+06	4020000.	0.05	1	0.62353E+05	4020000.
0.92000E+05	5917000.	0.05	1	0.55964E+05	5917000.
0.94000E+05	6522000.	0.05	1	0.57532E+05	6522000.
0.90000E+05	6891000.	0.05	1	0.54416E+05	6891000.
0.86000E+05	4460000.	0.05	1	0.51374E+05	4460000.

```
THERE IS  1 REGION(S) WITH DATA
AND  0 REGION(S) TO THE RIGHT WITHOUT DATA
THE UPPER BOUND(S) OF THE REGION(S) ARE (CYCLES):

        0.100E+37


EXOGENOUS INFORMATION


CONSTRAINT ON COEFFICIENT OF VARIATION, C:  0.0000

EXPLICIT CONSTRAINT ON m FOR EACH REGION:

REGION      # OF POINTS      LOWER BOUND      UPPER BOUND

    1            0              0.0000           0.0000


B LIVES:       EMPIRICAL

0.00100       0.164506E+05
0.00200       0.256184E+05
0.00300       0.328444E+05
0.00400       0.397100E+05
0.00500       0.454202E+05
0.00600       0.530106E+05
0.00700       0.583856E+05
0.00800       0.625631E+05
0.00900       0.677342E+05
0.01000       0.733181E+05
0.50000       0.334764E+07
```

Output File - LOWLIF

```
1,  5.E-5,  2171.08268607
2,  1.E-4,  2274.610282879
3,  1.5E-4,  5397.61433618
4,  2.E-4,  5436.913987152
5,  2.5E-4,  7590.725113991
6,  3.E-4,  8243.513935069
7,  3.5E-4,  9478.598493334
8,  4.E-4,  9592.334153456
9,  4.5E-4,  10961.29979166
10,  5.E-4,  11248.37224586
11,  5.5E-4,  12006.79530942
12,  6.E-4,  12394.79049961
13,  6.5E-4,  12458.42625798
```

```
14,  7.E-4,  12615.58511637
15,  7.5E-4,  13077.76799579
16,  8.E-4,  13245.47144751
17,  8.5E-4,  13298.6206169
18,  9.E-4,  13398.09257794
19,  9.5E-4,  14890.87886404
20,  1.E-3,  16450.60402927
21,  1.05E-3,  17930.50652629
22,  1.1E-3,  18318.76045862
23,  1.15E-3,  18616.07977373
24,  1.2E-3,  18825.78120489
25,  1.25E-3,  19031.35540271
26,  1.3E-3,  19896.02557763
27,  1.35E-3,  19896.45621919
28,  1.4E-3,  20283.58254505
29,  1.45E-3,  20716.21926102
30,  1.5E-3,  21090.96928527
31,  1.55E-3,  21771.34472699
32,  1.6E-3,  22473.12998514
33,  1.65E-3,  22483.11184718
34,  1.7E-3,  23031.93757268
35,  1.75E-3,  23576.6407008
36,  1.8E-3,  23744.0658441
37,  1.85E-3,  24557.7138378
38,  1.9E-3,  24806.64062718
39,  1.95E-3,  24983.14710955
40,  2.E-3,  25618.40563241
41,  2.05E-3,  25653.09540362
42,  2.1E-3,  26190.33441654
43,  2.15E-3,  26337.13572945
44,  2.2E-3,  28353.02541956
45,  2.25E-3,  28834.7318554
46,  2.3E-3,  29108.81760869
47,  2.35E-3,  29162.57978578
48,  2.4E-3,  29244.09472359
49,  2.45E-3,  29603.45152701
50,  2.5E-3,  29632.66087405
51,  2.55E-3,  30291.34679017
52,  2.6E-3,  30446.00942229
53,  2.65E-3,  30493.38478737
54,  2.7E-3,  30673.46359312
55,  2.75E-3,  30760.85836022
56,  2.8E-3,  31007.51798871
57,  2.85E-3,  32148.98623899
58,  2.9E-3,  32372.47132738
59,  2.95E-3,  32390.50914646
60,  3.E-3,  32844.36090394
61,  3.05E-3,  33014.88860404
62,  3.1E-3,  33190.12210164
63,  3.15E-3,  33270.0824175
```

```
64,  3.2E-3,  34615.02721604
65,  3.25E-3,  34748.27188751
66,  3.3E-3,  34872.98895736
67,  3.35E-3,  35068.65368964
68,  3.4E-3,  35096.39424284
69,  3.45E-3,  35281.89190532
70,  3.5E-3,  35425.55976141
71,  3.55E-3,  35897.72810911
72,  3.6E-3,  36560.07826949
73,  3.65E-3,  36588.46946974
74,  3.7E-3,  37605.65296311
75,  3.75E-3,  37978.29169689
76,  3.8E-3,  39305.80601728
77,  3.85E-3,  39374.22514173
78,  3.9E-3,  39490.47963762
79,  3.95E-3,  39699.64167016
80,  4.E-3,  39709.99000531
81,  4.05E-3,  40508.29704049
82,  4.1E-3,  41214.003737
83,  4.15E-3,  41506.81491461
84,  4.2E-3,  41532.92876058
85,  4.25E-3,  41622.05616043
86,  4.3E-3,  42243.61170326
87,  4.35E-3,  42632.96056193
88,  4.4E-3,  42744.1434916
89,  4.45E-3,  43060.05554056
90,  4.5E-3,  43148.21678663
91,  4.55E-3,  43425.31080851
92,  4.6E-3,  43485.79372142
93,  4.65E-3,  43665.25474881
94,  4.7E-3,  43679.23619109
95,  4.75E-3,  44087.79399035
96,  4.8E-3,  44466.30256251
97,  4.85E-3,  44838.15511878
98,  4.9E-3,  44938.80625138
99,  4.95E-3,  45160.62247766
100,  5.E-3,  45420.16962913
101,  5.05E-3,  45470.65979261
102,  5.1E-3,  45652.11464271
103,  5.15E-3,  46127.71679451
104,  5.2E-3,  46251.00996064
105,  5.25E-3,  46372.88535658
106,  5.3E-3,  47119.6325578
107,  5.35E-3,  47137.13100697
108,  5.4E-3,  48171.37806459
109,  5.45E-3,  48207.11856747
110,  5.5E-3,  48318.70721881
111,  5.55E-3,  48931.61143896
112,  5.6E-3,  49703.44909796
113,  5.65E-3,  49956.33191574
```

```
114,  5.7E-3,  50234.61968773
115,  5.75E-3,  50398.55301772
116,  5.8E-3,  50644.56677104
117,  5.85E-3,  51204.9658348
118,  5.9E-3,  52501.46119135
119,  5.95E-3,  52904.03713305
120,  6.E-3,  53010.6194896
121,  6.05E-3,  53167.75826465
122,  6.1E-3,  53357.64587097
123,  6.15E-3,  53468.23112726
124,  6.2E-3,  53929.93276736
125,  6.25E-3,  54082.80324984
126,  6.3E-3,  54293.44219992
127,  6.35E-3,  54346.43533946
128,  6.4E-3,  55234.56773908
129,  6.45E-3,  55326.77795268
130,  6.5E-3,  55585.55479447
131,  6.55E-3,  55938.43019878
132,  6.6E-3,  56350.38162224
133,  6.65E-3,  56711.10774186
134,  6.7E-3,  56817.21030027
135,  6.75E-3,  56967.09611928
136,  6.8E-3,  57346.04643495
137,  6.85E-3,  57566.47058465
138,  6.9E-3,  57613.30154789
139,  6.95E-3,  57832.43925853
140,  7.E-3,  58385.56620338
141,  7.05E-3,  58462.89978311
142,  7.1E-3,  58624.28036547
143,  7.15E-3,  58782.60363557
144,  7.2E-3,  58971.56159982
145,  7.25E-3,  59110.23542496
146,  7.3E-3,  59122.95734245
147,  7.35E-3,  59272.60177966
148,  7.4E-3,  59324.77926608
149,  7.45E-3,  59465.20911553
150,  7.5E-3,  59763.82855003
151,  7.55E-3,  60154.6430269
152,  7.6E-3,  60396.64734786
153,  7.65E-3,  60406.48823455
154,  7.7E-3,  60515.31715323
155,  7.75E-3,  61252.11016131
156,  7.8E-3,  61363.38086049
157,  7.85E-3,  61453.41837845
158,  7.9E-3,  61578.69974975
159,  7.95E-3,  61600.93010134
160,  8.E-3,  62563.0930965
161,  8.05E-3,  63269.80866235
162,  8.1E-3,  63291.9881826
163,  8.15E-3,  63950.16419736
```

```
164,  8.2E-3,  63965.346384
165,  8.25E-3,  64102.87159225
166,  8.3E-3,  64415.36565053
167,  8.35E-3,  64541.8794529
168,  8.4E-3,  65163.69082135
169,  8.45E-3,  65519.40846814
170,  8.5E-3,  66120.52340431
171,  8.55E-3,  66308.5054934
172,  8.6E-3,  66494.47817761
173,  8.65E-3,  66554.46816072
174,  8.7E-3,  66844.66829289
175,  8.75E-3,  67103.77873876
176,  8.8E-3,  67345.80119819
177,  8.85E-3,  67352.66901473
178,  8.9E-3,  67546.08780309
179,  8.95E-3,  67603.05652641
180,  9.E-3,  67734.1771025
181,  9.05E-3,  67883.78039904
182,  9.1E-3,  68326.94572489
183,  9.15E-3,  68594.12670141
184,  9.2E-3,  68746.50091648
185,  9.25E-3,  69099.14523026
186,  9.3E-3,  69250.94593986
187,  9.35E-3,  69337.50660218
188,  9.4E-3,  69548.02239665
189,  9.45E-3,  69554.70766341
190,  9.5E-3,  69635.84059297
191,  9.55E-3,  70031.91794349
192,  9.6E-3,  70150.2009716
193,  9.65E-3,  70318.54906011
194,  9.7E-3,  70342.87926757
195,  9.75E-3,  71264.7486166
196,  9.8E-3,  71823.56061707
197,  9.85E-3,  72118.48961609
198,  9.9E-3,  72605.2876764
199,  9.95E-3,  73300.5780415
200,  1.E-2,  73318.12226789
```

Output File - DUMP

```
Copyright (C) 1990, California Institute of Technology.  U.S. Government
Sponsorship under NASA Contract NAS7-918 is acknowledged.


RESULTS OF INFORMATION AGGREGATION CALCULATIONS


95% CONFIDENCE INTERVALS ON C AND m FOR EACH REGION
```

```
REGION:  1        Io = ( 0.092758541, 0.181539608)
                  Jo = ( 3.596348060, 5.874000250)

POINT ESTIMATES OF C AND m FOR EACH REGION

     REGION          E(C)              E(m)

       1         0.122759425       4.735174


POSTERIOR CREDIBILITY RANGE ON m FOR EACH REGION

REGION      LOWER BOUND      UPPER BOUND

    1           3.5963           5.8740


PARAMETER VALUES FOR MEDIAN S/N CURVE

NUMBER OF REGIONS:   1     E(BETAo) =  9.6555     E(k) = 14.2292

REGION        m                K          LIFE BOUND        STRESS BOUND

   1       4.73517       0.15458E+07      0.100E+37          0.00000E+00
```

3.B.2 LPFTP Turbine Drive Duct HCF Analysis Files

Selected input and output files for the LPFTP turbine drive duct "all driver" analysis are given here. The analysis program DCTHCF requires two input files, DCTHCD and RELATD, along with the force history files. Related material data was not used for this component and hence the RELATD file was empty. The input file DCTHCD is given below. The output files from a DCTHCF run are DCTHCO, LOWLIF, DUMP, RELATO, and IOUTPR. The DCTHCO, LOWLIF, and DUMP files are given below. The DCTHCO file contains an echo of the input data, output from the S/N material model, and the Blives. The LOWLIF file contains the lowest 200 (1% of total simulated) fatigue failure lives for the discharge duct, and they are shown plotted in *Figure 3-13*. The DUMP file contains the results of the materials characterization calculations, including estimated values of the S/N curve parameters.

Input File - DCTHCD

```
675
0
1
20000
2
0
0
10
0.001
0.002
0.003
0.004
0.005
0.006
0.007
0.008
0.009
0.010
0.40   0.40   0.00   0.00    0.0   0.0
0.00   0.00   0.00   0.00    0.0   0.0
1.00
1.05   1.45   0.50   0.50   10.   10.
1.26   1.74   0.30   0.70    0.5   10.
1.21   1.35   0.30   0.70    0.5   10.
2.00   2.00   0.15   0.866667
2.00   2.00   0.20   0.933333
0.90      1.10
0.80      1.20
0.90      1.10
0.40      0.60
0.40      0.60
0.40      0.60
0.40      0.60
0.85      1.15
0.80      1.20
-1.38629   0.95166
22
2138.0   6820.0   16775.0   16775.0   1080.0   1080.0
'XP'     1   42.744     0.0       0.0       0.0       0.0       0.0
'YP'     1   28.0675    0.0       0.0       0.0       0.0       0.0
'ZP'     1   16.239     0.0       0.0       0.0       0.0       0.0
'XT'     1    0.0     145.41      0.0       0.0       0.0       0.0
'YT'     1    0.0     169.26      0.0       0.0       0.0       0.0
'ZT'     1    0.0     152.29      0.0       0.0       0.0       0.0
'XM2'    1    0.0       0.0     41.675      0.0       0.0       0.0
'YM2'    1    0.0       0.0     42.187      0.0       0.0       0.0
'ZM2'    1    0.0       0.0     68.5355     0.0       0.0       0.0
'XM3'    1    0.0       0.0      0.0      202.675     0.0       0.0
```

```
'YM3'     1     0.0         0.0       0.0      202.305     0.0       0.0
'ZM3'     1     0.0         0.0       0.0      126.755     0.0       0.0
'XV2'     1     0.0         0.0       0.0        0.0      57.689     0.0
'YV2'     1     0.0         0.0       0.0        0.0      42.7605    0.0
'SIN1'    2    21.91435    43.9086   39.4836    60.53955  14.9129   12.88245
'SIN2'    2    78.54595     1.60925   0.973577  73.7664    4.589225  0.264931
'SIN3'    2    19.6242      3.35879   1.339263  32.92415   7.497715  0.721379
'SIN4'    2   166.3695      0.548139  4.24984  189.0855   22.3281    0.099988
'SIN5'    2    24.15575     1.04256   0.753309  18.54625   1.7687    0.285259
'SIN6'    2    14.80325     0.083479  0.238039  18.04635   3.721265  0.05662
'SIN7'    2    11.1594      1.61855   6.060575   8.033975  2.63346   0.58617
'SIN12'   2     6.76763     0.1371    0.394779  17.00245   1.566452  0.200407
1.00    1.00    1.00
5293.
6.00
0.70
2.0
0.118
0.166
2.7E+07
1
25.
1.5
0.00
30001
0.235      2.000000
0.300      4.800000
0.350      7.200001
0.400      9.600001
0.450     12.50000
0.500     15.80000
0.550     20.00000
0.580     24.00000
0.600     30.00000
0.600    200.0000
'75 F, INCOLOY 903'
158600.    186500.    6    20
7    -1.0    1
70000.       59900.
60000.       85300.
50000.      213100.
40000.      473900.
35000.      892100.
33000.      865100.
32000.      744100.
3    -1.0    2
30000.     2799400.
29000.     5631800.
28000.     2121200.
5    -1.0    1
```

```
70000.       29000.
60000.       53100.
50000.      142700.
40000.      170500.
35000.      385900.
1    -1.0    2
30000.     1201600.
1    -1.0    1
28000.      614800.
3    -1.0    2
28000.     3796000.
27000.     1345600.
26000.    18940700.
0.00
2    0
1.0E+06
1.0E+36
0.15
2    0.000     3.987284
2    0.000    12.57616
```

Output File - DCTHCO

INPUT DATA

DRIVERS		PARAMETER DISTRIBUTIONS	
		RHO	THETA
WELD OFFSET (%)	Be(0.40, 0.40)	U(0.00000, 0.00000)	U(0.0, 0.0)
	Be(0.00, 0.00)	U(0.00000, 0.00000)	U(0.0, 0.0)
	TEST = 1.00		
K WELD (OD)	Be(1.05, 1.45)	U(0.50000, 0.50000)	U(10.0, 10.0)
K WELD (ID)	Be(1.26, 1.74)	U(0.30000, 0.70000)	U(0.5, 10.0)
K GEOM (OD)	Be(1.21, 1.35)	U(0.30000, 0.70000)	U(0.5, 10.0)
LAMBDA RANDOM	k: U(2.00000, 2.00000)		
	COEFFICIENT OF VARIATION: 0.150		
	STRAIN GAGE FACTOR: 0.8666670		

LAMBDA SINE	k: U(2.00000, 2.00000) COEFFICIENT OF VARIATION: 0.200 STRAIN GAGE FACTOR: 0.9333330	
LAMBDA STATIC		U(0.90000, 1.10000)
DYNAMIC STRESS ANALYSIS		U(0.80000, 1.20000)
STATIC STRESS ANALYSIS		U(0.90000, 1.10000)
STRESS CARRYOVER FACTORS		
IN-PLANE AXIAL		U(0.40000, 0.60000)
OUT-OF-PLANE AXIAL		U(0.40000, 0.60000)
IN-PLANE CIRCUMFERENTIAL		U(0.40000, 0.60000)
OUT-OF-PLANE CIRCUMFERENTIAL		U(0.40000, 0.60000)
OVALITY ANALYSIS FACTOR		U(0.85000, 1.15000)
LAMBDA KOFF		U(0.80000, 1.20000)
DAMAGE MODEL ACCURACY		U(ln 0.25000, ln 2.59001)

LOADS INPUT

P LOADS (LBS)	T LOADS (IN.-LBS)	M2 LOADS (IN.-LBS)	M3 LOADS (IN.-LBS)	V2 LOADS (LBS)	V3 LOADS (LBS)
STATIC					
2138.0000	6820.0000	16775.0000	16775.0000	1080.0000	1080.0000
XP					
42.7440	0.0000	0.0000	0.0000	0.0000	0.0000
YP					
28.0675	0.0000	0.0000	0.0000	0.0000	0.0000
ZP					
16.2390	0.0000	0.0000	0.0000	0.0000	0.0000
XT					
0.0000	145.4100	0.0000	0.0000	0.0000	0.0000
YT					
0.0000	169.2600	0.0000	0.0000	0.0000	0.0000
ZT					
0.0000	152.2900	0.0000	0.0000	0.0000	0.0000
XM2					
0.0000	0.0000	41.6750	0.0000	0.0000	0.0000
YM2					

0.0000	0.0000	42.1870	0.0000	0.0000	0.0000
ZM2					
0.0000	0.0000	68.5355	0.0000	0.0000	0.0000
XM3					
0.0000	0.0000	0.0000	202.6750	0.0000	0.0000
YM3					
0.0000	0.0000	0.0000	202.3050	0.0000	0.0000
ZM3					
0.0000	0.0000	0.0000	126.7550	0.0000	0.0000
XV2					
0.0000	0.0000	0.0000	0.0000	57.6890	0.0000
YV2					
0.0000	0.0000	0.0000	0.0000	42.7605	0.0000
SIN1					
21.9144	43.9086	39.4836	60.5395	14.9129	12.8825
SIN2					
78.5460	1.6093	0.9736	73.7664	4.5892	0.2649
SIN3					
19.6242	3.3588	1.3393	32.9242	7.4977	0.7214
SIN4					
166.3695	0.5481	4.2498	189.0855	22.3281	0.1000
SIN5					
24.1558	1.0426	0.7533	18.5462	1.7687	0.2853
SIN6					
14.8032	0.0835	0.2380	18.0463	3.7213	0.0566
SIN7					
11.1594	1.6185	6.0606	8.0340	2.6335	0.5862
SIN12					
6.7676	0.1371	0.3948	17.0024	1.5665	0.2004

GEOMETRIC AND OTHER INPUT

K GEOM (ID)	1.00
K HOOP (OD)	1.00
K HOOP (ID)	1.00
LIMIT PRESSURE, PSI	5293.
BEND RADIUS, IN.	6.00
WELD DISTANCE FROM ELBOW TANGENCY LINE, IN.	0.700
DUCT INSIDE DIAMETER, IN.	2.00

MINIMUM WALL THICKNESS, IN.	0.1180
WALL THICKNESS AT BEND (ID), IN.	0.1660
ELASTIC MODULUS, PSI	0.270E+08
ANALYSIS LOCATION	1
ANGLE PHI (DEG)	25.0
STRESS-TIME HISTORY PERIOD, SEC	1.50
STRESS-TIME HISTORY NOISE FILTER, PSI	0.0
NUMBER OF TIME-VARYING LOADS	22
NUMBER OF POINTS IN HISTORIES	30001

MATERIAL INPUT

DESCRIPTION: 75 F, INCOLOY 903

YIELD STRENGTH	0.15860E+06
ULTIMATE STRENGTH	0.18650E+06
NUMBER OF POINTS	20

ORIGINAL S/N STRESS	ORIGINAL S/N LIFE	STRESS RATIO	REGION	TRANSFORMED S/N STRESS	TRANSFORMED S/N LIFE
0.70000E+05	59900.	-1.00	1	0.70000E+05	59900.
0.60000E+05	85300.	-1.00	1	0.60000E+05	85300.
0.50000E+05	213100.	-1.00	1	0.50000E+05	213100.
0.40000E+05	473900.	-1.00	1	0.40000E+05	473900.
0.35000E+05	892100.	-1.00	1	0.35000E+05	892100.
0.33000E+05	865100.	-1.00	1	0.33000E+05	865100.
0.32000E+05	744100.	-1.00	1	0.32000E+05	744100.
0.30000E+05	2799400.	-1.00	2	0.30000E+05	2799400.
0.29000E+05	5631800.	-1.00	2	0.29000E+05	5631800.
0.28000E+05	2121200.	-1.00	2	0.28000E+05	2121200.
0.70000E+05	29000.	-1.00	1	0.70000E+05	29000.
0.60000E+05	53100.	-1.00	1	0.60000E+05	53100.
0.50000E+05	142700.	-1.00	1	0.50000E+05	142700.
0.40000E+05	170500.	-1.00	1	0.40000E+05	170500.

```
0.35000E+05    385900.     -1.00     1     0.35000E+05    385900.
0.30000E+05   1201600.     -1.00     2     0.30000E+05   1201600.
0.28000E+05    614800.     -1.00     1     0.28000E+05    614800.
0.28000E+05   3796000.     -1.00     2     0.28000E+05   3796000.
0.27000E+05   1345600.     -1.00     2     0.27000E+05   1345600.
0.26000E+05  18940700.     -1.00     2     0.26000E+05  18940700.


THERE IS  2 REGION(S) WITH DATA
AND  0 REGION(S) TO THE RIGHT WITHOUT DATA
THE UPPER BOUND(S) OF THE REGION(S) ARE (CYCLES):

        0.100E+07
        0.100E+37


EXOGENOUS INFORMATION


CONSTRAINT ON COEFFICIENT OF VARIATION, C:  0.1500

EXPLICIT CONSTRAINT ON m FOR EACH REGION:

REGION      # OF POINTS      LOWER BOUND      UPPER BOUND

    1             2              0.0000           3.9873
    2             2              0.0000          12.5762


B LIVES:       EMPIRICAL

0.00100       0.274755E+05
0.00200       0.383248E+05
0.00300       0.505642E+05
0.00400       0.643003E+05
0.00500       0.785574E+05
0.00600       0.884030E+05
0.00700       0.999464E+05
0.00800       0.110974E+06
0.00900       0.122820E+06
0.01000       0.136070E+06
0.50000       0.713371E+09
```

Output File - LOWLIF

```
1,  5.E-5,  5603.765356757
2,  1.E-4,  5686.285311492
```

```
3,  1.5E-4,  6433.169421466
4,  2.E-4,  7077.980999079
5,  2.5E-4,  7996.58950548
6,  3.E-4,  10592.64629652
7,  3.5E-4,  11409.4933516
8,  4.E-4,  12283.72670257
9,  4.5E-4,  13612.466679
10,  5.E-4,  13864.93582738
11,  5.5E-4,  15001.04129354
12,  6.E-4,  17990.54681255
13,  6.5E-4,  23196.74710228
14,  7.E-4,  24591.82586467
15,  7.5E-4,  26092.29722913
16,  8.E-4,  26543.75670674
17,  8.5E-4,  26745.60283963
18,  9.E-4,  26802.3800698
19,  9.5E-4,  26993.4418659
20,  1.E-3,  27475.5326694
21,  1.05E-3,  27823.33684902
22,  1.1E-3,  29152.07648564
23,  1.15E-3,  29171.93138802
24,  1.2E-3,  29573.79403915
25,  1.25E-3,  29983.66505427
26,  1.3E-3,  30020.49929504
27,  1.35E-3,  30730.58813945
28,  1.4E-3,  31818.28147166
29,  1.45E-3,  32078.43432697
30,  1.5E-3,  32312.58705008
31,  1.55E-3,  33443.5928183
32,  1.6E-3,  33944.00211847
33,  1.65E-3,  34073.0826797
34,  1.7E-3,  34446.13242596
35,  1.75E-3,  34628.64657622
36,  1.8E-3,  34912.88128041
37,  1.85E-3,  35636.18811894
38,  1.9E-3,  37006.21294047
39,  1.95E-3,  38092.36954628
40,  2.E-3,  38324.78814331
41,  2.05E-3,  39263.60630392
42,  2.1E-3,  40174.96787758
43,  2.15E-3,  40467.65864107
44,  2.2E-3,  40572.75490531
45,  2.25E-3,  40585.81106176
46,  2.3E-3,  40799.03000649
47,  2.35E-3,  41315.82068212
48,  2.4E-3,  41657.95489419
49,  2.45E-3,  41972.4804694
50,  2.5E-3,  42114.67488451
51,  2.55E-3,  42529.3518521
52,  2.6E-3,  42581.81576417
```

```
53,  2.65E-3,  44327.46170315
54,  2.7E-3,  44817.43749491
55,  2.75E-3,  46465.8858277
56,  2.8E-3,  48511.14449324
57,  2.85E-3,  49314.87507409
58,  2.9E-3,  49613.19530952
59,  2.95E-3,  50021.7885656
60,  3.E-3,  50564.21599362
61,  3.05E-3,  52221.61596956
62,  3.1E-3,  52489.29502605
63,  3.15E-3,  53484.15740996
64,  3.2E-3,  53544.35435706
65,  3.25E-3,  53772.27288086
66,  3.3E-3,  54502.37085461
67,  3.35E-3,  54778.57663731
68,  3.4E-3,  55165.42363888
69,  3.45E-3,  56459.15886717
70,  3.5E-3,  56656.17288078
71,  3.55E-3,  57372.66680184
72,  3.6E-3,  59359.49645979
73,  3.65E-3,  59501.69612314
74,  3.7E-3,  60825.8373782
75,  3.75E-3,  60952.32209879
76,  3.8E-3,  61266.72189539
77,  3.85E-3,  61541.91532104
78,  3.9E-3,  62831.75816497
79,  3.95E-3,  63547.40623241
80,  4.E-3,  64300.33685851
81,  4.05E-3,  64990.7651771
82,  4.1E-3,  65693.61651306
83,  4.15E-3,  67062.36182379
84,  4.2E-3,  67952.65012623
85,  4.25E-3,  67966.85507035
86,  4.3E-3,  68414.1171338
87,  4.35E-3,  68526.89219322
88,  4.4E-3,  68860.78294691
89,  4.45E-3,  70528.3458314
90,  4.5E-3,  71379.60992727
91,  4.55E-3,  71678.38306004
92,  4.6E-3,  71695.41031714
93,  4.65E-3,  73126.40512159
94,  4.7E-3,  74014.94263623
95,  4.75E-3,  74873.24701067
96,  4.8E-3,  75093.57496214
97,  4.85E-3,  75901.18488815
98,  4.9E-3,  76837.83908576
99,  4.95E-3,  76976.54838642
100,  5.E-3,  78557.42795391
101,  5.05E-3,  78992.00096167
102,  5.1E-3,  79229.39570199
```

```
103,  5.15E-3,  79655.87573819
104,  5.2E-3,  79992.97567942
105,  5.25E-3,  80408.01544155
106,  5.3E-3,  81831.58969958
107,  5.35E-3,  82089.75634541
108,  5.4E-3,  82651.34975836
109,  5.45E-3,  83872.60081398
110,  5.5E-3,  85402.48252511
111,  5.55E-3,  85451.73880384
112,  5.6E-3,  85912.67397663
113,  5.65E-3,  86041.16338772
114,  5.7E-3,  86152.71655872
115,  5.75E-3,  86959.73810709
116,  5.8E-3,  87492.94913473
117,  5.85E-3,  87686.02957545
118,  5.9E-3,  88071.36981785
119,  5.95E-3,  88282.07265443
120,  6.E-3,  88403.03459386
121,  6.05E-3,  89183.98322008
122,  6.1E-3,  90536.43212354
123,  6.15E-3,  91120.61809887
124,  6.2E-3,  91948.27461359
125,  6.25E-3,  92638.90366091
126,  6.3E-3,  92853.75233303
127,  6.35E-3,  93050.65487485
128,  6.4E-3,  93524.76449977
129,  6.45E-3,  94354.12555006
130,  6.5E-3,  94792.44497588
131,  6.55E-3,  95745.49949854
132,  6.6E-3,  97765.41234892
133,  6.65E-3,  98664.81561846
134,  6.7E-3,  98769.64161344
135,  6.75E-3,  98935.8769087
136,  6.8E-3,  99079.62891364
137,  6.85E-3,  99121.49305396
138,  6.9E-3,  99839.57108528
139,  6.95E-3,  99852.70559686
140,  7.E-3,  99946.41616208
141,  7.05E-3,  99962.75543066
142,  7.1E-3,  100080.0446134
143,  7.15E-3,  100218.3024798
144,  7.2E-3,  101669.104322
145,  7.25E-3,  101816.5907939
146,  7.3E-3,  102081.8704252
147,  7.35E-3,  102318.2447821
148,  7.4E-3,  103613.7512834
149,  7.45E-3,  104392.6824486
150,  7.5E-3,  104418.6836832
151,  7.55E-3,  104657.3606114
152,  7.6E-3,  105911.0555323
```

```
153,  7.65E-3,  106932.51511
154,  7.7E-3,  107331.0389073
155,  7.75E-3,  108021.7003811
156,  7.8E-3,  108491.4387238
157,  7.85E-3,  109627.7429307
158,  7.9E-3,  109760.502436
159,  7.95E-3,  110859.1263592
160,  8.E-3,  110974.1482473
161,  8.05E-3,  111745.2881768
162,  8.1E-3,  112218.4228104
163,  8.15E-3,  112682.0621298
164,  8.2E-3,  114015.0054024
165,  8.25E-3,  114196.7326355
166,  8.3E-3,  115794.9572814
167,  8.35E-3,  115807.1656825
168,  8.4E-3,  115871.3692813
169,  8.45E-3,  117110.3954834
170,  8.5E-3,  117528.4808907
171,  8.55E-3,  117735.2485667
172,  8.6E-3,  117755.6719641
173,  8.65E-3,  117984.5071406
174,  8.7E-3,  118379.332936
175,  8.75E-3,  119797.4205213
176,  8.8E-3,  121633.2756584
177,  8.85E-3,  122248.3354606
178,  8.9E-3,  122588.7987535
179,  8.95E-3,  122778.3892267
180,  9.E-3,  122819.5130249
181,  9.05E-3,  122951.1159032
182,  9.1E-3,  123072.1599377
183,  9.15E-3,  124205.9447018
184,  9.2E-3,  124692.6470904
185,  9.25E-3,  125857.7661101
186,  9.3E-3,  125918.3411274
187,  9.35E-3,  126313.9718308
188,  9.4E-3,  126473.3023551
189,  9.45E-3,  127291.2592762
190,  9.5E-3,  128178.827365
191,  9.55E-3,  128187.0790466
192,  9.6E-3,  129780.1010373
193,  9.65E-3,  130930.0785701
194,  9.7E-3,  131940.5187697
195,  9.75E-3,  132256.5441974
196,  9.8E-3,  132812.2435942
197,  9.85E-3,  133010.3251245
198,  9.9E-3,  135402.23056
199,  9.95E-3,  135721.5964869
200,  1.E-2,  136070.0289122
```

Output File - DUMP

RESULTS OF INFORMATION AGGREGATION CALCULATIONS

95% CONFIDENCE INTERVALS ON C AND m FOR EACH REGION

```
     REGION:  1       Io = ( 0.080228861, 0.192291881)
                      Jo = ( 2.637740759, 4.360046378)
     REGION:  2       Io = ( 0.031044615, 0.121979338)
                      Jo = (-8.169760025,26.791736399)
```

POINT ESTIMATES OF C AND m FOR EACH REGION

REGION	E(C)	E(m)
1	0.113254264	3.498894
2	0.049734403	9.310988

RANGE ON m FOR EACH REGION IMPLIED BY C CONSTRAINT

REGION	LOWER BOUND	UPPER BOUND
1	3.0105	5.8711
2	6.0459	INFINITY

POSTERIOR CREDIBILITY RANGE ON m FOR EACH REGION

REGION	LOWER BOUND	UPPER BOUND
1	3.0105	3.9873
2	6.0459	12.5762

PARAMETER VALUES FOR MEDIAN S/N CURVE

```
NUMBER OF REGIONS:   2     E(BETAo) = 10.9339     E(k) = 14.2524

REGION        m              K          LIFE BOUND        STRESS BOUND

   1       3.49891     0.15780E+07      0.100E+07          0.30429E+05
   2       9.31103     0.13418E+06      0.100E+37          0.00000E+00
```

3.B.3 HPOTP Heat Exchanger Coil HCF Analysis Files

Selected input and output files for the HPOTP heat exchanger coil "all driver" analysis are given here. The analysis program HEXHCF requires two input files, HEXHCD and RELATD, along with the force history files. Annotated examples of the data file format for HEXHCD are given in *Figure 6-5*. Related material data was not used for this component and hence the RELATD file was empty. The input file HEXHCD is given below. *Section 6.1.10.1* contains a description of the input variables and a user's guide for running HEXHCF.

The output files from a HEXHCF run are HEXHCO, LOWLIF, DUMP, RELATO, and IOUTPR. The HEXHCO, LOWLIF, and DUMP files from an "all drivers" analysis of the HEX coil are given below. The HEXHCO file contains an echo of the input data, output from the S/N material model, and the B lives. The LOWLIF file contains the lowest 200 (1% of total simulated) fatigue failure lives for the discharge duct, and are shown plotted in *Figure 3-21*. The DUMP file contains the results of the materials characterization calculations, including estimated values of the S/N curve parameters.

Input File - HEXHCD

```
675
0
1
20000
2
0
0
10
0.001
0.002
0.003
0.004
0.005
0.006
0.007
0.008
0.009
0.01
0.10      0.10      0.00    0.00     0.0    0.0
```

```
0.00      0.00      0.00    0.00     0.0    0.0
1.00
1.00      1.00      0.00      0.00      0.0     0.0
1.20      3.50      0.1304    0.5652   10.     10.
0.1885    0.1915    0.50      0.50      0.5    20.
0.0113    0.0157    0.27273   0.27273   0.5    20.
2.00      2.00      0.15    1.00
2.00      2.00      0.20    1.00
 486.     666.    29.     56.5
 799.     908.    49.5    48.
3808.    4177.    69.     69.
0.50    1.50
0.80    1.20
0.80    1.20
0.90    1.10
0.80    1.20
0.60    1.40
-1.38629    0.95166
6
0.00      0.00      -0.07214    0.00       0.00       0.00
'XP'    1 0.856685 0.0       0.0       0.0       0.0       0.0
'YP'    1 0.62078  0.0       0.0       0.0       0.0       0.0
'XM3'   1 0.0      0.0       0.0       0.14102   0.0       0.0
'YM3'   1 0.0      0.0       0.0       0.355475  0.0       0.0
'SIN1' 2 0.269884 0.003043 0.009638 0.20535  0.347965 0.051646
'AERO' 3 0.0      0.0       0.0       0.07179   0.0       0.0
1.0    1.0    1.0    1.0
3640.
2
85.
1.00
0.0
17801
29000000.    8.8E-06    0.30
0.235      2.000000
0.300      4.800000
0.350      7.200001
0.400      9.600001
0.450     12.50000
0.500     15.80000
0.550     20.00000
0.580     24.00000
0.600     30.00000
0.600    200.0000
6
   21.95    0.001
   55.77    0.002
  144.85    0.005
  322.73    0.010
 1945.90    0.050
```

```
50688.0    0.660
'70 F, 321 STAINLESS STEEL ALLOY - WELDED'
27900.   76800.   1   13
13   -1.0   1
40000.     1000.
40000.     2000.
40000.     3000.
40000.     4000.
40000.     5000.
40000.     6000.
30000.    23000.
30000.    66000.
25000.    72000.
25000.   190000.
20000.   789000.
20000.  1070000.
20000.  1450000.
0.00
1    0
1.0E+36
0.00
0    0.000     0.000
0.0    0.0     0.0
```

Output File - HEXHCO

INPUT DATA

DRIVERS		PARAMETER DISTRIBUTIONS	
		RHO	THETA
WELD OFFSET (%)	Be(0.10, 0.10) Be(0.00, 0.00) TEST = 1.00	U(0.00000, 0.00000) U(0.00000, 0.00000)	U(0.0, 0.0) U(0.0, 0.0)
K WELD (OD)	Be(1.00, 1.00)	U(0.00000, 0.00000)	U(0.0, 0.0)
K WELD (ID)	Be(1.20, 3.50)	U(0.13040, 0.56520)	U(10.0, 10.0)
INNER DIAMETER	Be(0.1885, 0.1915)	U(0.50000, 0.50000)	U(0.5, 20.0)
WALL THICKNESS	Be(0.0113, 0.0157)	U(0.27273, 0.27273)	U(0.5, 20.0)

LAMBDA RANDOM k: U(2.00000, 2.00000)
COEFFICIENT OF VARIATION: 0.150
STRAIN GAGE FACTOR: 1.0000000

LAMBDA SINE k: U(2.00000, 2.00000)
COEFFICIENT OF VARIATION: 0.200
STRAIN GAGE FACTOR: 1.0000000

		MU	SIGMA
INNER TEMPERATURE	NORMAL:	U(486.0, 666.0)	U(29.0, 56.5)
OUTER TEMPERATURE	NORMAL:	U(799.0, 908.0)	U(49.5, 48.0)
INNER PRESSURE	NORMAL:	U(3808.0, 4177.0)	U(69.0, 69.0)

DYNAMIC AERO LOAD FACTOR	U(0.50000, 1.50000)
STATIC AERO LOAD FACTOR	U(0.80000, 1.20000)
DYNAMIC STRESS ANALYSIS	U(0.80000, 1.20000)
AERO STRESS ANALYSIS	U(0.90000, 1.10000)
LAMBDA KOFF	U(0.80000, 1.20000)
NEUBERS RULE	U(0.60000, 1.40000)
DAMAGE MODEL ACCURACY	U(ln 0.25000, ln 2.59001)

LOADS INPUT

P LOADS (LBS)	T LOADS (IN.-LBS)	M2 LOADS (IN.-LBS)	M3 LOADS (IN.-LBS)	V2 LOADS (LBS)	V3 LOADS (LBS)
STATIC AERO					
0.000000	0.000000	-0.072140	0.000000	0.000000	0.000000
XP					
0.856685	0.000000	0.000000	0.000000	0.000000	0.000000
YP					
0.620780	0.000000	0.000000	0.000000	0.000000	0.000000
XM3					

0.000000	0.000000	0.000000	0.141020	0.000000	0.000000
YM3					
0.000000	0.000000	0.000000	0.355475	0.000000	0.000000
SIN1					
0.269884	0.003043	0.009638	0.205350	0.347965	0.051646
AERO					
0.000000	0.000000	0.000000	0.071790	0.000000	0.000000

GEOMETRIC AND OTHER INPUT

K GEOM (OD)	1.00
K GEOM (ID)	1.00
K HOOP (OD)	1.00
K HOOP (ID)	1.00
EXTERNAL PRESSURE, PSI	3640.
ANALYSIS LOCATION	2
ANGLE THETA (DEGREES)	85.0
STRESS-TIME HISTORY PERIOD, SEC	1.00
STRESS-TIME HISTORY NOISE FILTER, PSI	0.0
NUMBER OF TIME-VARYING LOADS	6
NUMBER OF POINTS IN HISTORIES	17801
ANGLE THETA (RADIANS)	1.48
ELASTIC MODULUS, PSI	0.290E+08
COEFF OF THERMAL EXPANSION	0.88000000E-05
POISSONS RATIO	0.300

STRESS-STRAIN CURVE INPUT

MAXIMUM NUMBER OF SEGMENTS	6

STRESS-STRAIN PRODUCT	STRAIN VALUES
21.95	0.00100
55.77	0.00200
144.85	0.00500
322.73	0.01000
1945.90	0.05000
50688.00	0.66000

MATERIAL INPUT

DESCRIPTION: 70 F, 321 STAINLESS STEEL ALLOY - WELDED

YIELD STRENGTH 0.27900E+05

ULTIMATE STRENGTH 0.76800E+05

NUMBER OF POINTS 13

ORIGINAL S/N STRESS	ORIGINAL S/N LIFE	STRESS RATIO	REGION	TRANSFORMED S/N STRESS	TRANSFORMED S/N LIFE
0.40000E+05	1000.	-1.00	1	0.40000E+05	1000.
0.40000E+05	2000.	-1.00	1	0.40000E+05	2000.
0.40000E+05	3000.	-1.00	1	0.40000E+05	3000.
0.40000E+05	4000.	-1.00	1	0.40000E+05	4000.
0.40000E+05	5000.	-1.00	1	0.40000E+05	5000.
0.40000E+05	6000.	-1.00	1	0.40000E+05	6000.
0.30000E+05	23000.	-1.00	1	0.30000E+05	23000.
0.30000E+05	66000.	-1.00	1	0.30000E+05	66000.
0.25000E+05	72000.	-1.00	1	0.25000E+05	72000.
0.25000E+05	190000.	-1.00	1	0.25000E+05	190000.
0.20000E+05	789000.	-1.00	1	0.20000E+05	789000.
0.20000E+05	1070000.	-1.00	1	0.20000E+05	1070000.
0.20000E+05	1450000.	-1.00	1	0.20000E+05	1450000.

THERE IS 1 REGION(S) WITH DATA

```
AND  0 REGION(S) TO THE RIGHT WITHOUT DATA
THE UPPER BOUND(S) OF THE REGION(S) ARE (CYCLES):

        0.100E+37


EXOGENOUS INFORMATION


CONSTRAINT ON COEFFICIENT OF VARIATION, C:  0.0000

EXPLICIT CONSTRAINT ON m FOR EACH REGION:

REGION      # OF POINTS      LOWER BOUND      UPPER BOUND

    1            0              0.0000           0.0000



B LIVES:       EMPIRICAL

0.00100       0.771838E+07
0.00200       0.110621E+08
0.00300       0.143306E+08
0.00400       0.181705E+08
0.00500       0.206006E+08
0.00600       0.245673E+08
0.00700       0.278451E+08
0.00800       0.301220E+08
0.00900       0.326067E+08
0.01000       0.359317E+08
0.50000       0.175421E+11
```

Output File - LOWLIF

```
1,  5.E-5,  1479781.289269
2,  1.E-4,  3004876.487258
3,  1.5E-4,  3445826.573824
4,  2.E-4,  3963816.260295
5,  2.5E-4,  4037528.09434
6,  3.E-4,  4105125.884641
7,  3.5E-4,  4380491.704167
8,  4.E-4,  4589202.440686
9,  4.5E-4,  5285659.351945
10,  5.E-4,  5348788.569105
11,  5.5E-4,  5448780.289697
12,  6.E-4,  5673497.315382
```

```
13,  6.5E-4,  5756503.665433
14,  7.E-4,  5901122.14788
15,  7.5E-4,  5992467.420463
16,  8.E-4,  6099130.254685
17,  8.5E-4,  6236753.108872
18,  9.E-4,  6693325.086817
19,  9.5E-4,  7351647.786689
20,  1.E-3,  7718383.958808
21,  1.05E-3,  7868177.902472
22,  1.1E-3,  8082424.391728
23,  1.15E-3,  8130867.145248
24,  1.2E-3,  8410800.150164
25,  1.25E-3,  8490666.656294
26,  1.3E-3,  8535148.060287
27,  1.35E-3,  8979207.461742
28,  1.4E-3,  9105088.568738
29,  1.45E-3,  9364738.344999
30,  1.5E-3,  9496224.625237
31,  1.55E-3,  9598273.204801
32,  1.6E-3,  9633790.742194
33,  1.65E-3,  9807188.460706
34,  1.7E-3,  9905755.103738
35,  1.75E-3,  10192804.95354
36,  1.8E-3,  10252395.14266
37,  1.85E-3,  10705309.21556
38,  1.9E-3,  10767912.69693
39,  1.95E-3,  10867340.43723
40,  2.E-3,  11062070.15081
41,  2.05E-3,  11255641.20545
42,  2.1E-3,  11751449.73611
43,  2.15E-3,  12023472.49597
44,  2.2E-3,  12085322.16353
45,  2.25E-3,  12095466.70234
46,  2.3E-3,  12097250.13585
47,  2.35E-3,  12491067.59957
48,  2.4E-3,  12758632.94092
49,  2.45E-3,  13057469.48806
50,  2.5E-3,  13173851.63135
51,  2.55E-3,  13210510.88621
52,  2.6E-3,  13427543.61267
53,  2.65E-3,  13465648.7826
54,  2.7E-3,  13523692.04964
55,  2.75E-3,  13631616.97477
56,  2.8E-3,  13846292.93406
57,  2.85E-3,  13860630.26477
58,  2.9E-3,  14109263.07464
59,  2.95E-3,  14284922.59893
60,  3.E-3,  14330636.2891
61,  3.05E-3,  14728214.92948
62,  3.1E-3,  14829870.78647
```

```
63,  3.15E-3,  15091244.21511
64,  3.2E-3,  15342974.0025
65,  3.25E-3,  15420074.75321
66,  3.3E-3,  15422893.78037
67,  3.35E-3,  15638511.28351
68,  3.4E-3,  15946114.93471
69,  3.45E-3,  15980524.53372
70,  3.5E-3,  16279868.83655
71,  3.55E-3,  16375437.5627
72,  3.6E-3,  16397943.39711
73,  3.65E-3,  16635475.21379
74,  3.7E-3,  16642019.32203
75,  3.75E-3,  16819534.35861
76,  3.8E-3,  16930107.7936
77,  3.85E-3,  17897167.9116
78,  3.9E-3,  18060883.97599
79,  3.95E-3,  18141358.47696
80,  4.E-3,  18170490.68634
81,  4.05E-3,  18216391.60537
82,  4.1E-3,  18301817.92482
83,  4.15E-3,  18366179.92685
84,  4.2E-3,  18377286.10277
85,  4.25E-3,  18542064.30037
86,  4.3E-3,  18703119.18224
87,  4.35E-3,  18778146.2471
88,  4.4E-3,  19025340.88236
89,  4.45E-3,  19174037.51932
90,  4.5E-3,  19188576.59917
91,  4.55E-3,  19338320.0896
92,  4.6E-3,  19421080.93617
93,  4.65E-3,  19462969.41708
94,  4.7E-3,  19818515.90651
95,  4.75E-3,  19991339.85726
96,  4.8E-3,  20154722.27965
97,  4.85E-3,  20323197.58953
98,  4.9E-3,  20424278.42021
99,  4.95E-3,  20516960.82745
100,  5.E-3,  20600581.27911
101,  5.05E-3,  20982195.51449
102,  5.1E-3,  21286602.62778
103,  5.15E-3,  21536176.62897
104,  5.2E-3,  21619105.61789
105,  5.25E-3,  21692113.35097
106,  5.3E-3,  21820982.22142
107,  5.35E-3,  21979618.08444
108,  5.4E-3,  22168836.80603
109,  5.45E-3,  22259797.25835
110,  5.5E-3,  22653175.10462
111,  5.55E-3,  22925028.63644
112,  5.6E-3,  22984253.71787
```

```
113,  5.65E-3,  23529643.37564
114,  5.7E-3,  23556221.74841
115,  5.75E-3,  23880065.2457
116,  5.8E-3,  23992687.75068
117,  5.85E-3,  24290331.47328
118,  5.9E-3,  24330338.13695
119,  5.95E-3,  24555370.69535
120,  6.E-3,  24567304.15551
121,  6.05E-3,  24694668.57759
122,  6.1E-3,  24773379.48146
123,  6.15E-3,  24903674.65428
124,  6.2E-3,  24919553.96505
125,  6.25E-3,  24951568.50234
126,  6.3E-3,  25524327.86217
127,  6.35E-3,  25919175.18897
128,  6.4E-3,  26322117.84422
129,  6.45E-3,  26352051.25391
130,  6.5E-3,  26443563.88271
131,  6.55E-3,  26592214.12503
132,  6.6E-3,  26608410.70283
133,  6.65E-3,  26828702.36412
134,  6.7E-3,  26945248.00253
135,  6.75E-3,  27026953.52151
136,  6.8E-3,  27176462.20214
137,  6.85E-3,  27246360.5481
138,  6.9E-3,  27552759.52338
139,  6.95E-3,  27717394.02058
140,  7.E-3,  27845082.7874
141,  7.05E-3,  28264566.81855
142,  7.1E-3,  28267132.66918
143,  7.15E-3,  28508301.58202
144,  7.2E-3,  28517388.81253
145,  7.25E-3,  28770684.86102
146,  7.3E-3,  28808355.63171
147,  7.35E-3,  28974339.47578
148,  7.4E-3,  29130094.80862
149,  7.45E-3,  29131258.76974
150,  7.5E-3,  29194541.81925
151,  7.55E-3,  29294352.46579
152,  7.6E-3,  29388188.87586
153,  7.65E-3,  29444240.4738
154,  7.7E-3,  29541645.17309
155,  7.75E-3,  29643428.16885
156,  7.8E-3,  29693637.86088
157,  7.85E-3,  29714548.96468
158,  7.9E-3,  29801547.71799
159,  7.95E-3,  29892136.60004
160,  8.E-3,  30121980.7633
161,  8.05E-3,  30190071.31036
162,  8.1E-3,  30248124.40411
```

```
163,  8.15E-3,  30325107.65089
164,  8.2E-3,  30436443.99758
165,  8.25E-3,  30489332.79314
166,  8.3E-3,  30675818.13157
167,  8.35E-3,  30869018.14745
168,  8.4E-3,  30871951.16941
169,  8.45E-3,  30978760.43506
170,  8.5E-3,  31077171.69862
171,  8.55E-3,  31085731.82913
172,  8.6E-3,  31159676.69033
173,  8.65E-3,  31218713.54831
174,  8.7E-3,  31273807.6537
175,  8.75E-3,  31547129.63778
176,  8.8E-3,  31605498.65852
177,  8.85E-3,  32024029.52725
178,  8.9E-3,  32138469.20102
179,  8.95E-3,  32282195.66175
180,  9.E-3,  32606701.98199
181,  9.05E-3,  32853094.97354
182,  9.1E-3,  32947818.33784
183,  9.15E-3,  33003821.70516
184,  9.2E-3,  33239335.65172
185,  9.25E-3,  33305328.50143
186,  9.3E-3,  33540405.78944
187,  9.35E-3,  33597649.86919
188,  9.4E-3,  33693346.1913
189,  9.45E-3,  33979652.59362
190,  9.5E-3,  33995480.32142
191,  9.55E-3,  34120349.04351
192,  9.6E-3,  34169209.30027
193,  9.65E-3,  34297569.66375
194,  9.7E-3,  34879640.79331
195,  9.75E-3,  34907666.94819
196,  9.8E-3,  34941274.0184
197,  9.85E-3,  35018956.23174
198,  9.9E-3,  35504039.43814
199,  9.95E-3,  35658398.83892
200,  1.E-2,  35931735.01375
```

Output File - DUMP

RESULTS OF INFORMATION AGGREGATION CALCULATIONS

```
95% CONFIDENCE INTERVALS ON C AND m FOR EACH REGION

     REGION:  1        Io = ( 0.047421026, 0.113658328)
                       Jo = ( 7.136664079, 9.595369882)


POINT ESTIMATES OF C AND m FOR EACH REGION

     REGION          E(C)              E(m)

       1         0.066941413        8.366017


POSTERIOR CREDIBILITY RANGE ON m FOR EACH REGION

REGION      LOWER BOUND      UPPER BOUND

    1           7.1367           9.5954


PARAMETER VALUES FOR MEDIAN S/N CURVE

NUMBER OF REGIONS:   1     E(BETAo) = 19.5380     E(k) = 11.5536

REGION        m                K          LIFE BOUND        STRESS BOUND

   1        8.36602       0.10528E+06      0.100E+37          0.00000E+00
```

3.B.4 ATD-HPFTP Second Stage Turbine Disk LCF Analysis Files

Selected input and output files for the ATD-HPFTP second stage turbine disk "all driver" analysis are given here. The analysis program TRBPWA requires two input files: TRBPWD and RELATD. Annotated examples of the data file format for TRBPWD and RELATD input files are given in *Figures 6-7* and *6-2*. Related material data was not used for this component and hence the RELATD file was empty. The input file TRBPWD is given below. *Section 6.2.3* contains a description of the input variables and a user's guide for running TRBPWA.

The output files from a TRBPWA run are TRBPWO, LOWLIF, DUMP, RELATO, and IOUTPR. The TRBPWO, LOWLIF, and DUMP files are given below. The TRBPWO

file contains an echo of the input data, output from the S/N material model, and the B-lives. The LOWLIF file contains the lowest 200 (1% of total simulated) fatigue failure lives for the ATD Disk, and are shown plotted in *Figure 3-27*. The DUMP file contains the results of the materials characterization calculations, including estimated values of the S/N curve parameters.

Input File - TRBPWD

```
675
0
1
20000
50
2
0
0
10
0.001
0.002
0.003
0.004
0.005
0.006
0.007
0.008
0.009
0.010
-200.   200.   0.50   0.50   0.0   0.0
 200.   500.   0.00   0.00  10.0  10.0
0.95
37592.   507.
 0.80000   1.20000
 0.95000   1.05000
1.41   2.18   159807.   38600.
  1915.  0.91325   4.4435
 14749.  0.04   0.07   101.72
'PWA HPFTP 2ND TURBINE DISK'
00000.  198000.   1    9
 9   -1.0   1
160000.     636.
160000.     677.
160000.    1019.
140000.    4743.
130000.    3824.
130000.    4163.
120000.    3749.
120000.   11349.
110000.   39600.
0.
```

```
1    0
1.0E+36
0.00
0    0.000      0.000
```

Output File - TRBPWO

INPUT DATA

	DRIVERS	PARAMETER DISTRIBUTIONS	
		RHO	THETA
DELTA Tf	Be(-200.0, 200.0) Be(200.0, 500.0) TEST = 0.95	U(0.50000, 0.50000) U(0.00000, 0.00000)	U(0.0, 0.0) U(10.0, 10.0)
SPEED (RPM)	NORMAL: MEAN = 37592.	STAND. DEV. = 507.	
LAMBDA Kd	U(0.80000, 1.20000)		
LAMBDA Kt	U(0.95000, 1.05000)		

OTHER LOADS INPUT

STRESS ADJUSTMENT, Kd	1.410
STRESS CONCENTRATION, Kt	2.180
MECHANICAL STRESS (PSI)	159807.0
ROTATIONAL SPEED (RPM)	38600.
STRESS DUE TO METAL TEMPERATURE (PSI)	1915.0
SENSITIVITY OF METAL TEMPERATURE TO DELTA Tf	0.91325

SENSITIVITY OF STRESS DUE TO Tmetal (PSI/F) 4.44

STRESS DUE TO THERMAL GRADIENT (PSI) 14749.0

SENSITIVITY OF THERMAL GRADIENT TO DELTA Tf
FOR DELTA Tf < 0 0.040
FOR DELTA Tf >= 0 0.070

SENSITIVITY OF STRESS DUE TO THERM. GRAD. (PSI/F) 101.72

MATERIAL INPUT

DESCRIPTION: PWA HPFTP 2ND TURBINE DISK

YIELD STRENGTH 0.00000E+00

ULTIMATE STRENGTH 0.19800E+06

NUMBER OF POINTS 9

ORIGINAL S/N		STRESS		TRANSFORMED S/N	
STRESS	LIFE	RATIO	REGION	STRESS	LIFE
0.16000E+06	636.	-1.00	1	0.16000E+06	636.
0.16000E+06	677.	-1.00	1	0.16000E+06	677.
0.16000E+06	1019.	-1.00	1	0.16000E+06	1019.
0.14000E+06	4743.	-1.00	1	0.14000E+06	4743.
0.13000E+06	3824.	-1.00	1	0.13000E+06	3824.
0.13000E+06	4163.	-1.00	1	0.13000E+06	4163.
0.12000E+06	3749.	-1.00	1	0.12000E+06	3749.
0.12000E+06	11349.	-1.00	1	0.12000E+06	11349.
0.11000E+06	39600.	-1.00	1	0.11000E+06	39600.

THERE IS 1 REGION(S) WITH DATA
AND 0 REGION(S) TO THE RIGHT WITHOUT DATA
THE UPPER BOUND(S) OF THE REGION(S) ARE (CYCLES):

0.100E+37

EXOGENOUS INFORMATION

CONSTRAINT ON COEFFICIENT OF VARIATION, C: 0.0000

EXPLICIT CONSTRAINT ON m FOR EACH REGION:

REGION	# OF POINTS	LOWER BOUND	UPPER BOUND
1	0	0.0000	0.0000

B LIVES:	EMPIRICAL
0.00100	0.121108E+03
0.00200	0.155309E+03
0.00300	0.180471E+03
0.00400	0.200357E+03
0.00500	0.214710E+03
0.00600	0.230961E+03
0.00700	0.251356E+03
0.00800	0.263503E+03
0.00900	0.281120E+03
0.01000	0.288462E+03
0.50000	0.411175E+04

Output File - LOWLIF

1	0.500000E-04	15.2292
2	0.100000E-03	30.8418
3	0.150000E-03	34.1021
4	0.200000E-03	39.0600
5	0.250000E-03	51.4226
6	0.300000E-03	53.2745
7	0.350000E-03	58.0043
8	0.400000E-03	65.5637
9	0.450000E-03	71.9857
10	0.500000E-03	75.1110
11	0.550000E-03	75.8070
12	0.600000E-03	89.4144
13	0.650000E-03	103.456
14	0.700000E-03	104.278
15	0.750000E-03	105.559
16	0.800000E-03	107.647
17	0.850000E-03	107.784
18	0.900000E-03	114.712
19	0.950000E-03	116.542
20	0.100000E-02	121.108
21	0.105000E-02	124.069

22	0.110000E-02	124.429
23	0.115000E-02	124.546
24	0.120000E-02	129.185
25	0.125000E-02	131.056
26	0.130000E-02	132.799
27	0.135000E-02	133.245
28	0.140000E-02	133.803
29	0.145000E-02	134.375
30	0.150000E-02	136.029
31	0.155000E-02	136.142
32	0.160000E-02	146.670
33	0.165000E-02	149.321
34	0.170000E-02	149.350
35	0.175000E-02	149.919
36	0.180000E-02	152.232
37	0.185000E-02	152.349
38	0.190000E-02	152.559
39	0.195000E-02	152.949
40	0.200000E-02	155.309
41	0.205000E-02	155.585
42	0.210000E-02	156.888
43	0.215000E-02	157.319
44	0.220000E-02	158.105
45	0.225000E-02	158.928
46	0.230000E-02	159.245
47	0.235000E-02	160.929
48	0.240000E-02	161.168
49	0.245000E-02	163.429
50	0.250000E-02	164.862
51	0.255000E-02	166.070
52	0.260000E-02	168.230
53	0.265000E-02	169.043
54	0.270000E-02	169.055
55	0.275000E-02	174.029
56	0.280000E-02	175.739
57	0.285000E-02	176.429
58	0.290000E-02	176.966
59	0.295000E-02	178.398
60	0.300000E-02	180.471
61	0.305000E-02	180.738
62	0.310000E-02	181.203
63	0.315000E-02	181.368
64	0.320000E-02	182.887
65	0.325000E-02	184.505
66	0.330000E-02	184.510
67	0.335000E-02	184.919
68	0.340000E-02	185.591
69	0.345000E-02	185.607
70	0.350000E-02	186.154
71	0.355000E-02	191.204

72	0.360000E-02	191.649
73	0.365000E-02	193.389
74	0.370000E-02	195.028
75	0.375000E-02	195.336
76	0.380000E-02	197.925
77	0.385000E-02	198.473
78	0.390000E-02	199.333
79	0.395000E-02	199.871
80	0.400000E-02	200.357
81	0.405000E-02	203.074
82	0.410000E-02	206.303
83	0.415000E-02	207.010
84	0.420000E-02	207.449
85	0.425000E-02	207.492
86	0.430000E-02	207.952
87	0.435000E-02	208.420
88	0.440000E-02	209.027
89	0.445000E-02	209.282
90	0.450000E-02	209.696
91	0.455000E-02	210.907
92	0.460000E-02	211.559
93	0.465000E-02	211.829
94	0.470000E-02	212.364
95	0.475000E-02	212.551
96	0.480000E-02	213.054
97	0.485000E-02	213.175
98	0.490000E-02	214.526
99	0.495000E-02	214.554
100	0.500000E-02	214.710
101	0.505000E-02	215.661
102	0.510000E-02	215.751
103	0.515000E-02	216.391
104	0.520000E-02	216.600
105	0.525000E-02	217.116
106	0.530000E-02	217.569
107	0.535000E-02	217.849
108	0.540000E-02	219.640
109	0.545000E-02	219.643
110	0.550000E-02	220.485
111	0.555000E-02	221.658
112	0.560000E-02	222.904
113	0.565000E-02	223.053
114	0.570000E-02	224.775
115	0.575000E-02	225.854
116	0.580000E-02	227.973
117	0.585000E-02	228.482
118	0.590000E-02	228.934
119	0.595000E-02	230.314
120	0.600000E-02	230.961
121	0.605000E-02	231.353

122	0.610000E-02	232.023
123	0.615000E-02	232.187
124	0.620000E-02	234.333
125	0.625000E-02	234.820
126	0.630000E-02	236.077
127	0.635000E-02	236.604
128	0.640000E-02	237.671
129	0.645000E-02	238.349
130	0.650000E-02	239.269
131	0.655000E-02	239.967
132	0.660000E-02	240.050
133	0.665000E-02	242.428
134	0.670000E-02	244.809
135	0.675000E-02	245.703
136	0.680000E-02	248.848
137	0.685000E-02	250.122
138	0.690000E-02	250.135
139	0.695000E-02	251.327
140	0.700000E-02	251.356
141	0.705000E-02	251.544
142	0.710000E-02	252.696
143	0.715000E-02	252.731
144	0.720000E-02	252.826
145	0.725000E-02	254.045
146	0.730000E-02	255.588
147	0.735000E-02	255.936
148	0.740000E-02	258.845
149	0.745000E-02	259.559
150	0.750000E-02	259.613
151	0.755000E-02	260.046
152	0.760000E-02	260.628
153	0.765000E-02	261.008
154	0.770000E-02	261.185
155	0.775000E-02	261.531
156	0.780000E-02	262.128
157	0.785000E-02	262.237
158	0.790000E-02	262.727
159	0.795000E-02	263.178
160	0.800000E-02	263.503
161	0.805000E-02	264.066
162	0.810000E-02	264.301
163	0.815000E-02	264.491
164	0.820000E-02	264.728
165	0.825000E-02	265.586
166	0.830000E-02	269.652
167	0.835000E-02	271.928
168	0.840000E-02	272.150
169	0.845000E-02	273.784
170	0.850000E-02	274.667
171	0.855000E-02	274.995

172	0.860000E-02	275.158
173	0.865000E-02	278.007
174	0.870000E-02	279.032
175	0.875000E-02	280.049
176	0.880000E-02	280.089
177	0.885000E-02	280.380
178	0.890000E-02	280.779
179	0.895000E-02	280.885
180	0.900000E-02	281.120
181	0.905000E-02	281.155
182	0.910000E-02	281.284
183	0.915000E-02	281.394
184	0.920000E-02	281.707
185	0.925000E-02	283.283
186	0.930000E-02	283.324
187	0.935000E-02	283.371
188	0.940000E-02	283.556
189	0.945000E-02	284.575
190	0.950000E-02	284.579
191	0.955000E-02	284.692
192	0.960000E-02	284.880
193	0.965000E-02	285.136
194	0.970000E-02	285.480
195	0.975000E-02	285.854
196	0.980000E-02	285.907
197	0.985000E-02	286.616
198	0.990000E-02	287.837
199	0.995000E-02	288.408
200	0.100000E-01	288.462

Output File - DUMP

RESULTS OF INFORMATION AGGREGATION CALCULATIONS

95% CONFIDENCE INTERVALS ON C AND m FOR EACH REGION

REGION: 1 Io = (0.036692030, 0.112948100)
Jo = (5.734418000,11.972310000)

POINT ESTIMATES OF C AND m FOR EACH REGION

REGION E(C) E(m)

1	0.055495330	8.853366

POSTERIOR CREDIBILITY RANGE ON m FOR EACH REGION

REGION	LOWER BOUND	UPPER BOUND
1	5.7344	11.9723

PARAMETER VALUES FOR MEDIAN S/N CURVE

NUMBER OF REGIONS: 1 E(BETAo) = 22.9860 E(k) = 12.7338

REGION	m	K	LIFE BOUND	STRESS BOUND
1	8.85337	0.34214E+06	0.100E+37	0.00000E+00

TECHNICAL REPORT STANDARD TITLE PAGE

1. Report No. 92-15	2. Government Accession No.	3. Recipient's Catalog No.
4. Title and Subtitle An Improved Approach for Flight Readiness Certification--Methodology for Failure Risk Assessment and Application Examples. Vol I (untitled), Vol. II Software Documentation, Vol. III Structure and Listing of Programs		5. Report Date June 1, 1992 6. Performing Organization Code
7. Author(s) N. R. Moore, D. H. Ebbeler, L. E. Newlin, S. Sutharshana, M. Creager		8. Performing Organization Report No.
9. Performing Organization Name and Address JET PROPULSION LABORATORY California Institute of Technology 4800 Oak Grove Drive Pasadena, California 91109		10. Work Unit No. 11. Contract or Grant No. NAS7-918 13. Type of Report and Period Covered JPL Publication
12. Sponsoring Agency Name and Address NATIONAL AERONAUTICS AND SPACE ADMINISTRATION Washington, D.C. 20546		14. Sponsoring Agency Code RE67 BT-553-02-01-01-00

15. Supplementary Notes

16. Abstract

An improved methodology for quantitatively evaluating failure risk of spaceflight systems to assess flight readiness and identify risk control measures is presented. This methodology, called Probabilistic Failure Assessment (PFA), combines operating experience from tests and flights with engineering analysis to estimate failure risk. The PFA methodology is of particular value when information on which to base an assessment of failure risk, including test experience and knowledge of parameters used in engineering analyses of failure phenomena, is expensive or difficult to acquire.

The PFA methodology is a prescribed statistical structure in which engineering analysis models that characterize failure phenomena are used conjointly with uncertainties about analysis parameters and/or modeling accuracy to estimate failure probability distributions for specific failure modes. These distributions can then be modified, by means of statistical procedures of the PFA methodology, to reflect any test or flight experience. Conventional engineering analysis models currently employed for design of failure prediction are used in this methodology.

This report describes the PFA methodology and presents examples of its application. Conventional approaches to failure risk evaluation for spaceflight systems are discussed, and the rationale for the approach taken in the PFA methodology is presented. The statistical methods, engineering models, and computer software used in fatigue failure mode applications are thoroughly documented.

17. Key Words (Selected by Author(s))	18. Distribution Statement
Spacecraft Design, Testing, and Performance Quality Assurance and Reliability Structural Engineering Statistics and Probability	Unclassified; unlimited

19. Security Classif. (of this report)	20. Security Classif. (of this page)	21. No. of Pages	22. Price
Unclassified	Unclassified	258,371, 526	